AN EXPERIMENTAL INVESTIGATION AND LABORATORY SIMULATION OF ATMOSPHERIC FADING ON A 900 MHz TRANSHORIZON RADIO-LINK

by

MICHAEL N. NICOLAIDES

February, 1979

A Thesis submitted for the degree of
Doctor of Philosophy of the
University of London

Department of Electrical Engineering
Imperial College of Science & Technology
London, S.W.7

ABSTRACT

In this work, the results of an investigation on the performance of a transhorizon radio-link, operating at a frequency of 900 MHz, are presented together with the results obtained from a scale-model laboratory simulation of the radio-link.

The properties of the propagation medium (atmosphere) are extensively discussed with special emphasis on phenomena such as atmospheric turbulence, thermal stratification and convection. The existing theories of e.m. wave propagation are briefly presented together with some theoretical expressions describing the fading power spectrum of a radio signal received beyond the horizon.

The long-term variation of the received signal median level is studied on a daily, monthly and annual basis. In particular, the relation between the monthly median level and the monthly average of surface wind and relative sunshine is investigated in order to define the average weather conditions that characterise the "worst month" in propagation terms.

The fading power spectra of short-term records (3.5 mins. duration) of the received signal are estimated using digital methods and the effects of surface wind and static stability upon the fading characteristics are studied. Most of the fading characteristics have been classified into two categories, namely, α- and β-type. The surface wind component, U_n, normal to the propagation direction appears to affect considerably the former but not the latter. An empirical expression relating U_n to the power spectral density function is established for the α-type of fading. This expression describes adequately the observed

"spread" of the fading power spectrum when U_n increases. For U_n = 0 (zero mean surface wind across the propagation direction), it suggests a "-8/3" power-law dependence of the power spectral density upon frequency. This is in agreement with Tatarski's theoretical expression for line-of-sight propagation.

Static stability is also found to affect the fading spectrum of the received signal. For the β-type of fading, it appears to govern the power spectral density function and to be responsible for a transition in the exponent of the inverse power law describing this function.

The results from the laboratory model show that the effects of the atmospheric medium upon the received signal can be adequately simulated. Thus, fading characteristics similar to those observed on the full-scale link (α- and β-type) can be reproduced under controlled conditions of surface wind and vertical temperature gradient. The effect of U_n upon the fading power spectrum is successfully simulated, yielding a scale reduction factor of 52 between U_n's experienced on the full-scale link and those required to produce the same power spectra on the model system. The effect of increasing vertical temperature gradient (decreasing static stability) upon the fading spectrum can also be adequately simulated. The resulting spectrum "spread" is attributed to intense thermal turbulence in the "near ground" region.

ACKNOWLEDGEMENTS

The author would like to express his deep gratitude to his supervisor, Dr. W. G. Burrows, for his contribution to the initiation and completion of this work. His guidance and assistance on all aspects were invaluable.

He would also like to express his indebtedness to the Hellenic National Research Foundation and the Royal Society of London for partly financing this work.

Gratitude is also expressed for the suggestions and discussions rendered by Dr. R. H. Clarke, Dr. N. Mavrokoukoulakis and Mr. I. Mashhour.

The author is grateful to Mr. D. Sage for his technical assistance and to Helen Bastin for her excellent typing.

The author feels that he can hardly express in words his gratitude to his wife, Marie-Paule, for her unfaultering and continuous support.

TABLE OF CONTENTS

		Page
ABSTRACT		1
ACKNOWLEDGEMENTS		3
TABLE OF CONTENTS		4
CHAPTER 1	THE PROPAGATION MEDIUM	9
1.1	The Earth's Atmosphere	9
1.2	Spatial and Temporal Scales of Atmospheric Processes	12
1.3	The Well-Mixed Atmosphere - Vertical Distribution of Refractive Index	15
1.4	The Turbulent Atmosphere	19
1.4.1	The Nature of Atmosphere Turbulence - Significance of Atmospheric Stability	19
1.4.2	Convection and Thermal Turbulence in the Atmosphere	25
	A Disordered Atmospheric Convection	26
	B Ordered Atmospheric Convection	30
1.4.3	Spectral Structure of the Velocity, Temperature and Refractivity Fields in the Turbulent Atmosphere	32
1.4.4	The Effect of Buoyancy on the Spectrum of Atmospheric Turbulence	43
CHAPTER 2	THEORETICAL APPROACHES TO THE PROBLEM OF TRANSHORIZON PROPAGATION	58
2.1	Propagation by Refraction in a Standard Atmosphere: Effective Earth Radius-Modified Refractive Index	59

		Page
2.2	Wave Propagation in the Real Atmosphere	63
	2.2.1 Wave Propagation in an Atmospheric Duct	64
	2.2.2 Wave Propagation by Partial Reflection	70
	2.2.3 Wave Propagation by Scattering	76
	2.2.4 Dependence of Some Propagation Parameters on Carrier Frequency and the Refractivity Spectrum Model	83
2.3	The Problem of the Temporal Fluctuations of the Received Signal	89
CHAPTER 3	THE RADIO LINK: DESCRIPTION OF THE SYSTEM	94
3.1	The Transmitter (NUS-3860)	94
3.2	The Receiver (NUS-3863)	98
3.3	Recording Apparatus	103
3.4	The Propagation Path	104
CHAPTER 4	DATA PROCESSING	107
4.1	Meteorological Data	107
4.2	Received Signal Processing	110
	4.2.1 Some Theoretical Considerations of Spectrum Analysis	111
	4.2.2 The Estimation of the Power Spectrum	118
	4.2.3 A Suitable Measure of the Spectrum "Spread"	121
4.3	Simple and Partial Correlation and Linear Regression	125

		Page
CHAPTER 5	THE RADIO LINK: EXPERIMENTAL INVESTIGATION	128
5.1	Long-Term Effects of the Atmosphere Upon the Received Signal	129
	5.1.1 Monthly and 10-Day Median Received Signal Levels	129
	5.1.2 Diurnal Variation of the Received Signal Level	133
	5.1.3 Effects of Frontal Activity Upon the Received Signal Level	137
5.2	Short-Term Effects: Fast Fading	140
	5.2.1 Types of Fast Fading	140
	5.2.2 Influence of the Surface Wind Upon the Fading Spectrum: A Qualitative Investigation	143
	5.2.3 The Effect of the Surface Wind Upon the Different Spectral Components of the Fading Spectrum	148
	5.2.4 Influence of the Surface Wind Upon the Spectrum of the Two Types of Fading	151
5.3	Influence of the Static Stability Upon the Fading Spectrum	154
5.4	Influence of the Surface Wind Upon the Spectrum of the "α-type" of Fading: A Quantitative Investigation	160
	5.4.1 Influence of U_n Upon Different Ranges of the "α-type" of Fading Spectrum	161
	5.4.2 An Empirical Relationship Between U_n and the Power Spectral Density Function of the "α-type" of Fading	163
	5.4.3 Discussion	173
5.5	The Effect of Static Stability Upon the Power Spectrum of the "β-type" of Fading	175

			Page
	5.5.1	Experimental Investigation	176
	5.5.2	Discussion	193
CHAPTER 6	SIMULATION IN THE LABORATORY: THE AIMS AND REALIZATION		199
6.1	Introduction		199
6.2	Previous Work		202
6.3	Aims of the Laboratory Simulation and Advantages of the Adopted Method		205
6.4	Description of the Model		206
	6.4.1	The Propagation Path - the Transmitter, the Receiver	208
	6.4.2	The Wind Tunnel: Dynamic Similarity, Description	217
	6.4.3	The Schlieren Interferometer	226
6.5	Methods of Determining the Temperature and Velocity Profiles: Instruments, Calibrations		230
6.6	Data Recording and Processing		234
CHAPTER 7	SIMULATION IN THE LABORATORY: EXPERIMENTAL INVESTIGATION		236
7.1	The Propagation Medium		237
	7.1.1	Temperature and Refractive Index Profiles	238
	7.1.2	The Refractivity Field as Revealed by the Schlieren Interferometer	246
	7.1.3	Study of the Velocity Field in the Model Propagation Medium	251
7.2	Qualitative Simulation of the Two Types of Fading		260
	7.2.1	Experimental Results	261

		Page
	7.2.2 Discussion	264
7.3	Simulation of the Effect of the Surface Wind Upon the Fading Power Spectrum	268
	7.3.1 Experimental Results	269
	7.3.2 Discussion	279
7.4	Investigation of the Effect of Temperature Gradient Upon the Fading Power Spectrum	282
	7.4.1 Experimental Results	282
	7.4.2 Discussion	283
CHAPTER 8	CONCLUSIONS AND SUGGESTIONS FOR FUTURE WORK	289
8.1	Conclusions	289
8.2	Suggestions for Future Work	293
REFERENCES		295
APPENDICES		307

CHAPTER 1
THE PROPAGATION MEDIUM

1.1 The Earth's Atmosphere

The term "atmosphere" is used to define the gaseous envelope which is held to the Earth by gravitational attraction and which, in large measure, rotates with it. The atmosphere extends from the solid or liquid surface of the Earth to an indefinite height, its density asymptotically approaching that of interplanetary space. At heights of the order of 80 km. the atmosphere is barely dense enough to scatter sunlight to a visible degree. At about 30,000 km. a molecule moving as if in a rigid rotation with the Earth cannot be held by gravitational attraction; this height may be considered as an extreme upper limit of the atmosphere.

The atmosphere may be subdivided vertically into a number of "atmospheric shells". Temperature distribution is the most common criterion for denoting the various shells. The "troposphere" (= sphere of changes) is the lowest region of the atmosphere and is characterized by a decrease of temperature with height. Its upper limit is the "tropopause" at an altitude varying from about 16 km. near the equator to about 9 km. near the poles. This altitude exhibits a seasonal variation with a maximum in spring. The tropopause is defined as the lowest level at which the vertical temperature gradient, known as the lapse rate, decreases to $2^{o}C/km$. The atmospheric shell immediately above the tropopause is the "stratosphere" and is nearly isothermal. It extends from the tropopause to an altitude of about 50 km. (stratopause). The

outer shell is the "thermosphere" with a more or less steadily increasing temperature with height.

The distribution of various physico-chemical processes is another criterion for the subdivision of the atmosphere. Thus, the "ozonosphere" lying roughly between 10 and 50 km. is the region with an appreciable ozone concentration which plays an important part in the radiative balance of the atmosphere. The "ionosphere" is the region in which ionization of one or more of the atmospheric constituents is significant; it is subdivided basically into three layers with a fourth one occasionally present at 65 - 80 km. Due to its reflecting properties for a range of h.f. radio-frequencies, the ionosphere has been the subject of a thorough investigation as a propagation medium for long-range communications. According to the physico-chemical classification, the troposphere is the "neutrosphere" in which the atmospheric constituents are for the most part non-ionized.

Among the above-mentioned atmospheric shells the most important for Meteorology is the troposphere. It is in the troposphere that the weather phenomena occur and the atmospheric turbulence is most marked. The troposphere consists of "dry air" and water vapour. Dry air consists of N_2 (78%), O_2 (21%) and the rest is inert gases, CO_2, O_3, etc. Water vapour comprises up to 4% p.v. of the atmosphere near the surface but it is almost absent above the tropopause. To the above constituents, dust and pollutants must be added.

The troposphere itself can be subdivided into

different shells or layers. The first distinction is between "free atmosphere" and the "boundary layer". In the latter, significant amounts of heat, momentum and trace substances (water vapour, dust, etc.) are transported vertically by small-scale eddies. The upper region of the boundary layer may be ill-defined locally and its altitude is variable but usually below the 750 mb. isobaric surface (∿ 2500 m.). At the lower region of the boundary layer is the "surface layer" which extends from just above the Earth's surface up to a height of a few decametres, increasing in depth with increasing roughness of the Earth's surface. Below the surface layer is the "interfacial layer" containing the roughness elements of the Earth's surface. Very little is known about the processes at work in this very shallow layer. These processes are, nevertheless, very important because they prescribe the surface values of the eddy fluxes of momentum, heat and water vapour.

In the "free atmosphere", small-scale processes are less frequent than in the boundary layer. They occur only inside the convective clouds and the regions of large vertical wind shear in which they may be very strong. Between the free atmosphere and the boundary, there is generally a stable layer preventing the penetration of boundary layer turbulence into the free atmosphere. Only under wet-unstable conditions, moist convective elements rise through the stable layer and penetrate into the free atmosphere in the form of convective clouds.

1.2 Spatial and Temporal Scales of Atmospheric Processes

The whole range of activity occurring in the atmosphere, from the general (zonal) circulation down to the "microscales" of dissipation, can be characterized as atmospheric "processes". The sole source of energy supplied to the atmosphere is the sun[1,2]. This energy is received as radiation through interplanetary space. Other energy received by the surface of the Earth, such as that from the hot interior or radiated from celestial bodies other than the sun, is in such small amounts that it can be neglected. The power that the sun transmits to the Earth is equal to 1.8×10^{14} kw but about 40% of that is immediately reflected back to space[2]. Only a small fraction of this energy is converted into kinetic energy. The three ways of heat transfer are conduction, convection and radiation. As the atmospheric air is a very poor conductor, most of the heat transfer in the atmosphere is done by convection. Radiation is responsible only for the heat transfer between the Earth and its celestial environment. As a result of the zonal convective currents and the pressure-equalizing motions, a "stirring" of the atmosphere causes spatial and temporal fluctuations of the various meteorological quantities. The scale sizes of these fluctuations range from 10^{7}m. to 10^{-3}m. and their periods range from one year to fractions of a second[2]. Fluctuations with periods less than a year can be classified as follows:-

(a) Global fluctuations: their periods range from months to one week. They are of the greatest interest for long-range

weather prediction but they have been studied very little. At these very large scales ($\sim 10^7$m.), climatological statistics have shown that the amplitudes of monthly and seasonal fluctuations vary considerably from year to year for the same month or season[3]. This makes weather predictions based on one year data very unreliable.

(b) Synoptic fluctuations: their periods range from many hours to several days. Diurnal variations and frontal activity fall into this range. Their horizontal dimensions vary between 10^5 and 10^7m. It has been observed that their energy spectrum has a maximum for periods of four days[4]. They produce large horizontal wind velocity fluctuations, whereas they do not contribute much to vertical fluctuations and vertical mixing. In the small scale part of their spectrum there is a cascade energy transfer to even smaller scale motions. This transfer is due to the hydrodynamic instability of the quasi-horizontal synoptic motions[2]. Apart from the diurnal variation, the rest of the synoptic fluctuations originate mainly from a slantwise convection process arising from the existence of a horizontal gradient in temperature, a feature very common in regions outside low latitudes.

(c) Mesometeorological fluctuations: their periods range from one minute to a few hours and their scale sizes from 10^5km. down to 1 km. Here, intense fluctuations of atmospheric quantities are rather rare, mainly connected with thunderstorms or gravitational waves of large amplitude[2]. This relaxation of the atmospheric processes appears as a broad minimum in

the energy spectrum of any meteorological parameter as, for instance, horizontal wind velocity[4]. This low and flat minimum has the form of a "spectral gap"[3,4,5] and, in fact, separates the macro- from the micro-meteorological range. The lowest part of this gap corresponds roughly to periods of 20 minutes[2,4] or, according to others, 1 hour[3] depending on the altitude at which the atmospheric variable has been measured. Nevertheless, there is a general agreement about the scale-size of the corresponding fluctuations which is of the order of 10 km. This is the depth of the effective thickness of the atmosphere, as 80% of the atmospheric mass is contained in the lowest 10 km. layer[2]. Apparently, at this scale, three-dimensional fluctuations cease to exist, whereas two-dimensional fluctuations (quasi-horizontal) start developing a larger scale.

(d) Micrometeorological fluctuations: they have periods ranging from a fraction of a second to a few minutes. Their scale sizes vary from some hundreds of meters to the "micro-scales" of turbulent dissipation of the order of 1 mm.[2,3,6]. They are produced by mechanical and/or convective turbulence and they strongly depend on such factors as the roughness of the underlying terrain, the velocity of the mean motion, the height above the ground, the thermal stability of the atmosphere, etc. Small-scale eddying motions are a common feature of the boundary layer and they are generally more intense over land than over sea. Their linear dimensions are less than, or comparable to, their altitude above the Earth's surface.

1.3 The Well Mixed Atmosphere-Vertical Distribution of Refractive Index

The concept of a well mixed atmosphere has been introduced as an approximation of an idealized atmosphere[7.8]. Such an atmosphere would be the result of thorough mixing by mechanical and convective turbulence and molecular diffusion. Thus, a state of mechanical equilibrium between gravitational and buoyant forces would be achieved. A well mixed atmosphere can be considered homogeneous enough to allow the variation of the refractive index with height to be estimated.

It can be shown[7,9] that the variation of temperature, pressure and the partial pressure of the water vapour with altitude are respectively:-

$$T = T_o - \frac{g}{c_p} \cdot h \qquad (1.3.1)$$

where T_o is the temperature at a reference altitude, g the acceleration of gravity, c_p the specific heat at constant pressure and h the altitude.

$$p = p_o \left(1 - \frac{g}{c_p T_o} \cdot h \right)^{m_o c_p / R} \qquad (1.3.2)$$

where m_o is the molecular weight of dry air and R the universal gas constant.

$$e = \frac{m_o . a}{m_o'(1-a) + m_o . a} \cdot p \qquad (1.3.3)$$

where m_o, m_o' are the molecular weights of dry air and water respectively and a is the specific humidity.

Another quantity of special interest is the potential temperature defined as the temperature that an air parcel would assume if brought adiabatically from a certain altitude (and pressure) to a reference altitude (pressure). The potential temperature θ is given by[9]:-

$$\theta = T\left(\frac{p_o}{p}\right)^{(\gamma-1)/\gamma} = T\left(\frac{p_o}{p}\right)^{0.286} \qquad (1.3.4)$$

where T is the absolute temperature of the air parcel and $\gamma = c_p/c_v$ is the Poisson's constant. The gradient of potential temperature can be expressed in terms of the gradient of absolute temperature and the adiabatic lapse rate. Differentiating (1.3.4) in its logarithmic form yields:-

$$\frac{1}{\theta}\frac{d\theta}{dz} = \frac{1}{T}\frac{dT}{dz} - \left(\frac{\gamma-1}{\gamma}\right)\frac{1}{p}\frac{dp}{dz} \qquad (1.3.5)$$

but in accordance with the adiabatic equation:-

$$\left(\frac{\gamma-1}{\gamma}\right)\frac{dp}{p} = \left(\frac{dT}{T}\right)_{\text{adiabatic}} = \Gamma = -9.8^{o}C/km \qquad (1.3.6)$$

by means of (1.3.6), (1.3.5) becomes:-

$$\frac{1}{\theta}\frac{d\theta}{dz} = \frac{1}{T}\left(\frac{dT}{dz} - \Gamma\right) \qquad (1.3.7)$$

The quantity $\frac{g}{\theta}\frac{d\theta}{dz}$ is defined as the "static stability" of the atmosphere.

If the gradient of temperature in the atmosphere is more negative than the adiabatic lapse rate Γ, i.e. $\frac{g}{\theta}\frac{d\theta}{dz} < 0$, then a parcel of air displaced upwards adiabatically will always possess a temperature higher than that of the environment and it will continue rising. This is a situation of atmospheric "instability". On the contrary, if $\frac{g}{\theta}\frac{d\theta}{dz} > 0$, the same parcel of air would sink back to the level where its temperature is equal to the environmental temperature. Then the atmosphere is considered as thermally "stable". The condition $\frac{g}{\theta}\frac{d\theta}{dz} = 0$, i.e. $\frac{dT}{dz} = \Gamma$, corresponds to a thermally "neutral" atmosphere.

The refractive index of the atmospheric air is a function of temperature, pressure and partial pressure of water vapour[7,8,9]:-

$$n = 1 + \frac{1}{2}\left\{\frac{k_1}{T}(p-e) + \frac{k_2}{T} \cdot e\right\} \qquad (1.3.8)$$

The coefficients k_1 and k_2 have been experimentally evaluated[10,11] and the following values have been adopted:-

$$k_1 = 158.10^{-9}\ {}^{o}K/mb \quad , \quad k_2 = 136.10^{-9}\left[\frac{T+5,582}{T}\right]{}^{o}K/mb$$

Substitution of these values in (1.3.8) gives:-

$$(n-1) \cdot 10^6 = \frac{77.6}{T}\left[p + \frac{4810}{T} \cdot e\right] \qquad (1.3.9)$$

At this stage, a new quantity known as "coindex of refraction"[12] or "refractivity"[8] can be defined:-

$$N = (n-1).10^6 \quad \text{(N-units)} \tag{1.3.10}$$

From the above-mentioned properties of the "well-mixed" atmospheric air, it is apparent that the refractive index is a function of height. C.C.I.R.[13] has adopted the following expression for this variation:-

$$(n-1).10^6 = N = 289.e^{-0.136h} \quad \text{(h in km.)} \tag{1.3.11}$$

Differentiation with respect to height of the above expression gives the gradient of the coindex of refraction in a "well-mixed" atmosphere:-

$$\frac{dN}{dh} = -39.3.e^{-0.136.h} \quad \text{(N-units/km.)} \tag{1.3.12}$$

For low altitudes, up to 3 km., the decrease of the refractive index with altitude may be considered as linear with a constant gradient given by[7,12]:-

$$\frac{dN}{dh} = -40 \quad \text{(N-units/km.)} \tag{1.3.13}$$

In the real atmosphere, depending on weather conditions and geographical location, the refractive index gradient may vary between -20 and -80 N-units/km.[12].

1.4 The Turbulent Atmosphere

By the end of the last century, it was recognised that the flow of fluids may occur in either laminar or turbulent regimes and that the two of them are vastly different qualitatively and quantitatively. Early in this century, interest developed in the properties of atmospheric turbulence (for recollections see[14]). Up to now, the majority of these studies have examined turbulence in the atmospheric boundary layer as it can be studied with ground based instruments and it is almost ever present because of the thermal and mechanical conditions created by the surface.

1.4.1 The Nature of Atmospheric Turbulence - Significance of Atmospheric Stability

Whilst turbulence can be easily recognized if the properties of the flow are made visually apparent, it is very difficult to develop a satisfactory definition of the phenomenon. Lumley and Panofsky[15] have taken the approach of listing some of the essential features of turbulence rather than attempt a definition. Thus, turbulence is a mode of fluid motion that is three-dimensional, rotational, dissipative, non-linear, stochastic and diffusive with the transport occurring at time and length scales typically the same as those of the properties being transported.

The main causes for flow becoming turbulent in the atmosphere are spatial differences in the large scale temperature and wind velocity fields that arise for various reasons. Atmospheric processes responsible for these

differences are:-

(a) Frictional retardation of flow at the Earth's surface and, consequently, the formation of large vertical gradients of the wind velocity in the boundary layer.

(b) Development of thermal convection due to non-uniform heating of the Earth's surface.

(c) Cloud generation processes releasing latent heat by condensation or ice formation which changes the character of temperature and wind velocity fields.

(d) Interaction of air masses with different characteristics to form large horizontal and vertical differences in temperature and wind velocity fields near atmospheric fronts.

(e) Unstable growth of waves formed in inversion layers and near other atmospheric interfaces as, for instance, thermal caps.

(f) Deformation of the air flow by terrain irregularities.

These processes may act simultaneously, weakening or enhancing each other and thus creating turbulence of varying intensity.

A well-known factor determining the onset of mechanical turbulence in an originally laminar flow is the Reynolds number:-

$$Re = \frac{\upsilon . L}{\nu} \qquad (1.4.1a)$$

where υ is the flow velocity, L the characteristic dimension of the flow and ν the kinematic viscosity. For a critical value $Re = Re_{cr}$ inertial forces represented by the numerator

of (1.4.1a) overcome the viscous forces and tend to bring together volumes of fluid that are initially remote and possess different velocities thus creating an instability in the velocity field. Experiments in wind tunnels suggest values for Re_{cr} from 1500 to 5000, definitely no turbulence can occur at Re < 1160[16]. In the atmosphere most of the processes take place at high Re. For a breeze, motion of air in a monsoon and the general circulation of the atmosphere (zonal) the Re are respectively[16]:-

$$Re_1 = 1.10^8 \quad , \quad Re_2 = 4.10^{11} \quad , \quad Re_3 = 8.10^{12}$$

Obviously, atmospheric motions are expected to be always turbulent if Re is considered as the only criterion for the onset of turbulence. But Re does not account for turbulence due to convective motions, or for the effects of thermal stratification, thus it is a rather inadequate criterion for turbulence other than mechanical.

Richardson[17] considered the problem theoretically and developed criteria for the growth and decay of energy in turbulent motions in a thermally stratified medium. He assumed that the loss of turbulent kinetic energy is mainly due to work done against the buoyancy forces created by gravity in a vertically stable stratification. Thus he obtained his criterion for atmospheric turbulence from the equation for the turbulent energy balance:-

$$\frac{dE'}{dt} = K_M\left(\frac{d\bar{u}}{dz}\right)^2 - K_T \frac{g}{\theta}\frac{d\theta}{dz} - \varepsilon - D \qquad (1.4.1b)$$

where E´ is the turbulent kinetic energy, $\frac{d\bar{u}}{dz}$ is the mean velocity vertical gradient, θ is the potential temperature, K_M the eddy viscosity, K_T the thermal eddy diffusivity, ε the rate of dissipation into heat and D the rate of diffusion of turbulent energy. The first and second terms in the right side of (1.4.1b) represent respectively the rate of transfer of kinetic energy from the mean to the turbulent motion and the rate of conversion of turbulent kinetic energy into heat by eddy processes. If molecular effects, represented by ε and D are neglected, (1.4.1b) becomes:-

$$\frac{dE'}{dt} = K_M\left(\frac{d\bar{u}}{dz}\right)^2 - K_T\left(\frac{g}{\theta}\,\frac{d\theta}{dz}\right) \qquad (1.4.1c)$$

the ratio: $$Ri = \frac{g}{\theta}\,\frac{\frac{d\theta}{dz}}{\left(\frac{d\bar{u}}{dz}\right)^2} \qquad (1.4.1d)$$

is called the Richardson number and can be interpreted as the ratio of buoyancy forces to inertial forces.

The quantity: $$Rf = \frac{K_T}{K_M} \cdot Ri \qquad (1.4.1e)$$

is called the flux Richardson number[18] and compares the effect of thermal convection in generating turbulence to that of the mechanical forces creating turbulent kin. energy from the mean motion.

From (1.4.1c) and (1.4.1e) it follows that:-

$$\frac{dE'}{dt} = K_M\left(\frac{d\bar{u}}{dz}\right)^2 \left[1 - Rf\right] \qquad (1.4.1f)$$

therefore, if Rf = 1, the turbulent energy is constant as $\frac{dE'}{dt} = 0$. The significance of Ri becomes apparent from (1.4.4). Whenever $\frac{d\theta}{dz} > 0$ (stable thermal stratification) the rate of turbulent kin. energy production decreases, as the buoyancy forces oppose the mechanical development of turbulence. For $\frac{d\theta}{dz} < 0$ (unstable thermal stratification) the buoyancy forces promote the excitation and development of turbulence and convective turbulence is added to the mechanical one. Thermal instability is particularly important in the clouds and in the atmospheric boundary layer. Superadiabatic lapse rates are very common from the Earth's surface up to 500 or 1000 m. on cloudless days with strong differential heating of the ground. For values $\frac{d\theta}{dz}$ close to zero (neutral stratification) buoyancy has no effect on turbulence.

Generally, onset of turbulence may be expected in a thermally non-uniform atmosphere only when $Ri < Ri_{cr}$ where Ri_{cr} is a critical value smaller than $\frac{K_M}{K_T}$ as follows from (1.4.1f). Laboratory investigations[19] and measurements in the surface layer of the atmosphere[20] have shown that $\frac{K_M}{K_T}$ depends significantly on the thermal stratification and wind shear. Under convective conditions $\frac{K_M}{K_T} > 1$; whereas, for cases of stable stratification a < 1. Proudman[21] presented evidence that $\frac{K_M}{K_T} = 0.03$ to 0.05 for $4 < Ri < 10$, which means that turbulence may appear even for large values of Ri.

It was previously assumed that turbulent diffusion

due to spatial gradients of the turbulent kinetic energy are negligible (D = O). Nevertheless, such gradients occur quite often in the atmosphere either in the vertical (inversions, jets, thermal caps) or in the horizontal direction (variable terrain roughness, organized convective elements).

The value of the rate of the diffusive transfer D depends on the eddy viscosity K_M and the spatial gradient of turbulent energy $\frac{dE'}{dr}$. Therefore:-

$$D = K_M^{\,a} \left(\frac{dE'}{dr}\right)^b \qquad (1.4.1g)$$

The dimensions of the quantities involved are:-

$$D = \left[L^2, T^{-3}\right] \quad , \quad K_M = \left[L^2, T^{-1}\right] \quad , \quad \left(\frac{dE'}{dr}\right) = \left[L^1, T^{-2}\right]$$

and by applying dimensional analysis:-

$$a = \frac{1}{3} \quad , \quad b = \frac{3}{4}$$

Thus:-

$$D = K_M^{\,1/3} \left(\frac{dE'}{dr}\right)^{3/4} \qquad (1.4.1h)$$

Neglecting molecular dissipation ($\varepsilon = O$) and combining (1.4.1b) and (1.4.1h) gives:-

$$Ri_{cr} = \frac{K_M}{K_T} \{1 - K_M^{1/3} \left(\frac{dE'}{dr}\right)^{3/4}\} \qquad (1.4.1i)$$

It follows that Ri_{cr} depends not only on $\frac{K_M}{K_T}$ but also on the degree of the spatial non-uniformity of the turbulent field as expressed by $\frac{dE'}{dr}$, which in turn depends on the spatial agitation of the flow.

It becomes apparent that Ri_{cr} cannot be constant for non-uniform turbulence. Nevertheless, the condition $Ri < Ri_{cr}$ is a qualitative indication that turbulence is being created.

1.4.2 Convection and Thermal Turbulence in the Atmosphere

It has long been known from observations of soaring birds[22,23] and from the experience of glider pilots[24] that convection is one of the most common forms of atmospheric motion. A consequence of the development of atmospheric convection is the so-called thermal turbulence.

The energy of convection is a result of the heating of the Earth's surface due to solar radiation. In cases where condensation of water vapour occurs the necessary energy is provided by the latent heat released during this process.

There are two different kinds of atmospheric convection, the random or "disordered" and the organized or "ordered" one. Convective elements belonging to the first category are thermal "bubbles" and "plumes", jet-like currents and turbulent eddies of convective origin. The second category includes various forms of cellular circulation

in which the flow is regularly subdivided into circulation cells. These cells may be closed in analogy to Bénard cells developing in a fluid heated from below. Sometimes they exist in the form of parallel bands of ascending and descending currents.

A. Disordered Atmospheric Convection

Depending on the dynamic and thermal conditions of the atmosphere and the nature of the underlying terrain, the elements of disordered convection may be formed either as bubbles or as jets. The hypothesis that the convective elements are isolated masses of air warmer than the environment was put forward by Scorer and Ludlam[25] and developed by Malkus and Scorer[26], Priestley[27], Scorer and Ronne[28] and others.

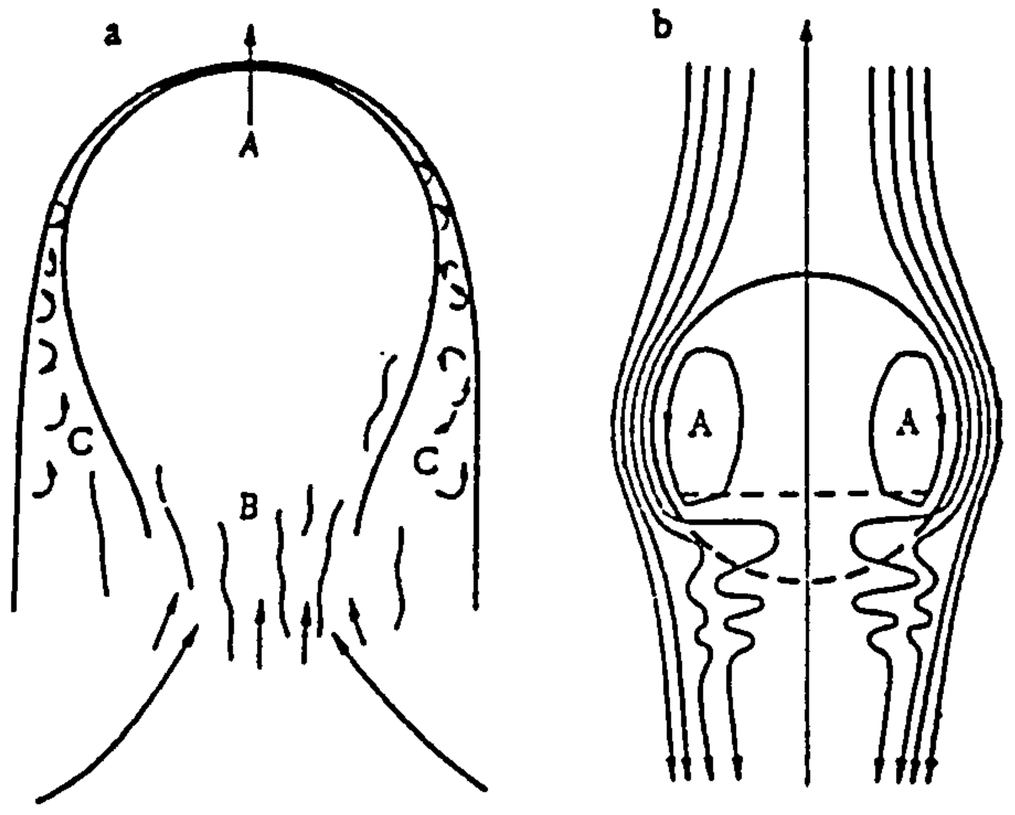

Fig. 1.1. The structure of a bubble. a) schematic of a bubble: (A) heated mass of air, (B) wake, (C) erosion layer; b) flow lines in an ascending bubble: (A) annular eddy.

(After Levine[30])

In their treatment, they considered that the upper part of a bubble, or "thermal cap", has a hemispheric shape whereas the lower part or "wake" is a trail of relatively colder air (see Fig. 1.1). During its ascent, a bubble is eroded and washed into its wake. It was also pointed out that small bubbles aggregate to form larger ones. The

ascent of a bubble depends on the stability of the surrounding air and it continues as long as the bubble possesses an excess of heat. As soon as it reaches a stable layer of air it may overshoot it due to the velocity it has already acquired and then describe damped oscillations about this level. In[27] a detailed investigation of the ascent of a thermal is given. Fig. 1.2 shows the growth and ascent of a thermal in the presence of a light wind. The origin of the freely floating thermals is not necessarily the ground; they may originate from an unstable layer near the ground, usually above a stably stratified layer or an inversion.

The theory of convective jets was put forward by Batchelor[29] and Priestley[18,27]. The base of jets can be either attached to the underlying ground or move freely along

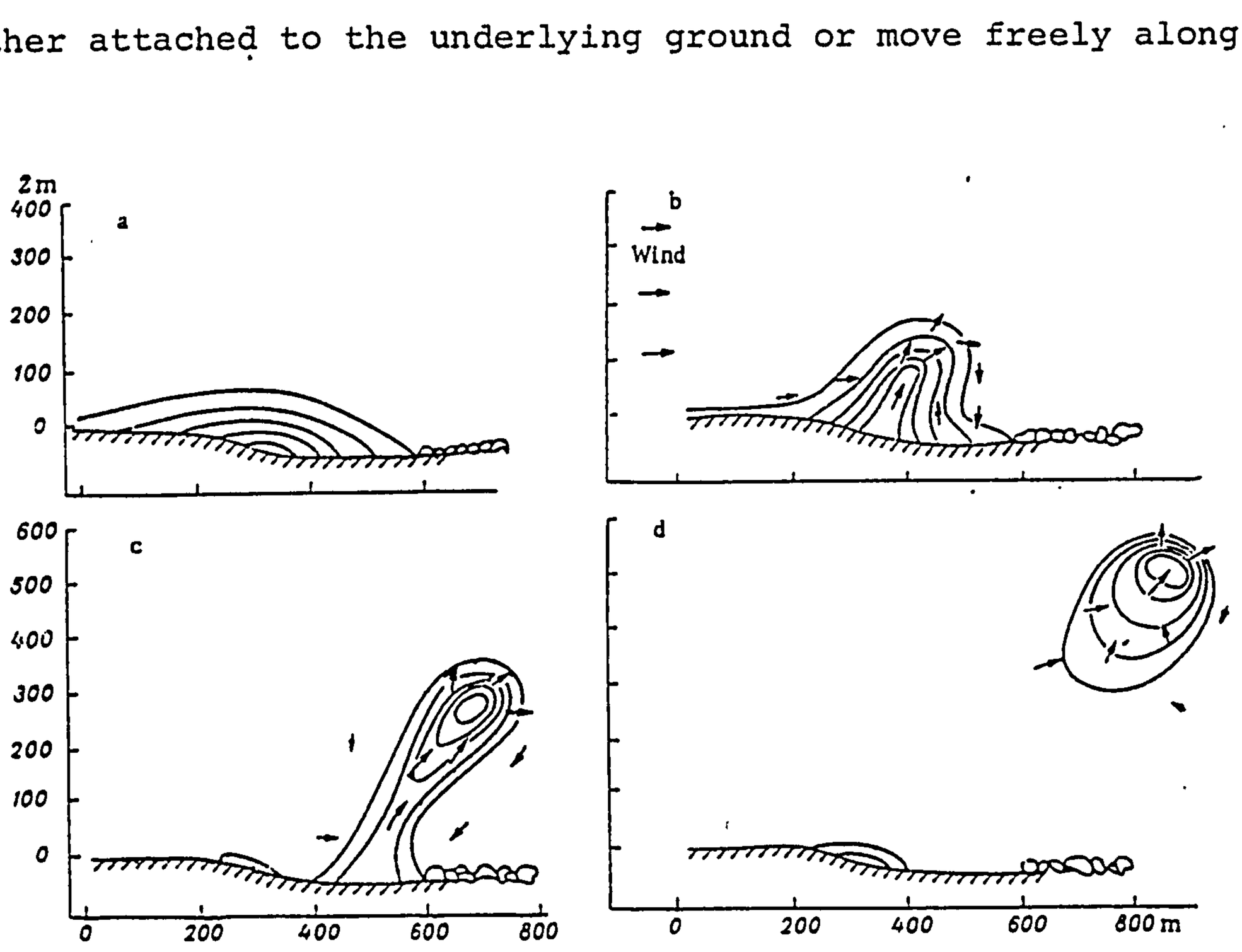

Fig. 1.2. Growth and ascent of a thermal in a light wind. (after Woodward[31]).

the wind. As the surface wind increases a convective jet may be detached from the ground and form a thermal bubble. The vacant surface area becomes the source of another jet after some time and another cycle of evolution starts. This illustrates that in the presence of a strong surface wind the convective elements finally acquire a shape of a bubble even if they have started as jets.

Disordered convection and thermal turbulence have been studied in the real atmosphere as well as in the laboratory. In the atmosphere, the methods of study vary from observations of birds and insects[22,23], flights of gliders[24,32] and aircraft[33] to Radar observations[34,35,36,37] and Acoustic soundings[38,39,40,37,41]. Quantitative information about the structure of the thermals have been provided up to now by aircraft flights equipped with fast-response, high-sensitivity instruments[33]. Radar observations give only qualitative results but, also, valuable visual supervision of the phenomenon. Acoustic soundings seem to provide both visual and quantitative information as it has been reported in[41].

Observational data shows that disordered convection and thermal turbulence obey a very pronounced daily variation. Overland observations show a maximum intensity in the hours around mid-day. In cases when thermals do not originate from the Earth's surface but from an unstable layer above the ground, they have always the shape of bubbles and not jets. Measurments determining the structure of disordered convective elements have been taken either above the surface layer and

under the base of cumulus clouds, or during horizontal aircraft flights[33]. Vulfson[33] has made detailed measurements of the mean dimensions and of the temperature excess at the centre of thermals at various altitudes. Some of his results are summarized in Table 1.1.

TABLE 1.1

Altitude m	Mean Dimensions (m.)		Mean Temperature Excess	
	Jets	Bubbles	Jets	Bubbles
10	42	31	0.64°C	0.54°C
30	49	37	0.23	0.18
50	55	43	0.23	0.19
100	61	46	0.23	0.18
300	68	58	0.15	0.14
500	70	61	0.12	0.11
1000	72	64	0.12	0.10
2000	74	65	0.10	0.09
3000	81	74	0.19	0.17

It can be seen from the Table that the dimensions of thermals change rapidly in the layer from 10 to 300 m. but they remain practically unchanged from 300 to 2000 m. The same is true for the temperature excess.

There seems to be a discrepancy between the dimensions shown in Table 1.1 and the ones reported by Radar observations [34,35,36] which suggest sizes of the order of 1 km. Observations with Acoustic sounders[38,39,40,41] have pointed towards smaller dimensions of the order of 200 m. more in agreement with aircraft measurements. It seems that convective elements "seen" by Radars are semi-organized cells

rather than bubbles, whereas Acoustic sounders, having a superior performance at low altitudes, can detect disorganized convection more accurately.

B. Ordered Atmospheric Convection

Ordered atmospheric convection belongs to the mesometeorological range of fluctuations and, in fact, consists the small-scale part of it. It is often called "cellular convection" due to the similarity between the convective elements and the Bénard cells developing in a fluid heated from below. As the top of thermal cells is usually a region of water vapour condensation, cumulus clouds mark the presence of such cells in the atmospheric boundary layer. This makes in situ measurements difficult and the basic data on the physical characteristics of ordered convection have been obtained by means of laboratory experiments[28,29,31,42] which have shown that:-

1. for ordered convection to exist in a layer, it is necessary that the vertical temperature gradient exceed some critical value depending mainly on the thickness of the convective layer and the intensity of turbulent diffusion;

2. the shape of the cells, their dimensions and the circulation inside a cell depend on the thickness of the convective layer, the thermal stratification and the wind shear.

Batchelor[29] pointed out that the criterion for the formation of convective cells in a layer is the Rayleigh number Ra defined as:-

$$Ra = \frac{g}{T} \frac{(\Gamma_d - \Gamma) h^4}{K_M . K_T} \qquad (1.4.2a)$$

where Γ_d and Γ are the adiabatic and the ambient lapse rates respectively, h the depth of the convective layer, T the ambient temperature and K_M, K_T the eddy viscosity and eddy thermal diffusivity.

Ordered cellular convection is replaced by thermal turbulence when the lapse rate increases and this situation corresponds to $Ra \simeq 50000$ [29]. If this value is substituted in (1.4.2a) along with the values $T = 280^{o}K$, $h = 300$ m., $K_M \simeq K_T = 1$ m.sec^{-1} [3] which are commonly encountered in the atmosphere, then $\Gamma_d - \Gamma = 0.17.10^{-3}\ ^{o}C.m^{-1}$ or $\Gamma_d - \Gamma = 0.17^{o}C/km.$, a value showing a slightly unstable stratification. Thus, one should expect cellular convection to occur for thermal stratifications from neutral to slightly unstable, whereas for moderately unstable conditions ordered convection must have been already replaced by disordered convection and thermal turbulence. Pellew and Southwell [43] found that for hexagonal Bénard cells the horizontal dimensions are 3.77h whereas, for circular cells, the diameter is 2.16h where h is the height of the cell.

Ordered convection has been studied in the atmosphere by Radars [34,35,44] and all observations agree that the horizontal dimensions of the cells are in the range 1 to 3 km. and that they can persist for 20 to 30 minutes. Hardy and Glover [45] report that when convective cells are drifting through the beam of a vertically pointing radar, they appear on a time-height display as undulating or irregular layers.

There also seems to be a general agreement about the shape of the ordered convective elements usually described as doughnut-shaped with warm air rising in their cores and colder air descending at their peripheries.

1.4.3 Spectral Structure of the Velocity, Temperature and Refractivity Fields in the Turbulent Atmosphere

The conversion of the energy of large scale motions into turbulent kinetic energy is an important feature of the atmospheric energy cycle. Energy flows to smaller and smaller wavelengths and is eventually dissipated by viscous forces into heat.

The quantitative description of this process became possible only after Taylor[46] realised that the velocity of a fluid is a random continuous function of position and time. This permitted the description of turbulence through its spatial autocorrelation function. Also the assumptions of homogeneity and isotropy greatly simplified the analysis. In the same investigation, Taylor proved experimentally that his assumptions were sound. In 1938 the same author[47] described the distribution of kinetic energy over the various wavenumber components of turbulence by means of the Fourier transform of the autocorrelation function. The kinetic energy spectrum of turbulence was described on a dimensional basis by A. N. Kolmogorov in 1941[48]. His treatment was based on the "similarity" hypothesis stating that the small-scale components of turbulence are approximately in statistical equilibrium. Kolmogorov postulated that:-

1. for a whole range of scale-sizes the transfer of

energy from one wavenumber to the other and its final dissipation depends on two parameters only, the kinematic viscosity ν of the fluid and the "energy dissipation rate" ε;

2. for scale sizes much greater than a certain size l_o, known as the "microscale" of turbulence, the transfer of energy is not affected by viscous forces and thus depends only on ε. The range containing these scale sizes is known as the "inertial subrange".

If the distribution of kinetic energy per unit mass with wavenumber is described by a spectral function $E(k)$, then the energy corresponding to a wavenumber k is $kE(k)$ and, according to the similarity hypothesis, depends on ε only. The dimensions of the quantities involved are:-

$$E(k) = \left[L^3, T^{-2}\right] \quad , \quad \varepsilon = \left[L^2, T^{-3}\right] \quad , \quad k = \left[L^{-1}, T^{o}\right]$$

The form in which the spectral function can be expressed is:-

$$E(k) = a.\varepsilon^m.k^n \qquad (1.4.3a)$$

where a is a constant and m, n exponents to be evaluated.

The dimensional equation is:-

$$\left[L^3, T^{-2}\right] = \left[L^2, T^{-3}\right]^m . \left[L^{-1}, T^{o}\right]^n \qquad (1.4.3b)$$

Hence: $m = \frac{2}{3}$, $n = -\frac{5}{3}$

and the spectral function can be written:-

$$E(k) = a.\varepsilon^{2/3}.k^{-5/3} \qquad (1.4.3c)$$

This is the well-known Kolmogorov's "-5/3 law" for the behaviour of the spectrum of turbulence in the inertial subrange.

The scale size at which the dissipation of kinetic energy into heat starts depends on the rate of dissipation ε and the physical properties of the fluid, in this case the kinematic viscosity ν. This dependence may be written:-

$$l_o \sim \varepsilon^a.\nu^b \qquad (1.4.3d)$$

$$\varepsilon = \left[L^2, T^{-3}\right] \quad , \quad \nu = \left[L^2, T^{-1}\right] \quad , \quad l_o = \left[L, T^o\right]$$

and finally:- $a = -\frac{1}{4}$, $b = \frac{3}{4}$

Thus:

$$l_o = \left(\frac{\nu^3}{\varepsilon}\right)^{1/4} \qquad (1.4.3e)$$

It has been found[49] that in the atmosphere l_o is of the order of 1 - 3 mm. Thus for scale sizes much greater than 1 mm., the kinetic energy spectrum must obey the -5/3 power law. In order to express the three-dimensional energy spectrum by means of (1.4.3c), the spatial autocorrelation function of the velocity field must be taken into consideration:-

$$R(\rho) = \int_{-\infty}^{\infty} E(k)\cos(\rho k)\,dk \qquad (1.4.3f)$$

i.e. the Fourier transform of the one-dimensional spectrum of the kinetic energy. It can be shown[49] that the three-dimensional spectrum is related to $R(\rho)$ through the expression:-

$$\phi(\vec{k}) = \frac{1}{2\pi^2 k} \int_{o}^{\infty} \rho.R(\rho)\cos(\rho k)\,d\rho \qquad (1.4.3g)$$

where: $k = |\vec{k}|$

Inversion of (1.4.3f) yields:-

$$E(k) = \frac{1}{\pi} \int_{o}^{\infty} R(\rho)\cos(\rho k)\,d\rho \qquad (1.4.3h)$$

Hence, by differentiation with respect to k:-

$$\frac{dE(k)}{dk} = -\frac{1}{\pi} \int_{o}^{\infty} \rho.R(\rho)\sin(k\rho)\,d\rho \qquad (1.4.3i)$$

Comparison of (1.4.3g) and (1.4.3i) gives:-

$$\phi(\vec{k}) = -\frac{1}{2\pi k}\frac{dE(k)}{dk} \qquad (1.4.3j)$$

Thus, for a one-dimensional spectrum obeying the "-5/3" power law (1.4.3c), the three-dimensional spectrum is:-

$$\phi(\vec{k}) = c^2.\varepsilon^{2/3}.\vec{k}^{-11/3} \qquad (1.4.3k)$$

where c^2 is a constant approximately equal to 0.11[49]. In the case of statistical isotropy of the velocity field, $\phi(\vec{k})$ is independent of direction and it may be written:-

$$\phi(\vec{k}) = \phi(k) = c^2.\varepsilon^{2/3}k^{-11/3} \qquad (49) \qquad (1.4.31)$$

The temporal spectrum of kinetic energy, i.e. the frequency spectrum, in the case when all the temporal variations are associated with a translation motion of constant velocity υ ("frozen field"), is given by[49]:-

$$W(\omega) = \frac{2\pi}{\upsilon}\int_{\omega}^{\infty} k.\phi(k)\,dk \qquad (1.4.3m)$$

Substitution of (1.4.31) into (1.4.3m) gives:-

$$W(\omega) = \frac{2\pi}{\upsilon} \cdot \frac{3}{5} c^2\varepsilon^{2/3}\left[\frac{\omega}{\upsilon}\right]^{-5/3} \qquad (1.4.3n)$$

Thus, the frequency spectrum obeys a "-5/3" power law in the case the velocity field is assumed to be "frozen". The velocity field is not the only turbulent field in the atmosphere. Temperature, humidity and refractive index undergo fluctuations due to turbulence. The fluctuations in temperature are caused by the transportation of eddies possessing a certain temperature to an environment with different temperature. In this way, temperature fluctuations

may develop at any point in a medium having a certain distribution of temperature. Following this argument and assuming that buoyancy does not interact with the velocity field, temperature can be considered as a conservative passive additive. Strictly speaking the temperature is not a passive additive, since deviations of T from a mean value give rise to buoyancy effects. Nevertheless, for very small deviations from the mean these effects may be considered negligible. This can be the case for an almost neutral stratification (Ri ≃ 0).

Tatarski[49] has given a complete description of the problem and the final result for the three-dimensional wavenumber spectrum of temperature fluctuations is:-

$$\phi_T(k) = 0.033\ C_T^2 . k^{-11/3} \qquad (1.4.3o)$$

There is an apparent similarity between (1.4.3e) and (1.4.3o) resulting from the assumption that the temperature fluctuations are solely due to the turbulent velocity field.

In (1.4.3o) the constant C_T^2 is called the temperature structure constant and is given by[49]:-

$$C_T^2 = a^2 . \chi . \varepsilon^{-1/3} \qquad (1.4.3p)$$

where a is a constant approximately equal to 1.34, ε is the kin. energy dissipation rate and χ can be expressed by means of the mean characteristics of the turbulent velocity and temperature fields as[49]:-

$$\varepsilon = K_M \left[\frac{dU}{dz}\right]^2 \quad , \quad \chi = K_T \left[\frac{dT}{dz}\right]^2 \qquad (1.4.3q)$$

where K_M, K_T are the eddy viscosity and eddy thermal diffusivity respectively, $\frac{dU}{dz}$ the mean vertical wind shear and $\frac{dT}{dz}$ the vertical temperature gradient. Thus (1.4.3p) can be written as:-

$$C_T^2 = a^2 \frac{K_T}{K_M 1/3} \left(\frac{dT}{dz}\right)^2 . \left(\frac{dU}{dz}\right)^{-2/3} \qquad (1.4.3r)$$

As a microscale of turbulence has been defined for the velocity field, similarly a temperature "microscale" can be defined as:-

$$l_T = \left(\frac{n^3}{\varepsilon}\right)^{1/4} \qquad (1.4.3s)$$

where n is the thermal diffusivity. In the atmosphere $\frac{n}{\nu}$ (Prandtl's number) is of the order of 0.75 and it follows from (1.4.3e) and (1.4.3s) that: $lo = 0.8 l_T$. Thus, dissipation in the atmosphere occurs at the same scale sizes for the velocity and temperature fields.

The frequency spectrum of temperature fluctuations is analogous to (1.4.3n) and obeys a "-5/3" power law:-

$$W_T(\omega) = 0.124 . \upsilon^{2/3} . C_T^2 . \omega^{-5/3} \qquad (1.4.3t)$$

The refractive index of atmospheric air for microwave frequencies is given by (1.3.9). The quantities T and e in

this expression are not strictly conservative. Nevertheless, it is possible to introduce instead of T and e the potential temperature θ and the specific humidity q in (1.3.9) which are both conservative additives as by definition they do not change during vertical displacements (provided that condensation of water vapour does not occur). The new expression for the coindex of refraction becomes[49] :-

$$N = \frac{77.6.p}{\theta - \gamma_d.z}\left(1 + \frac{7800}{\theta - \gamma_d.z}.q\right) \qquad (1.4.3u)$$

where z is the altitude and γ_d the adiabatic lapse rate.

Thus, N depends on the altitude z explicitly and also implicitly through the functions:-

p(z), θ(z) and q(z) and it can be written:-

$N = N(z, p(z), \theta(z), q(z))$

Thus, an air volume which is at an altitude z_1, has a coindex of refraction:-

$N_1 = N(z_1, p(z_1), \theta(z_1), q(z_1))$

If this volume is transported to an altitude z_2, the quantities θ and q do not change as they are conservative additives. The new N of the volume becomes:-

$N_1' = N(z_2, p(z_2), \theta(z_2), q(z_2))$

whereas the N of the new environment is:-

$$N_2 = N(z_2,\ p(z_2),\ \theta(z_2),\ q(z_2))$$

The difference in coindex of refraction between the transported volume and its environment is:-

$$\Delta N = N_1' - N_2 = \left(\frac{dN}{d\theta}\frac{d\theta}{dz} + \frac{dN}{dq}\frac{dq}{dz}\right)\Delta z \qquad (1.4.3v)$$

as z and p(z) are the same for the volume and its environment. In this case, the fluctuations in N are proportional to a quantity M which from (1.4.3u) and (1.4.3v) is[49,50]:-

$$M = -\frac{77.6}{T^2} \cdot 10^{-6}.p\left(1 + \frac{15600}{T}.q\right)\left(\frac{d\theta}{dz} - \frac{7800}{1+\frac{15600}{T}q} \cdot \frac{dq}{dz}\right) \qquad (1.4.3w)$$

The expression for the three-dimensional spectrum of the refractive index is given in[49] as:-

$$\phi_n(k) = 0.033\ C_n^2 \cdot k^{-11/3} \exp\left(-\frac{k^2}{k_m^2}\right) \qquad (1.4.3x)$$

where C_n^2 is the structure constant of the ref. index. The quantity k_m is related to the microscale of turbulence through the expression: $k_m = 5.92/l_o$[49]. Thus, for scale sizes of the order of 1 cm. and larger (1.4.3x) can be written:-

$$\phi_n(k) = 0.033\ C_n^2.k^{-11/3} \qquad (1.4.3y)$$

For optical wavelengths, the refractive index is independent of humidity and (1.4.3u) becomes:-

$$N = \frac{77.6}{T}.p \qquad (1.4.3z)$$

The fluctuations in N are related to the fluctuations in T by:-

$$\Delta N = - \frac{77.6}{T^2} \, p \, . \, \Delta T \qquad (1.4.3\gamma)$$

and the corresponding structure constants are related by the expression[49]:-

$$C_n^{\,2} = \left(\frac{77.6}{T^2} \, . \, 10^{-6}.p\right) \, . \, C_T^{\,2} \qquad (1.4.3\delta)$$

A lot of experimental work has been dedicated to the verification of the expressions (1.4.31), (1.4.3o) and (1.4.3y) or the corresponding expressions for the one-dimensional spectra which obey a "-5/3" power law. Considerable agreement has been found between experimental results and theory for the velocity field. Thus, Tsrang[51] using a mast 300 m. high, carried out measurements of horizontal and vertical wind components and temperature and found that the corresponding fluctuation spectra obeyed the "-5/3" power law. Burns[52] reported that the vertical wind component measured during aircraft flights at low altitudes has a fluctuation spectrum which in average obeys a "-5/3" law for a large range of scale sizes (15 - 2000 m.). Koprov[53] using the same

method found that spectra of the vertical wind component obeyed the "-5/3" law for altitudes up to 1000 m., whereas for greater altitudes and a stable stratification, the exponent was found to be greater than -5/3. Pinus and Shcherbakova[54] have found that for scale sizes from several hundreds of metres to some tens of metres and for neutral thermal stratification the spectra of the horizontal wind components obey the "-5/3" power law; for stable stratification, the spectra decreases more steeply than -5/3. Myrup's results[55] from aircraft flights show that as the atmosphere becomes unstable during the morning hours (around 08.00), the exponent of the inverse power law describing the spectrum of wind fluctuations undergoes a transition from greater values to the usual 5/3. Vinnichenko and Dutton[56] found that a -5/3 exponent prevails in the spectra of the horizontal wind components for sizes up to the synoptic scales.

Similar results have been obtained for spectra of temperature fluctuations. Gossard[57] making use of a captive balloon found that temperature spectra obeyed the "-5/3" law in an unstable layer with a large temperature gradient. Tsrang[58] found similar results from airborne and tower measurements of temperature spectra in the atmospheric boundary layer. Panofsky[59] from measurements at altitudes between 16 and 91 m. verified the "-5/3" law for spectra of temperature fluctuations. In[56] it was shown that although individual temperature spectra did not always agree with the "-5/3" law, their averaged values were well represented by this dependence.

Absolute humidity spectra measured by the captive balloon[57] and by optical methods[60] exhibit the same behaviour for scale sizes from 60 - 6 m.[57] and 100 - 4 m.[60].

Spectra of refractive index fluctuations have been measured in[57,61,62] and they were found to be in good agreement with the "-5/3" law especially for conditions of thermal instability.

1.4.4 The Effect of Buoyancy on the Spectrum of Atmospheric Turbulence

Although the validity of the similarity theory for the inertial subrange has found strong experimental support, it must be pointed out that a number of experimental investigations has shown significant deviations from the "-5/3" power law. Most of these deviations occur under conditions of thermal stability of the atmospheric layer under investigation. Quite often the deviations occur along with the "-5/3" law but for a different wavenumber range. In[57] spectra of atmospheric scalars were found to obey a law of the type $E_{\psi}(k) \sim k^{-n}$ where $5/3 < n < 7/3$. Shur[63] observed a transition in the exponent n from -3 to -5/3 as the environment was changing from stable to unstable. The transition was occurring at scale sizes of approximately 600 m. Lane in[61] reports that the exponents of refractive index spectra in the morning (stable stratification) varied in the range 1.64 - 2.55, whereas at around 13.00 hours (unstable conditions) the range of variation was shifted towards lower values (1.12 - 2.22). In[55] longitudinal velocity spectra taken in the early morning showed a

transition in the value of the exponent from -3 to -5/3. The transition was occurring for scale sizes $\gtrsim$ 70 m. As later in the day the stratification changed from stable to neutral and unstable, the spectral exponents acquired the familiar -5/3 value. In[64], Plate and Arya report that longitudinal and vertical velocity spectra measured in a wind tunnel obeyed a "-1" power law for a stably stratified boundary layer. Fichtl and Camp[65] measured temperature spectra by a rawisonde in the scale size range 50 - 2000 m. Their measurements suggest a spectral function with exponents changing from -3 to -1 for increasing wavenumber. In[66] measurements of temperature spectra obtained by a tethered balloon show that in the frequency range 0.2 to 2.0 Hz the exponent of the spectral function was varying in the range -0.6 to -3.5. The larger values were associated with stable conditions and intense temperature fluctuations, whereas exponents in the vicinity of -5/3 were likely to occur under any conditions.

The first attempt to explain theoretically the effect of buoyancy and, consequently stability, upon the spectral characteristics of atmospheric turbulence was made by Bolgiano[67,68]. He suggested that in a range of scale sizes (wavenumbers) the shape of the spectrum is determined only by the rate of production and dissipation of the mean-square fluctuations of the specific buoyancy forces. This range of wavenumbers was given the name " buoyant subrange " and may be considered as an extension of the inertial subrange. The effect of stratification in the buoyant subrange is that

it extracts kinetic energy from the turbulent motion transforming it into potential energy. The extraction of energy occurs over a whole range of scale sizes. A consequence of this is that the rate of inertial transfer of turbulent energy across the spectrum is reduced for increasing wavenumbers. Finally, the viscous dissipation rate ε may become much smaller than the rate at which turbulent energy is generated by the mean motion. The motions that, by working against buoyancy, convert kinetic energy into potential energy also generate deviations in density (temperature) from its mean distribution. Thus, mean-square temperature fluctuations are produced at a given rate and they break up into smaller scale components which are ultimately diffused into heat by molecular motion. In this way the kinetic energy that may have been converted into potential energy has the same fate as that which has been inertially transferred and dissipated by viscosity.

By assuming that for the buoyancy subrange the viscous dissipation rate $\varepsilon << \chi$ (rate of production of mean-square temperature fluctuations) and that viscosity and thermal diffusivity become active at much smaller scale sizes, Bolgiano gave the following spectral expressions for the one-dimensional wavenumber spectrum of kinetic energy and temperature:-

$$E(\kappa) \sim \chi^{2/5} (g/\theta_o)^{4/5} \kappa^{-11/5} \qquad (1.4.4a)$$

$$F_T(\kappa) \sim \chi^{4/5} (g/\theta_o)^{-2/5} \kappa^{-7/5} \qquad (1.4.4b)$$

where g is the acceleration of gravity and θ_o the mean potential temperature. For the inertial subrange the usual -5/3 forms apply. The expression (1.4.4b) applies for any conservative passive additive such as ref. index, for the buoyancy subrange.

Monin[69] obtained the same result by assuming that for very high stability the buoyant subrange does not depend on the rate of energy dissipation but is determined by two parameters only: the buoyancy parameter g/θ and the mean rate of production (and dissipation) χ of temperature fluctuations. From dimensional considerations the expression (1.4.4a) was obtained.

Shur in[63] obtained spectra of vertical velocities in stratified regions of the atmosphere; these spectra were adequately represented by a -3 power law at low wavenumbers undergoing a transition to the familiar -5/3 law at higher wavenumbers. To explain this behaviour, Shur attributed the loss of part of the kinetic energy of turbulence to the work done against buoyant forces. His explanation has the following basis.

In an atmosphere with stable stratification, a turbulent eddy must perform work against the buoyant forces. Thus, some of the eddy kinetic energy is converted into potential energy and contributes to a decrease of the stability. Eddies of small dimensions suffer little energy loss compared to large eddies which are more buoyant. It is clear that the loss of kinetic energy is not the same along the wavenumber range. In certain cases of high stability,

nearly all the energy of large eddies is expended against buoyancy forces and is not cascaded down to smaller eddies. Thus the spectrum of turbulence decreases very sharply at large wavenumbers. The quantitative result that Shur obtained through a "not rigorous" treatment, based mainly on dimensional analysis, is:-

$$E(\kappa) = c.\varepsilon^{2/3}\kappa^{-5/3}(1 + b.k^{-4/3}) \qquad (1.4.4c)$$

where c is a constant, ε the rate of dissipation and b a quantity defined as:-

$$b = \frac{4}{3}\ (2\pi)^{4/3}\ \frac{g}{\theta}\ \frac{d\theta}{dz}\ \varepsilon^{-2/3} \qquad (1.4.4d)$$

From (1.4.4c) it can be concluded that:-

$$\left.\begin{array}{ll} E(\kappa) \sim \kappa^{-3} & b.\kappa^{-4/3} >> 1 \\ E(\kappa) \sim \kappa^{-5/3} & b.\kappa^{-4/3} << 1 \end{array}\right. \qquad (1.4.4e)$$

Thus, the transition from the -3 to the -5/3 power law depends on the wavenumber and, from (1.4.4d), on the static stability parameter $\frac{g}{\theta}\ \frac{d\theta}{dz}$.

For high stability the -3 power law can dominate the spectral function for considerably high wavenumbers. Lumley[70] regarded the dissipation rate ε as a spectral energy flux and, in fact, when equilibrium is assumed, the amount of turbulent energy that is produced is also transferred through the spectrum and finally dissipated. For the inertial

subrange of turbulence ε is constant. A non-constant ε at a particular wavenumber means that energy is transferred into or out of the spectrum in that vicinity. If the local variation of ε with wavenumber $\frac{\partial \varepsilon}{\partial \kappa}$ is very small compared to the total variation of ε with κ $((\varepsilon/\kappa)/(\partial\varepsilon/\partial\kappa) >> 1)$, then the spectrum may be considered " locally " inertial and isotropic in wavenumber space. A consequence of this is that although there is a transfer of energy out of the spectrum due to work done by the eddies against buoyant forces, at any wavenumber " vicinity " the temperature fluctuations are solely determined by the velocity fluctuations exactly as in a Kolmogorov inertial subrange. Lumley found that the rate at which energy is leaving the spectrum is:-

$$\frac{d\varepsilon}{d\kappa} = - \frac{g}{\theta} \frac{\partial \theta}{\partial z} \, c . \varepsilon^{1/3} \kappa^{-7/3} \qquad (1.4.4f)$$

This is a non-linear first order equation for the spectral flux. Its solution gives[71]:-

$$\varepsilon^{2/3} = \varepsilon_o^{2/3} + \frac{g}{\theta} \frac{\partial \theta}{\partial z} \cdot \frac{c}{2} \kappa^{-4/3} = \varepsilon_o^{2/3} \left(1 + \left(\frac{\kappa}{\kappa_b}\right)^{-4/3}\right) \qquad (1.4.4g)$$

where ε_o is the final dissipation rate, c is a constant equal to $2\frac{K_M}{K_T}$ where K_T/K_M is the turbulent Prandtl's number approximately 0.03 for stable stratification[21]. Thus $c \simeq 66.6$. The quantity κ_b is given by:-

$$\kappa_b^{4/3} = \frac{c}{2} \frac{g}{\theta} \frac{d\theta}{dz} \varepsilon_o^{-2/3} \qquad (1.4.4h)$$

Due to the assumption of a " locally inertial" subrange the usual form of Kolmogorov may be used to describe the velocity fluctuations spectrum where ε is taken from (1.4.4g):-

$$E(\kappa) = a.\kappa^{-5/3} \left(1 + \left(\frac{\kappa}{\kappa_b}\right)^{-4/3}\right) \qquad (1.4.4i)$$

Apparently the result of Lumley is in exact agreement with the relationship given by Shur provided that $b = \kappa_b^{4/3}$. In fact from (1.4.4d) and (1.4.4h) accepting that $c \simeq 66.6$, it comes out that $b \simeq \frac{1}{2} \kappa_b^{4/3}$. This has the consequence that the transition from the -3 law to the -5/3 law occurs at smaller scale sizes for Lumley's model.

The above-mentioned models can be classified into two categories:-

(a) The Bolgiano-Monin model predicting a -11/3 power law for the spectrum of velocity fluctuations and a -7/5 law for the spectra of conservative passive additives in the " buoyancy subrange " .

(b) The Shur-Lumley model predicting a -3 power law for velocity and conservative passive additive spectra in the "buoyancy subrange", changing into the -5/3 power law for the inertial subrange proper. Their differences are a result of the initial hypotheses. In the Bolgiano-Monin model, the turbulence spectrum is determined by the rate of production and dissipation of the mean square fluctuations of the buoyancy forces. In the Shur-Lumley model the rate of work done against the mean gradient of temperature determines the spectrum.

Although these models give a satisfactory explanation to many of the previously mentioned experimental observations, they fail to predict a "-1" power dependence of the spectral function as reported by[64,65,66]. Neither do they give any predictions for the spectral expressions in the case of an unstable stratification. A different approach to the problem of the effect of stability upon the spectra of turbulent atmospheric motions has been introduced by the theory of interaction of the average and turbulent fields of temperature and wind velocity[71,72,73]. The main source of turbulent energy in the atmosphere is the energy of the mean motion. The intensity of turbulence and the turbulent transfer of momentum, or any conservative passive additive, are determined not only by the velocity gradients (vorticity) of the mean motion but also by the interaction of the vorticity of the mean motion $\left(\frac{d\bar{v}}{dz}\right)$ with the vorticity of the turbulent motion $\left(\frac{du}{dz}\right)$.

Tchen[71] distinguishes the case in which the vorticity of the basic (mean) motion is small compared with the vorticity of turbulence in a certain range of scale sizes from the case in which the vorticities are comparable. In the first case, there is no interaction between the two motions and the vorticity of the mean motion serves only as an energy input to the turbulent motion. In the second case, the comparable vorticities interact and this may lead to a strong resonance where the basic motion provides energy not only for the largest turbulent eddies but, also, for a whole range of scale sizes. In the atmosphere, this interaction

can be observed in the region of strong velocity and temperature gradients.

The predictions of Tchen[71] and later Gisina[72] for the kinetic energy spectrum are:-

A -5/3 power law for the case of weak interaction between the basic and the turbulent fields. In the dissipation subrange this law changes into -7 power law.

In the case of strong interaction, the spectrum of kinetic energy is given by the expression:-

$$E(\kappa) = \frac{\varepsilon}{\frac{K_T}{K_M}\frac{d\bar{v}}{dz}}\left[1 + \frac{g.\chi}{\theta.\varepsilon\frac{d\theta}{dz}}\right].\ \kappa^{-1} \qquad (1.4.4j)$$

where K_T/K_M is the turbulent Prandtl's number, ε the kinetic energy dissipation rate and χ the temperature dissipation rate.

In 1975, Tchen[73] published a work in which, through an elaborate mathematical method (cascade decomposition), the one-dimensional spectra of kinetic and potential energy for a stable or unstable stratification are expressed as a function of wavenumber for the following subranges:-
(a) Buoyancy subrange, (b) Inertial subrange with buoyancy mixing, (c) Inertial subrange, (d) Dissipation subrange.

In the case of stable stratification, the kinetic energy fluctuations are dampened and a conversion into potential energy occurs. In an unstable stratification, the effect of gravity is to amplify both the kinetic and potential energy fluctuations.

The results obtained by Tchen are summarized in Table 1.2.

The various subranges are characterized by different-spectral functions for the kinetic and potential energies and the exponent n can acquire the values -3, -1, -5/3 and -7 depending on the subrange. The transition occurs for specific wavenumbers separating the various subranges and given by the following expressions:-

(a) Kinetic energy spectra:-

$$\left.\begin{aligned} \kappa_{RN} &= \left\{\frac{R^{1/2}.N^2}{\varepsilon_u}\right\}^{1/2} \\ \kappa_{R_\varepsilon} &= \left\{\frac{R^{3/2}}{\varepsilon_u}\right\}^{1/2} \\ \kappa_\nu &= \left(\frac{\varepsilon_u}{\nu^3}\right)^{1/4} \end{aligned}\right\} \qquad (1.4.4k)$$

TABLE 1.2

Subranges of Kinetic and Potential Energy		KINETIC ENERGY SPECTRUM $E(\kappa)$			
		Buoyancy	Inertial with Buoyancy	Inertial	Dissipation
		κ_{RN}		κ_{R_ε}	κ_ν
POTENTIAL ENERGY SPECTRUM $G(\kappa)$	Buoyancy κ_{RN}	$E(\kappa) \sim \kappa^{-3}$ $G(\kappa) \sim \kappa^{-3}$			
	Inertial with Buoyancy κ_{R_ε}		$E(\kappa) \sim \kappa^{-1}$ $G(\kappa) \sim \kappa^{-1}$	$E(\kappa) \sim \kappa^{-5/3}$ $G(\kappa) \sim \kappa^{-1}$	
	Inertial $\kappa_{\chi\nu}$	$E(\kappa) \sim \kappa^{-3}$ $G(\kappa) \sim \kappa^{-1}$		$E(\kappa) \sim \kappa^{-5/3}$ $G(\kappa) \sim \kappa^{-5/3}$	
	Dissipation				$E(\kappa) \sim \kappa^{-7}$ $G(\kappa) \sim \kappa^{-7}$

(b) Potential energy spectra:-

$$\left.\begin{aligned} K_{RN} &= \{\frac{R^{1/2}N^2}{\varepsilon_U}\}^{1/2} \\ K_{R_\varepsilon} &= \{\frac{R^{3/2}}{\varepsilon_u}\}^{1/2} \\ K_\chi &= \left(\frac{\varepsilon_u}{\chi^3}\right)^{1/4} \end{aligned}\right\} \qquad (1.4.41)$$

where $N^2 = \frac{g}{\theta}\frac{d\theta}{dz}$, ε_u and ε_U and the dissipation rates of kinetic energy and potention energy respectively and R is a measure of the vorticity and is given by:-

$R = \varepsilon_u/K_M$ where K_M is the eddy viscosity

For unstable stratification, the spectral expressions remain as in Table 1.2 but the transition wavenumbers are given as:-

(a) Kinetic energy spectra:-

$$\left.\begin{aligned} \kappa_M &= \{\frac{M^3}{\varepsilon_U}\}^{1/2} \\ \kappa_{M_\varepsilon} &= \{\frac{M^3}{\varepsilon_u}\}^{1/2} \\ \kappa_\nu &= \{\frac{\varepsilon_u}{\nu^3}\}^{1/4} \end{aligned}\right\} \qquad (1.4.4m)$$

(b) Potential energy spectra:-

$$\left.\begin{aligned} K_M &= \{\frac{M^3}{\varepsilon_U}\}^{1/2} \\ K_{M_\varepsilon} &= \{\frac{M^3}{\varepsilon_u}\}^{1/2} \\ K_{\chi\nu} &= \{\frac{\varepsilon_u}{(\nu.\chi)^{3/2}}\}^{1/4} \end{aligned}\right\} \qquad (1.4.4n)$$

where $M^2 = -N^2$ and the rest of the quantities are as defined before.

An idea about the scale sizes corresponding to the transition wavenumbers can be given by the following numerical application:-

The values for ε_u given in[51] vary between 100 - 10 $cm^2.sec^{-2}$ and for ε_U between 150 - 50 $cm^2.sec^{-3}$. In[74] ε_U has an average value of 100 $cm^2.sec^{-3}$ for up to an altitude of 1000 m. Thus, the average values $\varepsilon_u = 50$ $cm^2.sec^{-3}$ and $\varepsilon_U = 100$ $cm^2.sec^{-3}$ seem appropriate. The value of K_M can be taken equal to $10^4 cm^2.sec^{-1}$ [3] and $\nu \approx \chi \approx 1.5$ $cm^2.sec^{-1}$. For $N^2 = 10^{-4} sec^{-2}$, the following values are obtained through (1.4.4k) and (1.4.4l):-

$$\kappa_{RN} = 3.76.10^{-2} m^{-1} \quad , \quad K_{RN} = 2.65.10^{-2} m^{-1}$$

$$\kappa_{R_\varepsilon} = K_{R_\varepsilon} = 2.65.10^{-1} m^{-1} \quad , \quad \kappa_\nu = K_\nu = 1.96.10^{2} m^{-1}$$

and for the corresponding scale sizes:-

$$l_{RN} = \frac{2\pi}{\kappa_{RN}} = 167 \text{ m} \quad , \quad L_{RN} = \frac{2\pi}{K_{RN}} = 236 \text{ m} \quad , \quad l_{R_\varepsilon} = L_{R_\varepsilon} \simeq 24 \text{ m}$$

and $l_\nu = L_\nu = 3.2.10^{-2}$ m

Thus, assuming that the buoyancy subrange starts with scale sizes in the vicinity of 2000 m (thermal cells), the "-3" regime covers 1 order of magnitude in scale size (2000 m. to 200 m.), the "-1" regime covers also 1 order of magnitude (200 m. to 20 m.) and the "-5/3" regime covers 3 orders of magnitude (20 m. to a few cms.).

When the stability decreases, the transition scale-size separating the "-3" and the "-1" regimes shifts to larger wavelengths. For $N^2 = 10^{-5}$ and the rest of the quantities the same as before:-

$\kappa_{RN} = 1.18.10^{-2} m^{-1}$ and $l_{RN} = 2\pi/\kappa_{RN} = 532$ m.

$K_{RN} = 8.4.10^{-3} m^{-1}$ and $L_{RN} = 2\pi/K_{RN} = 746$ m.

For conditions of instability, the expressions (1.4.4m) and (1.4.4n), for a very common value of $M^2 = 10^{-5} cm^{-2}$ and the rest of the quantities as before, give:-

$\kappa_M = K_M = 1.77.10^{-3} m^{-1}$ and $l_M = L_M = 3550$ m.

$\kappa_{M_\varepsilon} = K_{M_\varepsilon} = 2.51.10^{-3} m^{-1}$ and $l_{M_\varepsilon} = L_{M_\varepsilon} = 2500$ m.

Thus for unstable stratification the "-3" regime covers scale sizes larger than 3.5 km., the "-1" regime covers only a narrow range of scale sizes between 2.5 km. and 3.5 km. and the "-5/3" regime covers the whole range of scale-sizes from the dissipation microscale up to 2500 m.

Apparently Kolmogorov's "-5/3" law governs the whole micrometeorological range of fluctuations for unstable stratification and the small-scale part of it for stable stratification. Thus, it is the most common law for the spectral functions of atmospheric variables.

CHAPTER 2

THEORETICAL APPROACHES TO THE PROBLEM OF TRANSHORIZON PROPAGATION

In the years around 1935, after the discovery by Marconi (summer, 1932) that frequencies around 500 MHz. may be propagated beyond the optical horizon, theoreticians began their attempts to explain this phenomenon. Initially, their efforts were directed towards studying the diffraction effects due to the earth's curvature. Basically, the problem posed was that of diffraction by a sphere of diameter very much greater than a wavelength. The solution of this problem is not without difficulty even if the effects of the atmospheric gases are neglected. Solutions obtained after this simplification have given rise to what are collectively known as "theories of wave propagation in the ideal atmosphere". A detailed description of these theories is out of the scope of the present work. In general, they are not relevant to this investigation.

However, extensive research work, in the fields of transhorizon propagation and meteorology, revealed inadequacies in these early theories. Large discrepancies between experimental and theoretically predicted values of the field intensity existed for U.H.F. transmissions to distances well beyond the horizon. Also, the effects of the troposphere were found to be far from negligible. Considerable variations, both spatial and temporal, of the ref. index properties of this region were found to exist. This led to

new theoretical investigations taking into account the inhomogeneity of the troposphere for the purpose of attributing transhorizon propagation to the variations of the refractivity field. The resultant "theories of wave propagation in the real atmosphere" have proposed trans-horizon propagation via a number of different mechanisms.

2.1 Propagation by Refraction in a Standard Atmosphere: Effective Earth Radius-Modified Refr. Index

The first attempt to attribute propagation beyond the optical horizon to the mean properties of the atmospheric refr. index was made by Schelling, Burrows and Ferrell[75]. As mentioned in Chapter 1, in a "standard" atmosphere, the refr. index is decreasing with altitude. The path of a wave propagated in such a medium is curvilinear. An expression relating the curvature of a radio-ray to the gradient of the refr. index is given (see Appendix I for derivation):-

$$\frac{1}{\rho} = -\frac{1}{n}\frac{dn}{dh}\cos\theta \qquad (2.1.1)$$

where ρ is the radius of the ray-path curvature and θ is the angle between the ray-path and the surface of constant refr. index at an altitude h.

The curvature of an "effective earth" is defined as the difference between the curvatures of the real earth and the ray-path:-

$$\frac{1}{R_{eff.}} = \frac{1}{R} - \frac{1}{\rho}$$

then:-

$$R_{eff.} = k.R = \frac{1}{1/R - 1/\rho}$$

and:-

$$k = \frac{1}{1 + \frac{R}{n}\frac{dn}{dh}\cos\theta}$$

The values of θ are usually very small in tropospheric propagation, in which case $\cos\theta \simeq 1$ and:-

$$k = \frac{1}{1 + \frac{R}{n}\frac{dn}{dh}} \qquad (2.1.2)$$

For a "standard" atmosphere, the refr. index gradient has been given as (see Chapter 1 (1.3.13)):-

$$\frac{dn}{dh} = \frac{dN}{dh} \cdot 10^{-6} = -40.10^{-6} \text{ (units/km.)}$$

inserting this value in (2.1.2) and considering that $n \simeq 1$ and $R = 6370$ km.:-

$$k = \frac{1}{1 - 6.37.10^{3}.40.10^{-6}} \simeq \frac{4}{3} \qquad (2.1.3)$$

Thus, an "effective" earth radius of $R_{eff.} = \frac{4}{3}R$ would permit the propagation of a ray rectilinearly under "standard"

atmospheric conditions.

It is apparent from (2.1.2) that for any refr. index gradient there is a corresponding k-value. Therefore, it can be seen that there are conditions when short trans-horizon links may behave as though they were line-of-sight and, conversely, near the horizon line-of-sight links may behave as transhorizon.

Alternatively, one may use the concept of a modified refr. index with a gradient changing with altitude. When the departures of a ray-path from the straight are of interest, in which case a $k = \frac{4}{3}$ is assumed, one may remove the "standard" decrease of N with height by adding a quantity $\delta N = (h/4R).10^6$ to N(h). In this way, the "B unit is obtained"[76]:-

$$B(h) = N(h) + (h/4R).10^6 \qquad (2.1.4)$$

The profile of B in a standard atmosphere is a vertical line and any departure from this profile amounts to a deviation of the ray-path from the straight.

When propagation takes place over extended ranges, it is very helpful to use the concept of a "flat earth". In such a model, the terminals are "radio visible" but the ray-paths are curving upwards. As this corresponds to an infinite "effective earth" radius, then $k \to 0$ and from (2.1.2):-

$$1 + \frac{R}{n}\frac{dn}{dh} = 0 \quad , \quad \text{hence:} \quad \frac{dn}{dh} = -\frac{1}{R} \; (n \simeq 1)$$

For this case, the modified index of refraction is defined as:-

$$M(h) = N(h) + (h/R).10^6 \qquad (2.1.5)$$

The M-unit or "modified refractive index" has surface values in the vicinity of 300 and is an increasing function of altitude.

Both the B-unit and the M-unit are subject to certain limitations. These are due to the assumption of a "standard" atmosphere with a linear decrease of N with height. Investigations concerned with the variations of the k-value proved the inadequacy of the "linear decrease" model for N. It has been shown[76] that the k-values determined from actual meteorological measurements varied systematically as a function of climate. Later, Bean and Meany[77] have found that the annual variations in the monthly means of k were highly correlated with the corresponding monthly medians of radio field strengths for different parts of the U.S.A. This led to a development of a method predicting radio field strengths as a function of k[78]. Prompted by these realisations, other investigators[79] introduced new models of atmospheric refractive index, offering considerable improvement over the "4/3" model for applications at long distances and high elevations. These models adopt an exponential decrease of N with height. This is a more realistic model of the real atmosphere in view of the fact that the first term of (1.3.9), involving the factor P/T,

amounts to at least 70% of the total and is proportional to air density, a quantity assumed to decrease exponentially with height.

Nevertheless, it may be conveniently assumed that for the first 2-3 km. of the atmosphere, the "4/3" model is in essential agreement with the structure of N. Since it has been shown that 60% of the total bending of a ray occurs in the first kilometre above the earth's surface[79,80], then B and M units seem adequate enough to describe the refractivity profile for cases of propagation at moderate transhorizon distances (up to 200 km.) and at very small or zero elevation angles.

2.2 Wave Propagation in the Real Atmosphere

The theories attributing transhorizon propagation to the inhomogeneities of the troposphere, necessarily provide an atmospheric model representative of the propagation mechanism. Tropospheric models that have been extensively used in the past in propagation studies may be classified into the following categories:-

(a) Stratified atmosphere with transition layers where the refr. index gradient changes sign (inversions);

(b) Atmosphere with extensive layers or thin ones with limited horizontal extension, characterised by a gradient of refr. index exceeding that of the surrounding space and capable of reflecting incident e.m. radiation;

(c) Atmosphere containing turbulent eddies or "blobs" capable of scattering e.m. energy independently.

The propagation mechanisms related to the above-mentioned models are the following:-

1. Wave propagation in atmospheric "ducts", sometimes known as "trapping";
2. Propagation by partial reflection from extended or broken layer structures "feuillets" contained in the volume common to the transmitting and receiving aerial beams;
3. Propagation by "scattering" caused by turbulent eddies ("blobs"). In this mechanism only "blobs" contained in the "common volume" contribute to the transhorizon field.

2.2.1 Wave Propagation in an Atmospheric Duct

A theory of "ducting" was presented by Booker and Walkinshaw[81] in 1946. It is based on the concept of a flat earth model and, therefore, of a modified refr. index. When the gradient $\frac{dM}{dh}$ is positive, a propagated ray curves away from the earth's surface. For $\frac{dM}{dh} < 0$ a propagated ray-path curves towards the earth's surface. From (2.1.5) and (2.1.2), it can be shown that in such a case the k-factor becomes negative, thus it can be assumed that the effective earth's radius becomes negative in the presence of a negative $\frac{dM}{dh}$. In[81], these concepts are used in suggesting that certain M profiles may give rise to "guided wave modes" of

propagation in the troposphere.

To specify these modes of propagation and predict the field resulting from "ducting" at great distances, Booker and Walkinshaw initially considered an horizontally polarized wave and they proceeded to establish the conditions under which H waves are propagated in the atmosphere. The problem can be reduced to one of two-dimensions by considering an horizontal radiator of infinite length in the z-direction and studying the propagation on the x-y plane (see Figure 2.1):-

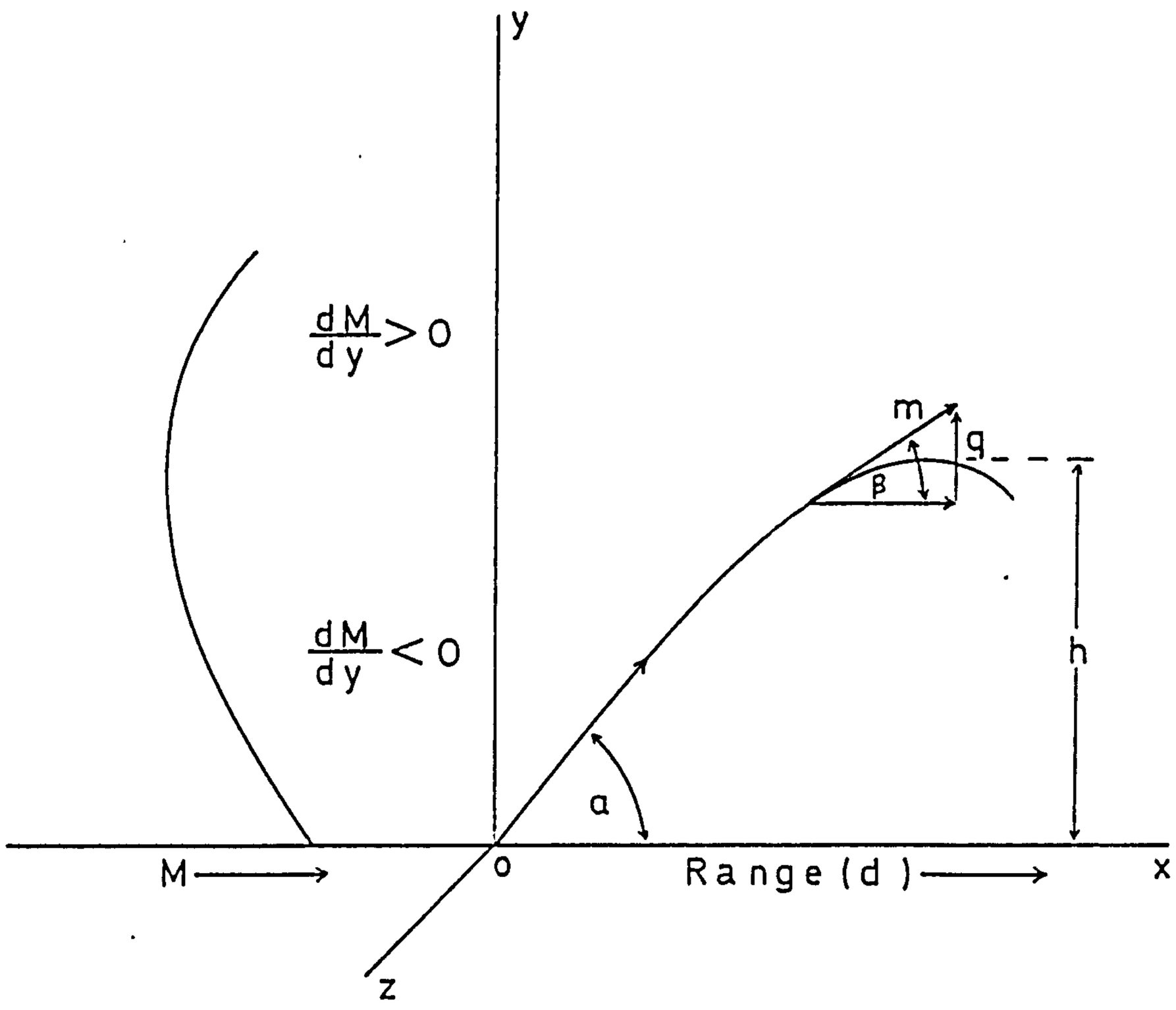

Figure: 2.1

Consider a wave launched at an angle α in a medium with a modified refr. index profile M(y) as in Figure 2.1a.

Due to the condition $\frac{dM(y)}{dy} < 0$ characterising the lower layer of the medium, the wave path curves towards the earth and at a height h, the propagation vector forms an angle β with the horizontal.

For this height, the wave function can be given as[7]:-

$$U = U_o \exp \{j\left[(\omega t) - 2\pi \frac{m(h)}{\lambda} (d\cos\beta + h\sin\beta)\right]\} \qquad (2.2.1a)$$

where $m(y) = M(y)/M(o)$ is the magnitude of the propagation vector.

The horizontal component of the propagation vector is normal to the direction of the refractivity gradient and it is independent of height. Thus, the vertical component of the propagation vector can fully describe the progress of the wave. From Snell's law:-

$M(y)\ \cos\beta = M(o)\ \cos\alpha$, and: $m(y)\ \cos\beta = \cos\alpha$

and for the vertical component of m(y):-

$q(y) = m(y)\ \sin\beta$

The wave function in (2.2.1a) can be expressed as:-

$$U = U_o \exp \{j\left[\omega t - k(r.\cos\alpha + q(y).y)\right]\}$$

and for any height in the duct:-

$$U = U_o \exp \{j\left[\omega t - k(r.\cos\alpha + \int_o^h q(y)\,dy\right]\}$$

Thus, the phase of the wave propagated in the duct depends on time and horizontal distance through the term:-

$$j(\omega t - k.r.\cos\alpha)$$

and on height through the term:-

$$-jk \int_o^h q(y)\,dy$$

As it is shown in Figure 2.1:-

$$q(y)^2 = m(y)^2 - \cos^2\alpha$$

Thus, for $y = h$, $q(h) = 0$ because $\beta = 0$ and $\sin\beta = 0$. For $y > h$, q is imaginary and negative. For $y < h$, q is real positive or negative.

The real values of q(y) indicate upgoing and down-going wave components present, corresponding to an incident and a reflected component respectively. The imaginary value of q(y) indicates that there is an upper boundary of the duct behaving as an inductive reactance, in such a line the transmitted and the reflected waves would interfere to give rise to a standing wave. The horizontal electric field associated with such a wave is given as:-

$$E = U_Y \frac{2}{\sqrt{q(y)}} \cos \left[\pi/4 = k\int qdh\right] e^{j\pi/4}$$

This standing wave also propagates along the horizontal direction as the factor exp{j(ωt - k.r.cosα)} suggests. For a given atmospheric duct, Booker and Walkinshaw[81] have shown that the resultant field at a distance r from a radiator is:-

$$E = E_o \frac{\frac{dM}{dh}}{2} \sqrt{r\lambda} \left| \sum_{n=1}^{\infty} \frac{\exp\left[j(\pi\alpha_n^2 . r/\lambda)\right]}{\alpha_n} . f_n(h_T) . f_n(h_r) \right|$$

where α_n is the characteristic angle of elevation for an H_n mode of propagation and the functions $f_n(h_T)$, $f_n(h_r)$ are the height functions of the transmitting and receiving aerials respectively. E_o is the free space value of the field.

As in waveguides, these ducts have a cut-off frequency. Unfortunately, this cut-off frequency is not well defined because the spatial limits of a duct are not easily defined. The maximum wavelength that may be propagated in a duct of given properties is approximately given by[12]:-

$$\lambda_{max} \text{ (m.)} = 2.5.h_o\sqrt{\Delta\bar{n}}$$

where h_o is the height of the duct in metres and $\Delta\bar{n}$ the variation of the refr. index inside the duct. Thus, for the present experiment and for $\Delta\bar{n} = 4.10^{-6}$ which is a typical value for average latitudes[83], the minimum duct height must be:-

$$h_{min} = \frac{\lambda_{max}}{2.5} .0.5.10^3 = 66m.$$

The conditions for the formation of an atmospheric duct usually depend on the temperature profile and temperature inversions are sometimes severe enough to cause a decrease of M with height without any vertical gradient of water vapour. An extensive description of the properties of atmospheric ducts and the conditions associated with their formation can be found in[9,82]. Briefly, these conditions are as follows:-

Surface ducts: (a) Flow of warm air over a cold and wet ground; (b) Radiative cooling of the ground during calm and cloudless nights.

Elevated ducts: Subsidence of an air mass in an area of high pressure. The descending air is compressed and thus warmed and dried; if this air is prevented from reaching the ground by low level clouds or fog, then an elevated duct is formed above the top of the clouds.

It has been shown[82] that even under the most favourable conditions, ducts above land occur less than 15% of the time. For a temperate climate, the frequency of occurrence is usually 4-5% of the time.

The non-permanent character of ducts has reduced the practical significance of the "ducting" theory during recent years. Nevertheless, abnormal propagation which may be attributed to ducting is sometimes of interest in the study of interference phenomena.

2.2.2 Wave Propagation by Partial Reflection

The theory of wave propagation by partial reflection has been based on the hypothesis that stable layers can appear in regions of the troposphere where the flow of air is laminar. Such layers are usually characterised by a discontinuity in the refr. index gradient due to the absence of turbulent mixing inside the layer. In the first theoretical studies[84,85] of the problem, it was assumed that the reflecting layers are not influenced by turbulence in the adjacent layers or by the vertical displacements of the troposphere. In such a case, the reflecting surfaces may be considered to be plane and horizontal and the geometry of the path can be described as in FIGURE 2.2:-

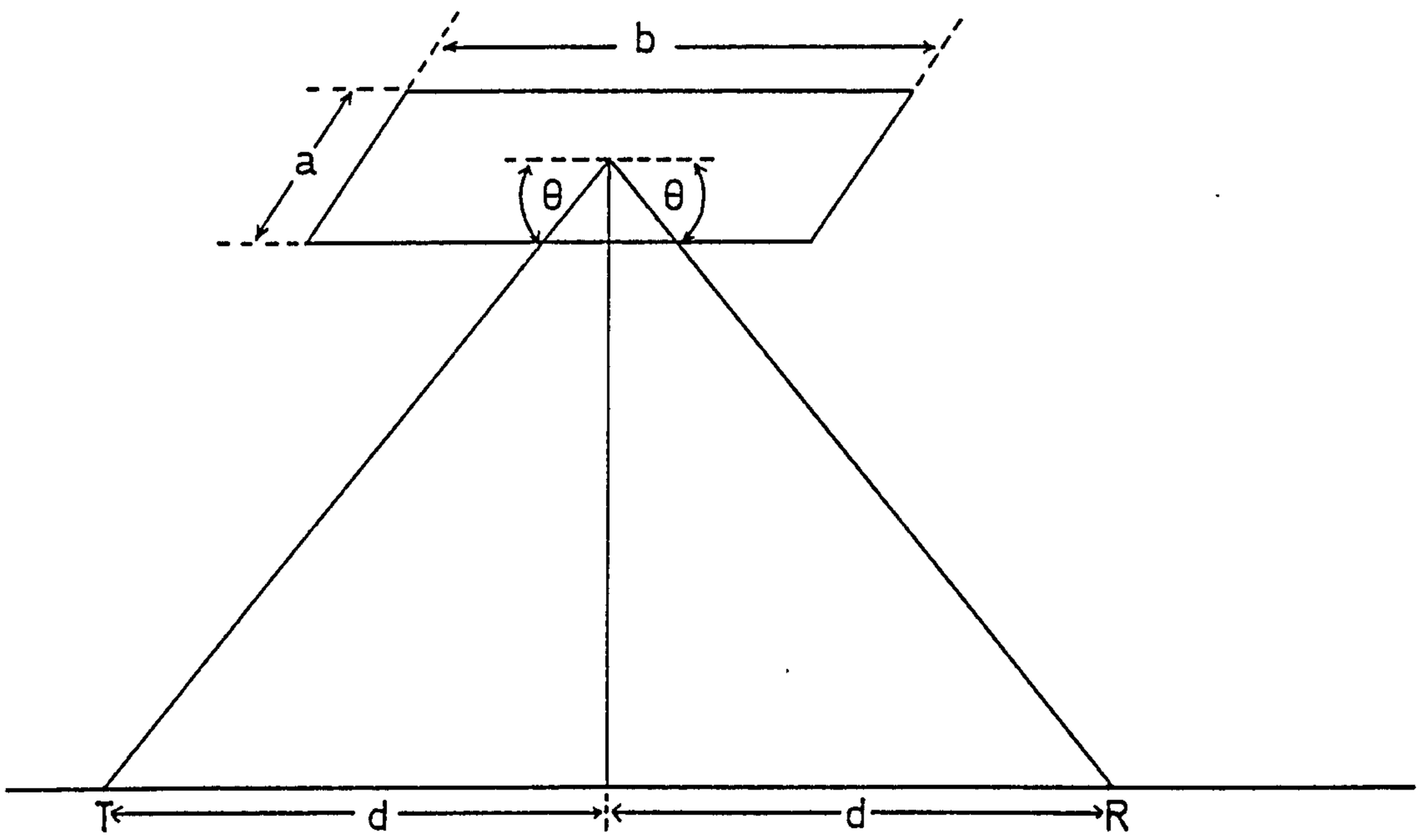

Figure 2.2

Considering each reflecting surface as a set of secondary (Huyghens) sources, the received power can be expressed as[ ]:-

$$P_R = P_T \frac{A_T . A_R}{\lambda^2 d^2} \left[C^2\left(\frac{a}{\sqrt{\lambda . d}}\right) + S^2\left(\frac{a}{\sqrt{\lambda . d}}\right)\right]\left[C^2\left(\frac{b.\theta}{\sqrt{\lambda . d}}\right) + S^2\left(\frac{b.\theta}{\sqrt{\lambda . d}}\right)\right] \quad (2.2.2a)$$

where A_T, A_R are the effective areas of the transmitting and receiving aerials, P_T is the transmitted power and C(z), S(z) are Fresnel integrals defined as[116]:-

$$C(z) = \int_0^z \cos\left(\frac{\pi}{2}t^2\right)dt \quad , \quad S(z) = \int_0^z \cos\left(\frac{\pi}{2}t^2\right)dt$$

C(z) and S(z) have the following properties[116]:-

$$\lim_{z\to\infty} C(z) = \frac{1}{2} \quad , \quad \lim_{z\to\infty} S(z) = \frac{1}{2}$$

$$\lim_{z\to 0} C(z) \simeq z \quad , \quad \lim_{z\to 0} S(z) = 0$$

Depending on the dimensions a and b of the reflecting surface relative to the axes $\sqrt{\lambda . d}$ and $\sqrt{\lambda . d}/\theta$ of the Fresnel ellipsoid, the expression (2.2.2a) can take the forms:-

(a) If $a >> \sqrt{\lambda . d}$ and $b >> \sqrt{\lambda . d}/\theta$, then:-

$$C\left(\frac{a}{\sqrt{\lambda . d}}\right) = C\left(\frac{b.\theta}{\sqrt{\lambda . d}}\right) = S\left(\frac{a}{\sqrt{\lambda . d}}\right) = S\left(\frac{b.\theta}{\sqrt{\lambda . d}}\right) = \frac{1}{2}$$

and:-

$$P_R = \frac{P_T . A_T . A_R}{4\lambda^2 . d^2} n^2 \qquad (2.2.2b)$$

where n is an amplitude reflection coefficient.

(b) If $a >> \sqrt{\lambda . d}$ and $b << \sqrt{\lambda . d}/\theta$, then:-

$$C\left(\frac{a}{\sqrt{\lambda . d}}\right) = S\left(\frac{a}{\sqrt{\lambda . d}}\right) = \frac{1}{2} \quad , \quad C\left(\frac{b.\theta}{\sqrt{\lambda . d}}\right) \simeq \frac{b.\theta}{\sqrt{\lambda . d}} \quad , \quad S\left(\frac{b.\theta}{\sqrt{\lambda . d}}\right) = 0$$

and:-

$$P_R = P_T \frac{A_T . A_R (b.\theta)^2}{2\lambda^3 d^3} . n^2 \qquad (2.2.2c)$$

(c) If $a << \sqrt{\lambda . d}$ and $b << \sqrt{\lambda . d}/\theta$, then:-

$$C\left(\frac{a}{\sqrt{\lambda . d}}\right) \simeq \frac{a}{\sqrt{\lambda . d}} \quad , \quad C\left(\frac{b.\theta}{\sqrt{\lambda . d}}\right) \simeq \frac{b.\theta}{\sqrt{\lambda . d}} \quad , \quad S\left(\frac{a}{\sqrt{\lambda . d}}\right) = S\left(\frac{b.\theta}{\sqrt{\lambda . d}}\right) = 0$$

and:-

$$P_R = P_T \frac{A_T . A_R . a^2 . (b.\theta)^2}{\lambda^4 . d^4} n^2 \qquad (2.2.2d)$$

The case (a) is rather unrealistic as, for moderate propagation distances and centimetric wavelengths, the dimension b is of the order of tens of kilometres. In the present experiment for instance:-

λ = 0.33m. , d = 70 km. , $\theta \simeq$ 8.2 mrd. , b $\simeq$ 18500 m.

It is more likely that b $\simeq$ a, then for a volume V common to the aerial beams and containing N contributing layers per unit volume, the received power can be given from (2.2.2c) as:-

$$P_R = P_T \frac{A_T . A_R . N . b^2}{2\lambda^3 . d^3} \int_V \theta^2 . n^2 dV \qquad (2.2.2e)$$

The above expression assumes that the dimensions and the number of layers per unit volume are constant in V. In[85], the solution of (2.2.2e) has been given in the form:-

$$P_R = P_T \frac{Q . \lambda^3}{3d^3 \Phi^5 a^2 (2+a/\Phi)} . f\left(\frac{a}{\Phi}\right) \qquad (2.2.2f)$$

where Φ is the angle of elevation of the transmitting and receiving aerials, a is the beamwidth of identical aerials and Q and $f\left(\frac{a}{\Phi}\right)$ are given as:-

$Q = 2.000\ k^2 . b^2 N$, i.e. a constant for the atmosphere in the common volume:-

$$f(a/\Phi) = 1 + (1 + a/\Phi)^{-4} - \frac{1}{8}\left(\frac{2 + a/\Phi}{1 + a/\Phi}\right)^4$$

The theory of propagation by partial reflection gives concrete answers to some basic problems involved in the planning and performance of a given transhorizon circuit.

Thus, from (2.2.2f) it can be seen that the transmission loss $L = \frac{P_R}{P_T} \sim \lambda^3$ and if (2.2.2d) is used in (2.2.2e) instead of (2.2.2c), then this dependence becomes $L \sim \lambda^2$.

Furthermore, in[112], the problem of the fading power spectrum has been considered and the proposed expression is:-

$$P(f) = \exp\left(-\frac{f^2}{2\sigma_e^2}\right) \qquad (2.2.2g)$$

the quantity $\sigma_e = (0.85\ \beta_e/\lambda).U.\sin\delta$

where β_e is the angle at which the power reflection coefficient becomes 1/2, U is the mean drift velocity of the reflecting layers and δ is the angle between the velocity vector and the propagation path.

The expression (2.2.2g) indicates that an increase of the drift velocity would result in a "spread" of the fading spectrum. Also, that the cross-path wind component accounts for the fading.

More recent theoretical work on this subject[86,87] has put forward a hypothesis which suggests that partial reflections from irregular layers or "feuillets" can be responsible for transhorizon propagation.

This theory takes into account the turbulence in the medium surrounding the stable layers which results in a "corrugation" of their surfaces. Two kinds of irregularities are distinguished - the "primary" having vertical and

horizontal dimensions of a few tens of metres and the "secondary" with vertical dimensions of a few hundreds of metres and horizontal dimensions of some kilometres. The former are a result of the adjacent turbulence; the latter are due to the vertical displacement of the air. Both "primary" and "secondary" irregularities in a "feuillet" may give rise to specular or to diffuse reflection depending on their orientation. Specular reflection results from "in phase" constructive interference of rays within a narrow solid angle. Diffuse reflection results from the interference of rays with a randomly distributed phase within a wider solid angle. The expression for the power due to specular reflection is given[12] as:-

$$P_{rs} = P_{fs} . a_s \frac{\delta n^2}{e^2} \frac{L^2 l_2^2}{l_1^2 H^2} (1 - \gamma^2) \frac{\lambda^3}{a^6 D} \qquad (2.2.2h)$$

and the power due to diffuse reflection:-

$$P_{rd} = P_{fs} . a_d \frac{\delta n^2}{e^2} \frac{L . l_2 . H}{h_1^2} (1 - \gamma^2) \frac{\lambda^2}{a^5 D} \qquad (2.2.2i)$$

where $a_d \simeq 6.2 \times 10^{-3}$, $a_s \simeq 1.2 \times 10^{-2}$, $\frac{\delta n}{e}$ is the refractive index gradient in the "feuillet", L and H are the horizontal and vertical dimensions of the "feuillet", l_1 and h_1 the horizontal and vertical dimensions of the "primary" irregularities, l_2 the horizontal dimension of the "secondary" irregularities, a is the angle of incidence, D the propagation distance, γ is the factor $\frac{\sin u}{u}$ where $u = 2\pi \frac{H}{\lambda} \theta$ and θ is the

angle of reflection.

The expressions (2.2.2h) and (2.2.2i) show a more rapid decrease of reflected power with frequency for specular reflection ($\sim \lambda^3$) than for diffuse reflection ($\sim \lambda^2$). The frequency dependence for the specular reflection are in agreement with the one proposed in the previous theory of partial reflections[85,112].

The temporal variations of a signal received through such a propagation mechanism are given in[12] by means of an approximate expression for the fading rate (number of positive transits across the median level):-

$$N = \frac{2a}{\lambda} U_n . 3\tau \qquad (2.2.2j)$$

where U_n is the component of the wind normal to the path and τ is the inclination of the discontinuity. No expression for the fading spectral function is proposed.

Although the theory of propagation by partial reflection has not been generally accepted as the main mechanism of transhorizon propagation, however, there is some experimental evidence[88,89] that for part of the time, transhorizon radio propagation may be accounted for by a reflection mechanism.

2.2.3 Wave Propagation by Scattering

Atmospheric turbulence as a possible cause for the scattering of transmitted radio waves was first suggested by Booker and Gordon[90] and Megaw[91], following the work of

Pekeris[92] on sound wave propagation. In these treatments the Born approximation (single-scatter) was introduced and since then, it has been consistently used. The weakness of these early theoretical approaches lie in the fact that an exponential autocorrelation function for the refractivity field is assumed. It was soon realised[93,94,95] that the model of turbulence proposed by Kolmogorov (see Subsection 1.4.3) was the most suitable for the description of the propagation medium and further research on the subject[96,97,49] proceeded along this line. Other investigators[98,99,100] developed original ideas for the dependence of the e.m. waves on the turbulent medium.

By considering a turbulent eddy as a "blob" having a different refr. index (dielectric constant) from its environment, Booker and Gordon showed that an aggregate of such "blobs", existing within the volume common to the transmitting and receiving aerial beams, can give rise to a considerable degree of energy scattering.

The wave equation for an inhomogeneous medium derived from Maxwell's equations gives for the electric field vector[101,102]:-

$$\nabla^2\vec{E} - \frac{1}{c^2}\frac{\partial^2}{\partial t^2}(\varepsilon.\vec{E}) = -\vec{\nabla}\left[\frac{1}{\varepsilon}\vec{E}.\vec{\nabla}\varepsilon\right] \qquad (2.2.3a)$$

Since the field oscillates much more rapidly than the dielectric constant, the time derivatives operate mainly on $\vec{E}$. Expressing the dielectric constant as $\varepsilon = \langle\varepsilon\rangle + \delta\varepsilon$, where $\langle\varepsilon\rangle$ is a mean and $\delta\varepsilon$ a fluctuating part and assuming

that $\langle\varepsilon\rangle \simeq 1$, (2.2.3a) can be written:-

$$\nabla^2\vec{E} - \frac{1}{c^2}(1 + \delta\varepsilon)\frac{\partial^2\vec{E}}{\partial t^2} = -\vec{\nabla}\left[\vec{E}.\vec{\nabla}\ln(1 + \delta\varepsilon)\right] \qquad (2.2.3b)$$

Considering that the field consists of an unperturbed part $\vec{E_o}$ and a scattered part $\vec{E_s}$, i.e. $\vec{E} = \vec{E_o} + \vec{E_s}$ and that $\ln(1 + \delta\varepsilon) \simeq \delta(\varepsilon)$ [49], then (see Appendix II):-

$$(\nabla^2 + k^2)\,\vec{E_s} = -k^2.\delta\varepsilon\,\vec{E_o} \qquad (2.2.3c)$$

The solution of this equation is [101,103]:-

$$\vec{E_s}(\vec{R}) = k^2\int_V G(\vec{R},\vec{r})\ .\ \delta\varepsilon(\vec{r},t)\ .\ \vec{E_o}(\vec{r})\,d^3\vec{r} \qquad (2.2.3d)$$

where V is the common scattering volume and $G(\vec{R},\vec{r})$ is the free-space spherical Green's function connecting the scattering "blob" at $\vec{r}$ and the receiver at $\vec{R}$ (see FIGURE 2.3). $G(\vec{R},\vec{r})$ is given by:-

$$G(\vec{R},\vec{r}) = \frac{e^{-jk|\vec{R}-\vec{r}|}}{|\vec{R} - \vec{r}|}$$

Since the receiver is always many wavelengths from the scattering "blobs", the far field approximation may be used:-

$$\vec{E}_s(\vec{R}) = \vec{E}_o.e^{-jk\vec{R}}\frac{k^2}{4\pi\vec{R}}\int_V \delta\varepsilon(\vec{r},t)\ \exp(j\vec{K}.\vec{r})\ d^3\vec{r} \qquad (2.2.3e)$$

where $\vec{K} = \vec{k}_1 - \vec{k}_2$ is the difference of the wave-number vectors before and after the scattering. If the scattering angle is θ, then from Bragg's condition:-

$$|\vec{K}| = \frac{4\pi}{\lambda} \sin \frac{\theta}{2} \qquad (2.2.3f)$$

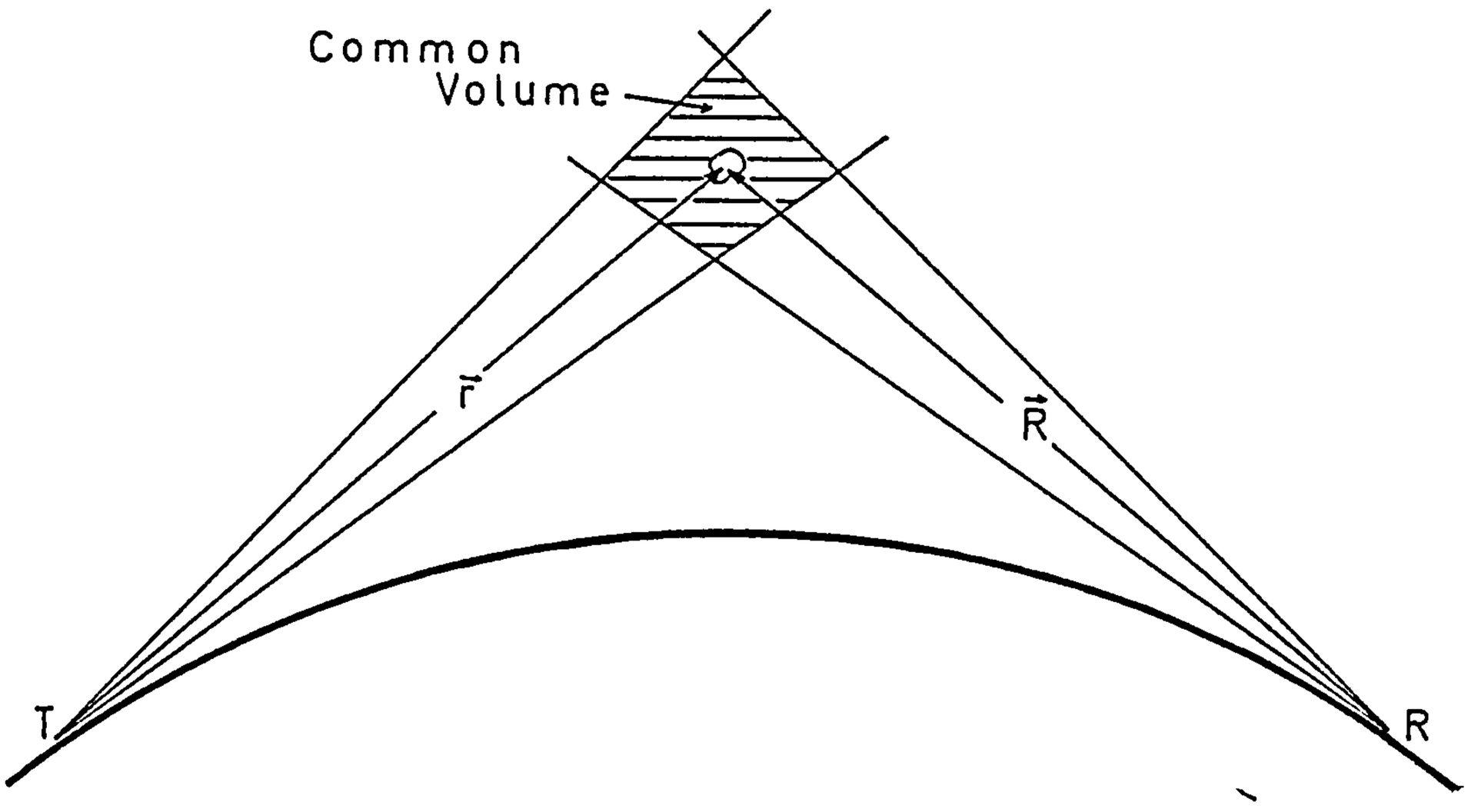

Figure 2.3

The above condition has the physical meaning that if the random scattering medium is considered as a set of spatial periodic diffracting gratings, then for given $\vec{k}_1$ and $\vec{k}_2$, the incident wave is diffracted only by that particular

grating whose wave-number satisfies (2.2.3f). Thus, scattering at a certain angle depends on only one spectral component of the inhomogeneities or, more accurately, on a narrow band of spectral components centered around K.

The mean scattered power per unit volume, per unit solid angle, per unit incident power characterises the average scattering capacity of each "blob" contained in the common volume V and is given by:-

$$\sigma = \frac{R^2}{V} \left| \frac{E_s(R)}{E_o} \right|^2 \qquad (2.2.3g)$$

This quantity is known as the "scattering cross-section".

From (2.2.3e):-

$$\left| \frac{E_s(\vec{R})}{E_o} \right|^2 = \frac{k^4}{16\pi^2 R^2} \int_V d^3r \int_V \delta\varepsilon(\vec{r},t) . \delta\varepsilon(\vec{r}',t) \exp\{j\vec{K}(\vec{r}-\vec{r}')\} d^3(\vec{r}-\vec{r}')$$

and:-

$$\sigma = \frac{k^4}{16\pi^2} \int_V \delta\varepsilon(\vec{r},t) . \delta\varepsilon(\vec{r}',t) \exp\{j\vec{K}(\vec{r}-\vec{r}')\} d^3(\vec{r}-\vec{r}')$$

The quantity $\delta\varepsilon(\vec{r},t).\delta\varepsilon(\vec{r},t)$ is the time dependent spatial autocorrelation function of the dielectric constant fluctuations. Assuming that the process is stationary in time and that the turbulent field is isotropic to give:-

$$\delta\varepsilon(\vec{r},t) . \delta\varepsilon(\vec{r}',t) = B_\varepsilon(\vec{r},\vec{r}') = B_\varepsilon(\vec{\rho}) \quad , \quad \vec{r}-\vec{r}' = \vec{\rho}$$

then:-

$$\sigma = \frac{\pi^2}{\lambda^4} \int_V B_\varepsilon(\vec{\rho}) \exp\{j\vec{K}.\vec{\rho}\} d^3\vec{\rho}$$

Taking into account that the correlation length of the dielectric constant in homogeneities is much smaller than the linear dimensions of the common volume V, then:-

$$\int_V B_\varepsilon(\vec{\rho}) \exp\{j\vec{K}.\vec{\rho}\} d^3\vec{\rho} = \iiint_{-\infty}^{\infty} B_\varepsilon(\vec{\rho}) \exp\{j\vec{K}.\vec{\rho}\} d^3\vec{\rho}$$

It should be noted that the right hand side of this equation is the Fourier transform of the autocorrelation function, i.e. the three-dimensional power spectrum, the scattering cross-section can be written:-

$$\sigma = \frac{\pi^2}{\lambda^4} \Phi_\varepsilon (\vec{K})$$

and from (2.2.3f):-

$$\sigma(\theta,\lambda) = \frac{\pi^2}{\lambda^4} \Phi_\varepsilon \left(\frac{4\pi}{\lambda} \sin \frac{\theta}{2}\right) \qquad (2.2.3h)$$

Thus, the scattering cross-section is a function of the wavelength of the transmitted wave and the scattering angle. The form of this function is determined by the three-dimensional power-spectrum of the dielectric constant fluctuations.

The ratio of the received-to-transmitted power, or otherwise "transmission loss" depends upon the integral of the scattering cross-section over the entire common volume. If the antenna gains of the beams intersected at the scattering point $d^3\vec{r}$ are G_T and G_R, then this ratio is given[101,103] as:-

$$L \doteq \frac{P_R}{P_T} = \frac{\lambda^2}{16\pi^2} \int_V \frac{G_T . G_R . \sigma(\theta,\lambda)}{R_1^2 . R_2^2} \, d^3r \qquad (2.2.3i)$$

where R_1, R_2 as shown in FIGURE 2.3.

If the aerial beams are narrow, then the scattering angle remains substantially constant over the common volume and the integral in (2.2.3i) can be collapsed to:-

$$L = \frac{P_R}{P_T} = \frac{\lambda^2}{16\pi^2} \, V \, \frac{G_R . G_T . \sigma(\theta,\lambda)}{\left[d/2\right]^2 \left[d/2\right]^2} \qquad (2.2.3j)$$

where $R_1 = R_2 \simeq d/2$, i.e. the common volume can be assumed to lie over the midpath area.

In this case, the scattering volume can be fully defined by the aerial beamwidths b (assumed identical) and the transmission path length d by:-

$$V \simeq 2(b.d/4)^3/\theta$$

where the average scattering angle θ is: $\theta \simeq d/R_{eff.}$ if $d << R_{eff.}$ (effective earth radius). Then, (2.2.3j) can be

written:-

$$L = \frac{P_R}{P_T} = \frac{R_{eff.}.b^3.\lambda^2}{32\pi^2.d^2} G_R.G_T.\sigma(\theta,\lambda) \qquad (2.2.3k)$$

Broad beam data are usually expressed with respect to the free-space power P_{fs} which would be received over an identical line-of-sight circuit.

Noting that[101,103]:-

$$\frac{P_{fs}}{P_T} = \frac{\lambda^2}{16\pi^2} \frac{G_T.G_R}{d^2}$$

the expression $L_s = \frac{P_R}{P_{fs}}$ known as "scatter loss" can be written:-

$$L_s = \frac{P_R}{P_{fs}} = d^2 \int_V \frac{\sigma(\theta,\lambda)}{R_1^2.R_2^2} d^3r \qquad (2.2.3l)$$

From the expressions (2.2.3i), (2.2.3k) and (2.2.3l), the importance of the scattering-cross-section as a factor determining the performance of a transhorizon radio link is evident. This, of course, assumes that the propagation mechanism is one of scattering.

2.2.4 Dependence of Some Propagation Parameters on Carrier Frequency and the Refractivity Spectrum Model

From the expressions (2.2.3i), (2.2.3k) and (2.2.3l), it can be seen that the quantities L and L_s depend, through $\sigma(\lambda,\theta)$, upon the transmitted radio-wavelength or the carrier

frequency. It was shown in the previous paragraph that the form of $\sigma(\lambda,\theta)$ depends solely on the function describing the three-dimensional refractivity spectrum. Thus, the choice of such a function determines the dependence of the quantities $\sigma(\lambda,\theta)$, L and L_s upon the carrier frequency.

Apart from the spectral functions suggested by the physical theories of fluid mechanics (see Subsections 1.4.3 and 1.4.4), there are other models which have been proposed for radio wave propagation[90,98,100] and have been extensively used in the past.

In[90] a spectral function of the form:-

$$\Phi_\varepsilon(\kappa) = 8\pi \frac{\langle \Delta\varepsilon^2 \rangle l_o^2}{\left[1+l_o^2\kappa^2\right]^2}$$

is proposed. This function for $l_o^2\kappa^2 >> 1$ can be written as:-

$$\Phi_\varepsilon(\kappa) = \Phi_\varepsilon^o . \kappa^{-4} \qquad (2.2.4a)$$

where Φ_ε^o is a constant. This spectral function corresponds to an exponential spatial autocorrelation function. Many authors[103,104,105] have pointed out the limited support this function receives from experimental evidence and the theory of fluid mechanics.

Another model has been proposed in[98] in an attempt to attribute refr. index fluctuations to pressure fluctuations induced by the turbulent velocity field

according to Bernoulli's law. The proposed spectral function takes the form:-

$$\Phi_\varepsilon(\kappa) = \left(\frac{U_o}{c}\right)^4 \frac{\kappa_o^{4/3}}{\kappa^{13/3}} \qquad (2.2.4b)$$

where U_o is the mean velocity and c the velocity of sound in air. However, it has been pointed out by Silverman[94] that the pressure fluctuations contribute very little to refr. index fluctuations which makes this approach rather unrealistic.

The mixing-in-gradient theory proposed by Villars and Weisskopf[106] and Wheelon[100] results in a κ^{-5} dependence for the three-dimensional wavenumber spectrum, which is in agreement with the Shur-Lumley model and the Tchen model for the "bouyancy subrange" ("-3" dependence for the one-dimensional wavenumber spectrum, see Subsection 1.4.4).

In general, all the models for the three-dimensional refractivity spectrum are functions of the form:-

$$\Phi_\varepsilon(\kappa) = \Phi_\varepsilon^{\,o} \cdot \kappa^{-n} \qquad n : \text{real} \qquad (2.2.4c)$$

where $\Phi_\varepsilon^{\,o}$ is a quantity independent of κ and varying from model to model.

From (2.2.3h) and (2.2.4c), the scattering cross-section can be written:-

$$\sigma(\lambda,\theta) = \frac{\pi^2}{\lambda^4}\,\Phi_\varepsilon^{\,o}\left[\frac{4\pi}{\lambda}\sin\frac{\theta}{2}\right]^{-n} \qquad (2.2.4d)$$

In most of the applications, θ is a very small angle and $\theta \simeq \sin\theta$, thus:-

$$\sigma(\lambda,\theta) = 2^{-n}\pi^{2-n} \cdot \Phi_{\varepsilon}{}^{o}\theta^{-n} \cdot \lambda^{n-4} \sim f_c{}^{4-n} \qquad (2.2.4e)$$

From this expression and (2,2,3k), (2,2,31) the following carrier frequency dependences can be derived:-

$$\text{Transmission Loss:} \quad \dot{L} = \frac{P_R}{P_T} \sim \lambda^{n-2} \sim f_c{}^{2-n} \qquad (2.2.4f)$$

$$\text{Scatter Loss:} \quad L_s = \frac{P_R}{P_{fs}} \sim \lambda^{n-4} \sim f_c{}^{4-n} \qquad (2.2.4g)$$

Another quantity that is affected by the model function representing the refr. spectrum, is the ratio of the scatter losses for two different wavelengths:-

$$L_{S1}/L_{S2} = (P_{R1}/P_{FS1}) \; / \; (P_{R2}/P_{FS2})$$

which is a measure of the wavelength or frequency dependence of the scattering mechanism. From (2.2.4f):-

$$\frac{L_{S1}}{L_{S2}} = \left(\frac{\lambda_1}{\lambda_2}\right)^{n-4} = \left(\frac{f_1}{f_2}\right)^{4-n} \qquad (2.2.4h)$$

This quantity is of special interest when frequence diversity is used with scaled aerials over the same path. The resulting carrier frequency dependences for the quantities σ, L, L_S,

L_{S1}/L_{S2} for different models of refractivity spectra are listed in TABLE 2.1.

TABLE 2.1

CARRIER FREQUENCY DEPENDENCES FOR DIFFERENT MODELS OF REFRACTIVITY SPECTRA

	Refractivity Spectrum	σ	L	L_S	L_{S1}/L_{S2}
Booker & Gordon (90)	$\frac{\Phi_\varepsilon{}^0}{\kappa^4}$	$f_c{}^0$	$f_c{}^{-2}$	$f_c{}^0$	$\left(\frac{f_{c1}}{f_{c2}}\right)^0$
Villars & Weisskopf (98)	$\frac{\Phi_\varepsilon{}^0}{\kappa^{13/3}}$	$f_c{}^{-1/3}$	$f_c{}^{-7/3}$	$f_c{}^{-1/3}$	$\left(\frac{f_{c1}}{f_{c2}}\right)^{-7/3}$
Kolmogorov (48) Tatarski (49,97)	$\frac{\Phi_\varepsilon{}^0}{\kappa^{11/3}}$	$f_c{}^{1/3}$	$f_c{}^{-5/3}$	$f_c{}^{1/3}$	$\left(\frac{f_{c1}}{f_{c2}}\right)^{1/3}$
Gisina (72) Tchen (71,73)	$\frac{\Phi_\varepsilon{}^0}{\kappa^3}$	$f_c{}^1$	$f_c{}^{-1}$	$f_c{}^1$	$\left(\frac{f_{c1}}{f_{c2}}\right)^1$
Shur-Lumley (70) Tchen (73)	$\frac{\Phi_\varepsilon{}^0}{\kappa^5}$	$f_c{}^{-1}$	$f_c{}^{-3}$	$f_c{}^{-1}$	$\left(\frac{f_{c1}}{f_{c2}}\right)^{-1}$
Bolgiano (67,68) Monin (69)	$\frac{\Phi_\varepsilon{}^0}{\kappa^{17/5}}$	$f_c{}^{-3/5}$	$f_c{}^{-7/5}$	$f_c{}^{-3/5}$	$\left(\frac{f_{c1}}{f_{c2}}\right)^{-3/5}$

As it can be seen from TABLE 2.1, there is a wide range of variation for the carrier frequency dependence. The subject has been experimentally investigated in the past with

results also varying over a wide range.

Thus, Bolgiano[107], using results from a previous experiment[108] in which scaled antennas had been employed, determined statistically the carrier frequency dependence of L_{S1}/L_{S2}. The results indicate that the dependence was not constant but varied from one time period to another. In 99% of the cases, the exponent of the dependence $L_S \sim f^q$ was found to be smaller than 1/3 (corresponding to the "-11/3" model), in 50% of the cases it was smaller than -1 (corresponding to the "-5" model) and in 1% of the cases it was found to be smaller than -2. The average value of the exponent was close to -1. Hirai, Nishikori et al[109] give a yearly median wavelength dependence of L_S for the range 100 - 3000 MHz. For f_c < 900 MHz the dependence was found to be $L_S \sim f_c^{\,0}$ whereas for f_c > 900 MHz the dependence was $L_S \sim f_R^{\,-1}$ (corresponding to the "-5" model). Ortwein et al[110] give an analysis of carrier frequency dependence using X-, S- and L-band signals on a 320 km. oversea path. For the lowest frequencies, the values of the exponent were found to be 1/3 ("-11/3" model) and -0.6 (closer to "-5" model). For the higher frequencies, the exponent was found to be 1/3. Ecklund and Wickerts[111] describe an experiment conducted at 1000 MHz and 3000 MHz over a 259 km. path with scaled antennas. Half-hour median values were used and the exponent q in the dependence $L_{S1}/L_{S2} \sim f_c^{\,q}$ was computed. The value of q was found to range from 1 to -3 with a statistical mean close to 1/3. The value of q was also found to be negatively correlated with the level of the

received power. The lowest values of q were observed during months of "good" reception, whereas, for months of "bad" reception, the value of q was greater and statistically around the value 1/3. The values of q for the 3000 MHz were more often in the vicinity of 1/3 than for the 1000 MHz. In this work, a radiometeorological explanation is offered, attributing these effects to a combined mechanism of scattering and partial reflection by "feuillets". Thus, scattering is the predominant mechanism for the highest frequency, resulting in a 1/3 carrier frequency dependence. For the lower frequency, the mechanism of partial reflection is more predominant, resulting in a dependence with smaller values of q.

Tatarski, in his monograph[49] dedicated to the study of e.m. wave scattering in the atmosphere, suggests that experimental results are often at variance with the theoretical prediction of 1/3 and attributes the discrepancy to mechanisms other than scattering.

2.3 The Problem of the Temporal Fluctuations of the Received Signal

This section is a brief summary of theoretical considerations of the problem of temporal fluctuations (fading) of a signal received beyong-the-horizon. Whilst the theory of propagation by "ducting" does not consider temporal fluctuations at all, the theory of propagation by partial reflection gives an expression for the fading power spectrum[112]. Thus:-

$$P(f) = \exp\{-\frac{f^2}{2(0.85\ \beta_e/\lambda)^2.U_n^2}\}$$

where β_e is the angle at which the power reflection coefficient becomes 1/2 and U_n is the cross-path component of the mean drift velocity. This is a one-sided, Gaussian-shaped function with its mean at zero. When U_n is increasing the spectrum "spreads" towards higher frequencies. Crawford et al[112] report that this model for the fading spectrum was successfully used in obtaining quantitative results.

Rice[113] proposes a function for the fading spectrum resulting from the work of Booker and Gordon[90] which has the form:-

$$P(f) = \exp\{-\frac{f^2}{2\sigma_a^2}\} \qquad (2.3.1)$$

where:-

$$\sigma_a = \left[(2u.\sin\theta/2)^2 + (U_n.1/r)^2\right]^{\frac{1}{2}}/\lambda$$

and u is the standard deviation of the wind velocity, U_n is the mean velocity normal to the path, l is a characteristic dimension of the common volume, r is the length of the path and θ is the scattering angle. This function is also Gaussian-shaped and an increase in either the U_n or u would cause a "spread" of the spectrum towards higher frequencies.

Tatarski[49] proposes an expression for the temporal

spectrum of the field envelope. It has the form:-

$$W(\Omega) = B.\Phi_{\varepsilon}(\vec{K}) \frac{1}{\sqrt{2\pi K^2\sigma_v^2/3}} \exp\{-\frac{(\Omega + \vec{K}.\vec{U_o})^2}{2K^2\sigma_v^2/3}\} \qquad (2.3.3)$$

where B is a constant depending on the geometry and the transmitted wavelength, Φ_{ε} is the three-dimensional refractivity spectrum, $\vec{K}$ is the scattering wavenumber, $\vec{U_o}$ is the mean drift velocity and $\sigma_v^2/3$ is the variance of the turbulent velocity field. As $\vec{K}$ = const., the refractivity spectrum enters the expression as a constant and the form of the function is determined solely by the exponential factor. This is again a Gaussian-shaped function centred around the frequency $-\vec{K}.\vec{U_o}$. Increasing $\vec{U_o}$ is not causing any "spread" of the spectrum, but only "shifting" towards higher frequencies.

A theoretical and experimental treatment of the problem is reported by Fehlhaber and Grosskopf[114,115] concerning two overland experiments with propagation paths of 418 km. and 242 km. and corresponding frequencies of 1715 MHz and 1850 MHz; by considering parameters in the time domain, they propose the following expression for the temporal autocorrelation function:-

$$R(\tau) = N5/6 \left[\tau.\left(\left(\frac{V_y}{L_y}\right)^2 + \left(\frac{V_z}{L_z}\right)^2\right)\right] . e^{-\frac{1}{2}\left(\frac{\tau}{\tau_o}\right)^2} \qquad (2.3.4)$$

where N5/6 is the Norton function:-

$$N5/6\left[\tau.\left(\left[\frac{V_y}{L_y}\right]^2+\left[\frac{V_z}{L_z}\right]^2\right)\right]=$$

$$=\frac{2^{5/6-1}}{\Gamma(5/6)}\cdot\left[\tau.\left(\left[\frac{V_y}{L_y}\right]^2+\left[\frac{V_z}{L_z}\right]^2\right)\right]^{5/6}\cdot K_{5/6}\left[\tau.\left(\left[\frac{V_y}{L_y}\right]^2+\left[\frac{V_z}{L_z}\right]^2\right)\right]$$

The quantities in (2.3.4) are the following - V_y and V_z the two normal to the propagation path drift velocities (propagation assumed along the x-axis), L_y and L_z the corresponding spatial correlation lengths, τ_o is the time constant of the fluctuations. Usually in the atmosphere, the vertical mean wind velocity is zero[3] and (2.3.4) can be written:-

$$R(\tau)=N_{5/6}\left[\tau\cdot\frac{V_y}{L_y}\right]\cdot e^{-\frac{1}{2}(\tau/\tau_o)^2} \qquad (2.3.5)$$

Unfortunately, there is no analytic function for the Fourier transform of (2.3.5) with the result that the corresponding frequency spectrum cannot be expressed analytically.

Nevertheless, for $\tau_o >> 1$, $e^{-\frac{1}{2}(\tau/\tau_o)^2} \approx 1$, and the exponential in (2.3.5) can be considered as a constant. In this case, the Fourier transform of $R(\tau)$ exists[116] and its analytic expression is:-

$$W(f) = A \frac{L_y/V_y}{(1 + (L_y/V_y)^2 . f^2)^{4/3}} \qquad (2.3.6)$$

For $(L_y/V_y)^2 . f^2 >> 1$, (2.3.6) can be written:-

$$W(f) = A(V_y/L_y)^{5/3} . f^{-8/3} \qquad (2.3.7)$$

This is an interesting result because the $f^{-8/3}$ dependence has been suggested by Tatarski[49] for the power spectrum of amplitude and phase fluctuations in line-of-sight paths.

From (2.3.7) it can be seen that an increase in cross-path mean wind velocity will cause a "spread" of the frequency spectrum towards higher frequencies.

CHAPTER 3

THE RADIO LINK : DESCRIPTION OF THE SYSTEM

A block schematic diagram of the system is shown in Fig. 3.1. Both the transmitting and receiving sections were manufactured by ITT Federal Laboratories, Nutley, New Jersey. They were especially designed as a complete system for high accuracy measurements of Transmission Path Loss in the U.H.F. band.

3.1 The Transmitter (NUS-3860)

A block diagram of the transmitting section is shown in Fig. 3.2. The Transmitter was crystal-controlled and provided a C.W. unmodulated output frequency of 900 MHz with a frequency stability of ± 6 Hz in 10 MHz. The power available at the output was 10 W.

The various stages of the transmitter, as shown in Fig. 3.2, can be briefly described as follows:-

(a) Stable Oscillator (NUS-3846):

As the Master oscillator for the transmitter, the Stable oscillator comprised of three stages of grounded-grid amplification driven by a grounded-grid crystal oscillator with an overall frequency stability approaching that of the crystal itself.

The crystal was type HC-6/U, manufactured in pairs. The members of each pair were matched to within ± 50 Hz of a difference frequency of 30/18 MHz. This was the first

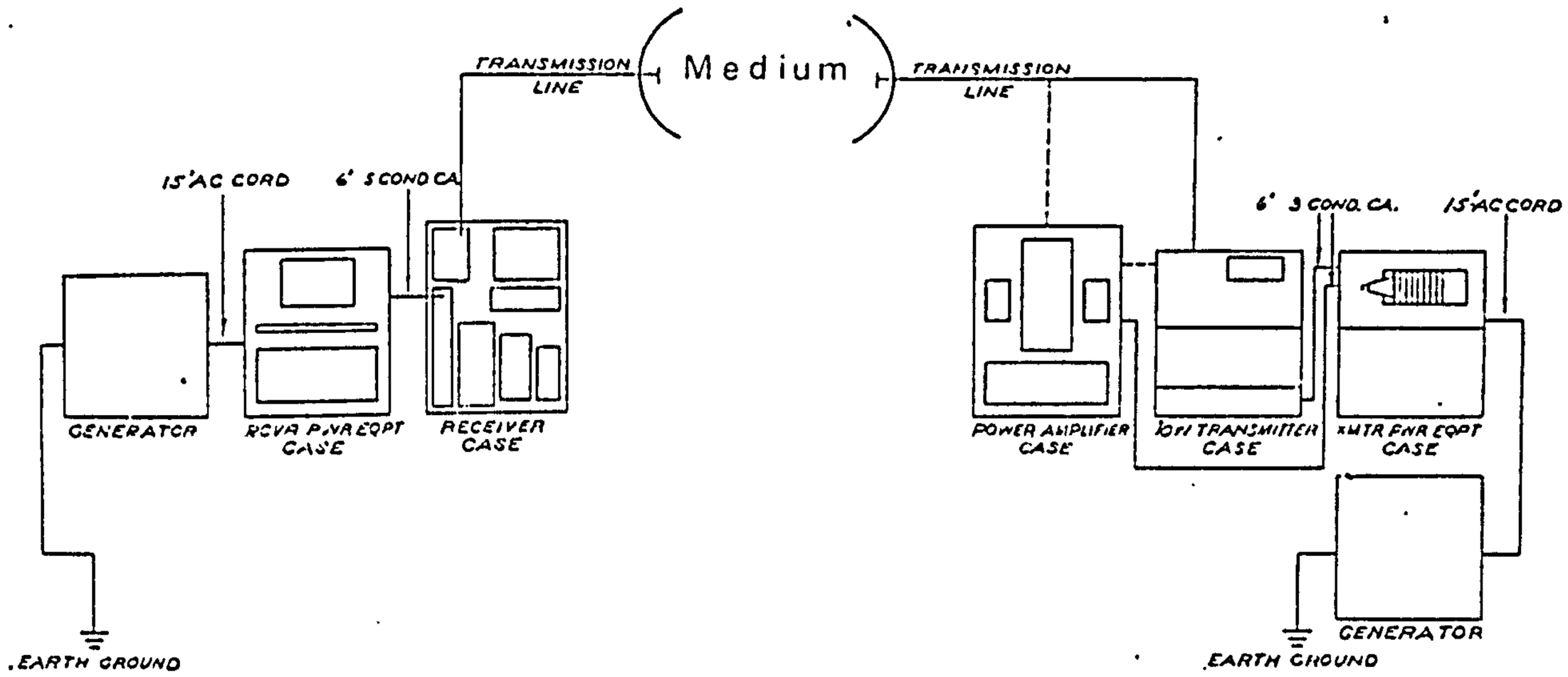

FIGURE 3.1 : Block schematic diagram of the Radio-system.

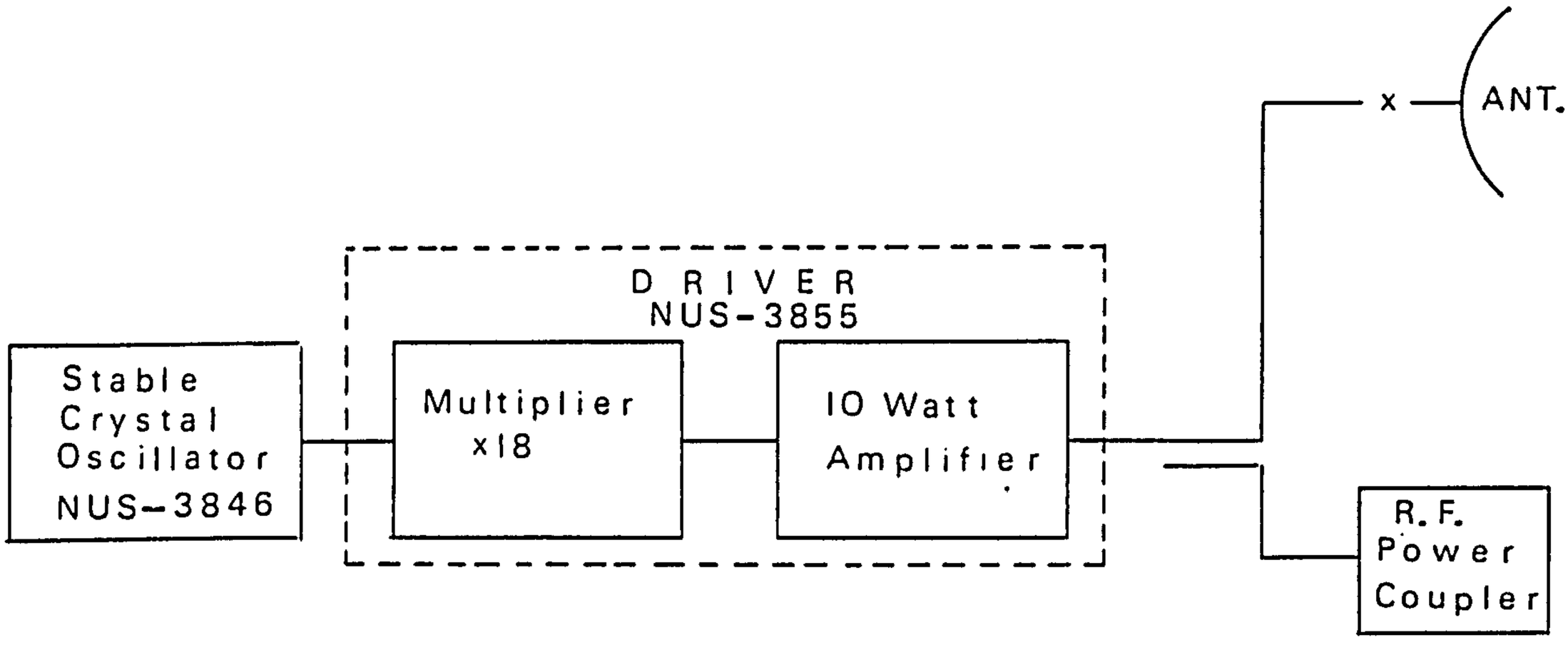

FIGURE 3.2: Block schematic diagram of the Transmitter.

receiver I.F. (30 MHz) divided by the crystal frequency multiplication factor (18). The higher frequency crystal of the pair was installed in the transmitter, thus, after the multiplication, the frequency to be transmitted was (48.33 MHz + 30/18 MHz) x 18 = 900 MHz.

The lower frequency (48.33 MHz) crystal was installed in the first local oscillator of the receiver. The crystal was mounted in an oven and kept at a constant temperature of $70^{o}C \pm 1^{o}C$ for an ambient temperature range of $-20^{o}C$ to $+50^{o}C$. The oven was constructed with a large outer case to provide ample thermal insulation.

(b) Driver (NUS-3855):

The function of the Driver was to multiply the frequency of the output signal from the stable oscillator by 18, and to amplify the signal at the final frequency to a power level of 10 watts. This R.F. power was then supplied, via a coaxial antenna feeder, to the transmitting antenna. Frequency multiplication and power amplification was accomplished by a succession of five vacuum tube stages as follows: amplifier, tripler, amplifier, tripler, doubler.

To permit accurate calibration of output power, a Micromatch Model 575.36 RF Power Coupler, manufactured by M. C. Jones Electronics Company, Bristol, Connecticut, was inserted into the transmission line connecting the driver output to the antenna.

The transmitting and receiving aerials were identical parabolic antennas of 12 ft. (3.66 m.) diameter.

Plate 3.1

Their beamwidth at the 3 dB points had been found from the relationship [11]:-

$BW = 68 \frac{\lambda}{D}$ (deg.) D = diameter, λ = wavelength

to be 6^{o} deg. approximately.

They were both provided with a horizontally polarized dipole feed and their elevation or "shoot" angle was zero. Plate 3.1 shows the receiving antenna on its supporting structure.

3.2 The Receiver (NUS-3863)

The Path Loss Measuring Receiver was essentially a very sensitive signal recording meter. Its threshold signal level, defined as signal equal to receiver noise, was determined by the receiver noise figure (9 dB or less above thermal). A 9 dB noise figure yielded a threshold signal level of - 138 dBm. The dynamic recording range of the receiver was 50 dB above threshold but the total range could be extended to 70 dB more by means of fixed attenuators in the input circuits.

A high inherent selectivity giving a 3 dB band-pass of 320 Hz was achieved by quadruple heterodyning with the following IFs: 30 MHz, 3.8 MHz, 262 KHz and 10 KHz. A block diagram is shown in Fig. 3.3.

In order to achieve the high degree of frequency stability necessary for an overall bandwidth of 0.35×10^{-4}% of the input frequency, each of the four local oscillators

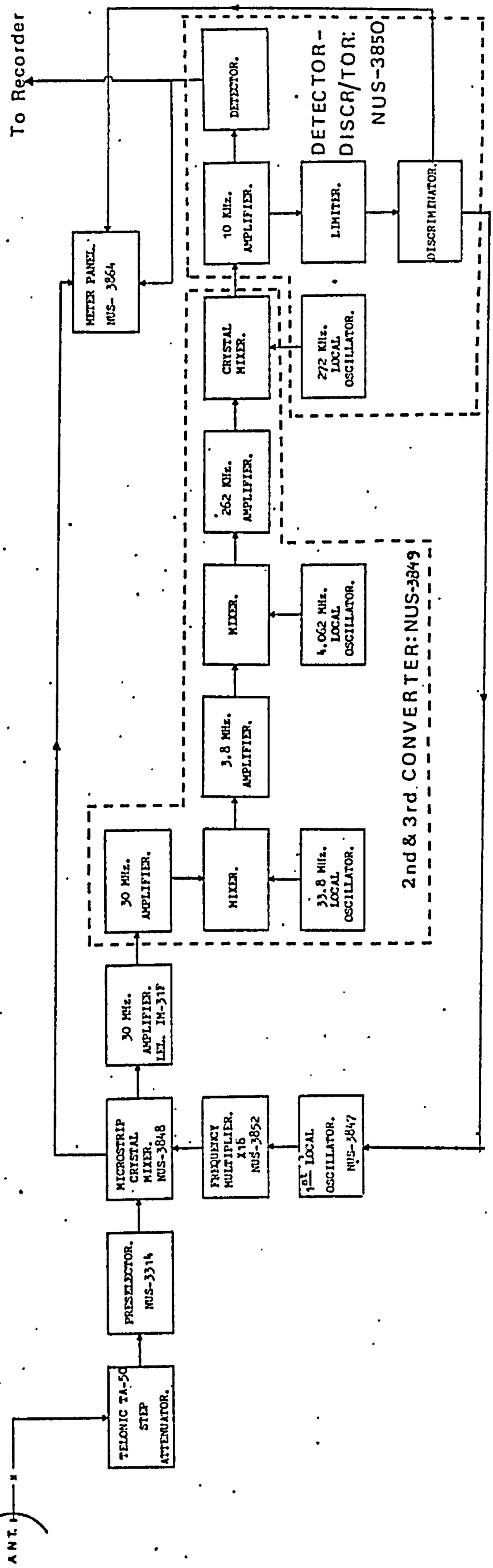

FIGURE 3.3: Block schematic diagram of the Receiver.

was crystal controlled and the first two were temperature stabilized. The effects of transmitter frequency drift and receiver local oscillator drifts were fully compensated by an automatic frequency control (AFC) loop from an output discriminator to the first local oscillator. If the overall drift was great enough to result in a last IF center frequency beyond the AFC capture range, then any of five crystals, 2 KHz apart, could be chosen by a switch at the third local oscillator to facilitate discriminator centering and capture.

A brief description of the units comprising the Receiver is the following:-

(a) Preselector (NUS-3314):

In order to eliminate image channel interference, a preselector in the form of a synchronous filter, tuned to the input frequency of the receiver, was provided to give a selectivity of 30 dB at ± 30 MHz and 50 dB at ± 40 MHz. The overall bandwidth was ± 3 MHz at the 3 dB points.

(b) First Local Oscillator (NUS-3847):

The first local oscillator was designed to cover the frequency range 46 to 51 MHz (with appropriate crystal). For this specific experiment, a 48.33 MHz crystal was employed. Frequency control was provided from the output descriminator which gave a frequency "pull" range of ± 115 Hz. This oscillator provided a signal at a stable frequency which, after multiplication by 18, was supplied to the mixer

to produce a first I.F. of 30 MHz.

(c) Local Oscillator Multiplier (NUS-3852):

Increasing the frequency of the signal from the first oscillator by a factor of 18, was obtained by four stages: a limiting amplifier, two triplers and a doubler. The output signal, at a frequency of 870 MHz and 30 MHz below the receiver operating frequency, was then applied to the first mixer.

(d) Mixer (NUS-3848):

This was a balanced mixer providing the first I.F. at 30 MHz generated from the receiver input signal and the output from the local oscillator multiplier.

(e) 30 MHz Amplifier:

This was an amplifier designed to provide 67 dB of gain for the 30 MHz output from the mixer. This gain was obtained from three cascaded low noise amplifier stages.

(f) Second and Third Converters (NUS-3849):

The second and third converters consisted of a 30 MHz amplifier, a 33.8 MHz local oscillator, a 3.8 MHz converter, a 4.062 MHz - 3.8 MHz oscillator-mixer, a 262 KHz amplifier, and a crystal mixer. Two stages of 30 MHz amplification provided a signal whose 3 dB bandwidth was approximately 100 KHz. Consequently, the selectivity of the 30 MHz amplifier provided ample rejection for the 3.8 MHz

image frequency. The 33.8 MHz second local oscillator was a crystal oscillator stabilized by means of an oven. The result of the 33.8 MHz - 30 MHz mixing provided a second I.F. of 3.8 MHz. This signal was converted into the third I.F. (262 KHz) after mixing with the output from a 4.062 MHz crystal oscillator. The frequency of this oscillator was variable in 2 KHz steps to ± 4 KHz away from 4.062 KHz by means of a manual selector switch which would connect any one of five crystals into the oscillator circuit. This provided a means of signal recapture by the AFC should the total frequency drift of Receiver versus Transmitter exceed the frequency pull range of the First Local Oscillator. The third I.F. signal was, thereafter, amplified by a 262 KHz amplifier and applied to a crystal mixer together with a 272 KHz signal provided by a local oscillator incorporated in the next stage.

(g) Detector Discriminator (NUS-3850):

This stage was composed of three circuits. The first was a 272 KHz crystal controlled local oscillator whose output was applied to the last mixer of the previous stage where it was mixed with the third I.F. to produce a 10 KHz signal or fourth I.F. The second circuit selectively amplified and rectified the 10 KHz signal to provide the D.C. output of the receiver. The third circuit was consisting of a limiter amplifier and a frequency discriminator which would detect the frequency error of the 10 KHz signal and derive a DC correction voltage for application to the

AFC input of the first local oscillator.

The built-in recorder of the Receiver was not used during the present experiment as its time constant of either five or ten seconds was not suitable for fast-fading measurements. Instead, the DC signal output of the detector was applied to a recording system suitable for either digital or continuous recordings.

3.3 Recording Apparatus

The recording apparatus was designed to provide facilities for the continuous low-speed recording of the d.c. signal from the Receiver output together with simultaneous high-speed digital recording in the form of punched paper-tapes. A block diagram of the recording system is shown in Fig. 3.4.

The first stage after the Receiver was a DC amplifier using a 741 OP-AMP integrated circuit. This was employed in order to increase the Receiver output signal level, which was in the range of some tens of a mV., to values of up to 1V required for the full deflection of the pen recorder. Thus, throughout the experiment a constant gain of 10 was adequate. There was also a provision for manual zero-setting so that the noise level could be adjusted to coincide with the zero level on the recorder chart.

A low-pass active filter followed, with a 3 dB cut-off frequency of 40 Hz. It was used to filter out any noise due to the mains supply.

The pen recorder used for the continuous recording

was a "RECORD" moving-coil equipment and its speed was set to 3"/hour.

For the digital high speed recordings, the signal was applied at the input of a "SOLARTRON" digital voltmeter whose sampling rate was externally set to 5 samples/sec by a simple pulse generator. The sampling rate was detected during the recordings by a frequency counter. The output of the D V/M was encoded into the C.D.C. version of the ASCll (8-track) code, suitable for processing by the I.C. Computer Unit.

The encoded signal was thence applied to a punch-drive unit and afterwards recorded on paper-tape by a high-speed paper punch.

There was also a facility for continuous monitoring of the received signal power Spectrum (fading-Spectrum) by means of a Real-Time Spectrum Analyser. This was arranged in order to ensure that frequencies higher than 2.5 Hz were not present in the fading spectrum of the received signal during the fast recordings. It also provided a good means of detecting the presence of aircraft on the transmission path during the recording. More extensive use of this facility was made during the laboratory simulation experiment where on-line fading spectra from the model were to be compared with fading spectra from the radio-link.

3.4 The Propagation Path

The transhorizon radio-link under investigation extended between SRDE, Christchurch, Dorset (transmitter)

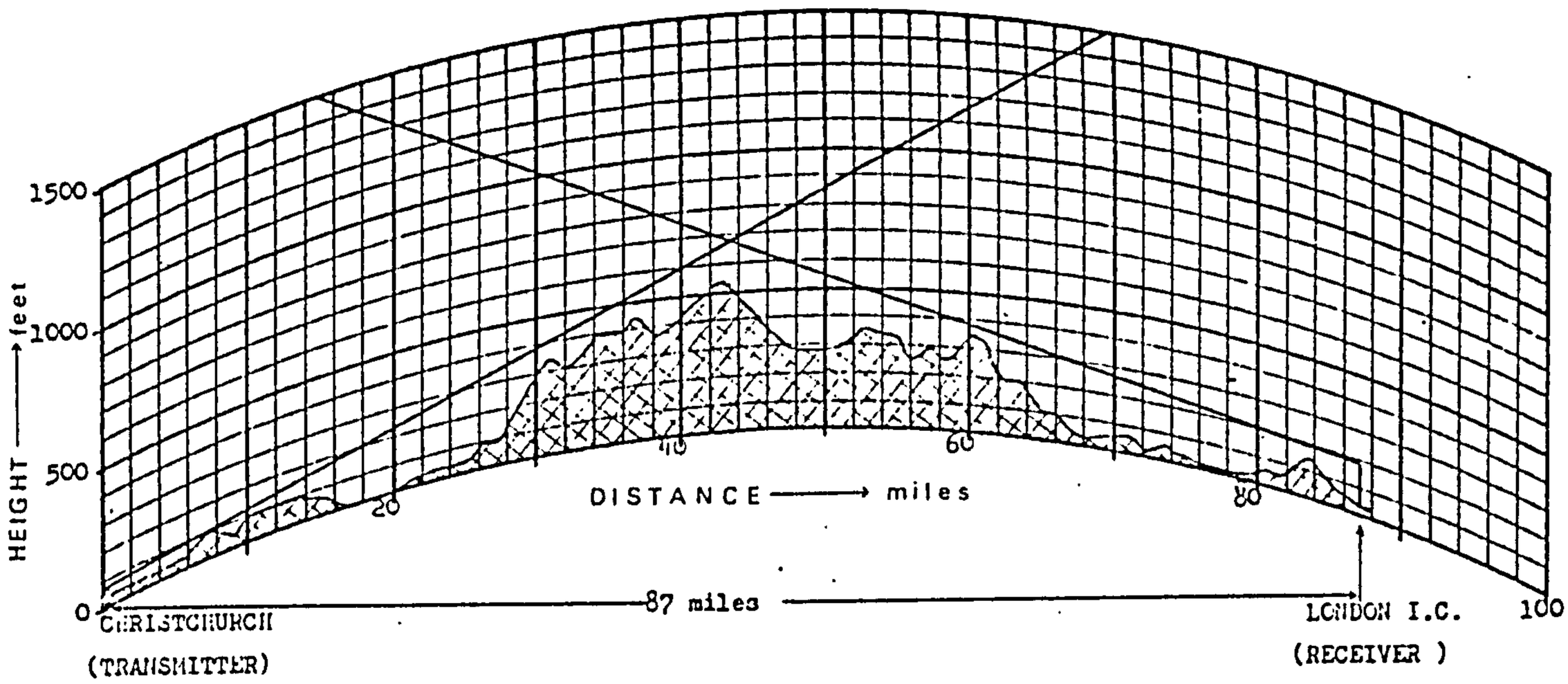

FIGURE 3.5: Vertical cross - section of the propagation Path terrain for a "4/3" effactive Earth radius.

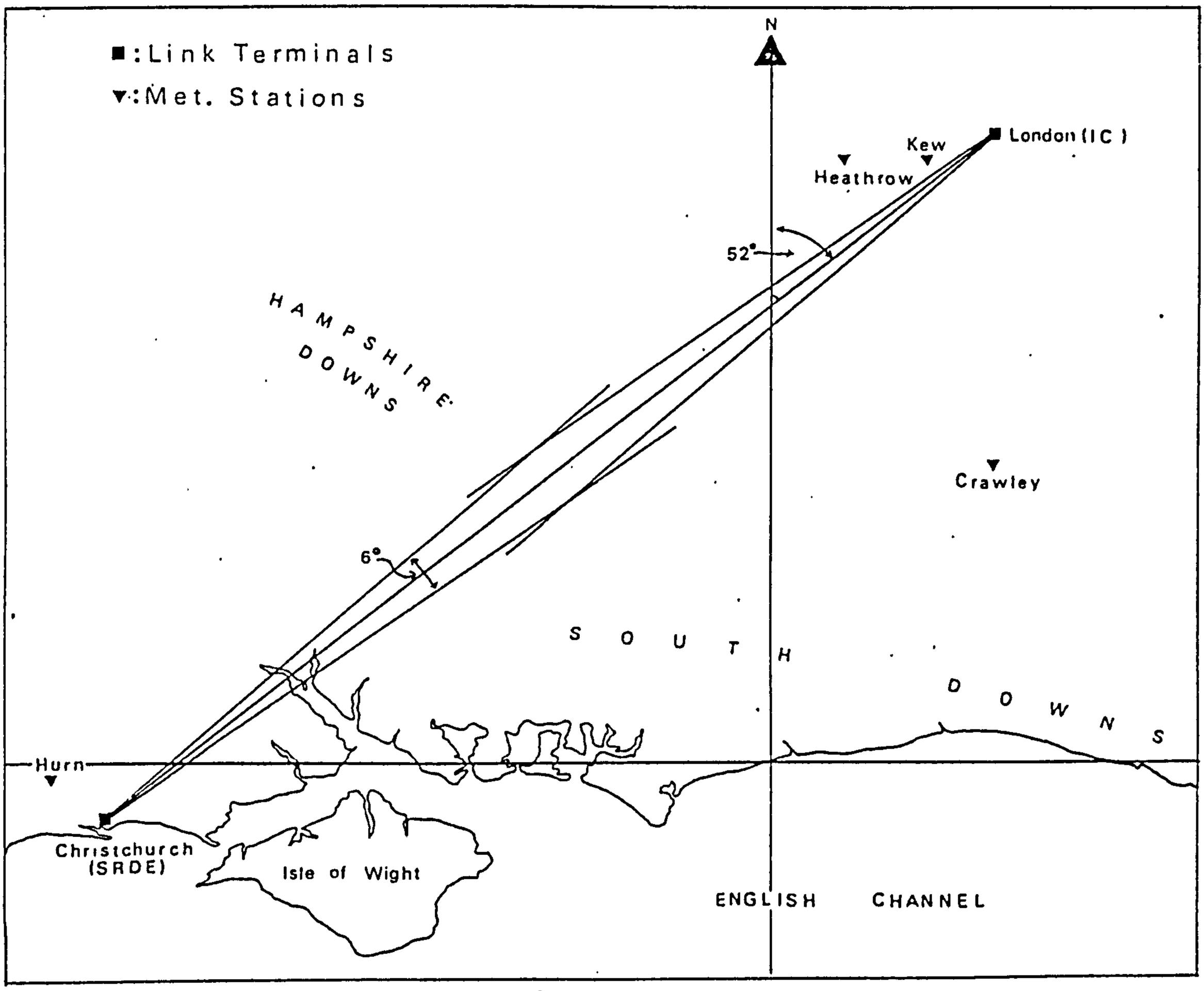

FIGURE 3.6: Geographic location and orientation of the Transhorizon Radio-link.

and Imperial College, South Kensington, London (receiver). The path length was 142 km. (87 miles). The transmitting antenna was sited at a height of 6 m. (20 ft.) above ground level at Christchurch. The receiving antenna was sited on the roof of the Electrical Engineering Department, Imperial College at a height of 44 m. (145 ft.) above ground level. Fig. 3.5 shows the path profile drawn for an effective Earth radius of $\frac{4}{3}$ R and allowing for the refractive effects of a standard atmosphere. It can be seen that the underlying terrain would not obstruct the axes of the two radio-beams.

It can also be seen that due to the morphology of the terrain, the "common volume" centre was only 50 - 60 m. above the ground. Thus, meteorological phenomena in the vicinity of the ground were likely to affect the performance of the radio link.

Fig. 3.6 shows the exact geographical location of the radio-link, the azimuthal angle between the propagation great circle and the North and the location of the Meteorological Stations with respect to the path.

For more than two-thirds of the path length, the underlying terrain was farmland with low vegetation or grass. The existing low hills are rolling gently and are cultivated. The rest of the terrain was urban area, south-west London and Southampton mainly, of the residential suburban type with relatively small structures. Thus, it can be suggested that the path profile, in propagation terms, might be assumed "smooth".

CHAPTER 4

DATA PROCESSING

4.1 Meteorological Data

All the Meteorological Data that has been used in the present investigation was obtained from the two Meteorological Office issues: the Daily Weather Report (D.W.R.) and the Daily Aerological Record (D.A.R.). The Daily Weather Report gives the results of surface observations made in the Northern Hemisphere, whilst the Daily Aerological Record gives the results of observations made in the upper atmosphere over the same region. These Reports are the only information available to the planning engineer and they are readily available from the Meteorological Office.

The essential surface Meteorological Data of interest and provided by the D.W.R. was: wind speed, wind direction and temperature. The results of observations made and recorded at 12.00 and 18.00 hours daily by the Meteorological Stations of Hurn, Kew and Heathrow, lying at distances of 5, 2 and 6 miles respectively from the propagation path, were used throughout the investigation.

The wind speed and direction Data is presented in the standard FM11D code for land Stations where the wind speed is given in knots (1 knot = 0.516 m/sec). The wind direction is given on a 01 - 36 scale, each unit corresponding to a compass direction. The interval between two consecutive units is 11¼ degrees.

For the purpose of this investigation, the wind

direction was considered in terms of the acute angle between the wind velocity vector and the propagation path. This angle was evaluated in the following way:

Let α be the azimuthal angle of the propagation path ($\alpha = 52^{o}$ deg.), θ_w the equivalent in degrees of the wind direction reported in the D.W.R. and ϕ the wind direction relative to the path. Then:-

$$\phi = \begin{cases} |\theta_w - \alpha| & \text{for } 0 \leq \theta_w \leq \frac{\pi}{2} + \alpha \\ |\pi - \theta_w + \alpha| & \text{" } \frac{\pi}{2} + \alpha < \theta_w \leq \frac{3\pi}{2} + \alpha \\ |2\pi - \theta_w + \alpha| & \text{" } \frac{3\pi}{2} + \alpha < \theta_w < 2\pi \end{cases} \quad (4.1.1)$$

Since the surface temperature is reported in ^{o}C, it was used as such.

In some instances, observations from a particular Meteorological Station were used separately. This was done in order to investigate the significance of the Station location with respect to the path, i.e. to what extent meteorological parameters recorded in the vicinity of one of the two terminals were related to the received signal. However, in most of the investigations, the three-Station-average values of the observations were used. It was considered that such an average is more representative of the value of a specific meteorological parameter over the whole of the path.

The upper air data, recorded twice daily (12.00 and 24.00 hours) at Crawley, 20 miles from the propagation path, was used to evaluate the temperature lapse rate for

the first kilometre of the atmosphere. This also allowed the Static Stability parameter to be determined for the same region by the following procedure.

Air temperature values at the altitude of the first standard isobaric surface (850 mb) were taken from the D.A.R. together with the height of this surface from mean sea-level. From these values and by means of a Tephigram (see Appendix III for example), the corresponding values of potential temperature at the 850 mb altitude were estimated. The potential temperature at the surface is almost equal to the actual surface temperature which was given in the D.A.R.

From the expression (1.3.7), it is known that the Static Stability is equal to:-

$$S = \frac{g}{\theta} \frac{d\theta}{dh} \quad (sec^{-2})$$

where g is the acceleration of gravity, θ the potential temperature and $\frac{d\theta}{dh}$ the vertical gradient of θ. As $\frac{1}{\theta} \frac{d\theta}{dh} = \frac{d(\ln\theta)}{dh}$, the above-mentioned expression can be written:-

$$S = g \frac{d(\ln\theta)}{dh} \simeq g \frac{\Delta \ln\theta}{\Delta h} \qquad (4.1.2)$$

where Δ denotes differences. This expression has been used for the practical evaluation of the Static Stability parameter after the substitutions:-

$$\Delta \ln\theta = \ln\theta_1 - \ln\theta_0 \text{ and } \Delta h = h_1$$

θ_1 and θ_0 being the potential temperatures at the altitude of 850 mb and at ground level respectively, and h_1 being the height of the 850 mb surface in metres.

4.2 Received Signal Processing

The envelope-detected received signal was sampled regularly twice a day at 12.00 hours and 18.00 hours, so that the time of recording would coincide with the time of meteorological observations carried out by the Meteorological Office. The duration of each recording (record length) was chosen to be 3½ minutes. In this way, the effects of micro-meteorological fluctuations (periods less than 3 minutes) were included, whereas the effects of mesometeorological fluctuations (periods greater than 10 minutes) were excluded. In fact, the 3½ minutes period falls into the "spectral gap" of atmospheric processes, already mentioned in Section 1.2. As a result, all the records were free of very low frequency variations, essentially from diurnal variations, etc.

During the time of sampling, the received signal was analysed by the SAI-51 real time Spectrum Analyser and the instantaneous spectrum was displayed on a cathode ray oscilloscope. An aircraft crossing the "common volume" could be detected from the Doppler shift and spread that appear in the spectrum. In such a case, the record was rejected and the measurement was repeated.

Spectral analysis was chosen as the most suitable method of investigating the fast fading characteristics of

the received signal. The reasons behind this choice were the following:-

(1) The fading power spectrum can be considered as the "response" of the propagation medium in the frequency domain. Thus, similarity between fading power spectra implies a similarity in the propagation conditions under which the corresponding signals have been received. The laboratory simulation experiment has been based on this assumption.

(2) Power spectral density functions can be easily expressed analytically. Thus, the effects of the propagation medium can be possibly identified from the variations they impose on the parameters of such analytic functions.

(3) As already discussed in Section 2.3, the problem of fading in a signal received beyond the horizon has been theoretically approached by means of the fading power spectrum. This allows for comparisons between experimentally obtained spectra and theoretically derived ones.

In what follows, some theoretical considerations involved in spectral analysis, together with some practical aspects, will be discussed.

4.2.1 Some Theoretical Considerations of Spectrum Analysis

The most common methods for the computation of power

spectra are[118]: (a) The "Blackman-Tuckey" method of computing the power spectral density function via its Fourier transform relation to the autocorrelation function, and, (b) The "Cooley-Tuckey" method of computing the power spectral density function via a Fast Fourier transform of the original time series. In the present investigation, the second method of computation has been selected because it does not require the intermediate computation of the Auto-correlation function. Thus, only one Fourier transform has to be performed and this reduces considerably the computer execution time. The Fourier transform pair for continuous signals can be written in the form:-

$$X(f) = \int_{-\infty}^{\infty} x(t) \exp\ (- j2\pi ft)\ dt$$

$$x(t) = \int_{-\infty}^{\infty} X(f) \exp\ (+ j2\pi ft)\ df \qquad (4.2.1a)$$

The corresponding form for sampled functions, known as the discrete Fourier transform, can be written as:-

$$X(n) = \sum_{k=0}^{N-1} x(k) \exp\ (- j2\pi nk/N)$$

$$x(k) = \sum_{n=0}^{N-1} X(h) \exp\ (+ j2\pi kn/n) \qquad (4.2.1b)$$

where k = 0, 1, ... N-1; n = 0, 1 .... N-1. The functions x(t), X(f) are generally complex.

The power spectrum of a time series x(k), k = 0, 1 .... N-1, is given by the expression:

$$P(n) = \frac{2\Delta t}{N} |X(n)|^2, \quad n = 0, 1 .... \frac{N+1}{2} \qquad (4.2.1c)$$

However, the transformation of x(k) via a F.F.T. and the computation of (4.2.1c) does not lead to adequately correct estimates of P(n) to give the power spectral density distribution of the original time series. The digital nature of a time series and its limited record length impose serious problems in the computation of the power spectrum. The most serious of them appear to be aliasing, leakage, reduction of the standard error of estimation and the picket-fence effect.

These problems have been considered in relevant monographs[118][119][120] and papers[121][122][123] and efficient methods to solve them have been proposed. In what follows, a brief description of the problems and the proposed methods for their solution will be discussed.

(1) Aliasing:

This is an effect which arises whenever an analogue signal is sampled at a rate much lower than the high frequency components present in the signal. If the sampling frequency is f_S, then the "folding" or Nyquist frequency of the power spectrum is $f_N = f_S/2$[118][119]. This is the frequency beyond which the spectrum is repeated as a mirror image. If a frequency higher than f_N is present in the analogue signal during sampling, then this frequency will

impersonate frequencies lower than f_N[118] and will appear as such in the frequency spectrum. For instance, if f_S = 10 Hz and f_N = 5 Hz, then a frequency of f = 6 Hz present in the original signal will appear in the frequency spectrum as a frequency component at $f' = f_N - f = 4$ Hz.

This problem may be overcome by fulfilling the condition:-

$$f_N = f_S/2 \geq f_h$$

where f_h is the highest frequency present in the original analogue signal. If f_h is known for a given signal, then f_S can be chosen accordingly. Otherwise, the original signal must be passed through a low-pass filter with cut-off frequency at most half the sampling frequency.

(2) Leakage:

This problem is due to the fact that the record has a finite length of duration. If this length is T seconds, then the record to be analysed is equivalent to the product of an infinite time series multiplied by a rectangular window W(t) of amplitude 1 and a width of T seconds. It is well-known[118][122] that the F.T. of the product of two functions is the convolution of the F.Ts of these functions. If the function to be transformed is a sinusoid with frequency f_1, then its spectrum should consist of a single spectral component at f_1. Instead, due to the process described before, the resulting spectrum is a

function of the form (sinx)/x centered about f_1. For a more composite time series, the (sinx)/x function appears in the place of every single spectral line. In this case, the sidelobes of neighbouring (sinx)/x functions may interfere creating frequency components which were not present in the original time-series. The contribution of a given frequency can be localised by reducing the "leakage" through the side-lobes. This can be achieved by multiplication of the time series by a data window which has lower sidelobes in the frequency domain than the rectangular data window.

A variety of such windows have been proposed[119], some of which are:-

The extended Cosine Bell, having the analogue form:-

$$A = 0.5\left(1 - \cos 2\pi \frac{5t}{T}\right), \text{ for: } 0 \leq t \leq \frac{T}{10} \text{ and } \frac{9T}{10} \leq t \leq T$$

$$A = 1 \qquad \text{for } \frac{T}{10} < t < \frac{9T}{10} \qquad (4.2.1d)$$

The Triangle or Bartlett window

$$A = 2t/t \qquad \text{for } 0 \leq t < T/2$$

$$A = 1\ 2t/T + 2 \qquad \text{for } T/2 \leq t \leq T \qquad (4.2.1e)$$

The Cosine or Hanning window

$$A = 0.5(1 - \cos 2\pi t/T) \quad \text{for } 0 \leq t \leq T \qquad (4.2.1f)$$

The Hamming window

$$A = 0.08 + 0.46(1 - \cos 2\pi t/T) \quad \text{for } 0 \leq t \leq T \qquad (4.2.1g)$$

The choice of any of these windows depends on the specific case; usually a considerable reduction of leakage is followed by a reduction in the main lobe height and a decrease of frequency resolution.

(3) d.c. spikes:

If the signal to be processed has a d.c. component, then the power spectrum will have a large peak at zero frequency. This will distort the very low frequency part of the spectrum and will reduce the relative magnitude of all the other frequency components.

The d.c. level can be easily set to zero by calculating and subtracting the mean of the original time series[122].

Sometimes the signal has a linear trend of the form: $x(t) = a + b \cdot t$. This is interpreted by the F.F.T. as a small section of a periodic function with a very low frequency and will result in an unwanted, very low frequency spike in the spectrum.

The removal of a linear trend involves the calculation of the regression line and slope of the original time series and their subtraction.

The process of excluding the mean and the trends from a time series is known as "prewhitening"[122].

(4) Reduction of the standard error of estimation and smoothing:

It has been shown[118][119] that the normalized standard error of estimation of a spectral component is:-

$$\varepsilon_r = \sqrt{\frac{2}{n}}$$

where n is the degree of freedom of the estimate. In the case of a "raw" estimate, i.e. an "unsmoothed" estimate resulting from the relation:-

$$P_{raw}(k) = |X(k)|^2 = \left[\mathrm{Re}\{X(k)\}\right]^2 + \left[\mathrm{Im}\{X(k)\}\right]^2 \qquad (4.2.1h)$$

the degrees of freedom are n = 2 because each $P_{raw}(k)$ is the sum of the squares of Re{X(k)} and Im{X(k)} which are two independent Gaussian variables[118]. Thus, for a "raw" estimate, n = 2 and ε_r = 1 and the spectral estimate is inconsistent.

The process of the reduction of ε_r is also called "smoothing" because of its effect of reducing the "roughness" of the spectrum whenever it is plotted. In practice, smoothing can be performed by two different methods[118].

The first method is by computing spectral estimates from q independent records and then averaging the q estimates at each frequency of a spectral component. This amounts to an ensembe smoothing procedure.

The second method is to smooth in the frequency domain. This can be achieved by averaging ℓ successive "raw"

components from a single record and substituting the resulting value at the $\ell/2$ position. This is repeated for successive intervals containing ℓ estimates each. It is easily proved[118] that if $q = \ell$, the two methods are equivalent.

After the smoothing procedure, the degrees of freedom for each smoothed estimate become $n = 2q$ or $n = 2\ell$ and the standard error of estimation is:-

$$\varepsilon_r = \frac{1}{\sqrt{q}}, \text{ for ensembe averaging of q records}$$

$$\varepsilon_r = \frac{1}{\sqrt{\ell}}, \text{ for frequency averaging of } \ell \text{ successive estimates}$$

An unwanted effect of smoothing in either way is the reduction of the final number of smoothed estimates and, consequently, the reduction of the frequency resolution.

4.2.2 The Estimation of the Power Spectrum

In this subsection, a description will be given of the adopted methods for the solution of the previously discussed problems. Each of these methods is described under the heading of the specific problem which must be overcome.

(1) Aliasing:

Preliminary tests and on-line analysis of the received signal by means of the real-time spectrum analyser

had revealed that the spectrum almost never had components with frequencies higher than 2.5 Hz. Therefore, a sampling rate of 5 Hz was chosen, corresponding to a folding frequency of 2.5 Hz. For safety, the range 2 - 2.5 Hz was excluded from further analysis. Thus, even if components of up to 3 Hz were occasionally present, they would not alias the part of the spectrum under consideration. As the mains supply is always a potential source of unwanted frequency components, an active filter with a cut-off frequency of 40 Hz was used after the detection.

(2) Leakage:

To avoid leakage, a Hamming data window was used with the analogue form given in equation (4.2.1g) and a digital form:-

$$A(k) = 0.08 + 0.46(1.0 - \cos 2\pi k/N) \quad k = 1 \ldots N$$

This operation in the computer program was performed by the subroutine TAPER.

The Hamming data window was chosen because it suppresses the highest side-lobe - 41.9 dB below the major lobe. At the same time, the frequency resolution is reduced by only 80%[123].

(3) Prewhitening:

The signal was prewhitened by the subtraction of its mean value and of any linear trend, if present. The

operation in the computer program was performed by the subroutine REGRE.

After these operations, the resulting time series was Fourier transformed by means of an F.F.T. subroutine (FASTF)[124]. The execution time for this subroutine running on the CDC 6400 was 0.357 seconds for N = 1024 number of samples[125].

The output of the F.F.T. consisted of two arrays containing the real and imaginary parts of the transform. The power spectral estimates were computed by means of (4.2.1h) for N/2 = 512 samples.

(4) Smoothing:

The next operation was smoothing of the spectral estimates and, consequently, the reduction of the normalised standard error of estimation. That was performed by means of a "running" average in the frequency domain of the form:-

$$P(n) = \frac{1}{q+1} \sum_{q=1}^{11} P_{raw}(n+q) \qquad n = 0, \ldots \frac{N}{2} - 11$$

The smooth estimates obtained by this procedure had 22 degrees of freedom and the standard error of estimation was $\varepsilon_r = \frac{1}{\sqrt{11}} = 0.3$, i.e. 33%.

An advantage of this "running" average procedure was that $\frac{N}{2} - q = 501$ estimates were obtained whereas, by the usual averaging procedure, only $\frac{N}{29} \simeq 22$ estimates would be obtained. After smoothing, each set of spectral estimates were normalised to the value of the maximum estimate. In

this way, all the spectra had estimates ranging from 0 to 1 and could be plotted on the same scale, a fact that facilitated the quantitative comparison of different spectra.

Finally, the normalised linear spectrum was plotted by means of the subroutine POWPLO in the KINGMATIC system of the CDC 6400. In part of the investigation, a logarithmic spectrum with fewer, but more consistent, spectral components was needed. In this case, the already smoothed estimates were further averaged in groups of 10. That increased the degrees of freedom of the resulting estimates to n = 2 . 11 . 10 = 220 and the standard error of estimation was reduced to:-

$$\sqrt{\frac{2}{220}} = \frac{1}{\sqrt{110}}\ 0.095 \simeq 10\%$$

A least-square polynomial fitting subroutine (EOZABF) was used to fit a curve to these estimates and the result was plotted on logarithmic scale (subroutine LOGPLO).

Figure 4.1 is a block diagram of the steps followed by the computer program. Sections A and B refer to the two different smoothing and plotting procedures.

A list of the main program and the subroutines can be found in Appendix IV.

4.2.3 A Suitable Measure of the Spectrum "Spread"

After the processing of the first few records, it became apparent that the spectrum "spread" towards higher frequencies was a dominant effect. In order to establish a

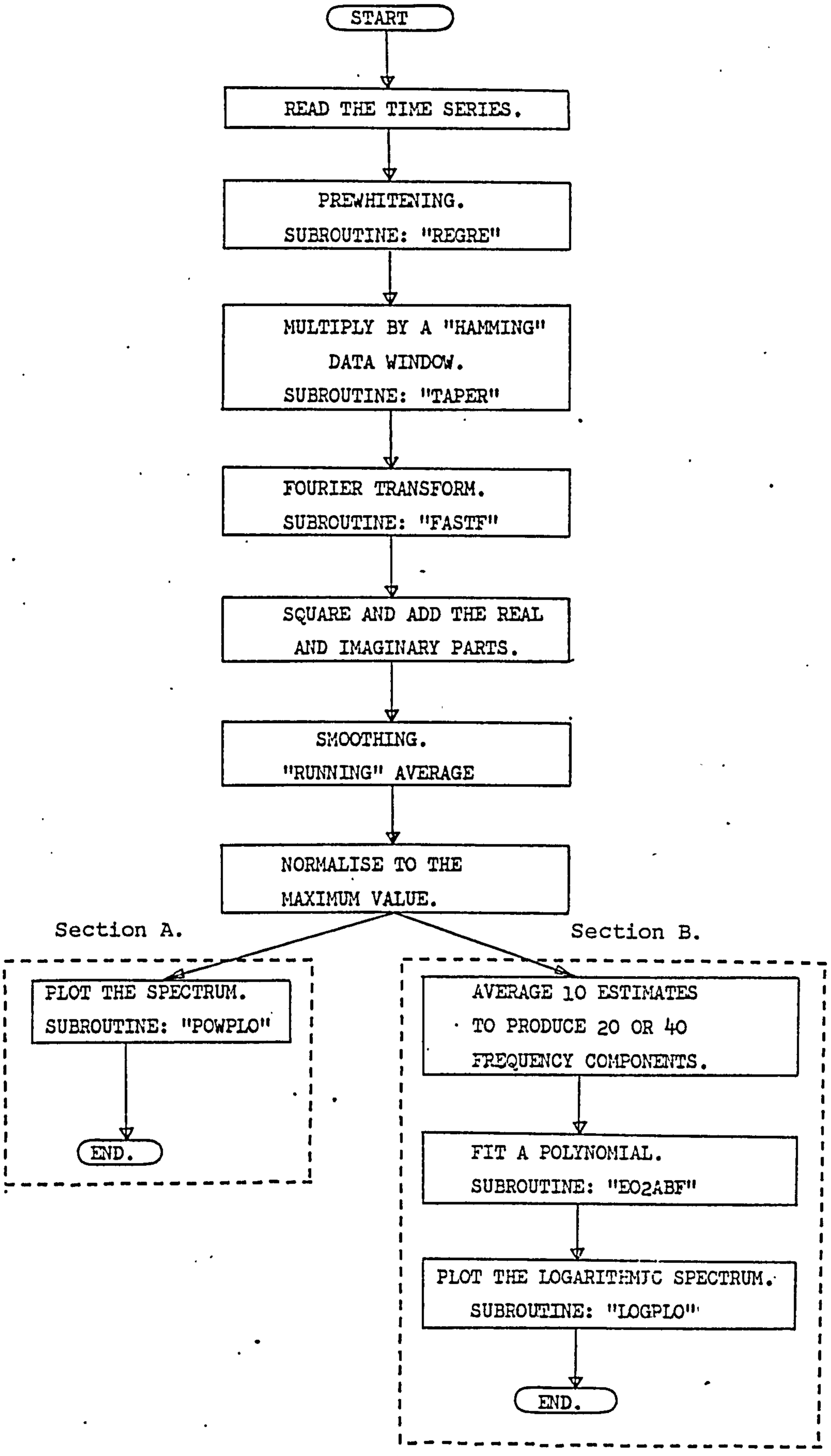

FIGURE 4.1: "Flow-chart" of the programme and subroutines for the estimation and plotting of the fading Power Spectrum.

qualitative relationship between the meteorological parameters under investigation and this effect, a suitable measure of the "spread" should be found. Fig. 4.2 shows a fading spectrum with apparent "spread". It can be seen that due to the irregular shape of the spectrum, more than one frequency may correspond to a fixed value of normalised power (say 0.5 or $1/\ell$). Thus, it would be rather dubious to use a measure of this type for the spectrum "spread".

On the other hand, only one spectral component corresponds to a certain frequency. For this reason, the magnitude of a fixed spectral component at f = 1 Hz was chosen as the most suitable measure of the spectrum "spread". The only reason for the choice of this particular component was that it lies in the middle of the spectral range under consideration (0 to 2 Hz).

In part of this investigation, instead of the fading Power Spectrum, the fading Amplitude Spectrum or simply the "fading Spectrum" has been used. This is defined as:-

$$W(f) = \sqrt{P(f)}$$

Its use had been dictated by the fact that $W(f) \geq P(f)$ because $P(f) \leq 1$ for any f. Thus, estimations of spectral components from plots could be made with smaller normalised standard error of estimation. Indeed, if dP is the error in the estimation of P, then:-

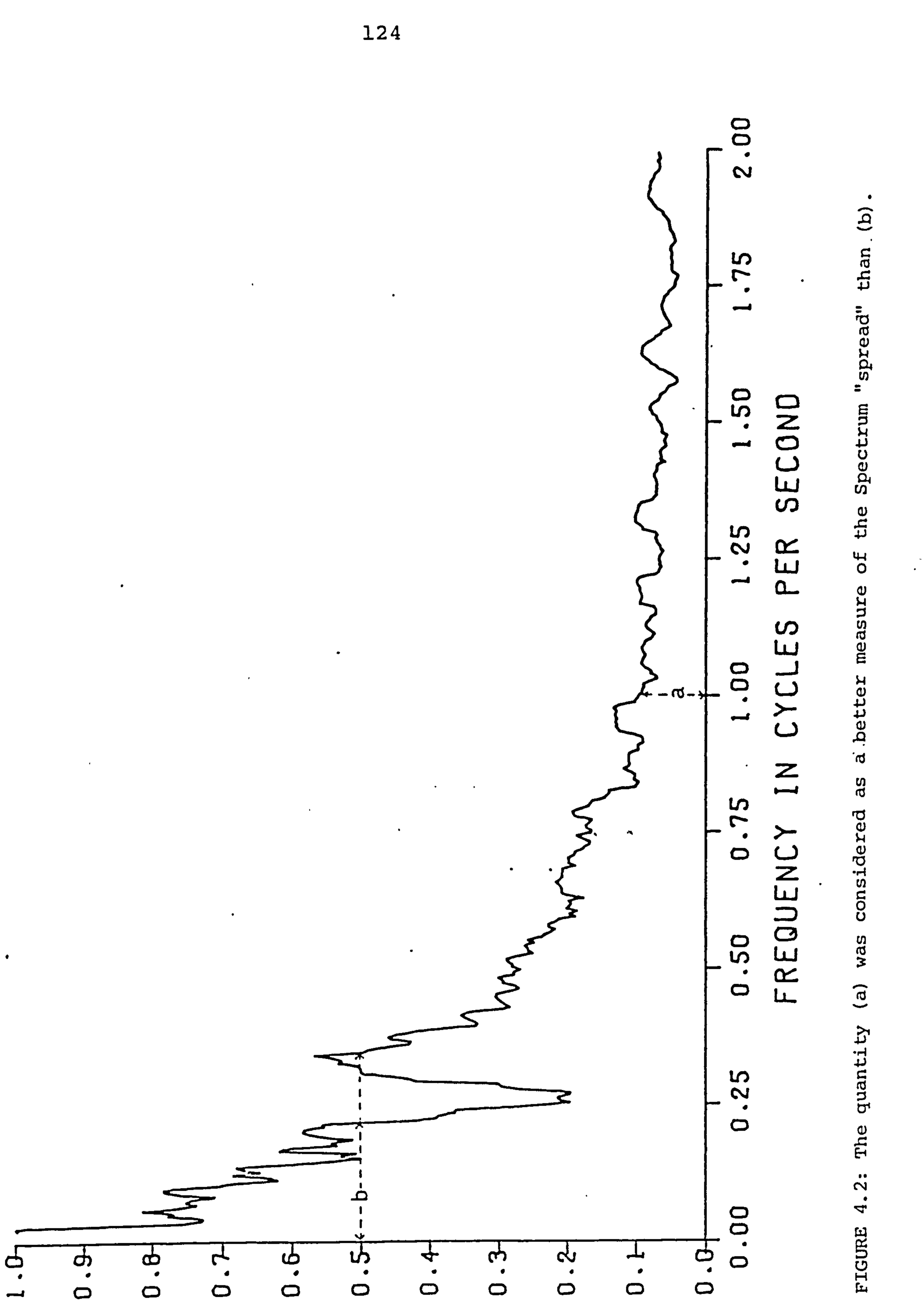

FIGURE 4.2: The quantity (a) was considered as a better measure of the Spectrum "spread" than (b).

$$\varepsilon_r = \frac{dP}{P}$$

and:-

$$\varepsilon_r' = \frac{d(P^{\frac{1}{2}})}{P^{\frac{1}{2}}} = \frac{1}{2}\,\frac{P^{-\frac{1}{2}}dP}{P^{\frac{1}{2}}} = \frac{1}{2}\,\frac{dP}{P} = \frac{1}{2}\,\varepsilon_r$$

4.3 Simple and Partial Correlation and Linear Regression

For many problems, it is of primary interest to know whether two or more random variables are inter-related. The existence of an inter-relationship and its relative strength can be measured in terms of a correlation coefficient defined as[126]:-

$$r_{xy} = \frac{n \cdot \sum_{i=1}^{n} x_i\, y_i - \sum_{i=1}^{n} x_i \cdot \sum_{i=1}^{n} y_i}{\left[\left(n \sum_{i=1}^{n} x_i^2 - \left(\sum_{i=1}^{n} x_i\right)^2\right)\left(n \sum_{i=1}^{n} y_i^2 - \left(\sum_{i=1}^{n} y_i\right)^2\right)\right]^{\frac{1}{2}}} \qquad (4.3.1)$$

where x_i, y_i are the random variables and n is the number of pairs of such variables.

The correlation coefficient r_{xy} lies between - 1 and 1 and has a bounding value only when there is a perfect linear relationship between the variables. A non-linear relationship or a data scatter would force the value of r towards zero.

Sometimes, it is of interest to be able to calculate the correlation coefficient between two variables

with the effect of one or more other variables removed. Such a correlation coefficient is known as a partial correlation coefficient and is given as[126]:-

$$r_{xy,z} = \frac{r_{xy} - r_{xz} \cdot r_{yz}}{\left[(1 - r_{xz}^2)\ (1 - r_{yz}^2)\right]^{\frac{1}{2}}} \qquad (4.3.2)$$

where x, y are the variables whose correlation is investigated and z is the variable whose effect is to be removed.

In some cases during the present investigation, the value of the coefficient of correlation between two variables suggested that a linear relationship could exist between the variables and that predictions could be made for one of them based upon specific values of the other.

The description of the relationship between two random variables by a linear model is the subject of regression analysis. The details can be found in any mathematical textbook[118][126]. The basic problem of linear regression is the estimation of the two parameters a (intercept) and b (slope) of the relationship:-

$$y = a + b \cdot x$$

This is usually done by the method of minimising the sum of the squared deviations of the observed values from the predicted values of y (least-squares fit). This method yields the expressions:-

$$a = \frac{\sum_{i=1}^{n} x_i \cdot \sum_{i=1}^{n} (x_i \cdot y_i) - \sum_{i=1}^{n} y_i \cdot \sum_{i=1}^{n} x_i^2}{\left[\sum_{i=1}^{n} x_i\right]^2 - n \cdot \sum_{i=1}^{n} x_i^2} \qquad (4.3.3)$$

$$b = \frac{\sum_{i=1}^{n} x_i \cdot y_i - \frac{1}{n} \cdot \sum_{i=1}^{n} x_i \cdot \sum_{i=1}^{n} y_i}{\sum_{i=1}^{n} x_i^2 - \frac{1}{n}\left[\sum_{i=1}^{n} x_i\right]^2} \qquad (4.3.4)$$

In the present investigation, correlation and linear regression have been performed by the same computer routine (SR of the STATPAK library) in the APL/360 system. A description and listing of the routine can be found in Appendix V.

CHAPTER 5

THE RADIO-LINK: EXPERIMENTAL INVESTIGATION

This chapter contains a detailed description of the experimental procedure, and the results obtained from the investigation of atmospheric fading experienced on the UHF transhorizon radio-link.

The investigation has been divided into two sections, the first concerning the long-term variations in median received signal level on a monthly and annual basis, the second dealing with the fast-fading characteristics of the received signal on a 3.5 mins. time-basis. In the former section, monthly averages of some meteorological parameters in relation to the monthly median level of the received signal are investigated, together with the influence of frontal activity upon the performance of the radio-link.

In the latter, the effects of some meteorological parameters upon the fading spectrum of the received signal are investigated both qualitatively and quantitatively.

It is anticipated that the results from this study will serve as a guideline for the simulation of the same effects in the laboratory.

5.1 Long-Term Effects of the Atmosphere Upon the Received Signal

For the study of long-term effects, the continuous records from the pen recorder have been used. The signal level is given in the form of attenuation relative to the maximum level of signal recorded during the period of measurements.

The meteorological Data used in this study was provided by the Monthly Weather Report, issued by the Meteorological Office. Each Report contains average and extreme values of temperature, sunshine, surface wind velocity and precipitation recorded during a month at various Meteorological Stations in the United Kingdom.

The long-term effects studied were the following:-

(a) Monthly and 10-day median levels for the year 1973 in relation to the monthly averages of some meteorological parameters.

(b) Diurnal variations under different weather conditions.

(c) Influence of the frontal activity upon the signal.

5.1.1 Monthly and 10-Day Median Received Signal Levels

Continuous recordings during the year 1973 could be carried out only during the day as the transmission time was limited between 09.30 and 18.30 hours. Thus, the reported median levels represent daytime values only. The

a) MONTHLY & 10-DAY MEDIAN LEVEL BELOW MAXIMUM RECORDED. YEAR: 1973

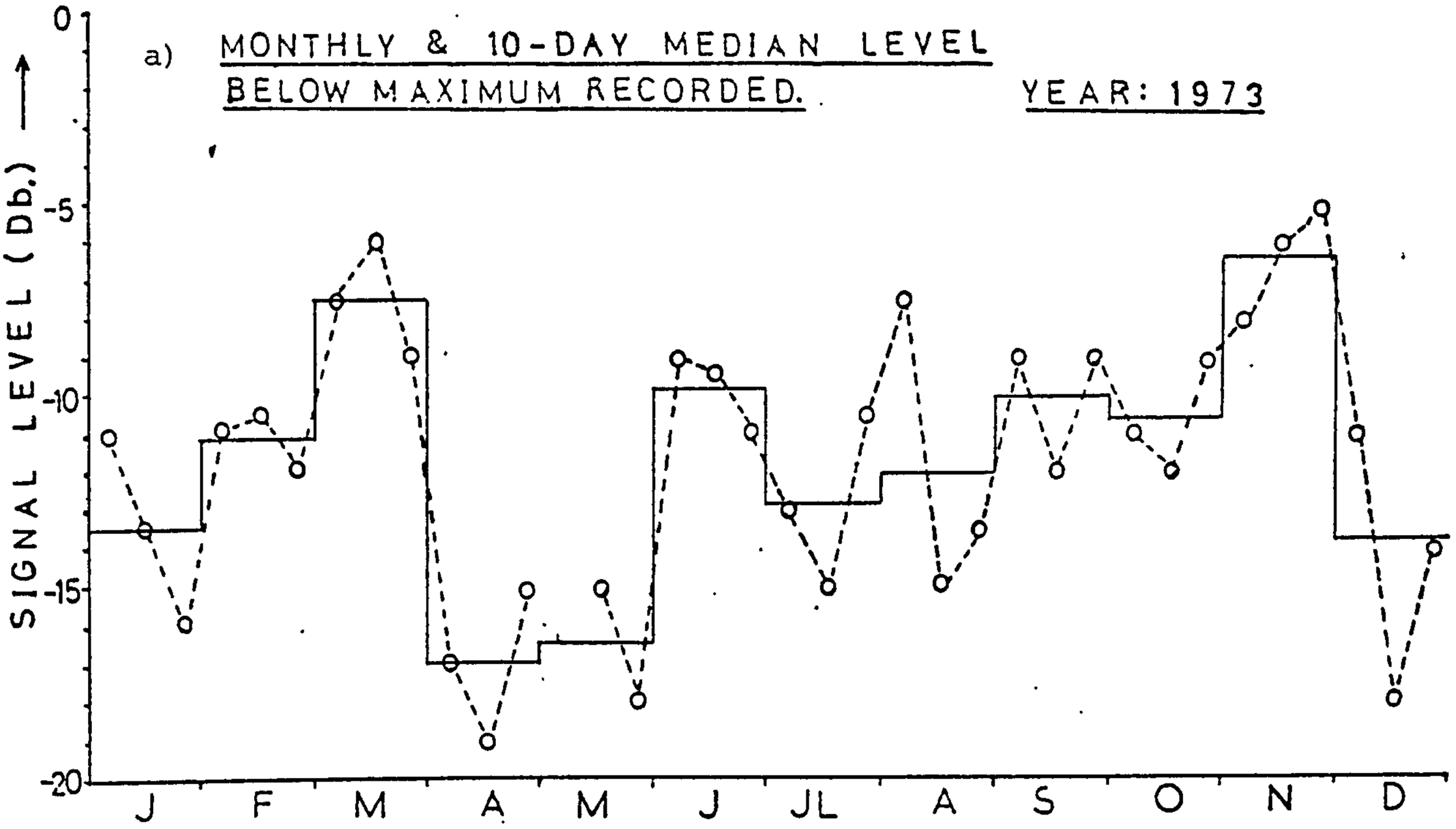

b) WIND MONTHLY AVERAGE

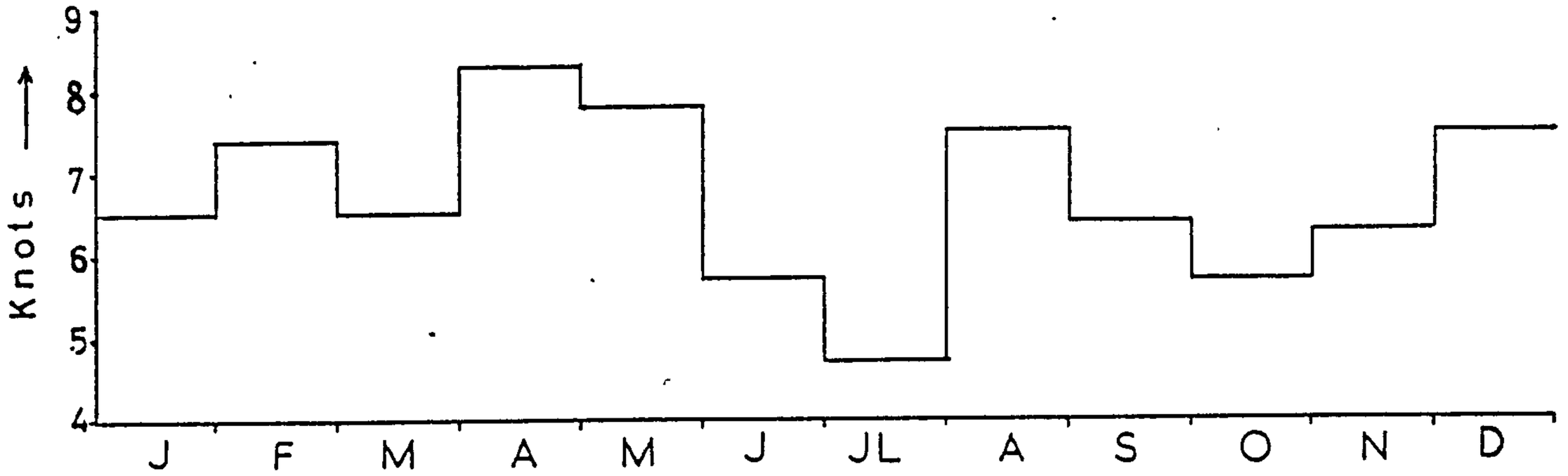

c) % OF SUNSHINE RELATIVE TO MONTHLY AVERAGE.

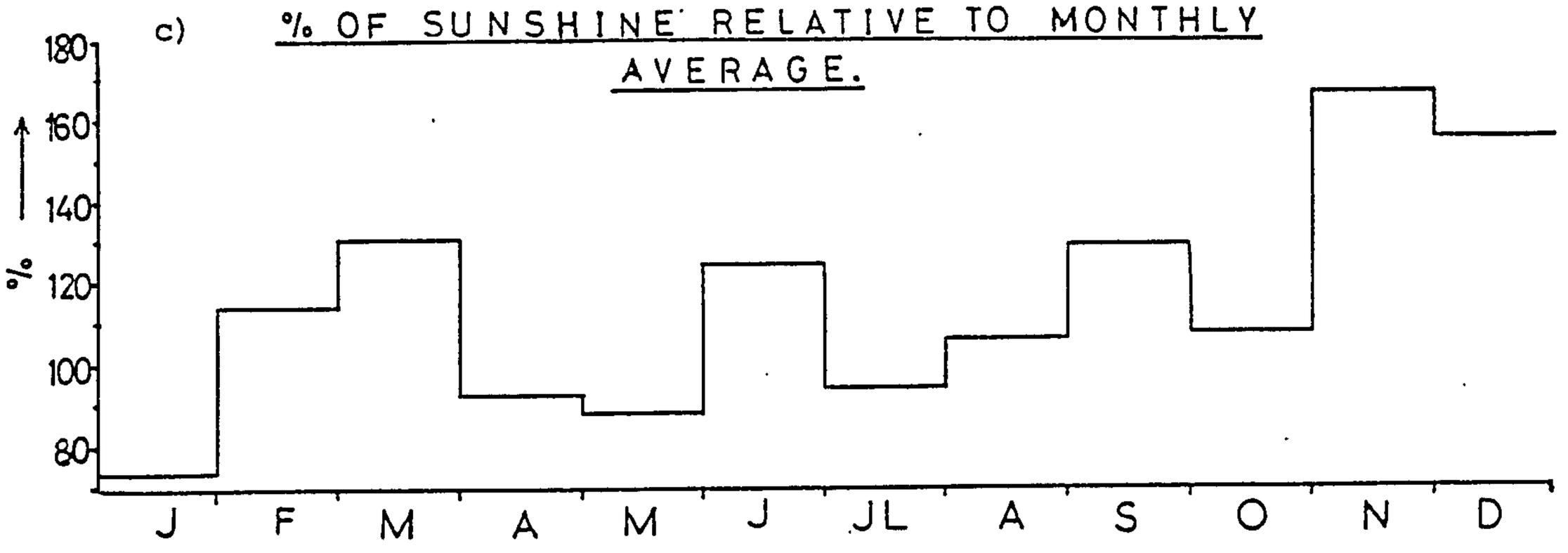

FIGURE 5.1: Monthly and 10-day (o--o) median level of the received signal for the year 1973 (a). Also, monthly average of the surface wind (b) and relative sunshine (c) for the same year.

10-day median levels were obtained by averaging the daily median levels. The resulting 10-day medians were averaged to produce the median level for the whole month.

In Fig. 5.1a, the annual variation of the signal level during 1973 is shown. The "worst month" of the year was April with only a slight improvement during May. The "best month" was found to be November followed by March.

A subject of specific interest for the planning radio engineer is the effect of the average weather conditions over a period of time, one month for instance, upon the performance of a radio-link. Such average weather conditions are expressed by the monthly averages of sunshine, surface wind velocity, surface temperature and precipitation. As precipitation is not expected to affect the propagation conditions at these frequencies, the rest of the monthly average meteorological parameters were considered in connection with the monthly median levels of the received signal for the whole of the year 1973.

These meteorological parameters (i.e. surface temperature, surface wind and sunshine) are of special importance for the energetics of the weather. Sunshine is the main source of energy for the atmosphere and wind and convection are the main agents for the transfer of energy from one scale of atmospheric processes to another.

The effect of these parameters can be readily produced over a given surface in the laboratory; heating providing the effects of sunshine/surface temperature and wind-tunnel techniques producing surface winds. For these reasons, a simple correlation test, as

described in Section 4.3, was performed between the monthly median levels of the received signal and monthly average values of surface temperature, surface wind velocity and relative sunshine recorded at the Meteorological Station at Kew. The correlation test between the monthly median level of the signal and the monthly surface temperature did not reveal any significant correlation between these quantities.

On the other hand, the monthly average wind velocity was found to be negatively correlated with the monthly median levels of received signal with a correlation coefficient:-

$$\rho_{(\text{Wind, Med.Level})} = -0.52$$

whereas, the relative monthly sunshine was found to be positively correlated with a coefficient:-

$$\rho_{(\text{Rel.Sunshine, Med.Level})} = 0.65$$

The probability that these coefficients represent uncorrelated quantities is approximately 5% as can be seen from the tables of correlation coefficient (Appendix VI). The results revealed by the correlation tests can also be yielded by visual inspection of Figs. 5.1a, 5.1b and 5.1c.

The fact that the monthly median level is higher for a "sunny" month has been realised by many investigators (127)(77)(128) and has received various explanations. Stickland and Smith-Rose[127] suggest that it might be due to the large reflactive index gradients occurring during

the warm months and the consequent bending of the propagated rays due to large k-values according to the expression (2.1.2). Bean and Meany[77] add the possibility of partial reflections or ducting caused by inversions. Tests performed by Bullington et al[128] at 505 and 4.090 MHz over transhorizon paths have shown that higher signal levels are likely to occur during summer and autumn with the explanation that temperature and humidity are higher during the summer. An attempted correlation with the average wind, carried out in this investigation, did not yield any significant result.

An original proposition put forward by Belatini[129] and developed by Burrows in[130] seems to be supported by the present observations. According to this proposition, the transhorizon field, or at least a part of it, can be accounted for by the presence of "convective cells" acting as divergent lenses. As mentioned in Chapter 1, these cells are a common feature in the atmospheric boundary layer and their formation is favoured by strong insolation and inhibited by strong winds. The correlation coefficients found give a support to this proposition without contradicting any of the other hypotheses mentioned.

5.1.2 Diurnal Variation of the Received Signal Level

The mean signal level of the received signal, expressed in hourly median values, was found to vary in a different way for various weather conditions and for different seasons of the year. Nevertheless, some features of the diurnal variation were occurring in a systematic way.

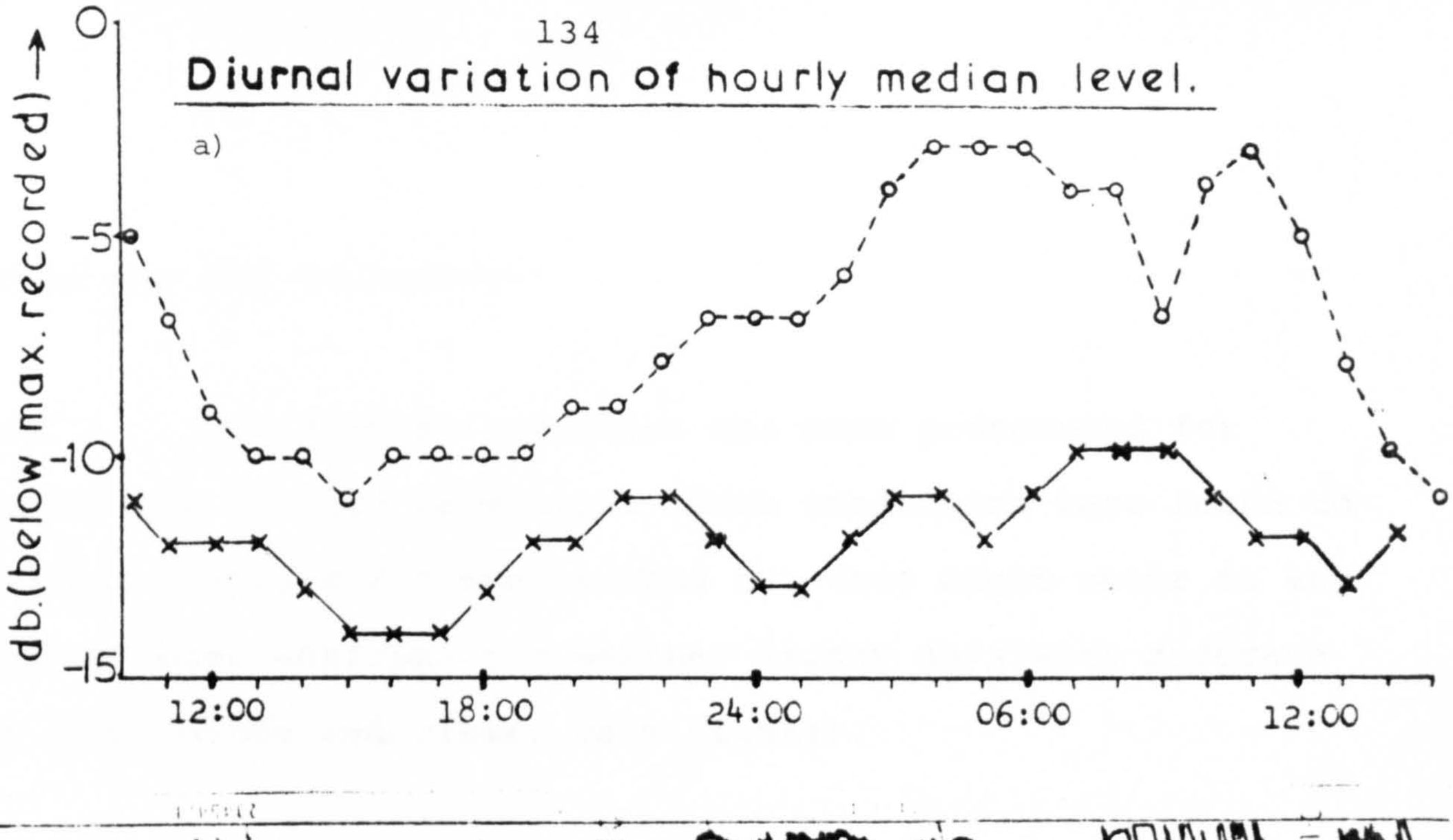

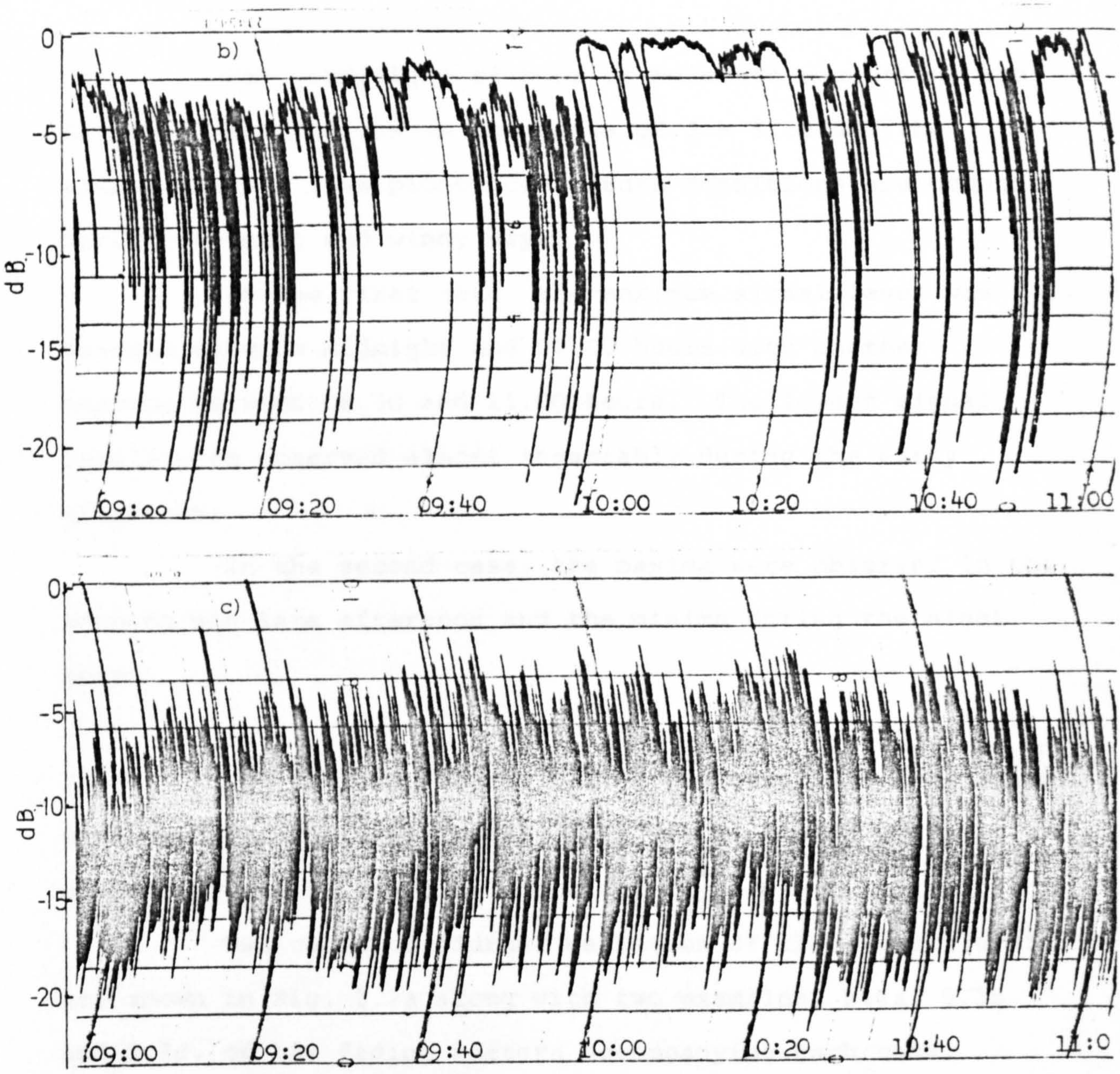

FIGURE 5.2: Diurnal variation of the received signal under favourable (o--o) and unfavourable (x--x) conditions(a). Fading pattern under these conditions (b and c respectively).

These are the following:-

(a) The diurnal variation was more pronounced for conditions of good reception. Such conditions were found to prevail during the summer months but they might occur in any season under anticyclonic weather (sunny days with moderate or light winds and clear, calm nights).

(b) For conditions of poor or moderate reception, the diurnal variation was in the range of 3 - 6 dB and the phenomenon was less pronounced. Such conditions are common during overcast and windy days.

In the first case, the maximum signal level was reached between midnight and 06.00 hours with another maximum between 08.30 and 11.00 hours. The lowest signal levels were observed almost invariably during the early afternoon.

In the second case, the maxima were observed in the morning and late afternoon and the minima during the night hours.

(c) The rapidity of the fading was generally increasing with decreasing signal level. Thus, rapid fading was a common feature of overcast and windy days.

Two cases of diurnal variation of the signal level are shown in Fig. 5.2a along with two examples, Figs. 5.2b and 5.2c, of the fading pattern accompanying each case.

These observations are in general agreement with results obtained during three experiments of transhorizon propagation described by Kerr[9]. The propagation paths in these experiments varied from 38 to 70 miles and the wavelength from 6.6 m. to 9 cm. One of these systems had been in operation in the south of England between Wembley and Haslemere under precisely the same climatic conditions as the present experimental investigation. Angell and Foot[131] also describe an experimental study of a transhorizon link at 3480 MHz between Wembley and Star Point (173 miles). Half of this path almost coincides with the path of the present experiment. The features of the diurnal variation for this link show many similarities with the ones observed during the present investigation. For example, the period from 20.00 to 06.00 hours was the most likely to produce high signal levels, whilst minima were observed more frequently in the early afternoon. Plots of the transmission loss versus time for small, average and large diurnal variation were similar to the ones shown in Fig. 5.2. In both these experiments, the high signal levels observed during calm and clear nights were attributed to a "ducting" mechanism due to the presence of temperature inversions favoured by anticyclonic conditions.

Rider[132] describes an experiment at 858 MHz over a 200 mile path where, again, the diurnal variation of hourly median level is in general agreement with the diurnal cycle observed in the present experiment. In this work, the high signal levels during the night hours are attributed to super-

refraction with a partial reflection from layers as a supplementary cause.

5.1.3 Effects of Frontal Activity Upon the Received Signal

During the period of measurements, 26 cases of a front crossing the propagation path were observed. From the Daily Weather Report, it was found that 15 of these cases were cold fronts, 9 were warm fronts and 2 were occluded. A summary of the effects of these fronts upon the median level and the fading pattern is the following:-

(a) All of the cold fronts caused a drop in hourly median level ranging from - 20 dB (below maximum recorded) down to noise level. The effect was most pronounced for fronts coming from the north-east and containing Continental polar air. These fronts were causing absolute fade-outs with only a few outbursts of detectable signal, usually caused by aircraft crossing the propagation path (Fig. 5.3a). Fronts coming from the west and north-west and containing cold or polar maritime air were causing drops of the received signal to levels which were low but still detectable. The fading in these cases was rapid with sharp maxima and minima, rather similar to those present during windy and overcast days (Fig. 5.3b). Four of the cold fronts were accompanied by squalls producing a variable mean level with relative changes of - 12 to - 15 dB. The fading during the crossings of a squall line was rapid but not very deep with a fading range of 9 to 12 dB.

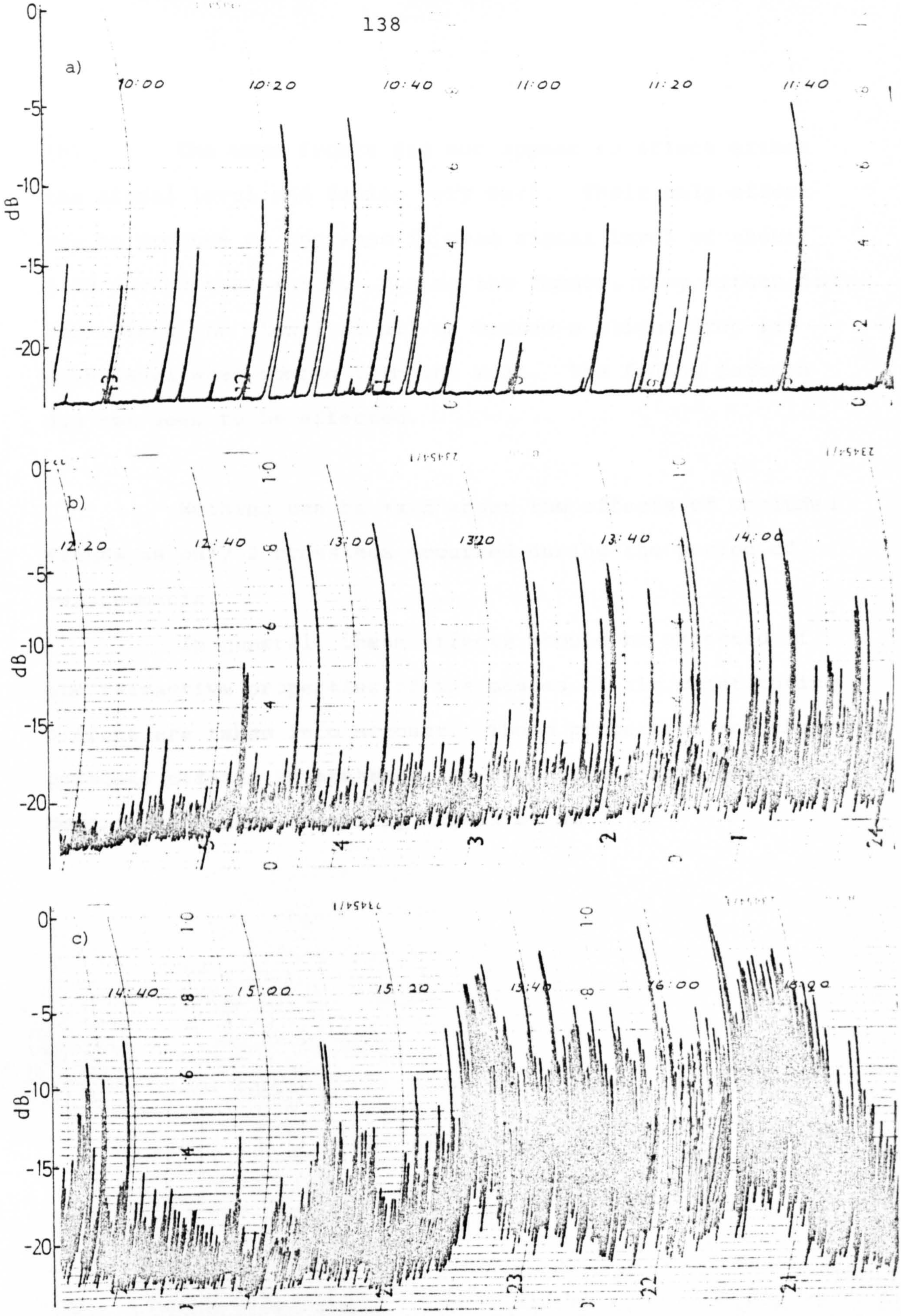

FIGURE 5.3: Fading during the passage of: (a) A cold front containing polar continental air, (b) a cold front containing polar maritime air, (c) a warm front.

(b) The warm fronts did not appear to affect either the signal level and fading very much. Their only effect was to produce an increase in mean signal level of about 6 dB during the winter. During the summer, they either did not affect the signal at all or caused a slight drop in mean level when coming from the west. The fading pattern did not seem to be affected.

Nothing can be said about the effects of occluded fronts as only 2 crossings occurred during the period of measurements.

In general, these effects should be expected if the refractive properties of the masses of air constituting a front are taken into account. These properties and their possible effects on transhorizon radio links have been described in some detail by Angell et al[131].

5.2 Short-term Effects: Fast Fading

In long-term investigations of a signal received beyond the horizon the main feature to be studied is the median level and its variations. In short-term investigations (record lengths < ½ hour) the median level is usually steady and the feature that becomes of primary interest is the variation of the instantaneous level of the received signal or "fast fading".

As the fast fading is of a more or less random character[113,94,103,49] the most suitable means of studying it is through such stochastic quantities as, the probability distribution, the autocorrelation function and the power spectrum. In the present investigation the power spectrum has been considered as the best means of studying the fast fading for reasons already discussed in Section 4.2.

5.2.1 Types of Fast Fading

As the signal records were accumulated, it became apparent that two distinct types of fading exist. These types of fading were given the names "α-type" and "β-type" of fading and will be referred to as such from here onwards.

The characteristics of these types of fading are as follows:-

α-type: It is characterized by rapid and deep fades with sharp maxima and minima. The mean level usually lies half-way between maximum and minimum. The fading rate varies from 0.3 Hz to 1.0 Hz and the fading range between 8 - 10 dB. It may occur during any period of the year and at any time of

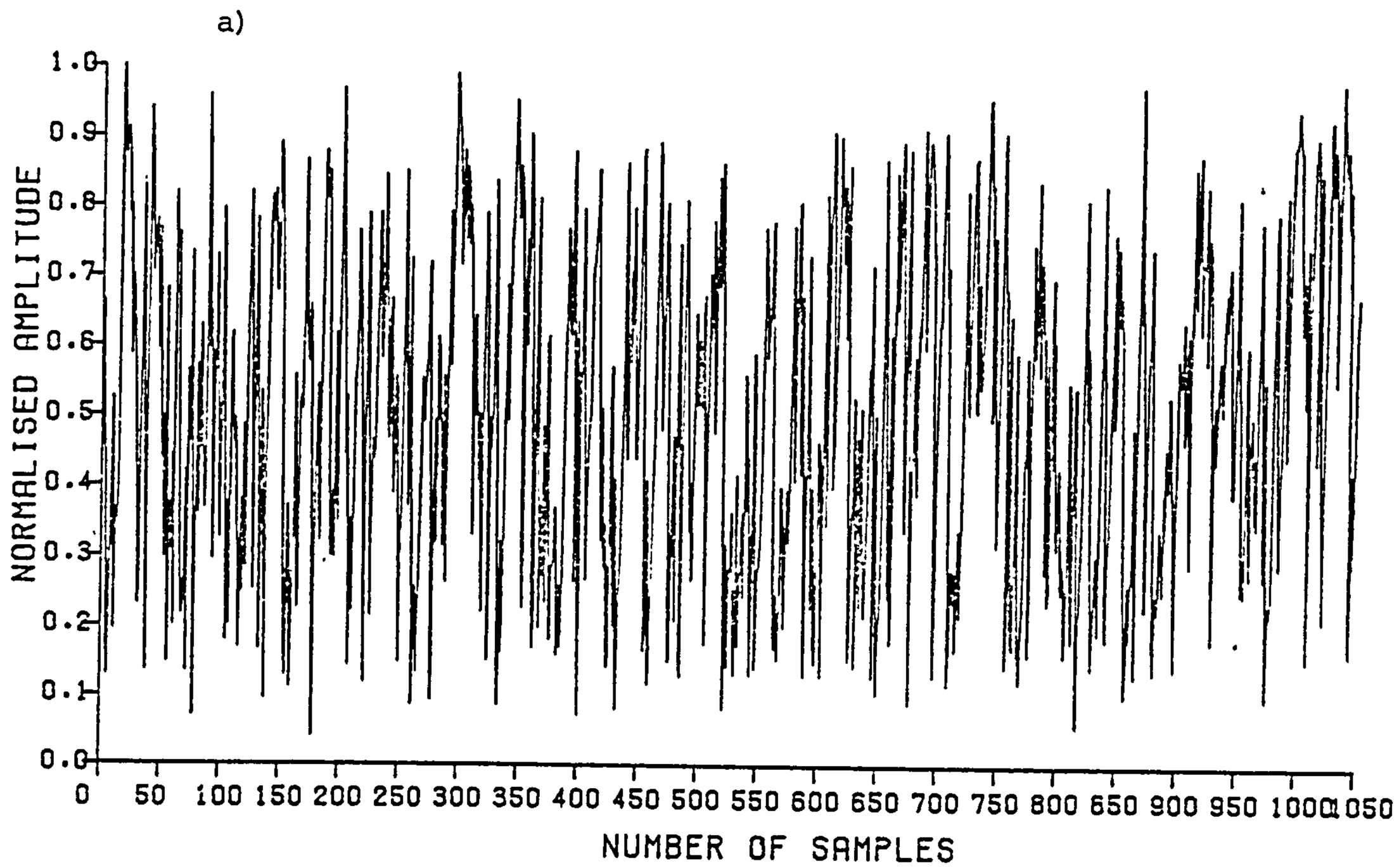

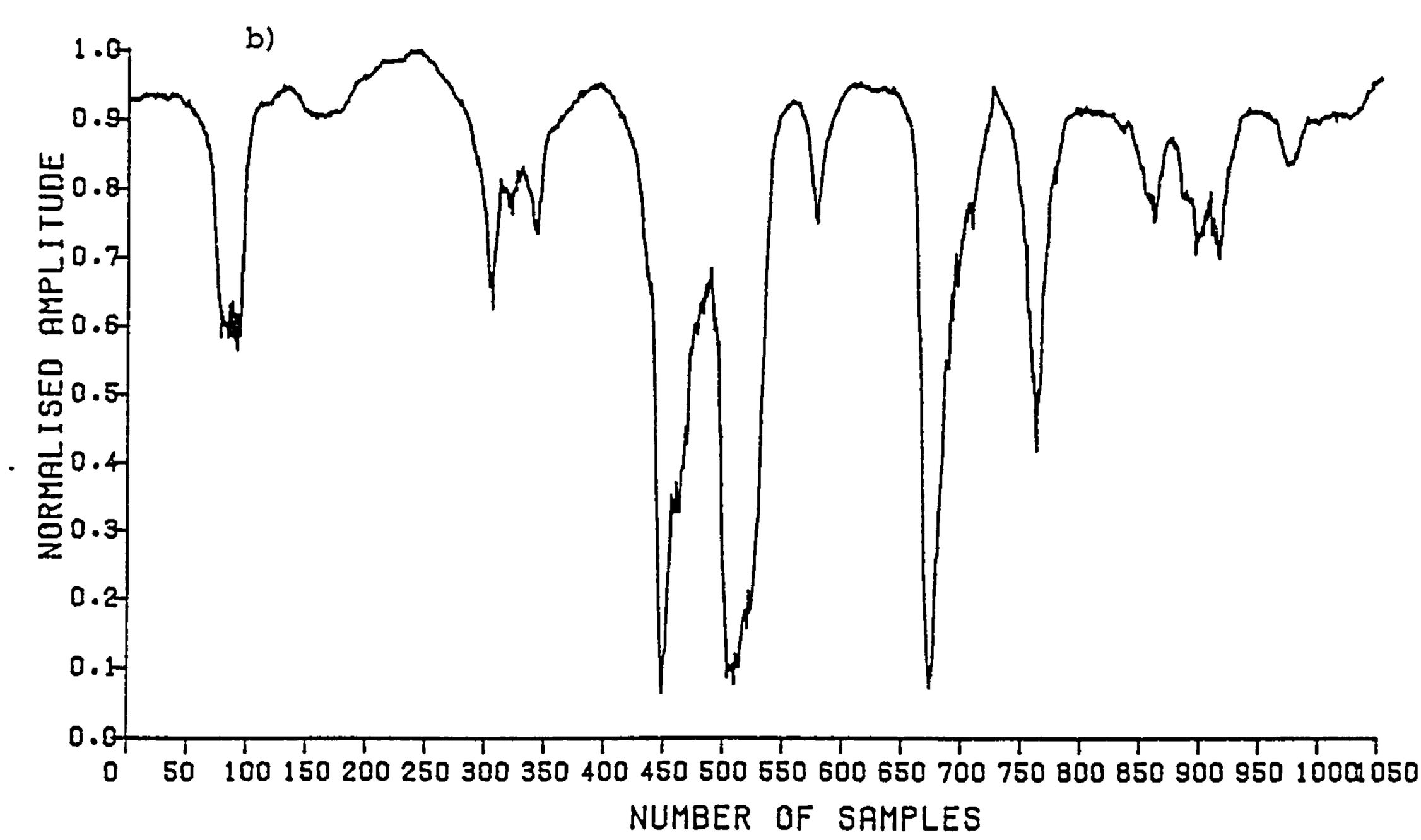

FIGURE 5.4: Examples of "α-type" (a) and "β-type" (b) of fading observed on the full scale radio - link (record length = 3.5 mins).

the day. It is favoured by poor weather conditions (overcast and windy days). It is the most common type of fading accounting for 85 - 90% of the cases.

β-type: It is characterized by broad maxima with a "round top" and sharp, deep minima. The mean signal level lies close to the maxima. The fading rate is usually less than 0.2 Hz and the fading range is of the order of 12 dB. It occurs during the early hours of the day mainly in the summer months but sometimes in spring or autumn under anticyclonic conditions. It is favoured by light or moderate winds and strong insolation. Two characteristic cases are shown in Fig. 5.4.

Similar types of fading have been observed during other investigations. For a transhorizon link operating at a frequency of 203.5 MHz over a path length of 160 nautical miles studies carried out by Kitchen and Richards[133] have revealed various types of fading. Among these the α and β type, as described here, are easily recognizable. In this investigation the α-type is attributed to a purely scattering mechanism whereas the β-type, to interference from a few components partially reflected by low-altitude inversions. Nicolis[134] reports that for a 237 km oversea link operating at 180 MHz similar types of fading have been observed. Again, the α-type is attributed to scattering whereas the β-type, to a "transitional" mechanism ranging between "single duct" propagation and scattering.

5.2.2 Influence of the Surface Wind Upon the Fading Spectrum. Qualitative Investigation

Among meteorological parameters that affect the fading spectrum of a signal received beyond the horizon, the surface wind can be considered as being of primary importance. Although not directly related to the dielectric constant properties of the propagation medium, the wind affects the distributions of other meteorological parameters such as temperature and humidity which define the refracting properties of the medium. If the wind is considered as a sum of a "mean" and an "eddying" motion then its role in the atmosphere becomes clearer. The "mean" motion can transport existing inhomogeneities and provides energy for the creation of new ones. The "eddying" motion, along with the convective activity, is the source of inhomogeneities in the refractivity field but can also destroy existing stratified layers by mixing. Thus, whichever of the theories of propagation is accepted for the real atmosphere, the effect of the wind upon the characteristics of the received signal is inevitable.

However, theoretical and experimental investigations on this subject are not very extensive. Thus, Rice[113] and Silverman[95] relate the normal-to-the-path component of the wind to both the frequency spectrum and fading rate of the received signal fluctuations. Fehlhaber[115] suggests that the drift velocity normal to the path appears as a parameter of the spatial and temporal autocorrelation functions of the received signal. Wheelon[103] gives an integral equation for the signal temporal autocorrelation function which contains the cross-path wind velocity as a variable of an indefinite

function. Tatarski[49] proposes a spectral function for field envelope fluctuations which is dependent on the cross-path wind velocity.

Rider[132] has carried out correlation tests between fading rate and fading range and the longitudinal and transverse wind components at an altitude of 2400 m. Angell and Foot[131] have calculated the correlation coefficients between fading rate and the total and normal to the path wind velocity at an altitude of 1500 m.

The present investigation has been directed towards establishing qualitatively any existing relationship between the fading spectrum and the surface wind and then seeking quantitative results. In view of that, no theoretical expression relating the wind velocity to the fading spectrum has been a priori postulated.

After processing the first few records with the method described in Chapter 4, it became apparent that the most variable feature of the fading spectrum was its "spread". The magnitude of the 1.0 Hz spectral component was chosen as the most suitable measure of this "spread", for reasons discussed in Subsection 4.2.3.

Surface wind data from the Meteorological Stations at Hurn, Kew and Heathrow were used separately and also to provide an average. The influence of the total surface wind velocity together with its longitudinal and transverse components upon the "spread" of the spectrum, was examined by means of a correlation test (see Section 4.3). The resulting correlation coefficients are listed in Table 5.1.

TABLE 5.1

COEFFICIENTS OF CORRELATION BETWEEN SPECTRUM "SPREAD" AND SURFACE WIND VELOCITY FOR 3 METEOROLOGICAL STATIONS

Meteorological Station	WIND COMPONENT		
	Total Wind	Longitudinal Component	Normal Component
Hurn	0.52	0.05	0.57
Kew	0.39	0.02	0.56
Heathrow	0.38	- 0.05	0.50
Average	0.50	- 0.02	0.65

From the table for correlation coefficients in Appendix VI, it can be seen that the critical correlation coefficient for 100 degrees of freedom and for the 1% significance level is 0.321. Thus for 122 degrees of freedom (124 observations used in the present test) it must be even smaller. All the coefficients in Table 5.1, except the ones for the longitudinal component, are greater than 0.321, consequently, they are significant for the 1‰ level. The coefficients for the longitudinal component show uncorrelated quantities. The conclusions which may be drawn from the examination of the results in Table 5.1 may be summarized as follows:-

(a) Increasing total wind velocity is causing more spectrum "spread".

(b) The longitudinal component of the surface wind does

not affect the fading spectrum in any consistent manner.

(c) The spectrum "spread" is affected mainly by the normal to the path component (the corresponding correlations have the highest coefficients).

(d) Among the data from the three meteorological stations the ones originating from Hurn are best correlated with the spectrum "spread".

(e) The average value from the three stations is satisfactorily correlated with the "spread" of the fading spectrum and it can be considered as a good criterion for the surface wind velocity over the whole of the path.

These results are in general agreement with previous experimental investigations. For example, Angel and Foot[131] report that coefficients of correlation between fading rate and wind observations, from an altitude of 1500 m, were found to be 0.35 and 0.45 for the total wind and the normal to the path component respectively. Rider[132] has shown that the fading rate and the normal to the path component of the wind at 2400 m are correlated with a coefficient of 0.5. In[112] it is reported that the rate of fading has been found to be a strong function of the horizontal drift wind across the path.

The fact that the fading spectrum is mainly affected by the normal to the path component of the wind has received the following explanation by Tatarski[49] in his theoretical treatment of line-of-sight propagation.

The fading is mainly due to destructive interference

between waves transmitted via the "shortest" path and waves scattered at the vicinity of a Fresnel ellipsoid and having travelled distances differing by $n \cdot \frac{\lambda}{2}$, $n = 1, 3, 5 \ldots$ A Fresnel ellipsoid is highly elongated along the direction of propagation and its major axis is approximately equal to the path length L, whereas its minor axis is $2\sqrt{\lambda \cdot L} << L$. A scattering "blob" drifted by the mean wind away from the great circle of propagation will reach the first Fresnel ellipsoid in a time $\tau = \frac{\sqrt{\lambda \cdot L}}{U_n}$, where U_n is the cross-path component of the wind. At the same time the "blob" will have travelled along the path (major axis) a distance $x = \frac{U_p}{U_n} \sqrt{\lambda \cdot L}$. In general, $x << L$ unless:-

$$\frac{U_p}{U_n} \simeq \frac{L}{\sqrt{\lambda \cdot L}} = \sqrt{\frac{L}{\lambda}}$$

The value $\sqrt{\frac{L}{\lambda}}$ is of the order of 10^3 for most of the applications. Thus, the condition $U_p \simeq 10^3 U_n$, under which the along the path component would produce the same fading as the normal to the path component, is a very improbable case.

The same reasoning can be applied to transhorizon propagation and explain the predominant influence of the cross-path component upon the fading spectrum.

The fact that the wind observations from Hurn, in the vicinity of the transmitter, are better correlated with the spectrum "spread" seems to indicate that inhomogeneities near the transmitting site contribute more to the signal fluctuations. A theoretical explanation in the form of a "path-weighting filter function" has been given by Lee and

Harp[135] but for line-of-sight propagation only. No theoretical explanation has been found so far for transhorizon propagation. However, it is anticipated that the laboratory simulation will provide an explanation for this effect.

5.2.3 The Effect of the Surface Wind Upon the Different Spectral Components of the Fading Spectrum

Qualitative investigation up to this stage was limited to correlations between the surface wind and the 1.0 Hz spectral component of the fading spectrum which has been chosen as a measure of the spectrum "spread".

However, in order to acquire a more complete idea of the effect the surface wind has upon the whole of the fading spectrum, the procedure described in Subsection 5.2.2 was repeated for 7 different spectral components corresponding to frequencies of 0.1, 0.25, 0.5, 0.75, 1.0, 1.5 and 2.0 Hz. These spectral components were correlated with the total surface wind at the three Meteorological Stations and with the 3-station average. The coefficients of correlation can be found in Table 5.2.

For 124 available pairs of measurements (i.e. 122 degrees of freedom) all the correlation coefficients are above the critical one for the 1‰ significance level (see Table for Correlation Coefficients in Appendix VI).

The values of the correlation coefficients indicate that the high frequency part of the spectrum is more affected by the surface wind. This is probably due to the fact that this part of the fading spectrum is affected by small scale turbulence of mechanical origin and, therefore, more sensitive to changes of the surface wind.

TABLE 5.2

COEFFICIENTS OF CORRELATION BETWEEN SPECTRAL COMPONENTS AND SURFACE WIND VELOCITY AT 3 METEOROLOGICAL STATIONS

Spectral Component	CORRELATION COEFFICIENTS			
	Hurn	Kew	Heathrow	Average
0.1 Hz	0.318	0.270	0.312	0.358
0.25 Hz	0.401	0.283	0.338	0.486
0.5 Hz	0.511	0.331	0.357	0.554
0.75 Hz	0.517	0.354	0.364	0.586
1.0 Hz	0.528	0.387	0.385	0.587
1.5 Hz	0.533	0.438	0.411	0.610
2.0 Hz	0.529	0.451	0.417	0.615

Again, data originating from Hurn Meteorological Station at the vicinity of the transmitting site appear to be better correlated with the magnitude of the spectral components. This effect has been already observed and reported in Subsection 5.2.2. Another interesting observation is that the 3-station average appears to be a better estimate than data originating from a particular Meteorological Station. This is probably due to the fact that the average is more representative of the wind conditions over the whole of the path.

A test for correlation between the above-mentioned spectral components and the normal to the path wind component of the average surface wind yielded the following coefficients:-

TABLE 5.3

COEFFICIENTS OF CORRELATION BETWEEN SPECTRAL COMPONENTS AND THE NORMAL TO THE PATH COMPONENT OF THE AVERAGE WIND

Spectral Component	0.1 Hz	0.25 Hz	0.5 Hz	0.75 Hz	1.0 Hz	1.5 Hz	2.0 Hz
Correl. Coefficient	0.497	0.537	0.616	0.638	0.651	0.646	0.631

As expected, the normal to the path wind component is better correlated with the spectral components than the total wind velocity. The effect is more apparent for the high frequency part of the spectrum.

5.2.4 Influence of the Surface Wind Upon the Spectrum of the Two Types of Fading

It was mentioned in Section 5.2, that Kitchen and Richards[133] and Nicolis[134] have attributed the two types of fading, referred to as α- and β-type in the present investigation, to different propagation mechanisms. However, in none of these investigations was it attempted to study the influence of the wind, either at the surface or at any height above the ground, upon the characteristics of the observed types of fading. Moreover, in the course of this investigation, it was observed that the β-type of fading could appear with almost identical characteristics under various surface winds ranging from very light to moderate. For these reasons, it was decided that the influence of the surface wind upon the two types of fading should be investigated separately.

As a first step towards this investigation, the magnitude of the 1.0 Hz spectral component (spectrum "spread") was plotted against the corresponding values of the 3-station average of the surface wind for all the available fading spectra. This plotting had the form of a scatter diagram and is shown in Fig. 5.5. Different marks indicate points belonging to the α- or β-type of fading.

From Fig. 5.5, it becomes immediately apparent that the β-type of fading is very little affected by the surface wind, whilst for the α-type of fading, increasing wind velocity causes an increase in the "spread" of the fading spectrum. As a second step in establishing an idea about this effect, the measurements were divided into two

□ : "α - type" of fading.

△ : "β - type" of fading.

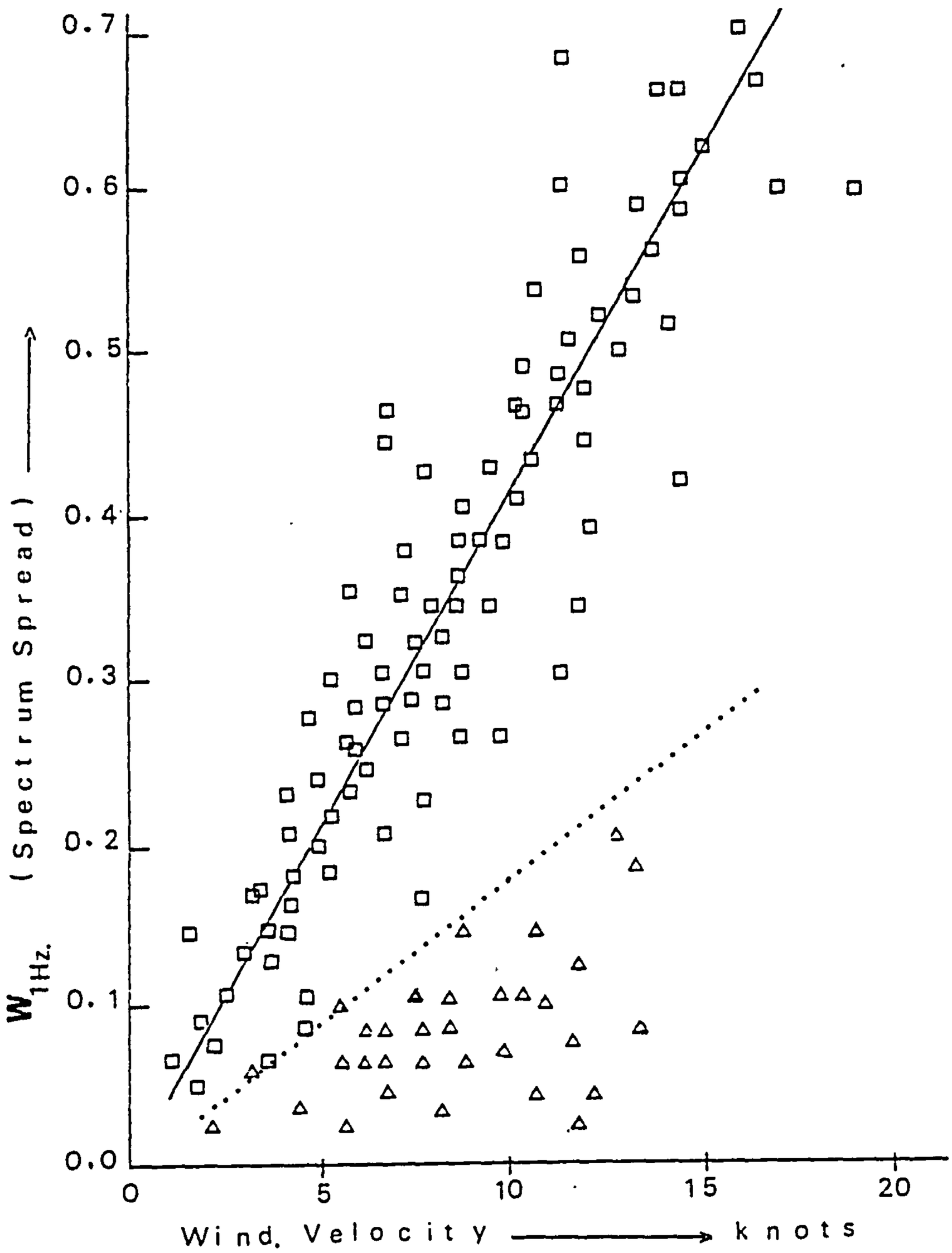

FIGURE 5.5: Effect of the surface wind velocity upon the Spectrum "spread" of the two types of fading.

groups, according to the type of fading, and the spectrum "spread" was correlated with the surface wind for each group separately. The computed correlation coefficients are listed in Table 5.4.

TABLE 5.4

COEFFICIENTS OF CORRELATION BETWEEN SPECTRUM "SPREAD" AND SURFACE WIND VELOCITY FOR THE 2 TYPES OF FADING

Type of Fading	df	METEOROLOGICAL STATION			
		Hurn	Kew	Heathrow	Average
α-type	90	0.687	0.632	0.654	0.743
β-type	30	0.061	0.192	0.132	0.173

All the coefficients for the α-type of fading are significant at the 1% confidence level. They indicate a strong correlation between the spectrum "spread" and the surface wind velocity. They also indicate that the average value of the surface wind is better correlated with the "spread" than data from any particular station. The correlation coefficients for the β-type of fading show no significant correlation and by checking their values against the corresponding critical values in the Table for Correlation Coefficients (Appendix VI), it can be concluded that there is more than 10% probability that the quantities are totally uncorrelated.

The available meteorological data does not provide enough evidence for explaining, with certainty, why the surface wind does not affect the spectrum of the β-type of fading.

Correlation tests between surface wind and wind at an altitude of 850 mb (approximately 1500 m.), with observations from Crawley Meteorological Station, revealed that the wind at this altitude is highly correlated with the surface wind, both in speed (correlation coefficient: 0.873) and in direction (correlation coefficient: 0.718). Therefore, it would not be very sound to assume that this effect is solely due to the fact that the atmospheric structures responsible for the β-type of fading are situated at considerable altitudes above the surface.

It is more likely that the atmospheric structures responsible for the β-type of fading are very little affected by light or moderate winds irrespective of altitude. Such structures can be stratified layers or large thermal "cells" which would be slowly advected under the influence of a light or moderate surface wind. It is expected that the laboratory simulation will throw more light into the nature of these structures.

5.3 Influence of the Static Stability Upon the Fading Spectrum

The importance of the static stability in the troposphere has been already discussed in Section 1.3. Important parameters such as the Richardson number Ri, the Rayleigh number Ra and the coindex of refraction gradient

depend explicitly on the static stability through the expressions (1.4.1d), (1.4.2a) and (1.4.3w) respectively.

Also, in Subsection 1.4.4, it has been shown that the spectral function for atmospheric turbulence may undergo a transition from one inverse-power law to another under the influence of buoyancy. In both the theories of Shur[63] and Lumley[70] and of Tchen[71,73] this transition depends on the value of the static stability (expressions (1.4.4d) and (1.4.4h) for the Shur-Lumley model and (1.4.41) and (1.4.4k) for the Tchen model).

For these reasons it was decided that the effect of the static stability parameter upon the fading spectrum should be investigated.

A definition of static stability and the method used for its evaluation has been given in Section 4.1. The necessary upper atmosphere meteorological data originates from Crawley Meteorological Station, where upper-air temperature observations are carried out only twice a day at 12.00 h and 24.00 h. For this reason, only mid-day signal records were used.

As previously, a correlation test was used in order to specify any qualitative relationship between static stability and the "spread" of the fading spectrum. The correlation coefficient was found to be: - 0.672 for 65 pairs of measurements.

From the Table for Correlation Coefficients (Appendix VI) it can be seen that for 60 degrees of freedom and for the 1‰ confidence level the critical coefficient is 0.408, thus the correlation coefficient between static stability and

spectrum "spread" can be considered as very significant.

The sign of the correlation coefficient suggests that increasing static stability corresponds to narrower fading spectra. This should be expected in view of the fact that in a stably stratified atmosphere the turbulence is suppressed whereas in an unstable atmosphere, the turbulence is enhanced.

In the above calculation of the correlation coefficient, the effect of the wind velocity upon the spectrum has not been taken into account. As a further step, the measurements were divided into three groups according to the wind velocity at the time of the recording. These three groups are: 18 measurements for wind velocities in the range 1 - 6 knots (light winds), 28 measurements for the range 6 - 12 knots (moderate winds) and 17 measurements for the range 12 - 18 knots (strong winds).

The correlation coefficient was computed for each of these groups and the results are listed in Table 5.5.

TABLE 5.5

COEFFICIENTS OF CORRELATION BETWEEN STATIC STABILITY AND SPECTRUM "SPREAD" FOR DIFFERENT WIND f

WIND: 1 - 6 knots		6 - 12 knots		12 - 18 knots	
df	corr. coeff.	df	corr. coeff.	df	corr. coeff.
16	- 0.751	26	- 0.798	15	- 0.879

These coefficients are well above the critical ones for the corresponding degrees of freedom at the 1% confidence level. Therefore, they can be considered as being very significant.

From Table 5.5, it can be seen that increasing surface wind velocity appears to enhance the correlation between spectrum "spread" and static stability.

This effect will be discussed in what follows with the additional aid of the diagram in Fig. 5.6 which represents a scatter diagram of spectrum "spread" versus static stability for the three ranges of wind velocity already considered.

The solid-line curves represent the trend of variation of the "spread" with static stability, for the three groups of wind velocities. From visual inspection of Fig. 5.6, the following conclusions can be drawn in respect of the effect of static stability upon the fading spectrum:-

1. High static stability (S) reduces the "spread" whereas low positive, or negative static stability induces a large "spread", i.e. rapid fading. This is apparent for any of the three groups of wind velocities.

2. This effect is less pronounced for light winds whereas for strong or even moderate winds, the "spread" increases more rapidly with decreasing S. From the curve No. 1 (light winds) in Fig. 5.6, it can be seen that when the static stability falls from 15.10^{-5} sec^{-2} to 2.10^{-5} sec^{-2}, the relative increase in "spread" is approximately 240%.

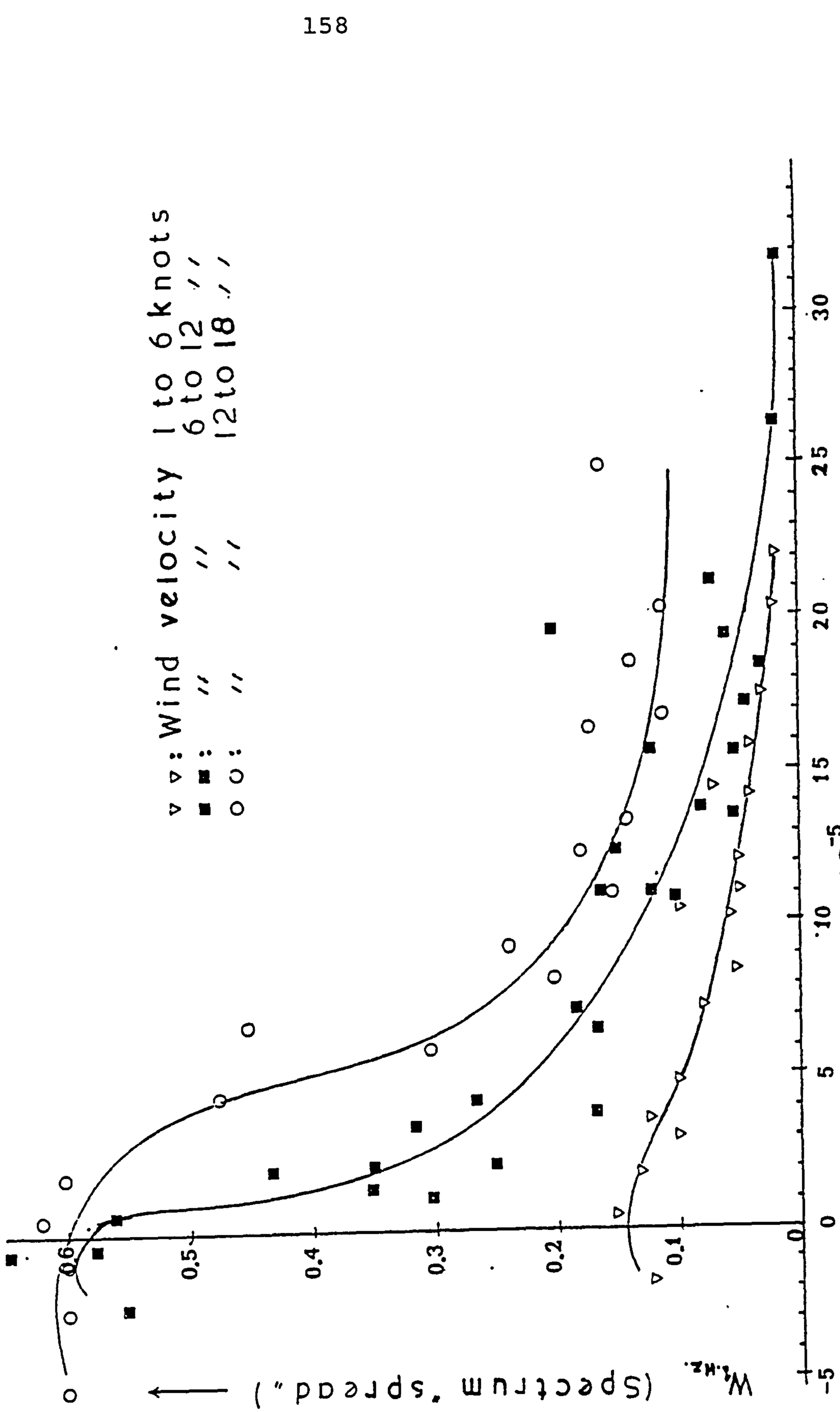

FIGURE 5.6: Effect of the static stability upon the "spread" of the fading Spectrum.

For moderate winds (curve No. 2), the same drop in S causes a relative increase in "spread" of approximately 340%.

It was qualitatively shown in the previous Subsections 5.2.2 and 5.2.3 that increasing surface wind, and especially its normal to the path component, is responsible for rapid fading by drifting scattering inhomogeneities through the common volume. To this factor, two more can be added: the number of scattering "blobs" contributing to fading; and their size. Obviously the greater the number of these "blobs", the more rapid the resulting fading, since at a certain moment more of them will have the right position in space (vicinity of a Fresnel zone) to cause destructive interference. The importance of the size becomes apparent from the Bragg condition (2.2.3f): the smaller the blob size, the larger is the corresponding scattering angle and regions of the common volume remote from the great circle of propagation start contributing to fading.

In view of these facts, the previously mentioned effects can be explained as follows:-

(a) According to the discussion in Subsection 1.4.1, high static stability is likely to suppress turbulent motion in the atmosphere even in the presence of a strong wind. This is due to the fact that for 5 >> O Ri > Ri_{cr}, and buoyancy forces are opposing any mechanically produced turbulence. Under these conditions only large eddies can be maintained for considerable periods of time because their buoyancy is greater, but such eddies contribute very little

to fast fading. Conversely, conditions of low or negative static stability can lead to $Ri < Ri_{cr}$ and then the onset and maintenance of turbulence is promoted by the buoyancy forces. This increases the number of eddies and favours the maintenance of those of smaller size.

(b) When light winds are prevailing, turbulence is mainly due to convection. Thus, even for low or negative static stability, the fading is mainly due to relatively large (see Table 1.1) convective elements drifting through the common volume. In the presence of stronger winds, mechanical turbulence is added to the convective one thus increasing the number of inhomogeneities. Also, more energy is fed to the spectrum of turbulence by the mean motion and is cascaded down to small-size eddies. Thus, the relative "effectiveness" of a strong or moderate wind in producing rapid fading, is enhanced under conditions of low positive or negative static stability.

5.4 Influence of the Surface Wind Upon the Spectrum of the "α-type" of Fading: A Quantitative Investigation

The qualitative investigation described in Section 5.2 provided evidence that the surface wind, and especially its component U_n normal to the propagation path, considerably affects the fading characteristics of a signal received beyond the horizon and causes a "spread" of the fading spectrum towards higher frequencies.

Spectral components, corresponding to different frequency ranges of the fading spectrum, were found to be affected by the surface wind (see Subsection 5.2.3) and this

effect was more pronounced for components in the high frequency part of the spectrum.

Fading spectra belonging to the α-type category were found to be particularly affected by the surface wind, whilst those of the β-type did not appear to be affected by this meteorological parameter in any consistent manner. The very significant correlation coefficients between spectrum "spread" and U_n (see Table 5.4) suggest that a quantitative relationship between the "α-type" of fading spectrum and U_n could be established. For this type of fading, such a relationship would lead to an empirical formula connecting the power spectral density function to the surface wind velocity U_n in the direction normal to the propagation path.

This empirical formula could be thereafter compared with the theoretical predictions for the power spectral density function of atmospheric fading, given in Section 2.3, and also serve as a guideline for the laboratory simulation of the same effect.

5.4.1 Influence of U_n Upon Different Ranges of the "α-type" of Fading Spectrum

Prior to seeking a quantitative relationship between U_n and the power spectral density function of the α-type of fading, it was considered necessary to investigate the effect of U_n upon the different ranges of the spectrum for this type of fading.

From each of 92 available fading spectra belonging to the "α-type" category, seven spectral components 0.1, 0.25, 0.5, 0.75, 1.0, 1.5 and 2.0 Hz were considered. Seven sets

of measurements were thus formed, each containing 92 spectral components of the same frequency.

As in Subsection 5.2.3, each of these sets was tested for correlation with the corresponding values of U_n. A 3 meteorological station average value of U_n was considered to represent better the surface wind conditions over the whole of the propagation path and, therefore, such average values of U_n were used instead of data from a particular meteorological station.

The correlation test yielded coefficients shown in Table 5.6.

TABLE 5.6

COEFFICIENTS OF CORRELATION BETWEEN U_n AND SPECTRAL COMPONENTS FOR THE "α-type" OF FADING

SPECTRAL COMPONENT	0.1 Hz	0.25 Hz	0.50 Hz	0.75 Hz	1.0 Hz	1.5 Hz	2.0 Hz
CORR. COEFFICIENT	0.497	0.666	0.733	0.802	0.776	0.762	0.738

Entering the Table of the Correlation Coefficient (Appendix VI) for 90 degrees of freedom, it can be seen that all of the coefficients in Table 5.8 are well above the critical value for the 1‰ significance level. Thus, the probability that the quantities are uncorrelated is less than 1‰.

These results reveal that the spectral components

in the different frequency ranges of the fading spectrum are increasing in magnitude when U_n increases.

There is, therefore, a strong indication that a power spectral density function, describing the whole of the power spectrum of the "α-type" of fading, might be affected by U_n in a consistent way, allowing for more quantitative conclusions to be drawn about the effect under investigation.

5.4.2 An Empirical Relationship Between U_n and the Power Spectral Density Function of the "α-type" of Fading

After the encouraging results reported in the previous subsection, it was decided that a quantitative empirical relationship between U_n and the power spectral density function of the "α-type" of fading could be established.

For this purpose an analytical expression should be found which would: (a) describe as accurately as possible all the available power spectra of the "α-type" of fading, and, (b) contain U_n as a parameter.

This was achieved through the following procedure:-

1. The correlation coefficients in Table 5.6 suggested that the relation between U_n and each of the spectral components might be a linear one, since a correlation test is essentially a test for linearity as well[118,126]. Such a linear relation would have the form:-

$$W(f_i) = \alpha_i + \beta_i \cdot U_n \qquad i = 1, 7 \qquad (5.4.2a)$$

where $W(f_i)$ is the magnitude of each of the 7 spectral components considered, f_i is the corresponding frequency and α_i, β_i are the constants of each regression line (intercept and slope respectively). The index i indicates each of the 7 spectral components under consideration.

Since the correlation coefficient is a rather qualitative indication that two sets of variables are linearly related (unless it is equal to 1 or - 1), another more powerful method was used to test the linearity between each of the spectral components $W(f_i)$ and U_n.

Each set of 92 spectral components $W(f_i)$ and the corresponding values of U_n were used as an input to a computer program based on the subroutine EO2ABF (see Appendix IV).

This subroutine examines least-square polynomial approximations which fit a set of data points; in this case $(W(f_i), U_n)$. The degree of the polynomials can vary from zero to an integer m set by the user. These polynomials have the form:-

$$f(x) = F(1) + F(2) \cdot x + F(3) \cdot x^2 + ... + F(N + 1) \cdot x^m$$

The subroutine can select the degree J, $(0 \leq J \leq m)$, of the polynomial which fits the given data points best. The criterion for the selection of J is that the sample variance resulting from each trial is minimised. The degree J of the best fitting polynomial is given by the program as an output parameter. For all the 7 spectral components, the best fitting polynomial was found to be of the first degree

although polynomials up to the fifth degree were tested by the program.

2. After it had been established that the magnitude of each of the 7 spectral components depended linearly on U_n, the constants α_i, β_i of the expression (5.4.2a) should be determined so that each spectral component could be expressed as a linear function of U_n. For this purpose, the APL/360 system was used and the calculations were performed by means of the routine SR (STATPACK package) (see Appendix V). This routine, as already discussed in Section 4.3, estimates the constants of a linear regression line by means of the expressions (4.3.3) and (4.3.4) using the least-squares method. The values of α_i (intercept) and β_i (slope) corresponding to each line of regression between a spectral component and U_n are listed in Table 5.7.

TABLE 5.7

CONSTANTS OF LINEAR REGRESSION BETWEEN EACH OF THE 7 SPECTRAL COMPONENTS AND U_n

Spectral Compon.	0.10 Hz	0.25 Hz	0.50 Hz	0.75 Hz	1.0 Hz	1.5 Hz	2.0 Hz
α_i	0.651	0.301	0.128	0.073	0.039	0.010	0.007
β_i	0.021	0.031	0.037	0.037	0.037	0.036	0.034

With the intercept (α_i) and slope (β_i) of each regression line known, the 7 lines representing the expression (5.4.2a) were plotted on the same graph in Fig. 5.7. This graph has the form of a nomogramme showing the increase in amplitude of each of the 7 spectral components when U_m increases in the range from 1 to 18 knots. With the aid of this graph, for a given wind velocity U_n, 7 components of the fading spectrum could be determined. It must be recalled here that these components do not belong to the "Fading Power Spectrum" P(f), but to the "Fading Spectrum" W(f) (see Subsection 4.2.3). Thus, in order to obtain 7 estimates of the fading power spectrum for a given U_n, the values of the fading spectral components obtained from the graph in Fig. 5.7 must be squared. These 7 estimates are adequate for plotting the fading power spectral density function for a given U_n, as shown in Fig. 5.8. This graph represents the fading power spectra, or rather the corresponding power spectral density functions, for 8 different values of U_n ranging from 2 to 16 knots. The effect of increasing U_n upon the power spectral density. function of the "α-type" of fading is apparent.

3. Visual inspection of Fig. 5.8 suggested that the fading power spectral density function might obey an inverse power law of the form:-

$$P(f) \sim f^{-n} \qquad (5.4.2b)$$

Such a function, when plotted with both axes

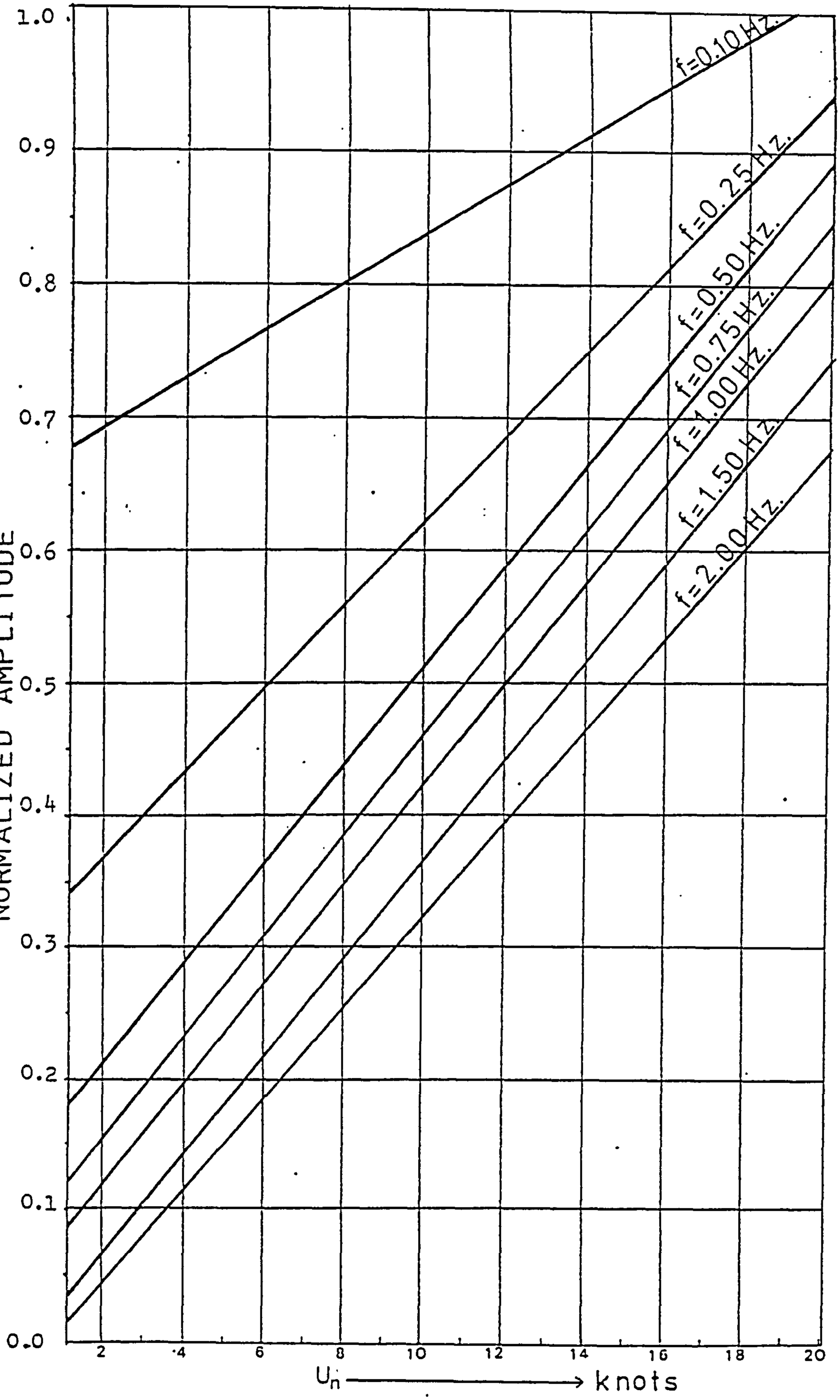

FIGURE 5.7: Regression lines showing the linear dependence of different spectral components on U_n. The graph has the form of a nomogram.

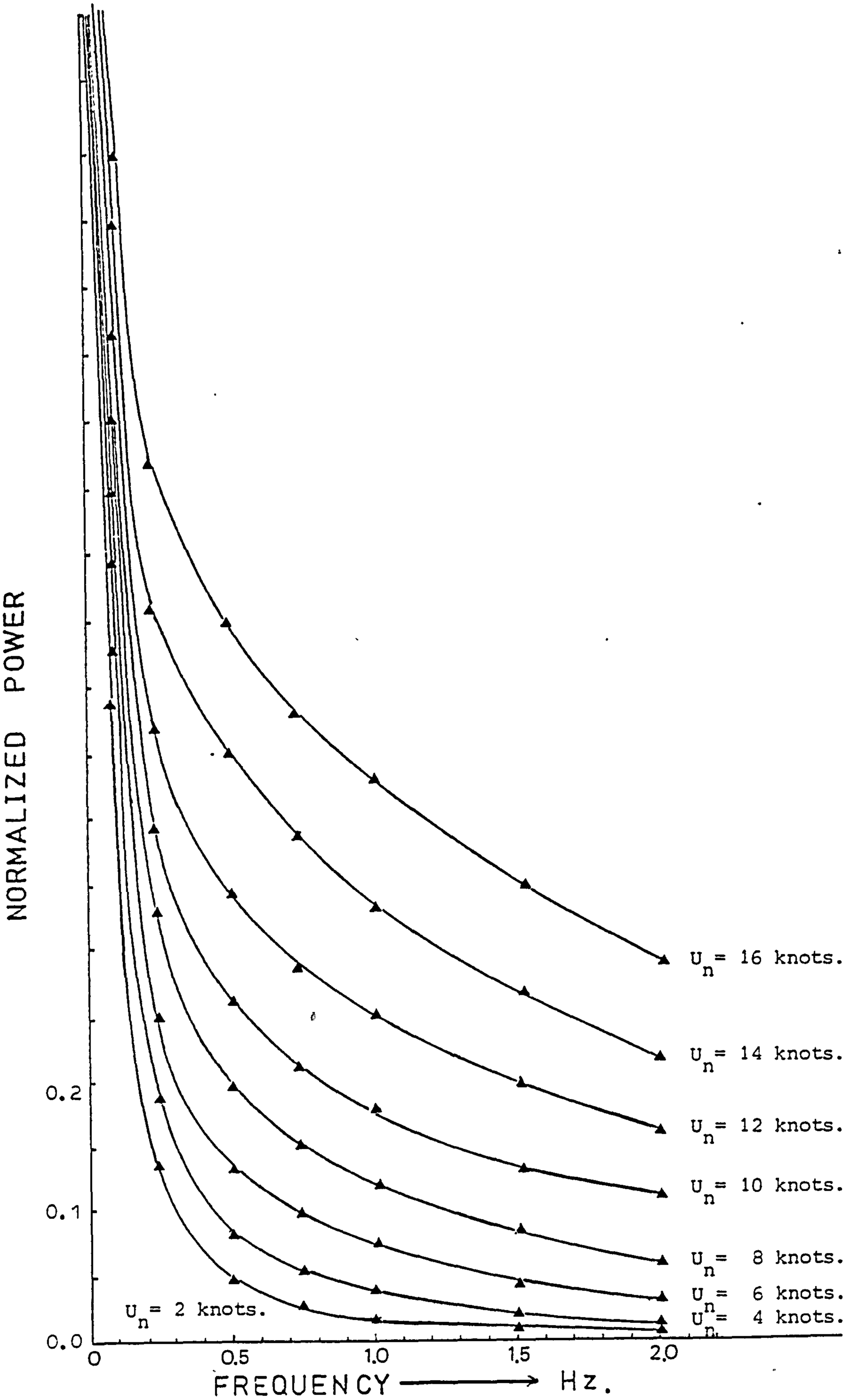

FIGURE 5.8: The effect of increasing U_n upon the Power Spectrum of the "α- type" of fading.

logarithmic, is represented by a straight line with a slope $n = - \frac{\log (P(f))}{\log f}$. Fig. 5.9 shows such a logarithmic plot which indicates that the power spectral density function, for various U_n, obeys an inverse power law. The exponent n appears to be constant for values of U_n from 16 to 6 knots. For lower values of U_n, the exponent n seems to increase for spectral components above 1 Hz. However, in this part of the spectrum the normalized power is some 13 dB, or more, below maximum, for U_n < 6 knots, as it can be seen from Fig. 5.9. It is, therefore, possible that under these conditions the spectral estimates in this range are aliased by the receiver noise to a certain degree.

Nevertheless, to a great extent, the exponent n would appear to be a constant parameter of the power spectral density function, depending only on the normal to the path component U_n of the surface wind.

4. From Fig. 5.9 it can be seen that the exponent n (slope of the logarithmic power spectra) decreases when U_n increases. This was further confirmed by the respective values of n and U_n contained in Table 5.8.

The graph shown in Fig. 5.10 represents the variation of n with increasing U_n and suggests an inverse proportionality between these two quantities. This led to the construction of another graph, also shown in Fig. 5.10, relating to the inverse of the exponent 1/n to the values of U_n (the corresponding values of 1/n are also shown in Table 5.8).

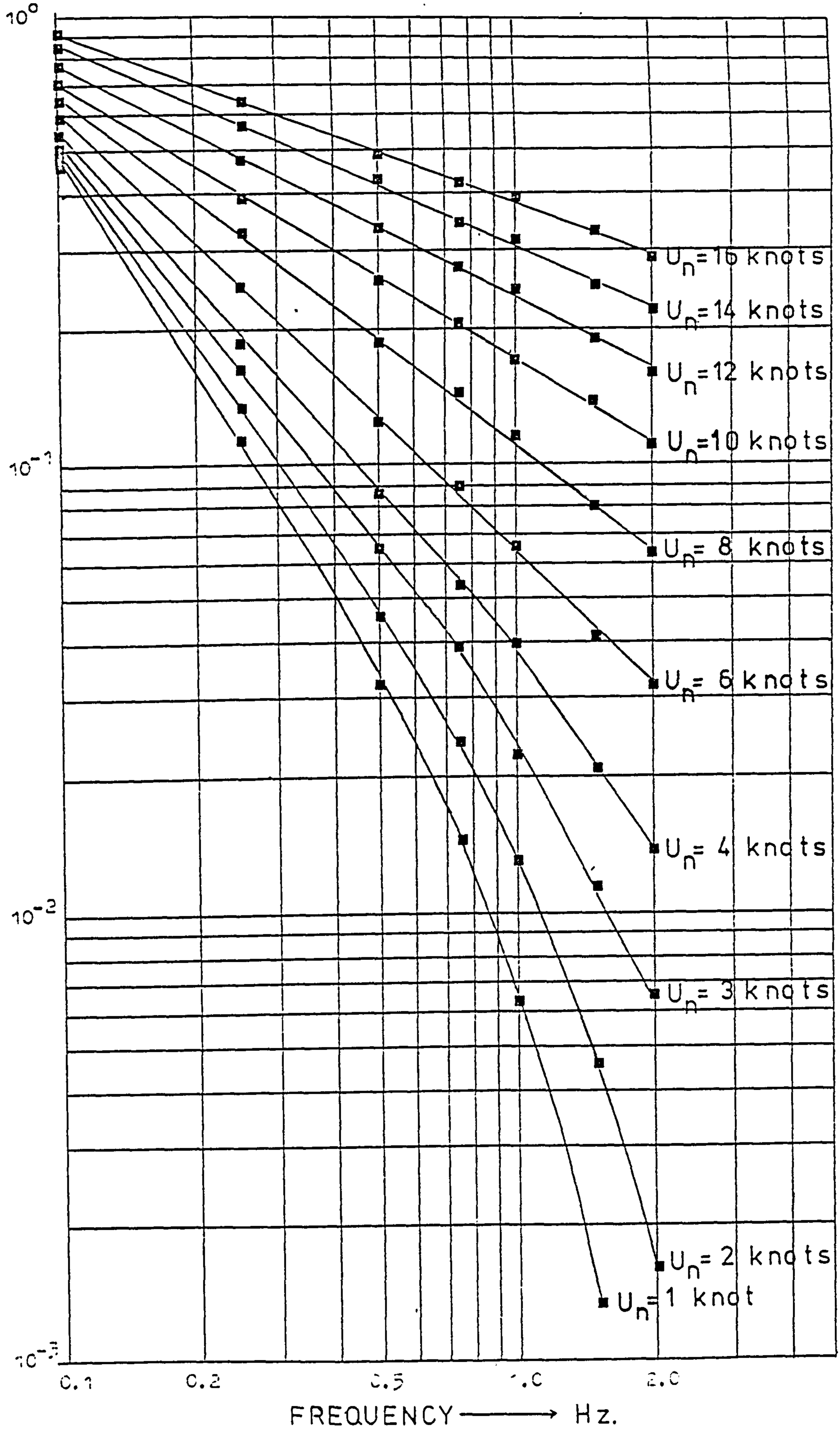

FIGURE 5.9: The effect of U_n upon the logarithmic Power Spectrum of the "a - type" of fading.

TABLE 5.8

U_n knots	n	1/n
16	0.392	2.56
14	0.459	2.18
12	0.513	1.95
10	0.614	1.63
8	0.786	1.27
6	0.876	1.14
4	1.12	0.89
3	1.28	0.78
2	1.47	0.68
1	1.87	0.535

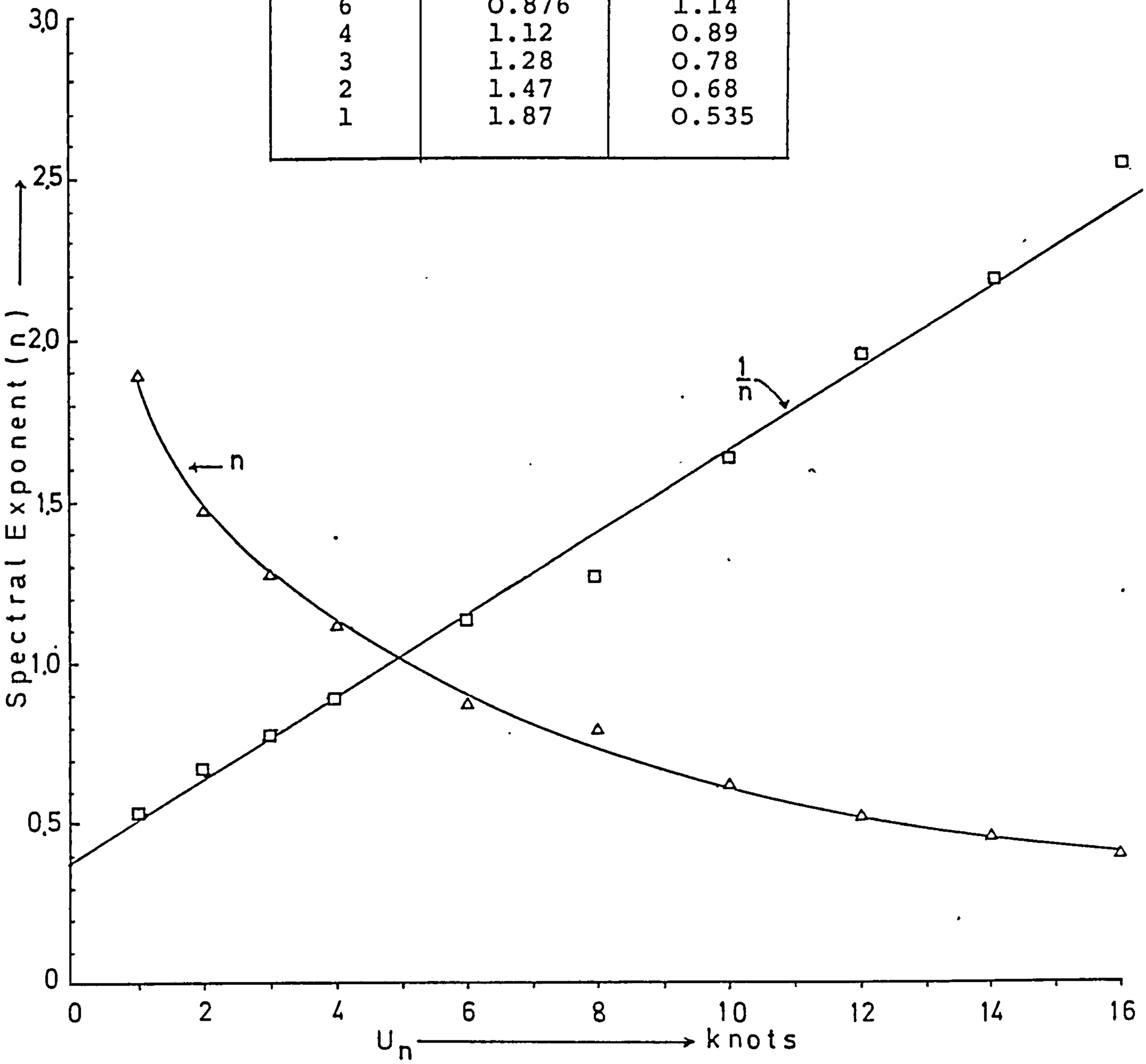

Fig. 5.10 Variation of the spectral exponent (n) and its inverse (1/n) with U_n.

The apparent linear relationship between 1/n and U_n suggested by this graph, led to a quantitative test for linear regression between 1/n and U_n by means of the APL/360 routine SR (see Appendix V). The results obtained from this routine for the 10 pairs of data (1/n, U_n) listed in Table 5.8 were the correlation coefficient, which was found to be 0.995, and the constants of the regression line, which were estimated as:-

Intercept: 0.366 Slope: 0.131

The fact that the correlation coefficient was found to be almost 1 confirmed that 1/n depended linearly on U_n. With the values of intercept and slope calculated by the routine, the relationship becomes:-

$$1/n = 0.36 + 0.131 \cdot U_n \quad (U_n \text{ in knots}) \tag{5.4.2c}$$

A combination of (5.4.2c) with (5.4.2b) gave the following empirical expression for the dependence of the power spectral density upon frequency with U_n as a parameter:-

$$P(f) \sim f^{-\{1/(0.366 + 0.131 \cdot U_n)} \tag{5.4.2d}$$

for $0.1 \leq f \leq 2.0$ Hz

It must be noted that this empirical expression does not describe the power spectral density function in the range 0 to 0.1 Hz, as this range had not been considered in the analysis. The sampling epoch (record length) in this

study had been kept constant at 3.5 mins throughout the measurements. Therefore, frequencies less than $1/3.5\ min^{-1} \simeq 5 \times 10^{-3}$ Hz would not be represented in the power spectrum with any accuracy. Moreover, this is the range where the power spectrum attains its maximum and, therefore, the form of the power spectral density function changes from an increasing to a decreasing function of f. This would impose considerable difficulties on the analytic description of the power spectrum in this range.

However, P(f) is a normalised power spectral density function, such that $P(f_m) = 1$, where f_m is the frequency at which the maximum of the power spectrum occurs. To account for this property of P(f), the expression (5.4.2d) can be written:-

$$P(f) \sim \left(\frac{f}{f_m}\right)^{-1/(0.366 + 0.131\ .\ U_n)} \qquad (U_n \text{ in knots}) \qquad (5.4.2e)$$

This new expression does not alter the dependence of P(f) on f and, moreover, satisfies the condition $P(f_m) = 1$.

5.4.3 Discussion

Expression (5.4.2e) is a purely empirical relationship showing the dependence of the normalized fading power spectrum upon the normal to the path velocity component of the surface wind. It should be appreciated that another analytic treatment of the same experimental data would result in another expression fitting the data equally well. However, for the purposes of the present investigation, the expression (5.4.2d) was considered adequate as it describes

the effect of increasing U_n in producing a "spread" of the fading power spectrum towards higher frequencies. This effect, as already discussed in Section 2.3, has been accounted for by various theoretical models proposed by Crawford et al[112], Rice[113] and Fehlhaber and Grosskopf[114,115]. In some of these cases[112,114,115], the theoretical models (power spectral density functions) are supported by experimental data as well.

Another very interesting feature of (5.4.2e) is that for $U_n = 0$ the dependence of power spectral density upon frequency becomes:-

$$P(f) \sim \left(\frac{f}{f_m}\right)^{-1/0.366} = \left(\frac{f}{f_m}\right)^{-2.74} \qquad (5.4.3a)$$

The value - 2.74 of the exponent is very close to the value $-8/3 \simeq -2.67$ proposed by Tatarski[49] for the power spectral density function of amplitude fluctuations in line-of-sight propagation.

The condition $U_n = 0$ does not imply that the propagation medium is absolutely at rest but corresponds to a case where turbulence is fully developed in the propagation medium and there is no mean transport velocity across the direction of propagation. Thus, the main source of Doppler spread and shift has ceased to exist and fading is mainly due to the evolution of turbulence in the atmosphere. The fact that this type of fading has a power spectral density function obeying (to a great extent) a - 8/3 law, as in the case of line-of-sight propagation, indicates that the refractive index in homogeneities

responsible for the fading cover a whole range of wave-numbers. Since, a "- 8/3" law for the power spectrum of amplitude fluctuations is a consequence of a one-dimensional refractive index spectrum obeying a "- 5/3" power law[49], the refractive index inhomogeneities causing the "α-type" of fading are expected to be in the inertial range of turbulence characterised by the - 5/3 spectral exponent (see Subsection 1.4.3).

5.5 The Effect of Static Stability Upon the Power Spectrum of the "β-type" of Fading

It was reported in Section 5.3 that the static stability of the first 1.5 km of the atmosphere was found to be the second meteorological parameter, other than the surface wind, to affect the fading spectra of the received signal.

In the case of the "β-type" of fading, the effect of the surface wind upon the fading spectrum was found to be altogether insignificant (see Subsection 5.2.4 and Fig. 5.5). It was, therefore, thought that a close examination of the power spectra of the "β-type" of fading could reveal the effects of the static stability of the atmospheric medium.

The investigation on the effect of U_n upon the power spectral density function of the "α-type" of fading, revealed that the spectral exponent n can be quantitatively related to a specific meteorological parameter, namely, U_n, and possibly to the spectral exponent of the refractivity field, at least in the case when $U_n = 0$. It was, therefore, decided that the spectral exponent n was the most suitable parameter of the power spectral density function to be considered in this

investigation.

5.5.1 Experimental Investigation

The procedure adopted to determine the effects of the static stability of the medium, for conditions associated with the "β-type" of fading, may be outlined as follows.

1. Each available fading power spectrum, belonging to the "β-type" category, was plotted on logarithmic scales, so that an inverse power law, possibly governing the power spectral density function, could be readily detected. Since all the fading spectra were decreasing very rapidly, only the frequency range up to 0.6 Hz was examined. In order to increase the consistency of the spectral estimates, further averaging in the frequency domain was performed as described in Subsection 4.2.2. This had the effect of reducing the standard error of estimation to less than 10% (see Subsection 4.2.2).

2. A least-squares polynomial was fitted to the resulting spectral estimates by means of the routine E02ABF (see Appendix IV). By this method a more complete picture of each power spectrum was obtained.

The power spectra resulting from this process are shown in Figs. 5.11 - 5.25.

From these plottings it can be seen that the slope of the logarithmic power spectra is nearly constant for most of the frequency range under consideration. In a few cases, the spectral exponent n appears to vary gradually

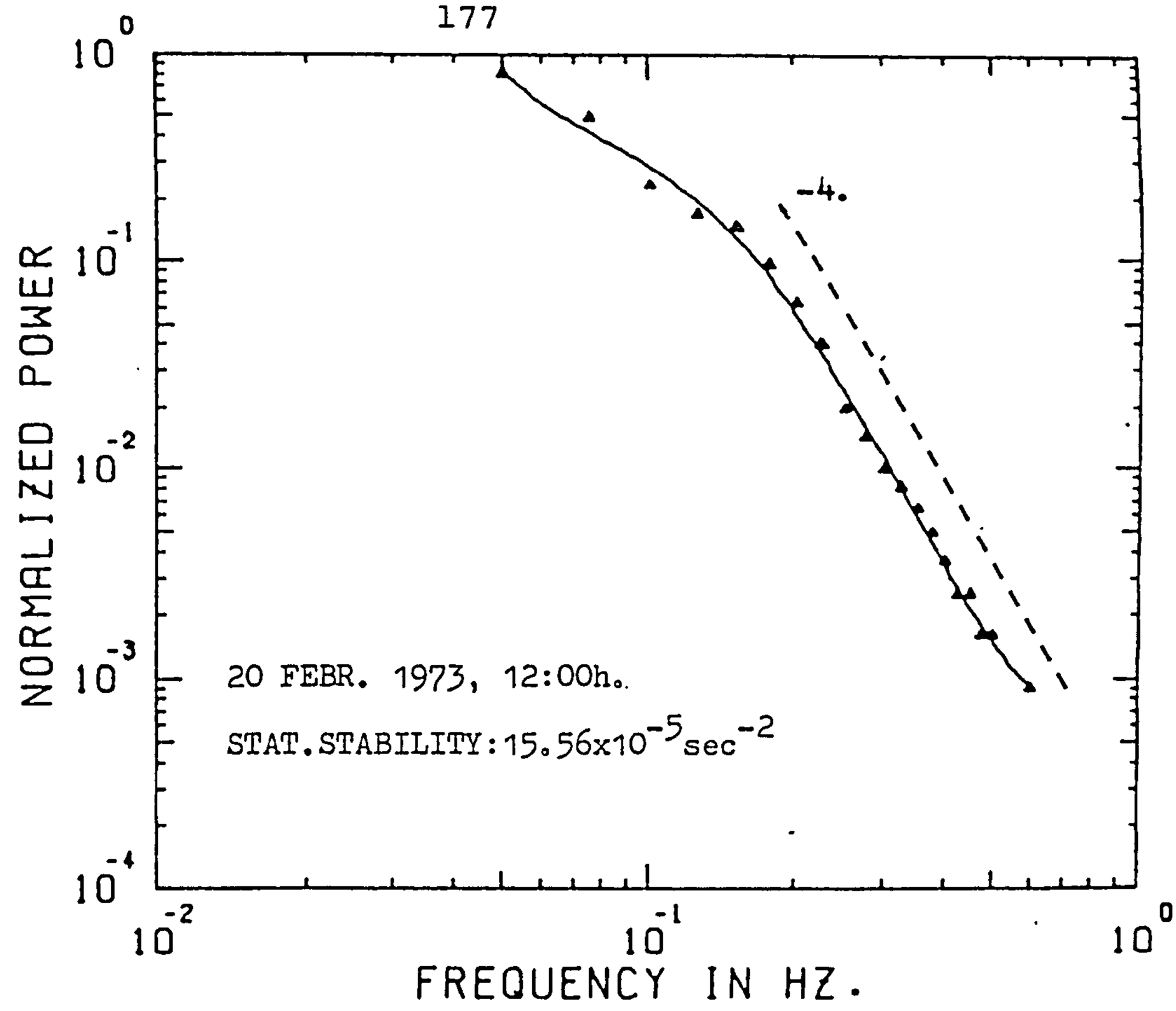
NORMALIZED POWER
10^{0}
10^{-1}
10^{-2}
10^{-3}
10^{-4}
-4.
20 FEBR. 1973, 12:00h.
STAT.STABILITY: $15.56 \times 10^{-5} sec^{-2}$
10^{-2}
10^{-1}
10^{0}
FREQUENCY IN HZ.

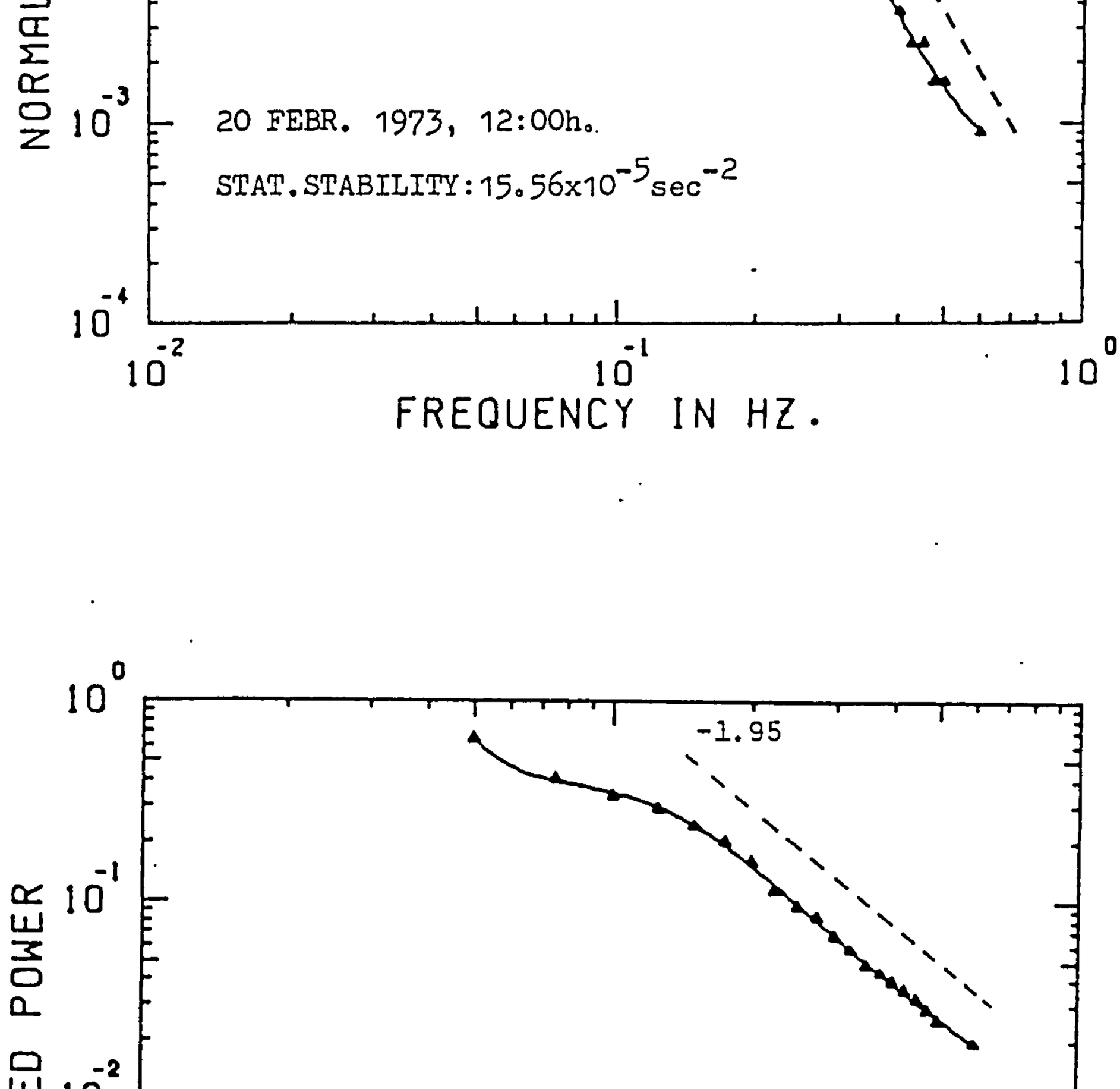
NORMALIZED POWER
10^{0}
10^{-1}
10^{-2}
10^{-3}
10^{-4}
-1.95
13 MARCH 1973, 12:00h.
STAT.STABILITY: $0.46 \times 10^{-5} sec^{-2}$
10^{-2}
10^{-1}
10^{0}
FREQUENCY IN HZ.

FIGURE 5.1i

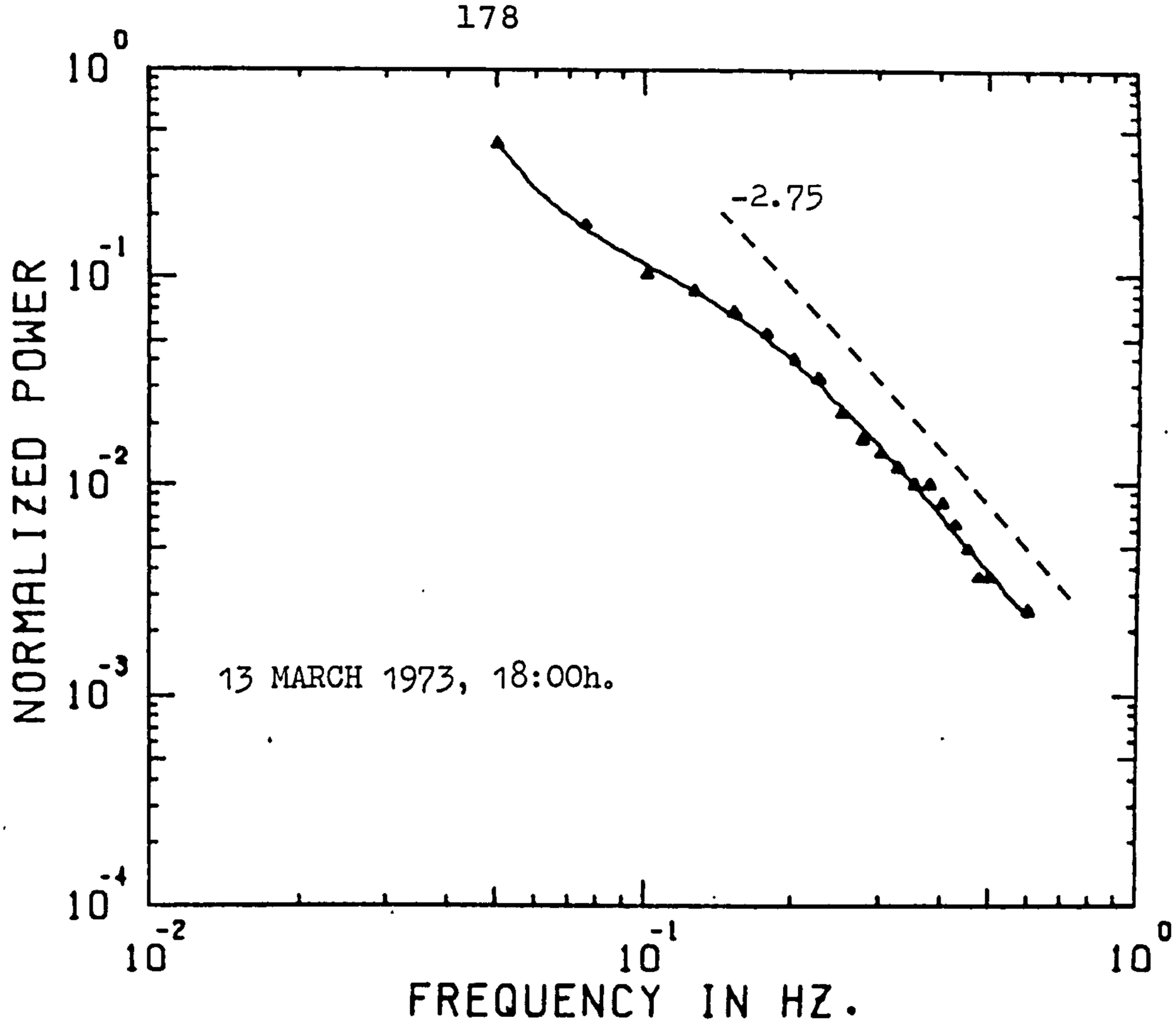
NORMALIZED POWER
10^{0}
10^{-1}
10^{-2}
10^{-3}
10^{-4}
-2.75
13 MARCH 1973, 18:00h.
10^{-2}
10^{-1}
10^{0}
FREQUENCY IN HZ.

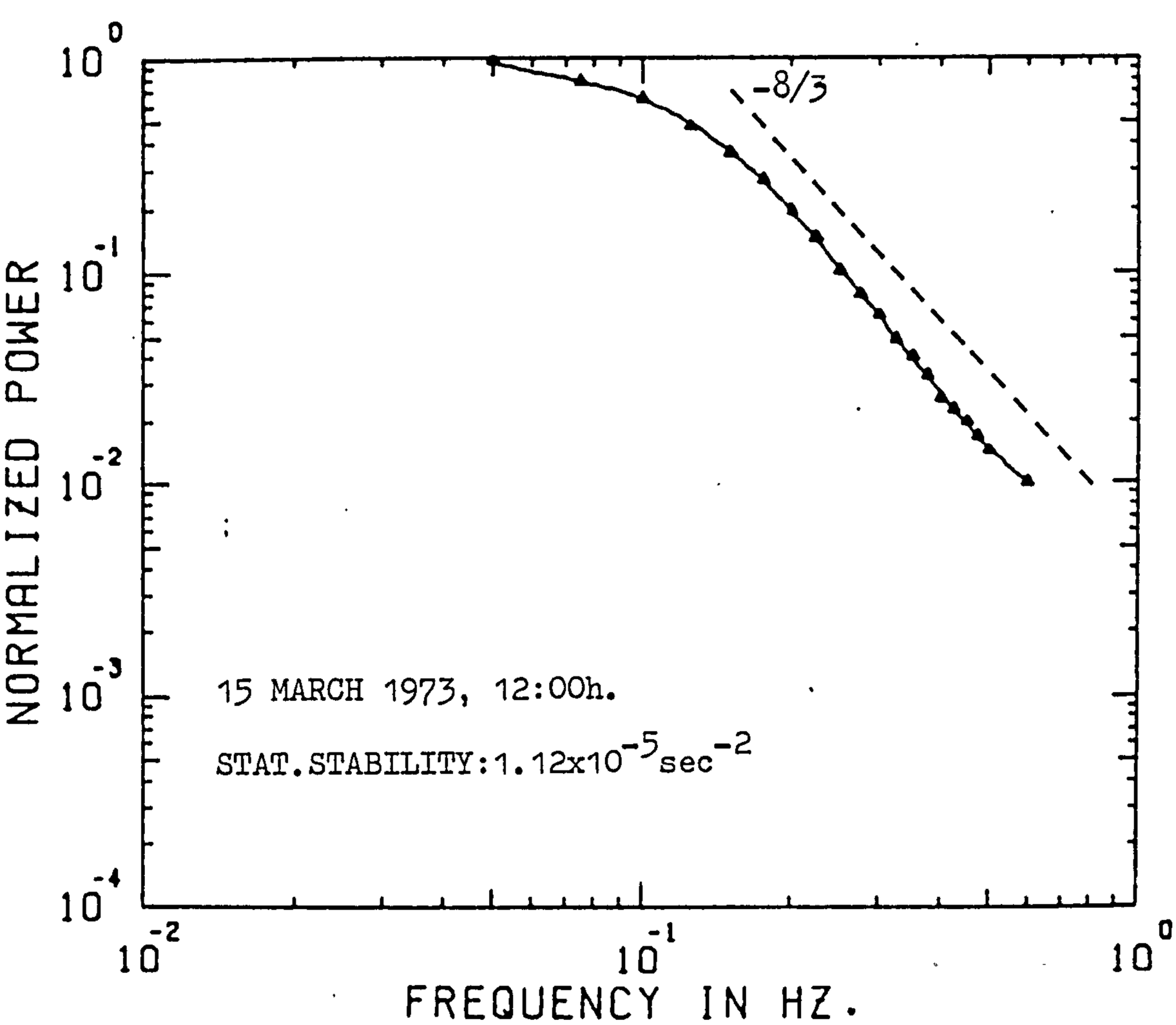
NORMALIZED POWER
10^{0}
10^{-1}
10^{-2}
10^{-3}
10^{-4}
-8/3
15 MARCH 1973, 12:00h.
STAT.STABILITY: $1.12 \times 10^{-5} sec^{-2}$
10^{-2}
10^{-1}
10^{0}
FREQUENCY IN HZ.

FIGURE 5.12

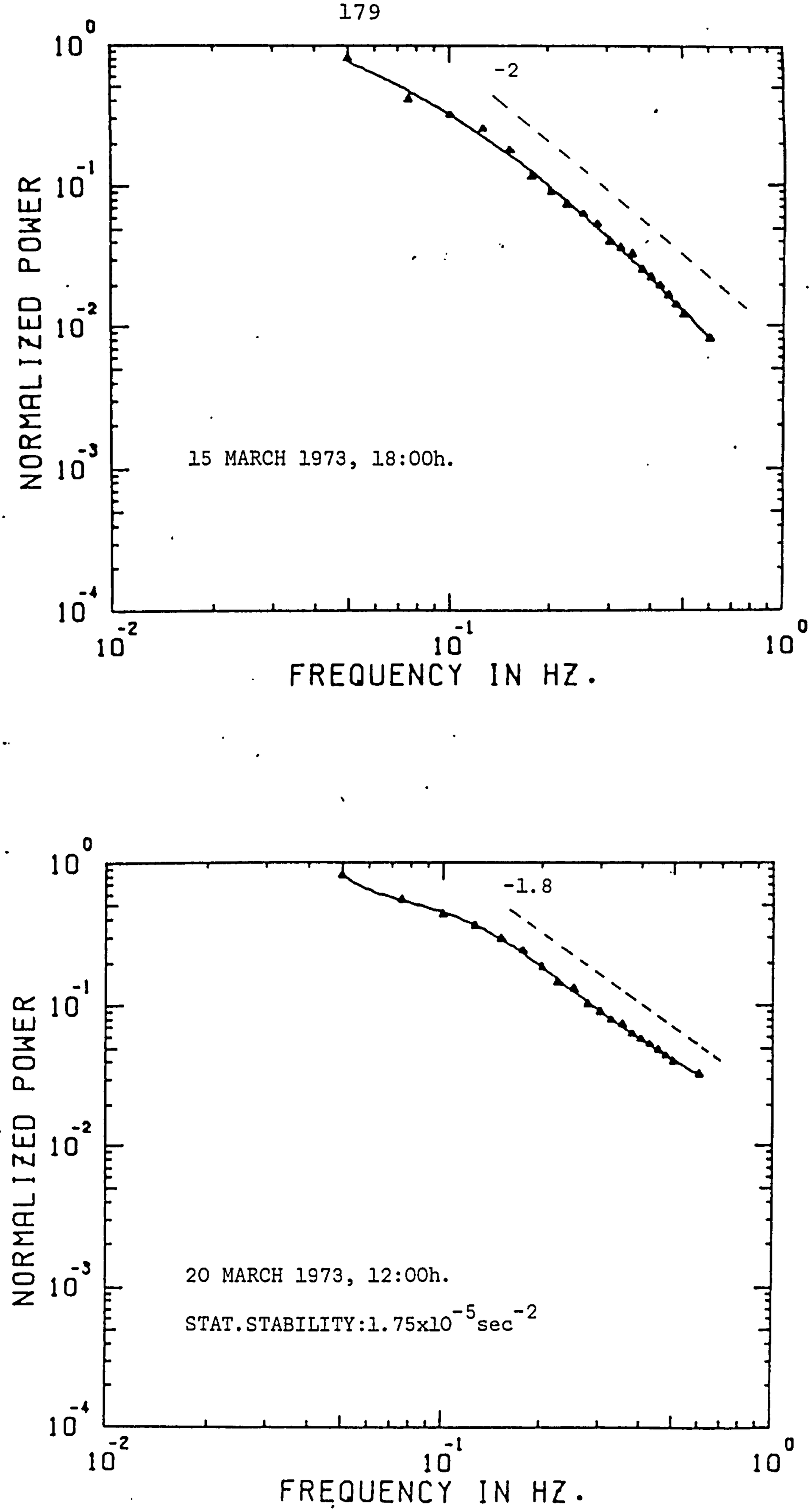
NORMALIZED POWER
10^{0}
10^{-1}
10^{-2}
10^{-3}
10^{-4}
-2
15 MARCH 1973, 18:00h.
10^{-2}
10^{-1}
10^{0}
FREQUENCY IN HZ.
NORMALIZED POWER
10^{0}
10^{-1}
10^{-2}
10^{-3}
10^{-4}
-1.8
20 MARCH 1973, 12:00h.
STAT.STABILITY:1.75x10^{-5}sec^{-2}
10^{-2}
10^{-1}
10^{0}
FREQUENCY IN HZ.

FIGURE 5.1 3

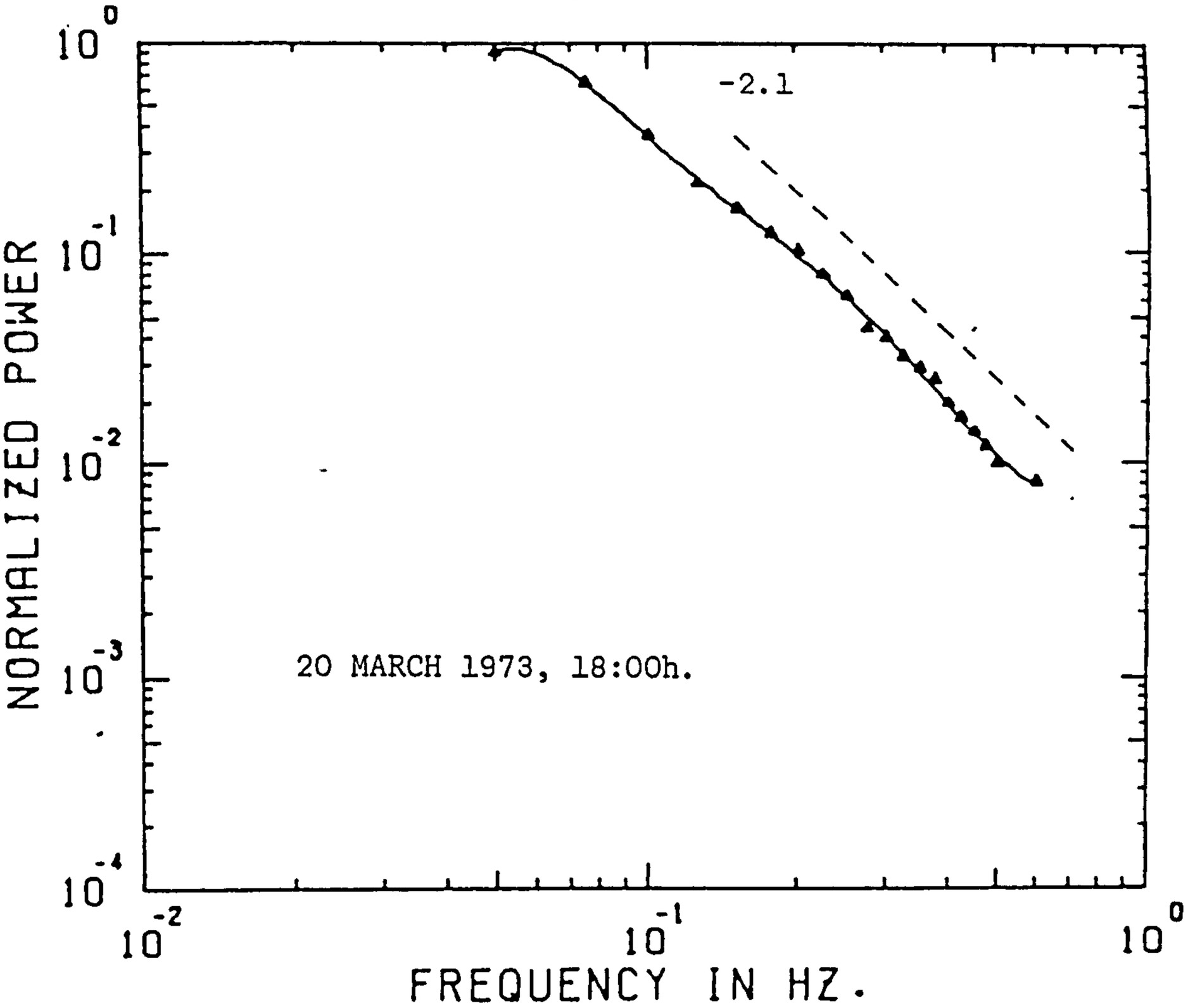
NORMALIZED POWER
10^{0}
10^{-1}
10^{-2}
10^{-3}
10^{-4}
-2.1
20 MARCH 1973, 18:00h.
10^{-2}
10^{-1}
10^{0}
FREQUENCY IN HZ.

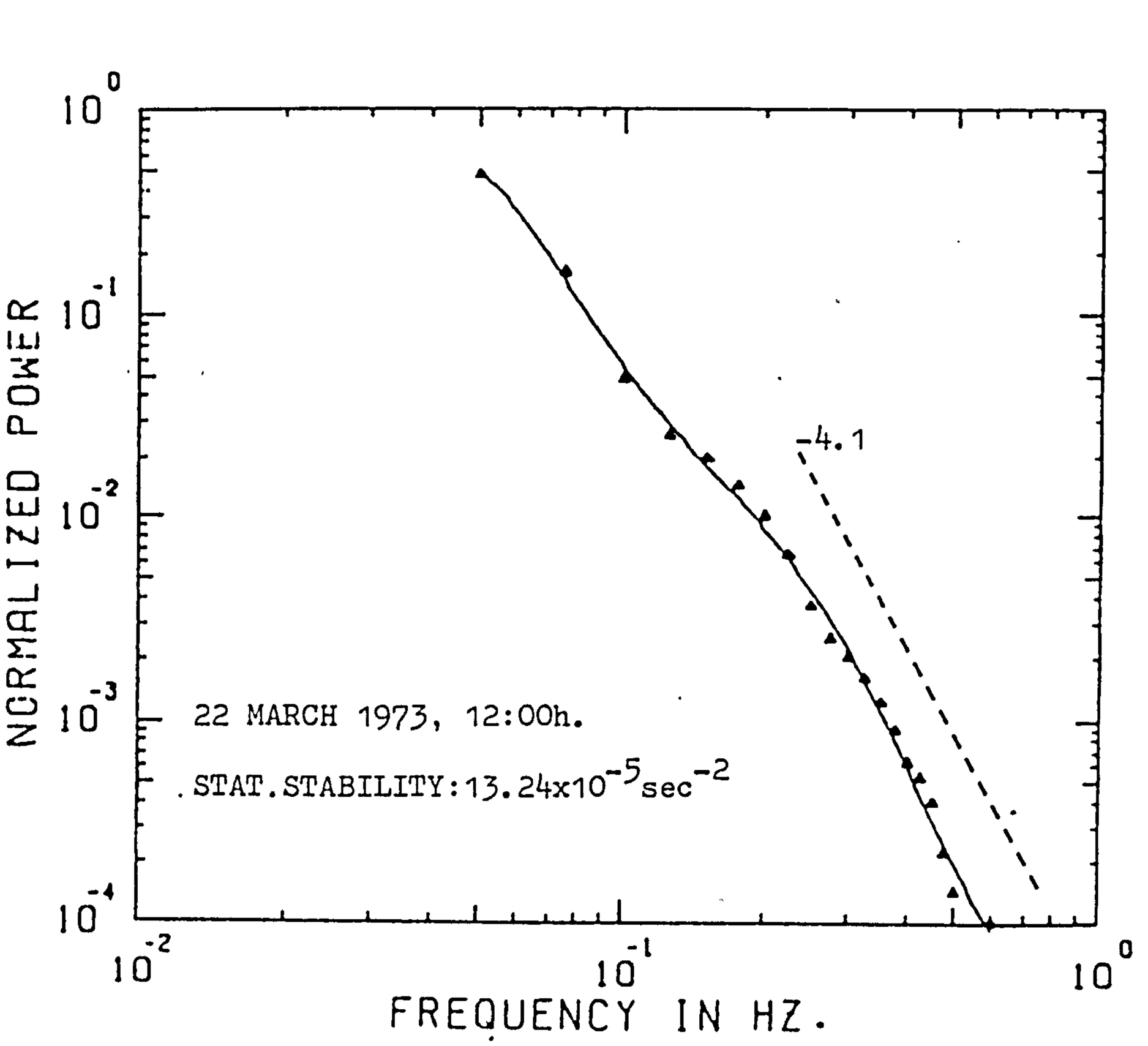
NORMALIZED POWER
10^{0}
10^{-1}
10^{-2}
10^{-3}
10^{-4}
-4.1
22 MARCH 1973, 12:00h.
STAT.STABILITY: 13.24×10^{-5} sec^{-2}
10^{-2}
10^{-1}
10^{0}
FREQUENCY IN HZ.

FIGURE 5.14

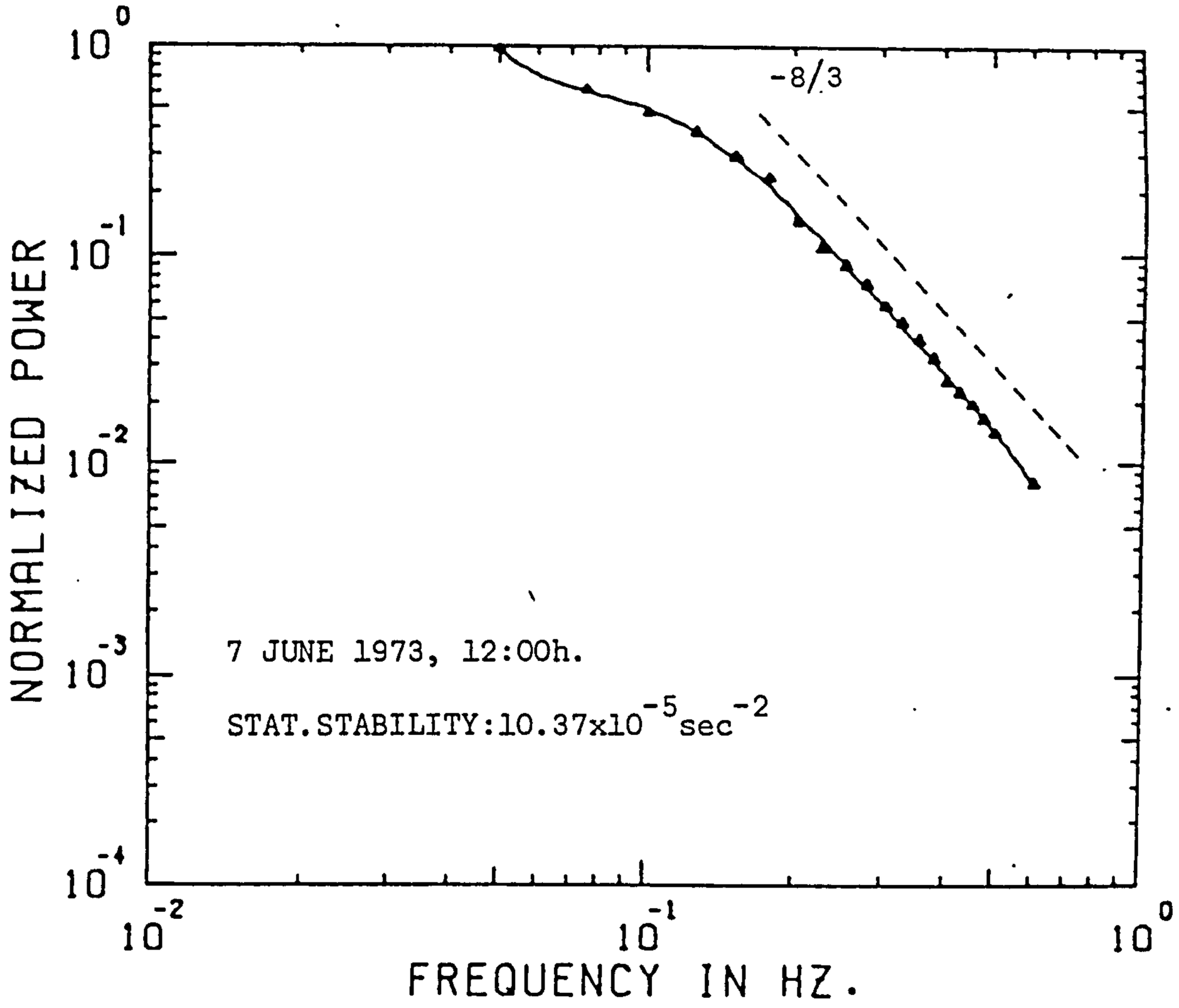
NORMALIZED POWER
10^{0}
10^{-1}
10^{-2}
10^{-3}
10^{-4}
-8/3
7 JUNE 1973, 12:00h.
STAT.STABILITY:10.37x10^{-5}sec^{-2}
10^{-2}
10^{-1}
10^{0}
FREQUENCY IN HZ.

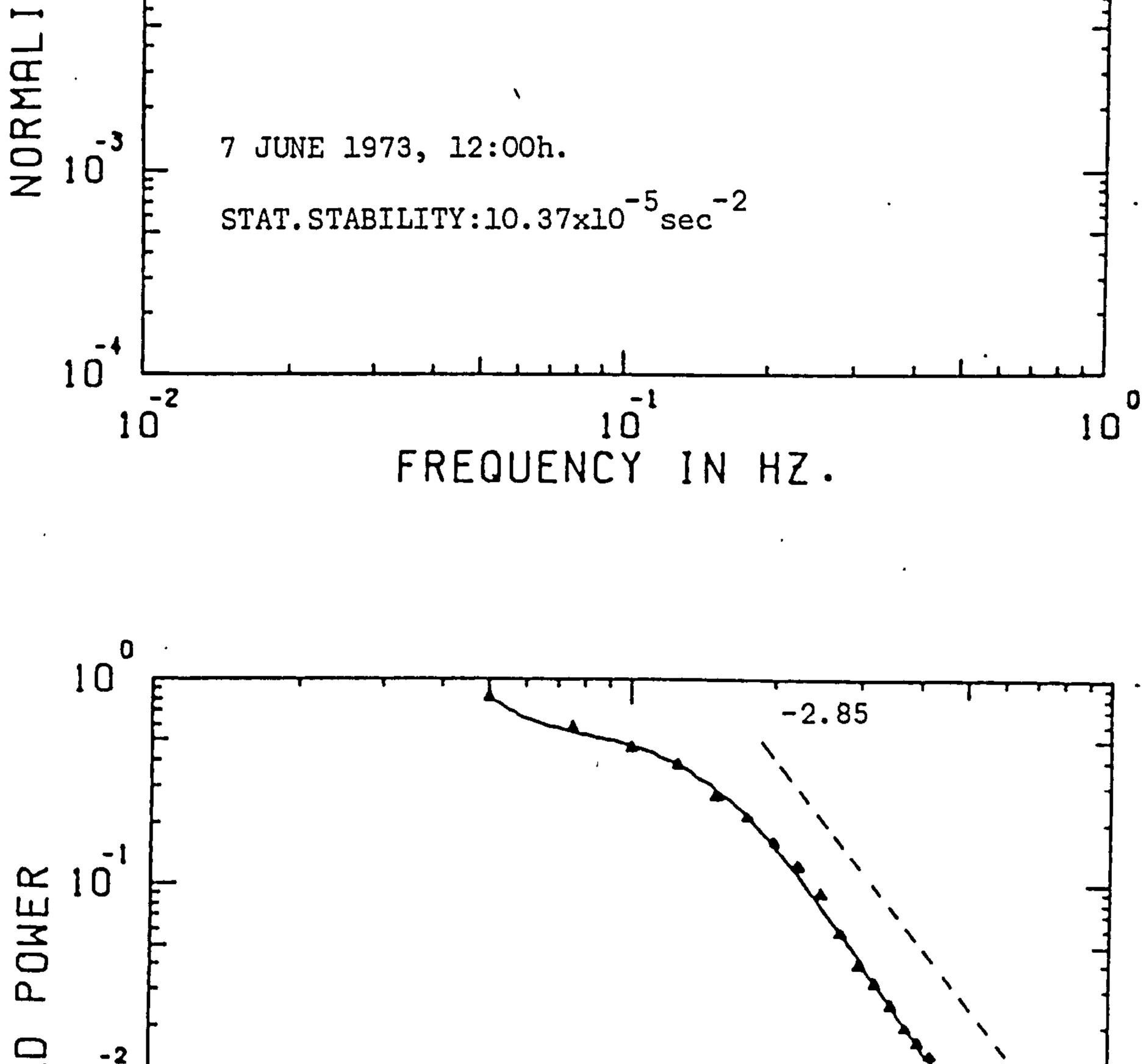
NORMALIZED POWER
10^{0}
10^{-1}
10^{-2}
10^{-3}
10^{-4}
-2.85
7 JUNE1973, 18:00h.
10^{-2}
10^{-1}
10^{0}
FREQUENCY IN HZ.

FIGURE 5.15

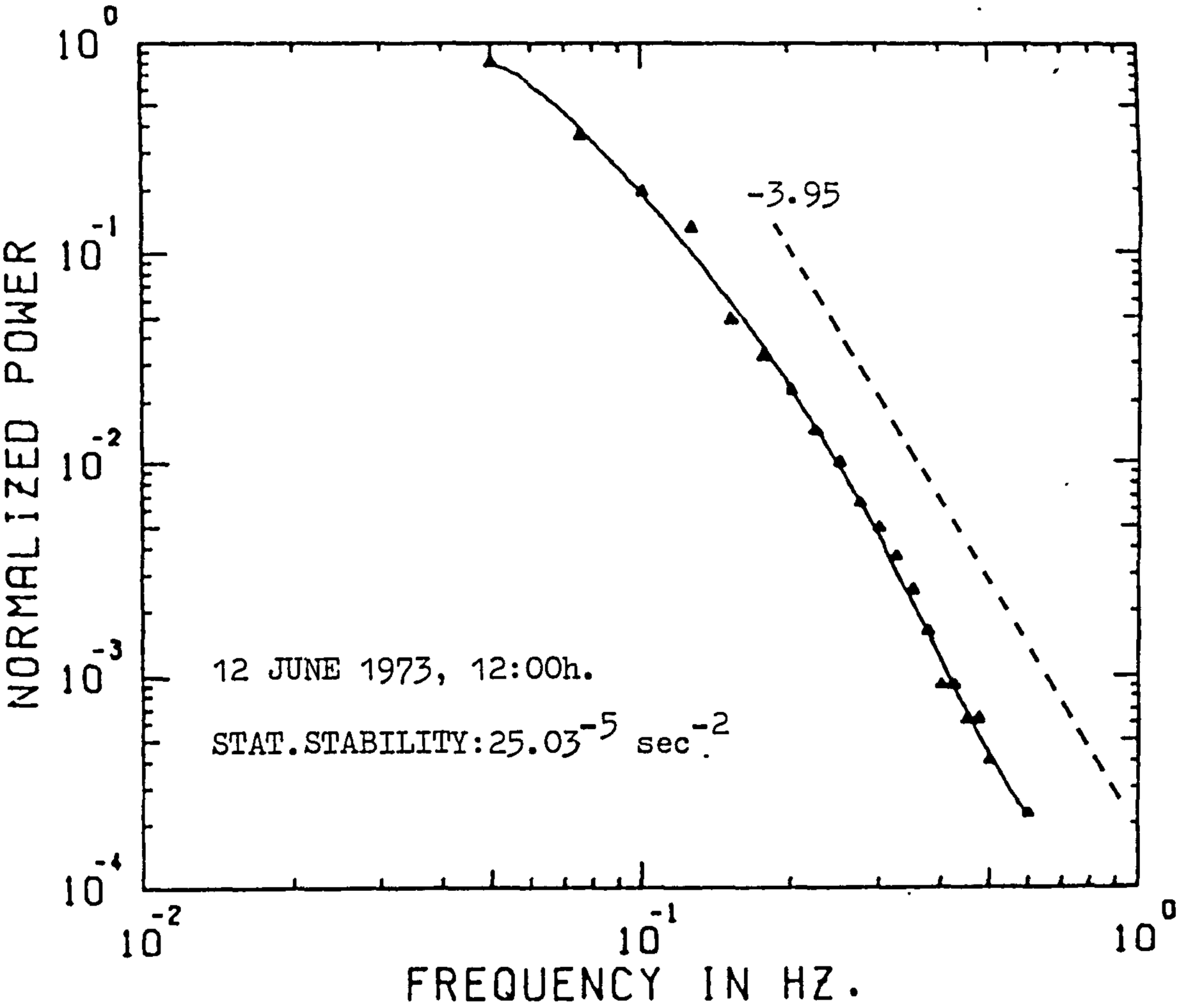
NORMALIZED POWER
10^{0}
10^{-1}
10^{-2}
10^{-3}
10^{-4}
-3.95
12 JUNE 1973, 12:00h.
STAT.STABILITY:25.03^{-5} sec^{-2}
10^{-2}
10^{-1}
10^{0}
FREQUENCY IN HZ.

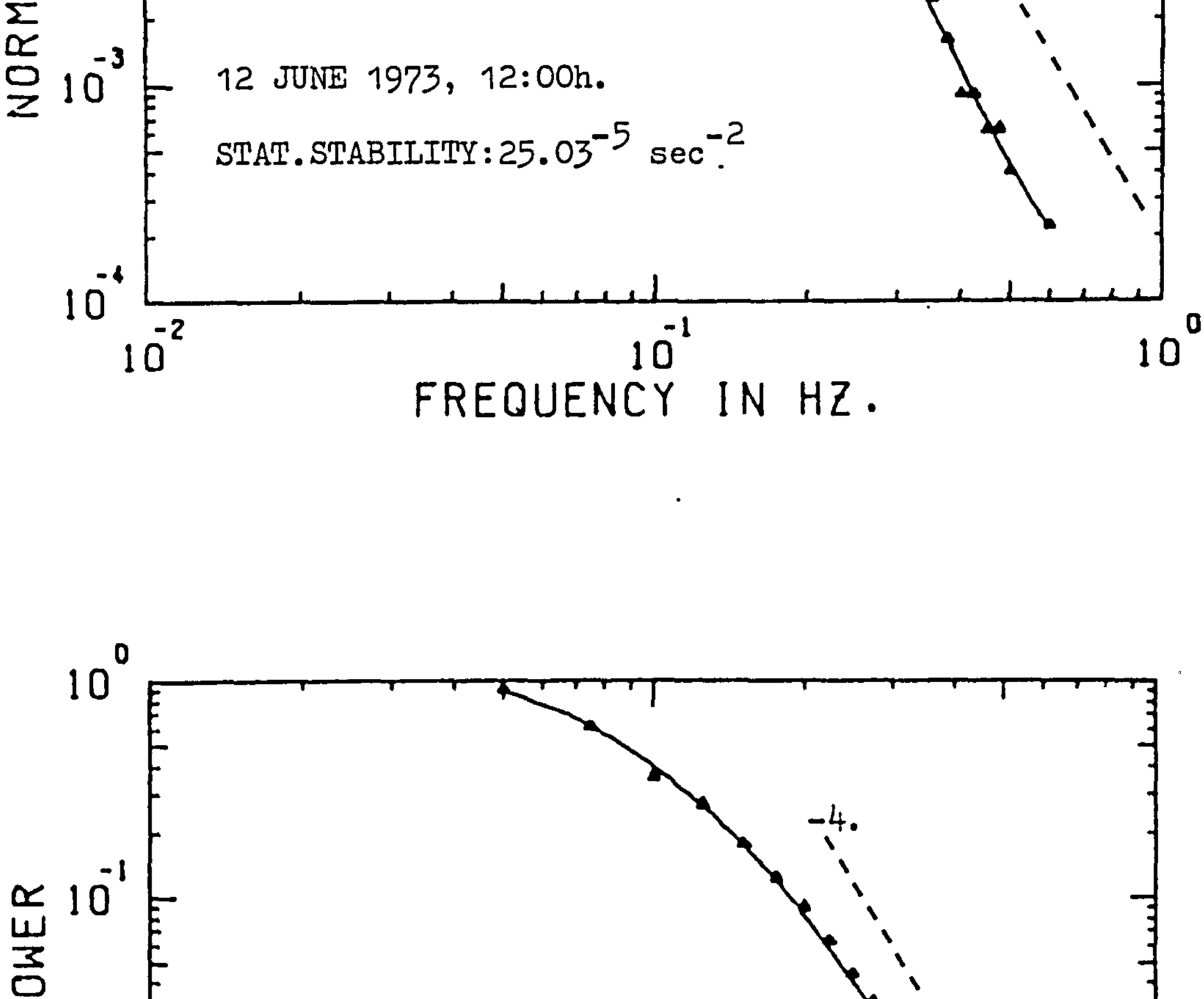
NORMALIZED POWER
10^{0}
10^{-1}
10^{-2}
10^{-3}
10^{-4}
-4.
12 JUNE 1973, 18:00h.
10^{-2}
10^{-1}
10^{0}
FREQUENCY IN HZ.

FIGURE 5.16

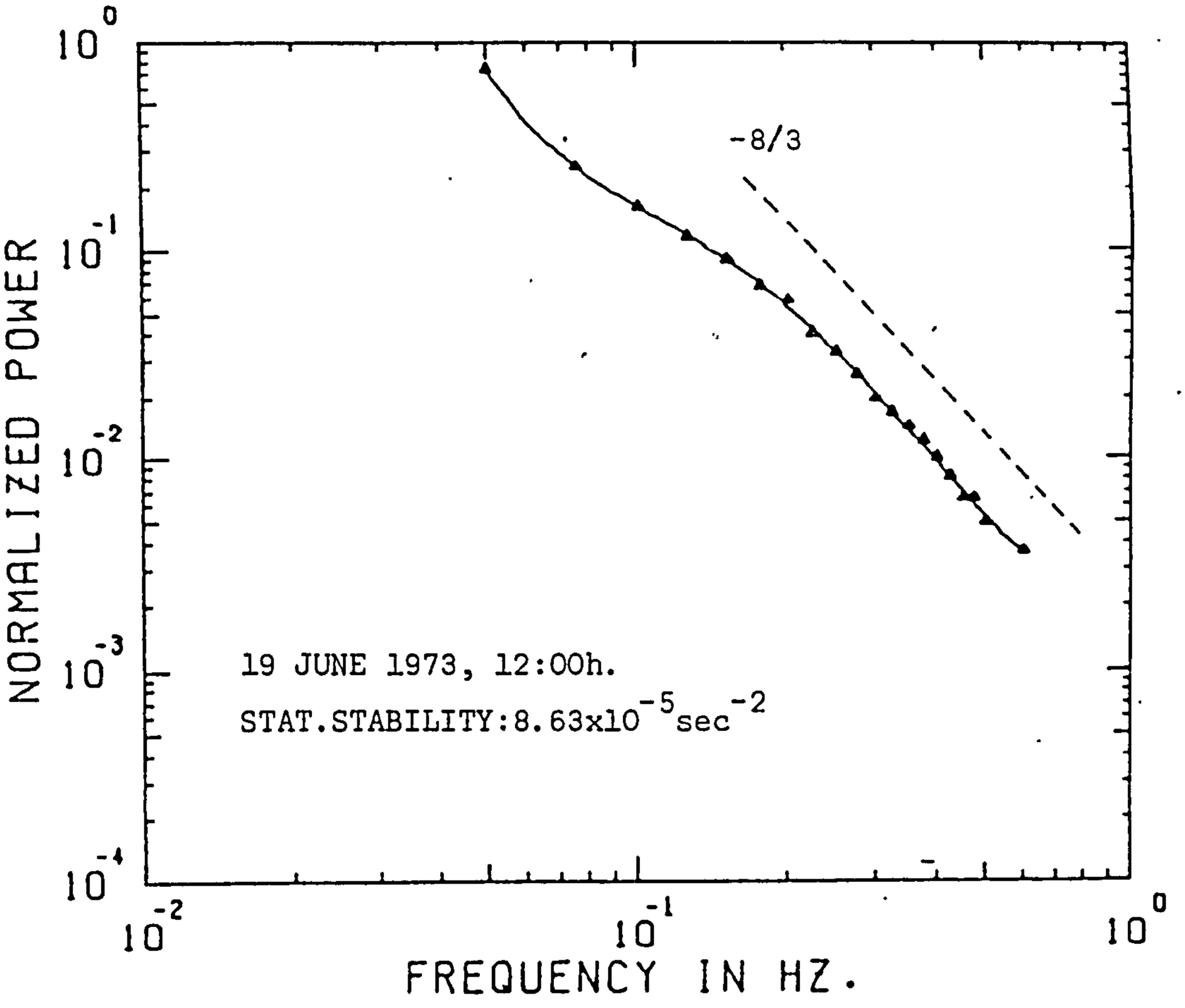
NORMALIZED POWER
10^{0}
10^{-1}
10^{-2}
10^{-3}
10^{-4}
-8/3
19 JUNE 1973, 12:00h.
STAT.STABILITY:8.63x10^{-5}sec^{-2}
10^{-2}
10^{-1}
10^{0}
FREQUENCY IN HZ.

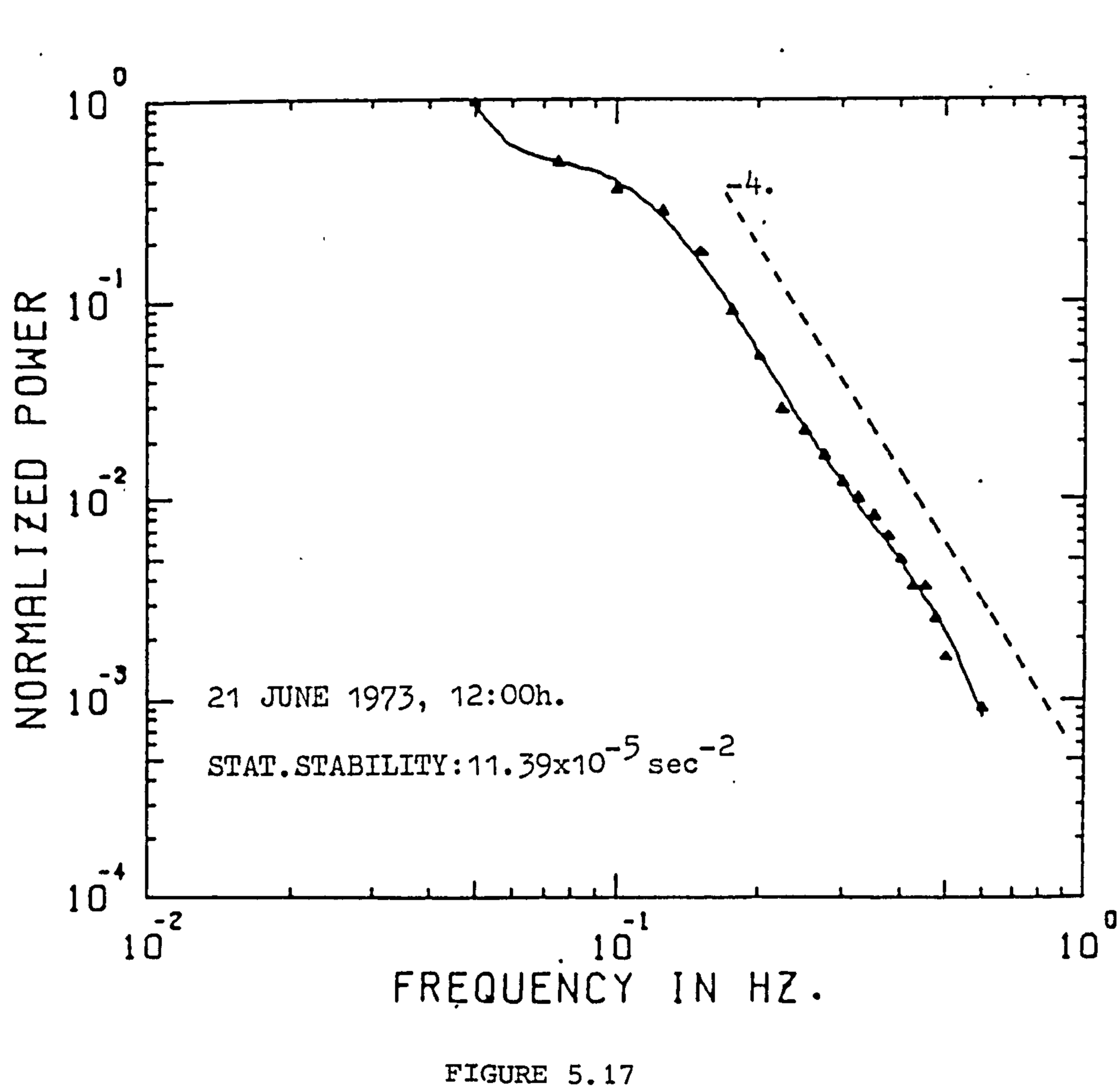
NORMALIZED POWER
10^{0}
10^{-1}
10^{-2}
10^{-3}
10^{-4}
-4.
21 JUNE 1973, 12:00h.
STAT.STABILITY:11.39x10^{-5} sec^{-2}
10^{-2}
10^{-1}
10^{0}
FREQUENCY IN HZ.

FIGURE 5.17

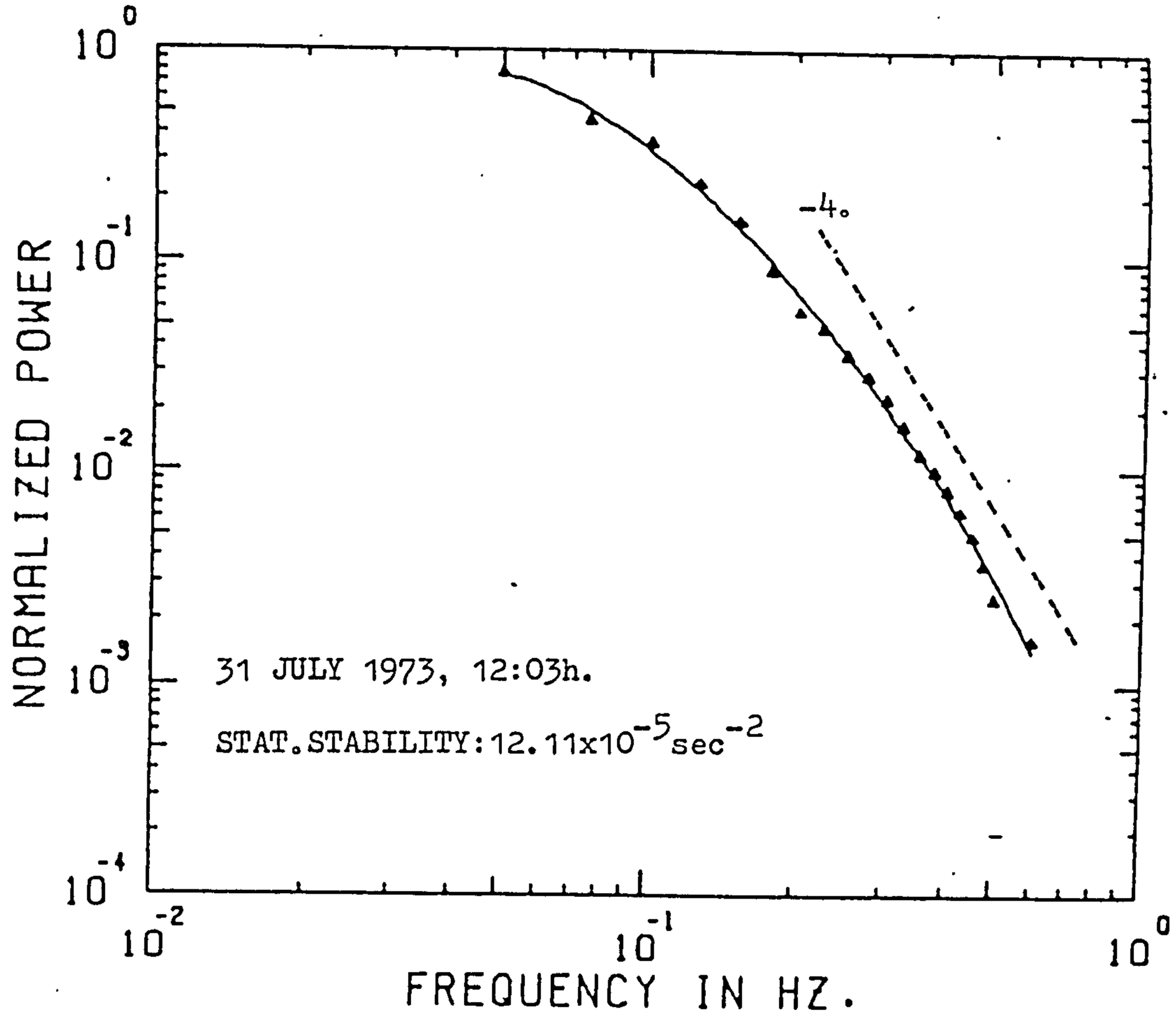
NORMALIZED POWER
10^{0}
10^{-1}
10^{-2}
10^{-3}
10^{-4}
-4
31 JULY 1973, 12:03h.
STAT.STABILITY: $12.11 \times 10^{-5} sec^{-2}$
10^{-2}
10^{-1}
10^{0}
FREQUENCY IN HZ.

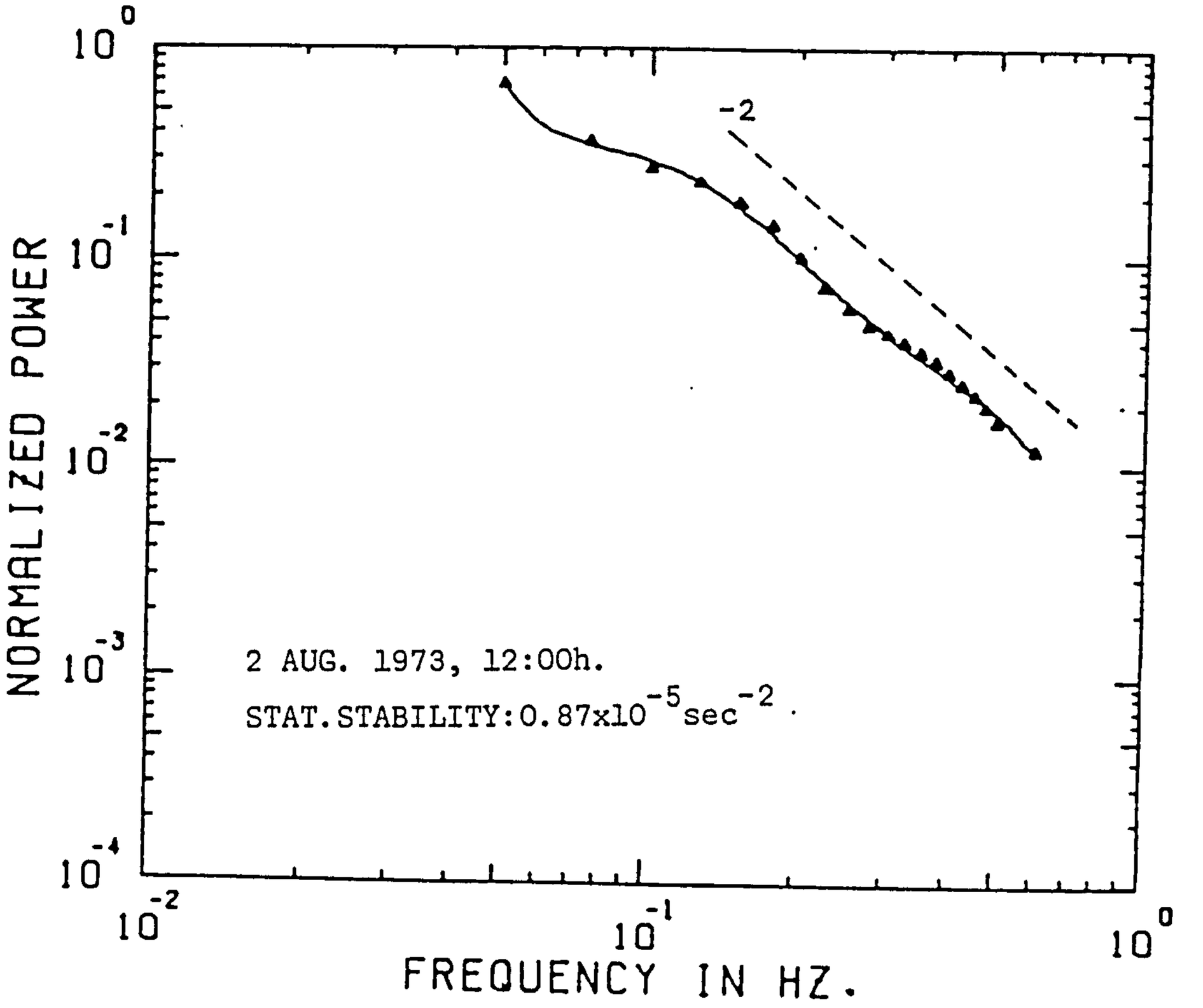
NORMALIZED POWER
10^{0}
10^{-1}
10^{-2}
10^{-3}
10^{-4}
-2
2 AUG. 1973, 12:00h.
STAT.STABILITY: $0.87 \times 10^{-5} sec^{-2}$
10^{-2}
10^{-1}
10^{0}
FREQUENCY IN HZ.

FIGURE 5.18

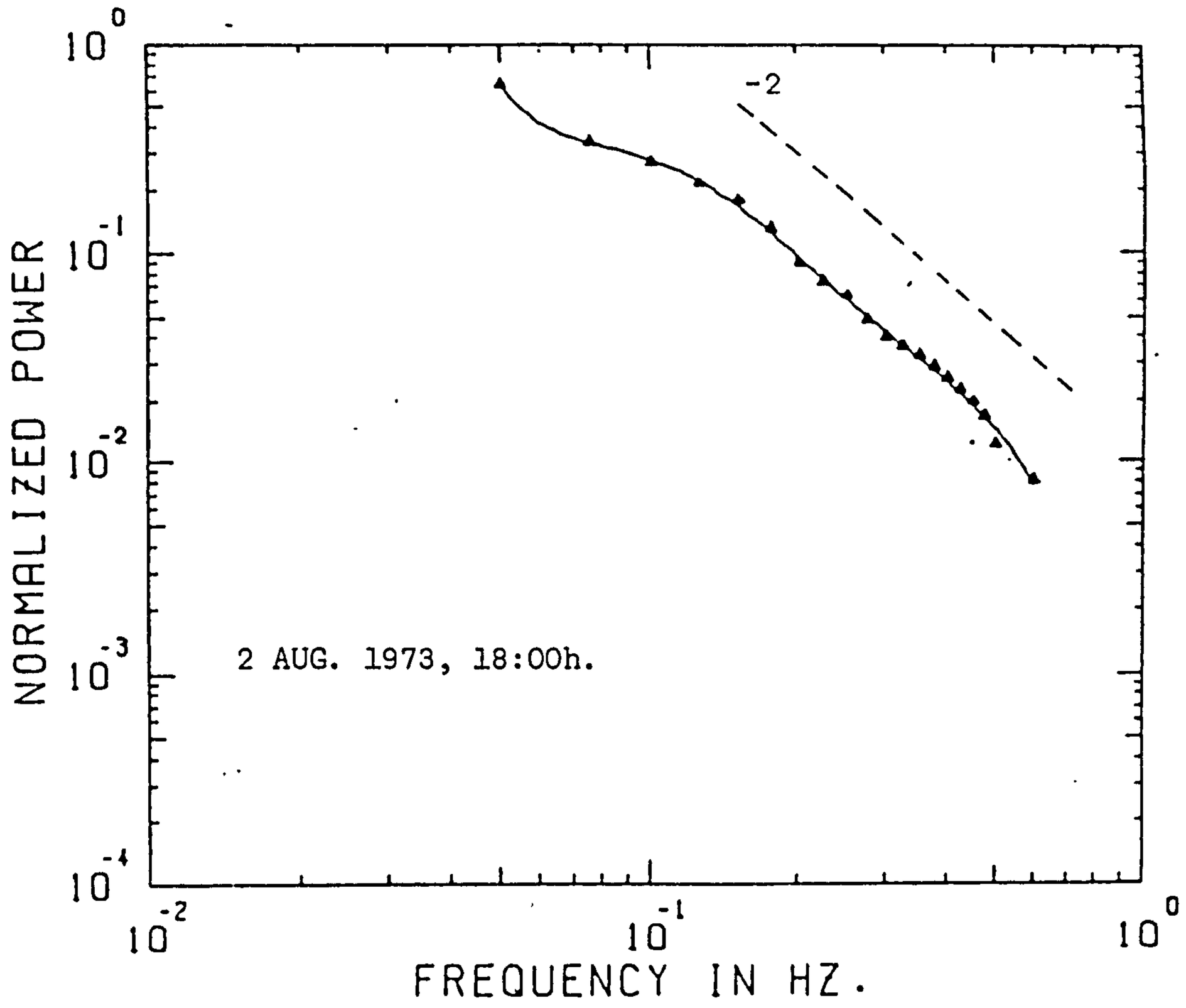
NORMALIZED POWER
10^{0}
10^{-1}
10^{-2}
10^{-3}
10^{-4}
-2
2 AUG. 1973, 18:00h.
10^{-2}
10^{-1}
10^{0}
FREQUENCY IN HZ.

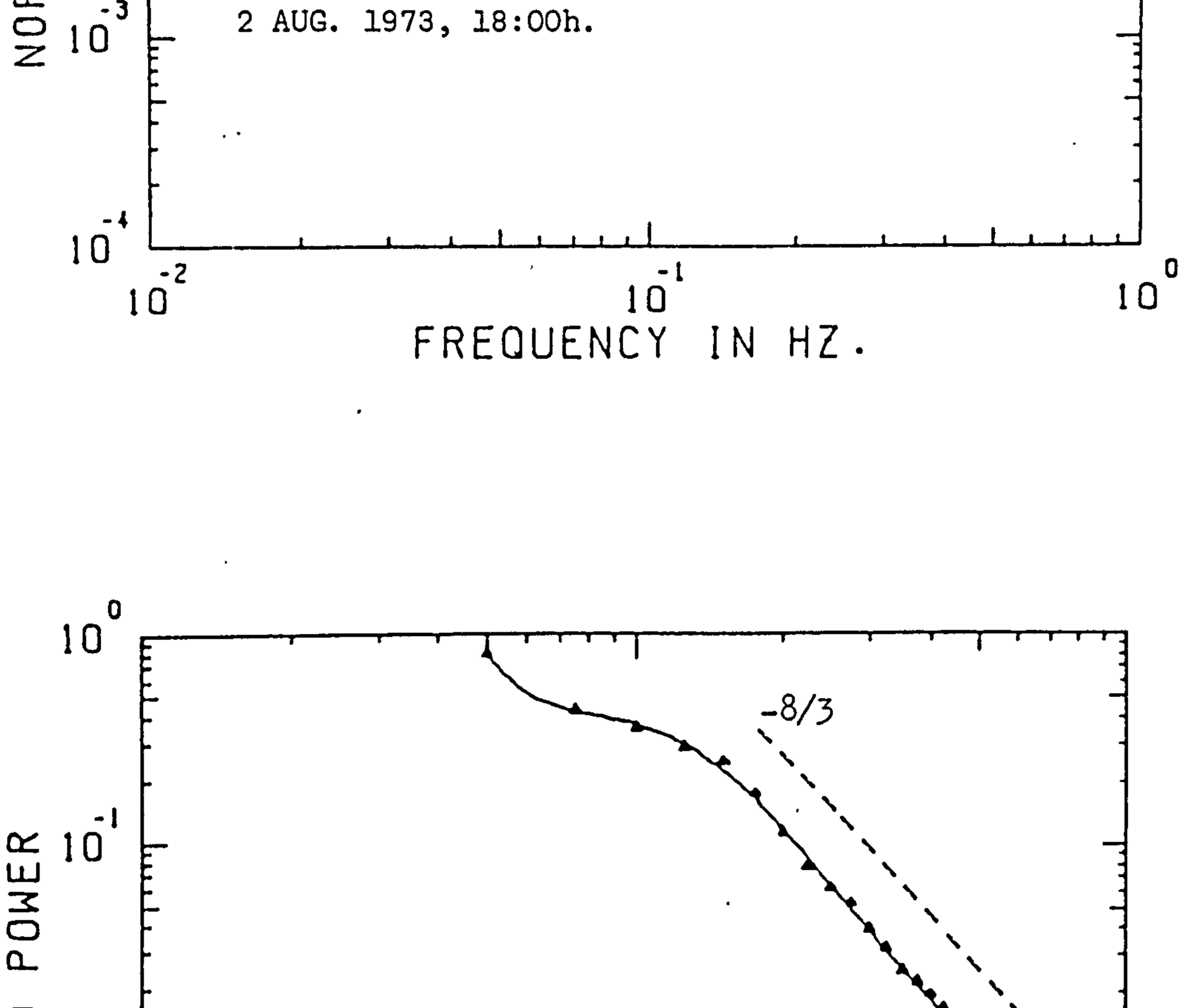
NORMALIZED POWER
10^{0}
10^{-1}
10^{-2}
10^{-3}
10^{-4}
-8/3
4 SEPT. 1973, 12:00h.
STAT. STABILITY: $10.61 \times 10^{-5} sec^{-2}$
10^{-2}
10^{-1}
10^{0}
FREQUENCY IN HZ.

FIGURE 5.19

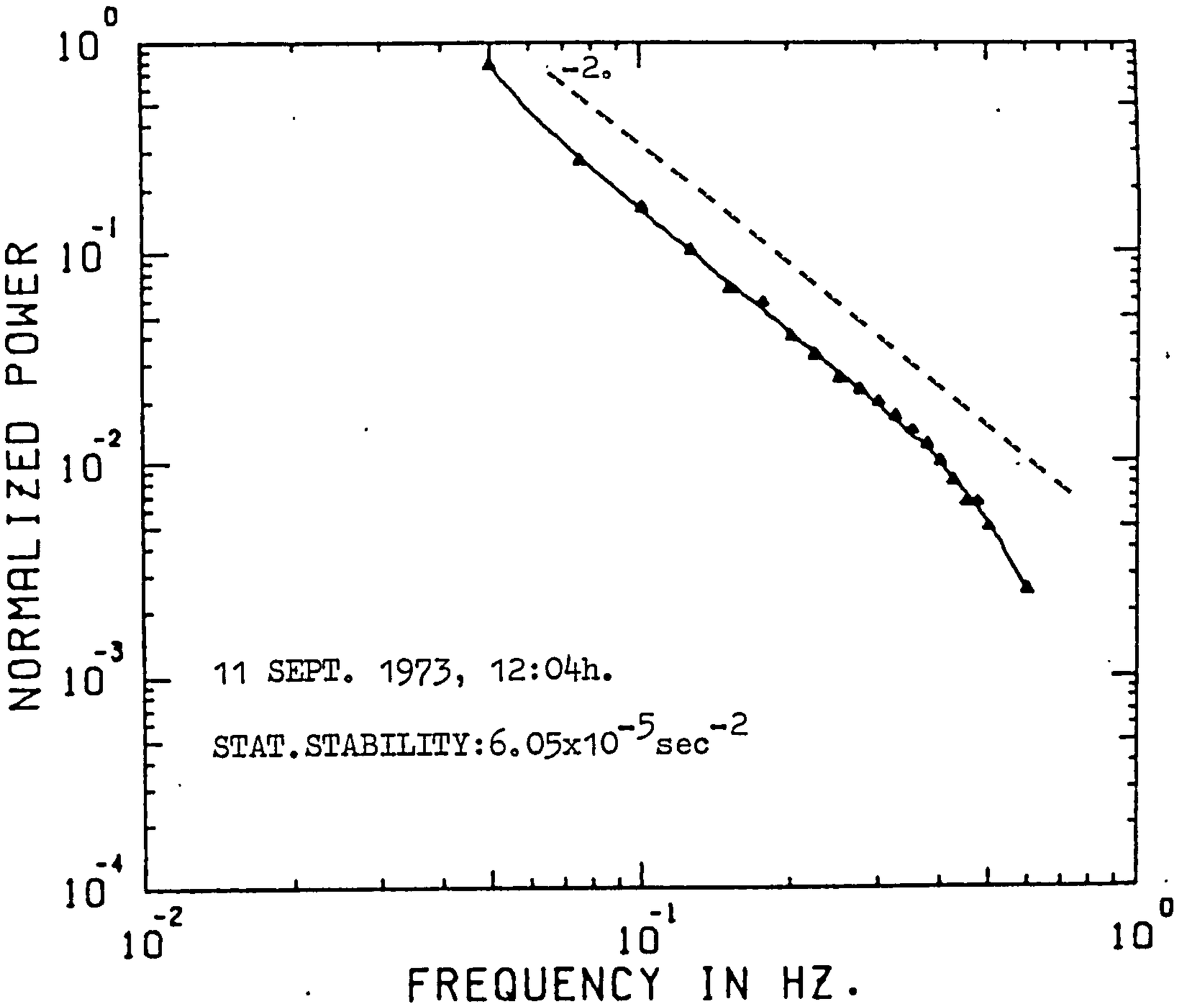
NORMALIZED POWER
10^{0}
10^{-1}
10^{-2}
10^{-3}
10^{-4}
-2.
11 SEPT. 1973, 12:04h.
STAT.STABILITY:6.05x10^{-5}sec^{-2}
10^{-2}
10^{-1}
10^{0}
FREQUENCY IN HZ.

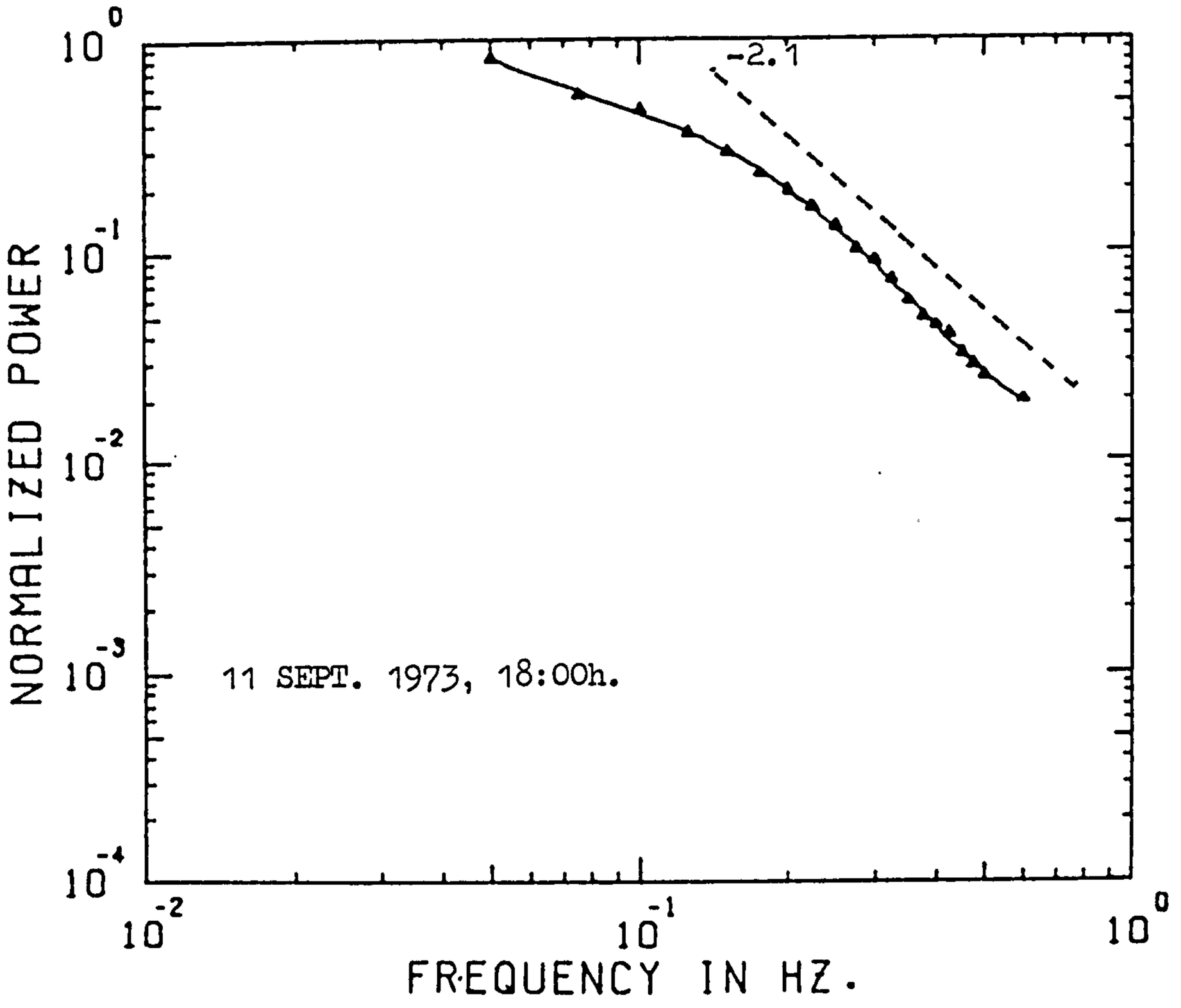
NORMALIZED POWER
10^{0}
10^{-1}
10^{-2}
10^{-3}
10^{-4}
-2.1
11 SEPT. 1973, 18:00h.
10^{-2}
10^{-1}
10^{0}
FREQUENCY IN HZ.

FIGURE 5.20

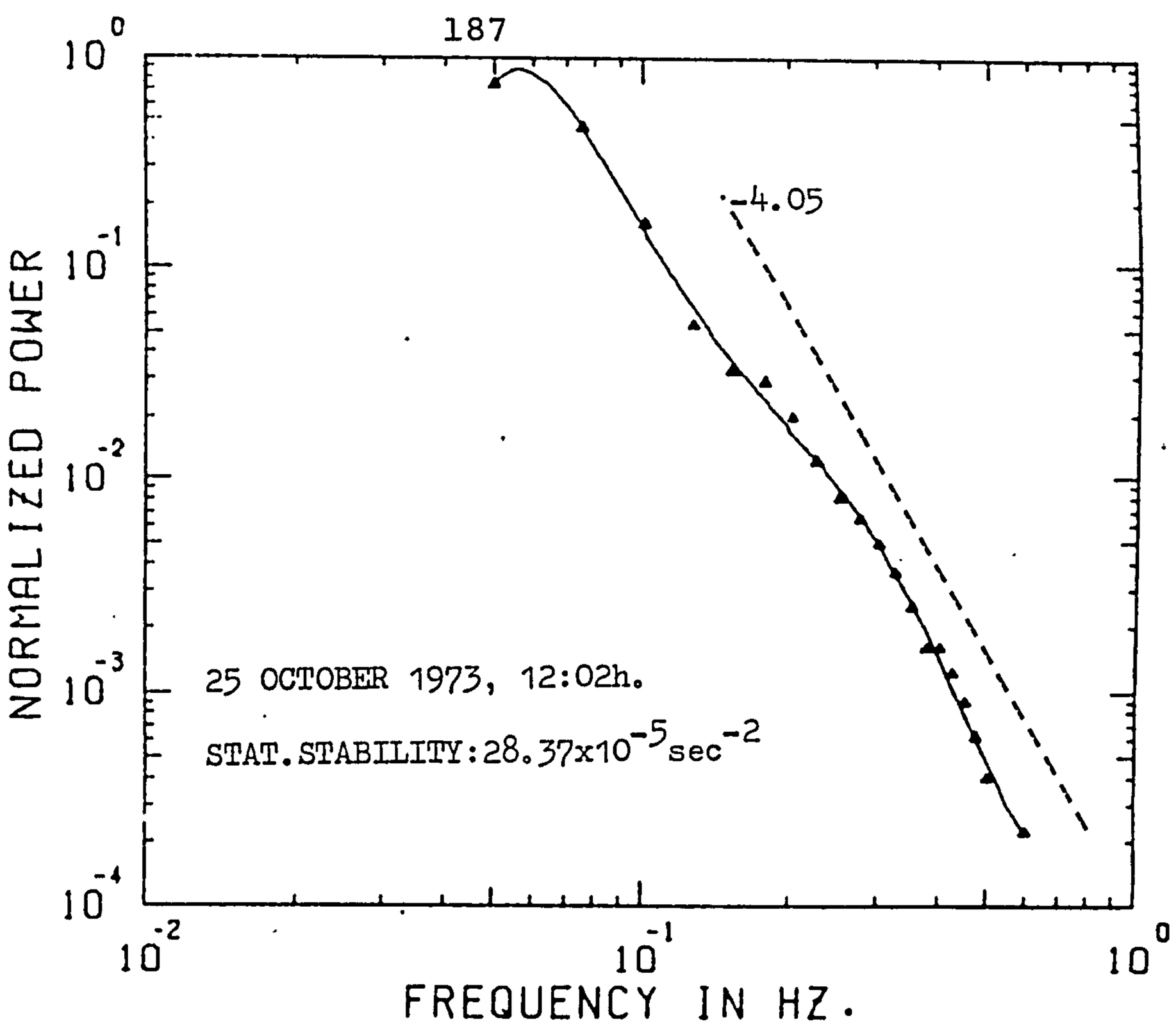
187
-4.05
NORMALIZED POWER
25 OCTOBER 1973, 12:02h.
STAT. STABILITY: 28.37x10^-5 sec^-2
FREQUENCY IN HZ.

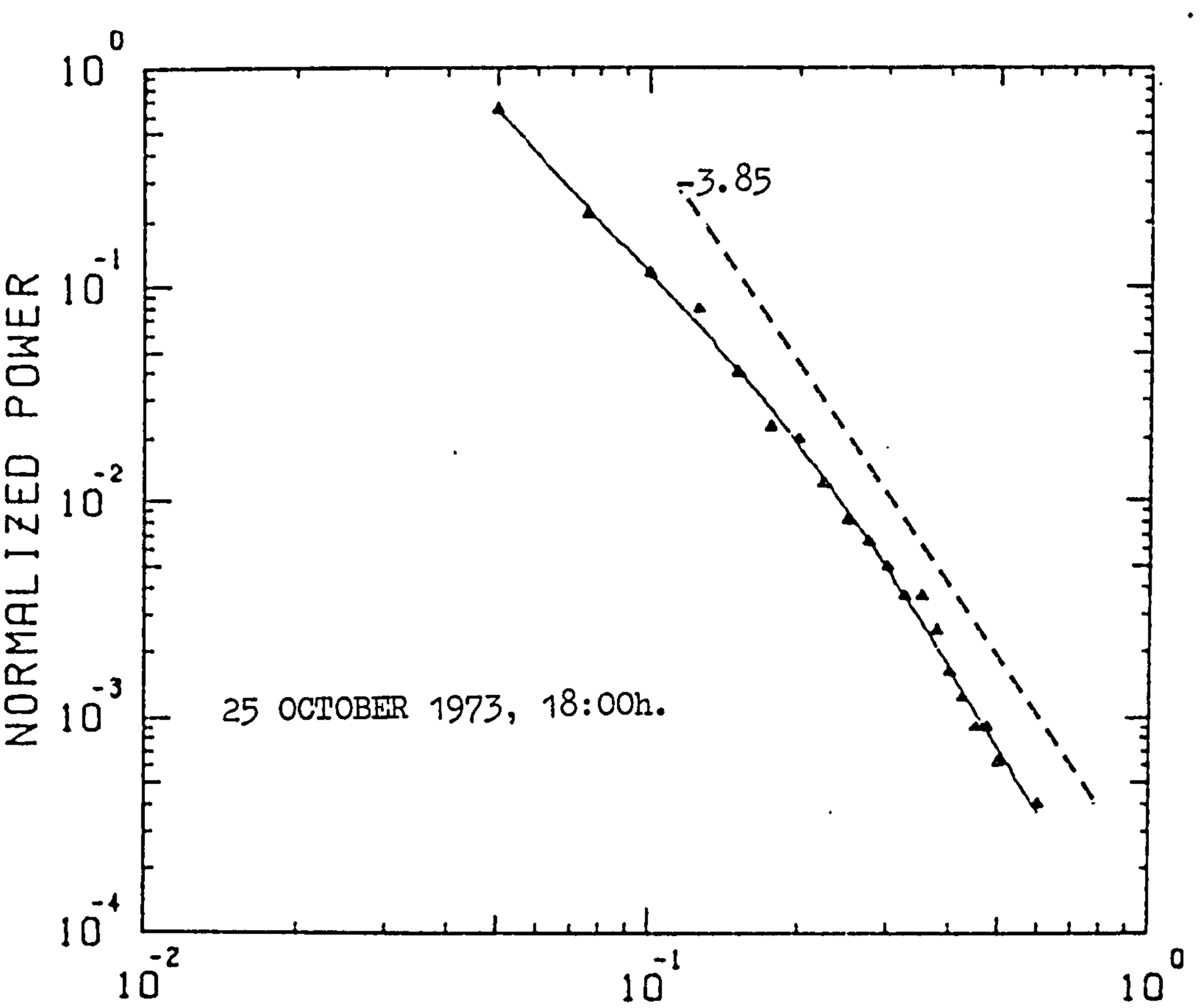
-3.85
NORMALIZED POWER
25 OCTOBER 1973, 18:00h.
FREQUENCY IN HZ.

FIGURE 5.21

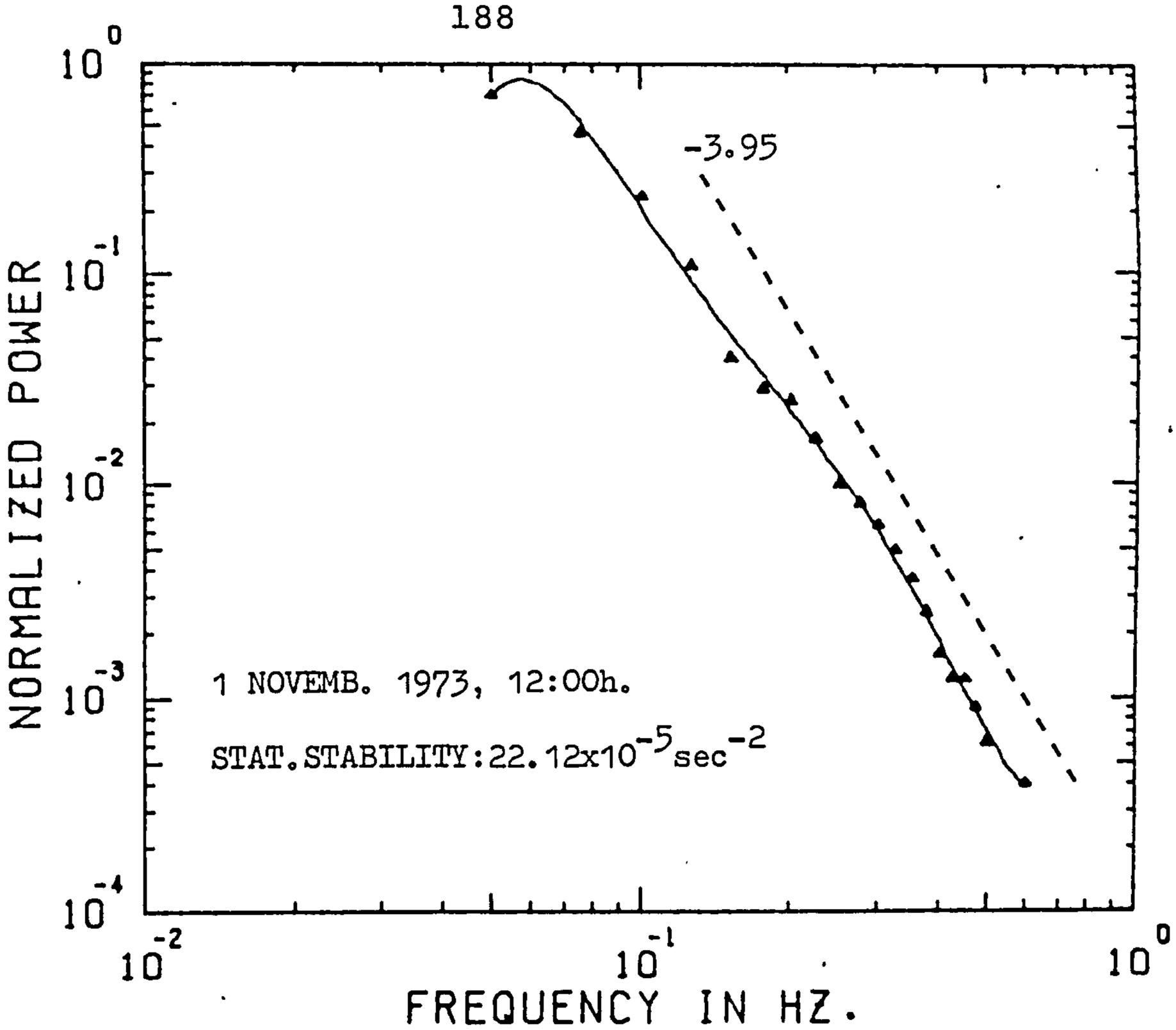
NORMALIZED POWER
10^{0}
10^{-1}
10^{-2}
10^{-3}
10^{-4}
-3.95
1 NOVEMB. 1973, 12:00h.
STAT.STABILITY:22.12x10^{-5}sec^{-2}
10^{-2}
10^{-1}
10^{0}
FREQUENCY IN HZ.

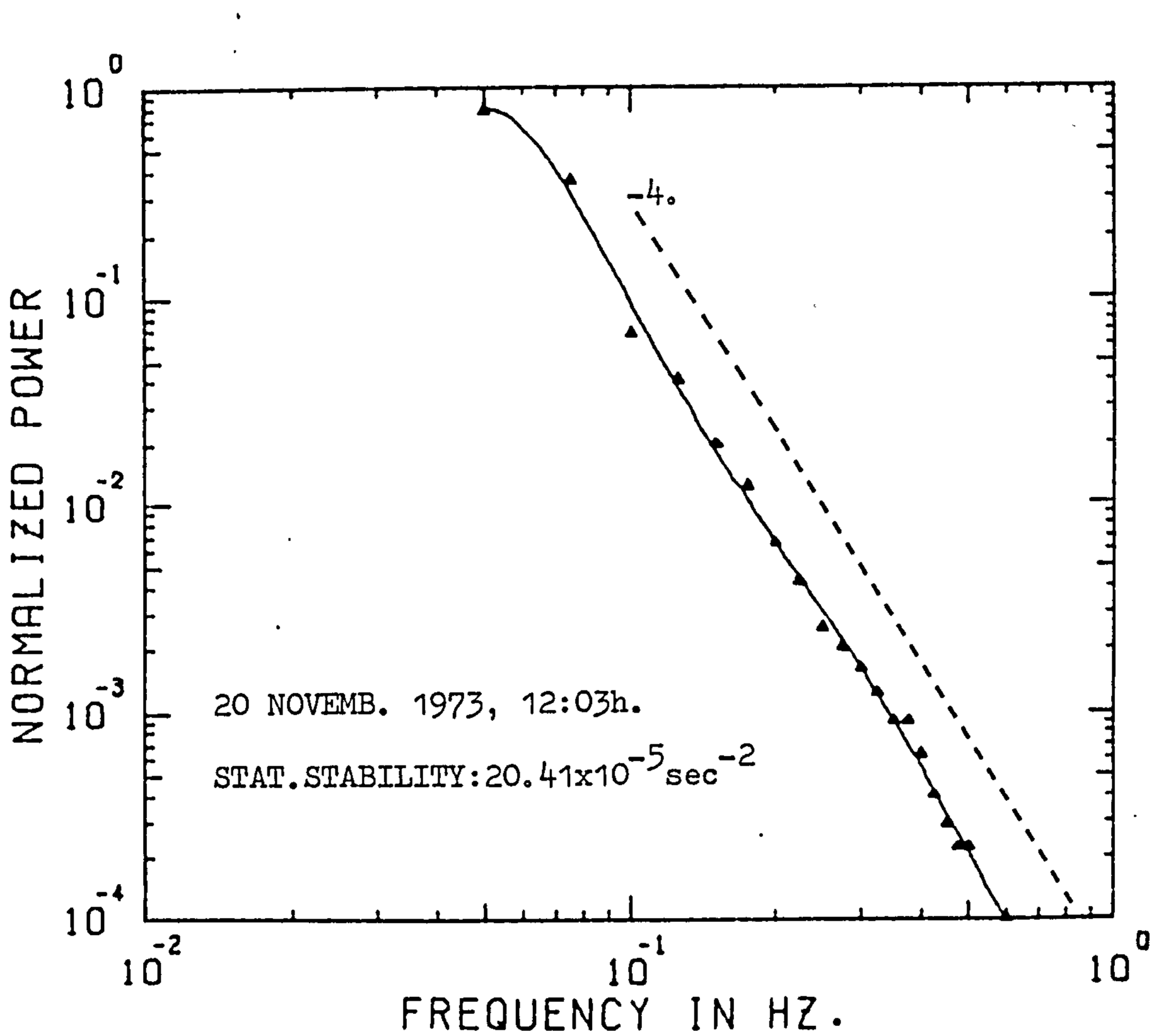
NORMALIZED POWER
10^{0}
10^{-1}
10^{-2}
10^{-3}
10^{-4}
-4.
20 NOVEMB. 1973, 12:03h.
STAT.STABILITY:20.41x10^{-5}sec^{-2}
10^{-2}
10^{-1}
10^{0}
FREQUENCY IN HZ.

FIGURE 5.22

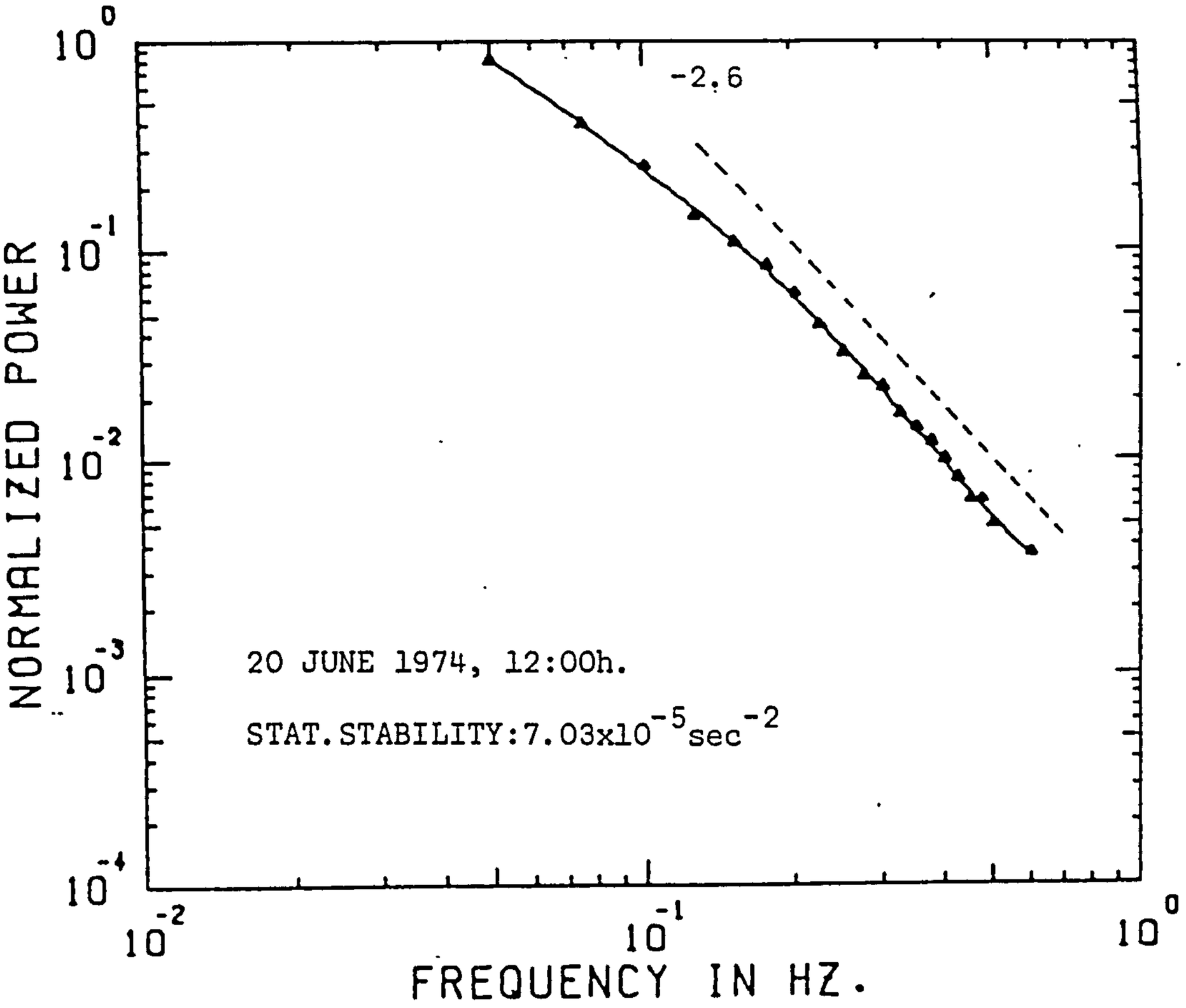
NORMALIZED POWER
10^{0}
10^{-1}
10^{-2}
10^{-3}
10^{-4}
-2.6
20 JUNE 1974, 12:00h.
STAT.STABILITY:7.03x10^{-5}sec^{-2}
10^{-2}
10^{-1}
10^{0}
FREQUENCY IN HZ.

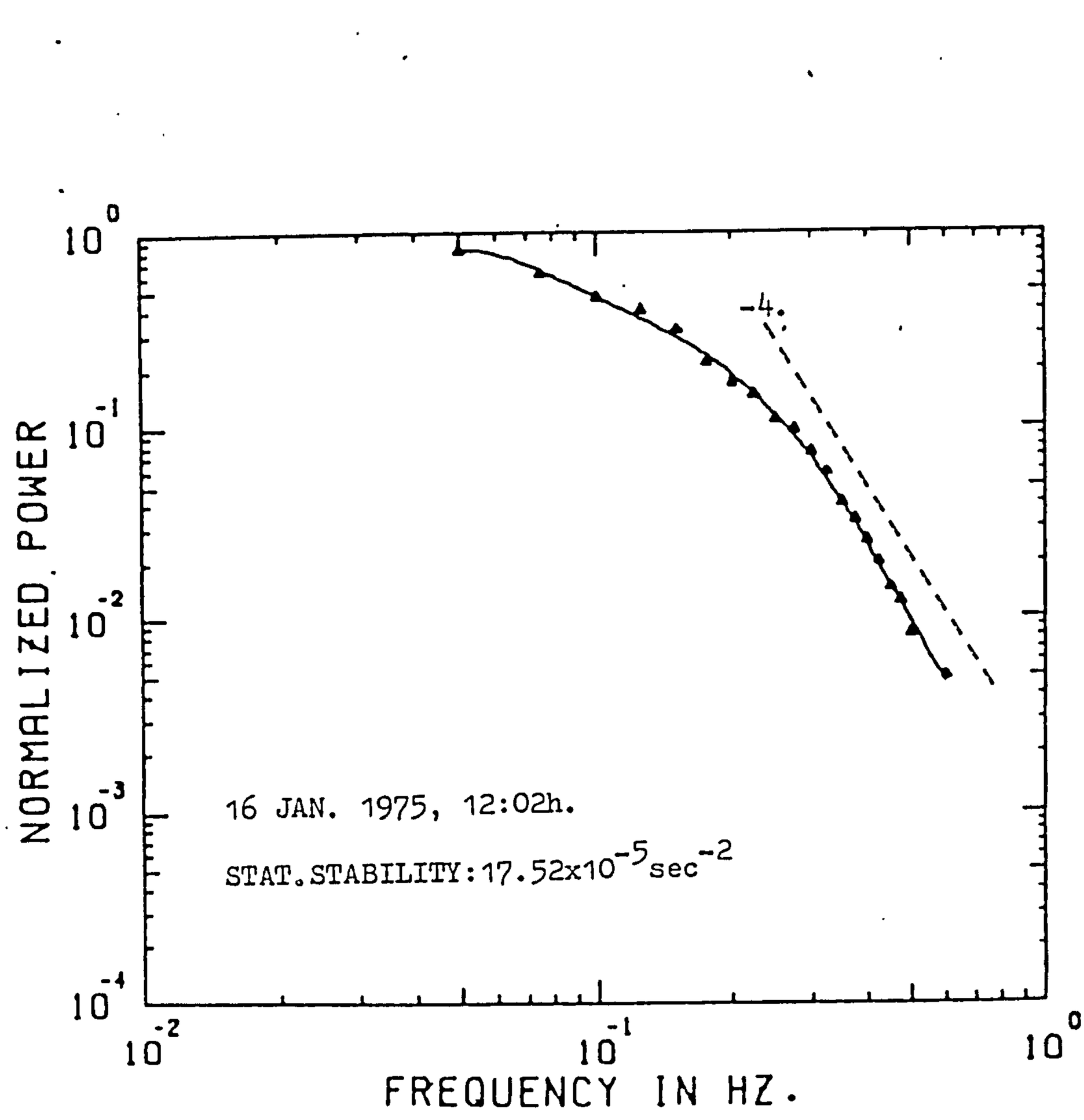
NORMALIZED POWER
10^{0}
10^{-1}
10^{-2}
10^{-3}
10^{-4}
-4
16 JAN. 1975, 12:02h.
STAT.STABILITY:17.52x10^{-5}sec^{-2}
10^{-2}
10^{-1}
10^{0}
FREQUENCY IN HZ.

FIGURE 5.23

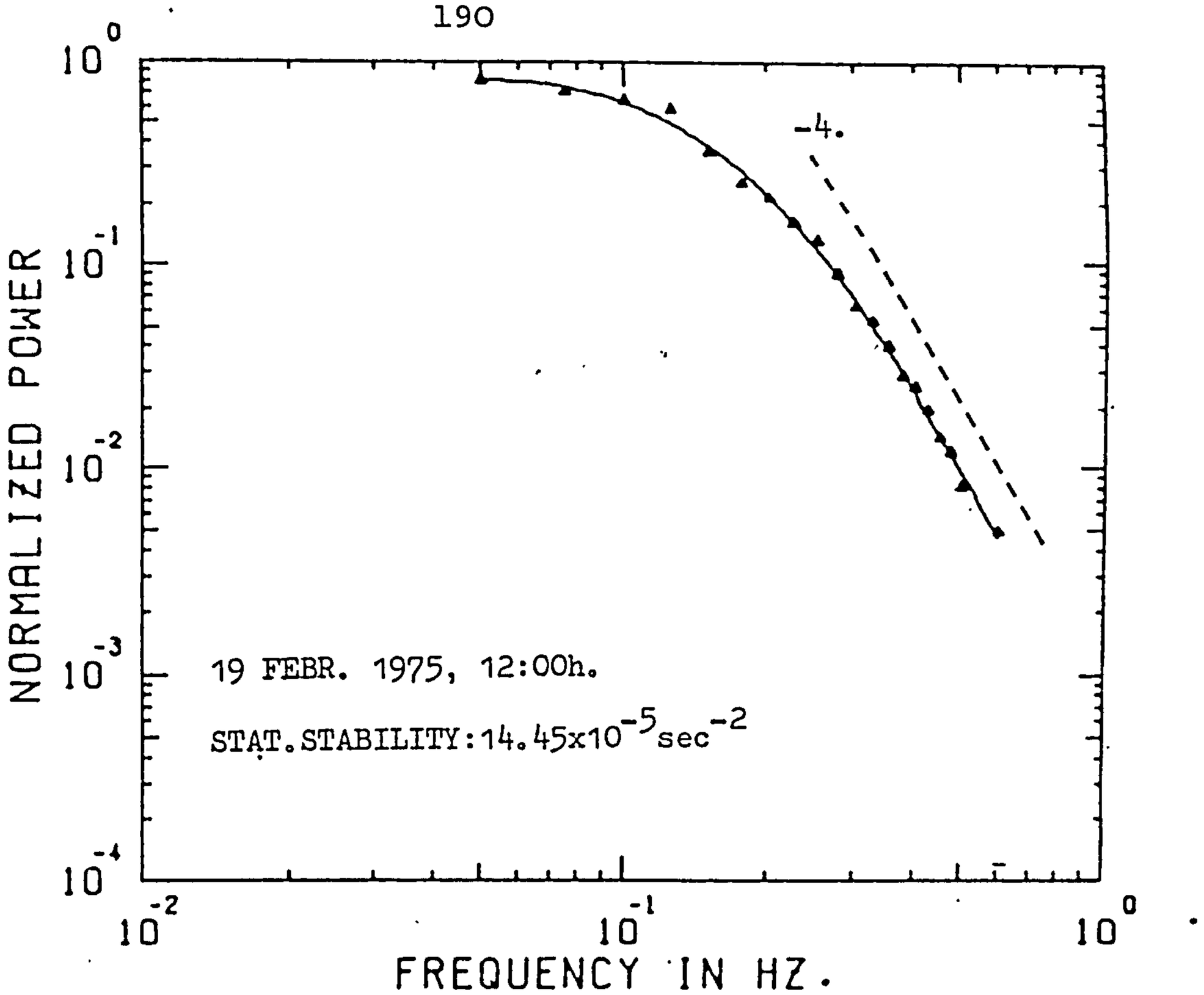
NORMALIZED POWER
10^{0}
10^{-1}
10^{-2}
10^{-3}
10^{-4}
-4.
19 FEBR. 1975, 12:00h.
STAT.STABILITY:14.45x10^{-5}sec^{-2}
10^{-2}
10^{-1}
10^{0}
FREQUENCY IN HZ.

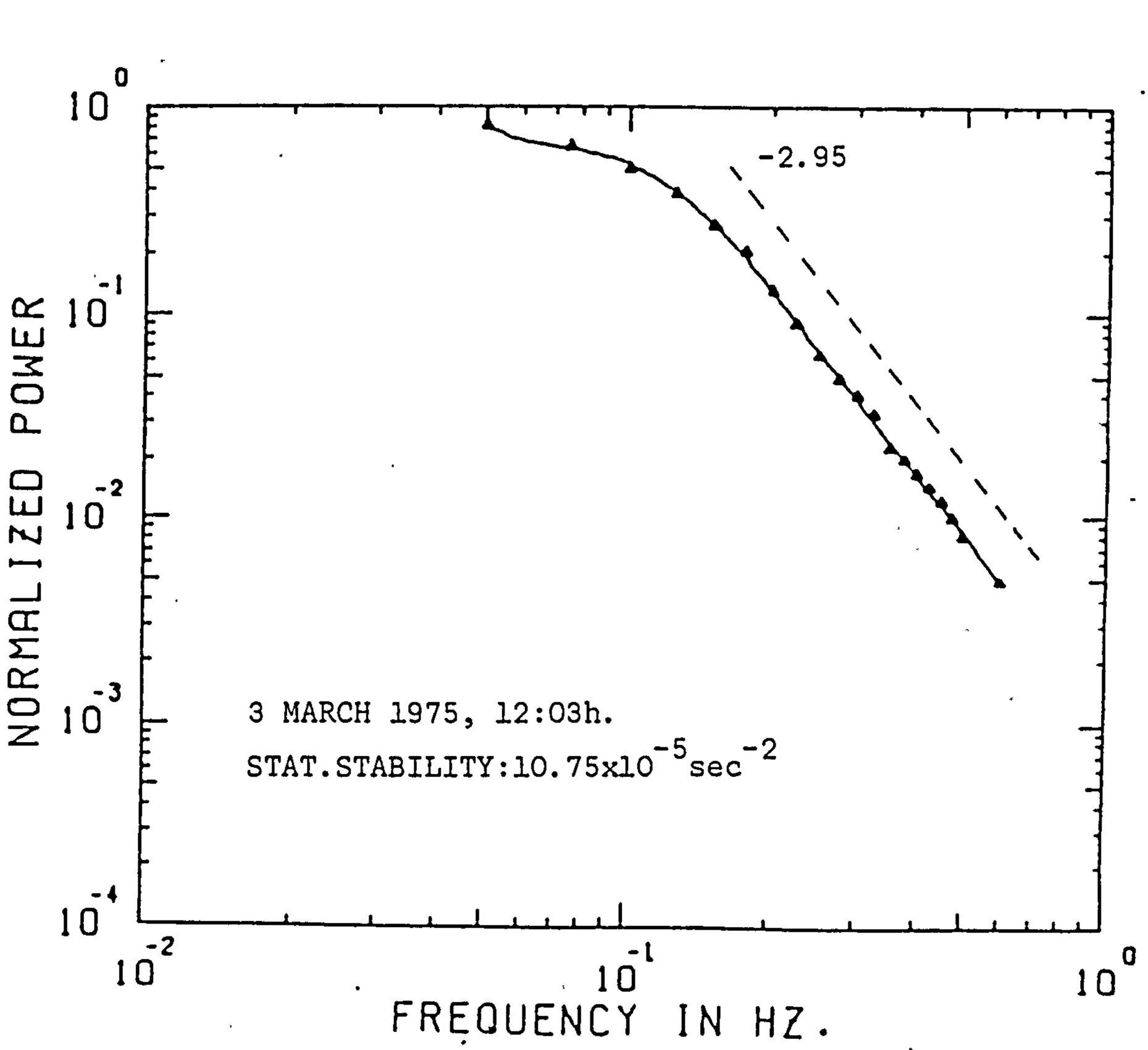
NORMALIZED POWER
10^{0}
10^{-1}
10^{-2}
10^{-3}
10^{-4}
-2.95
3 MARCH 1975, 12:03h.
STAT.STABILITY:10.75x10^{-5}sec^{-2}
10^{-2}
10^{-1}
10^{0}
FREQUENCY IN HZ.

FIGURE 5.24

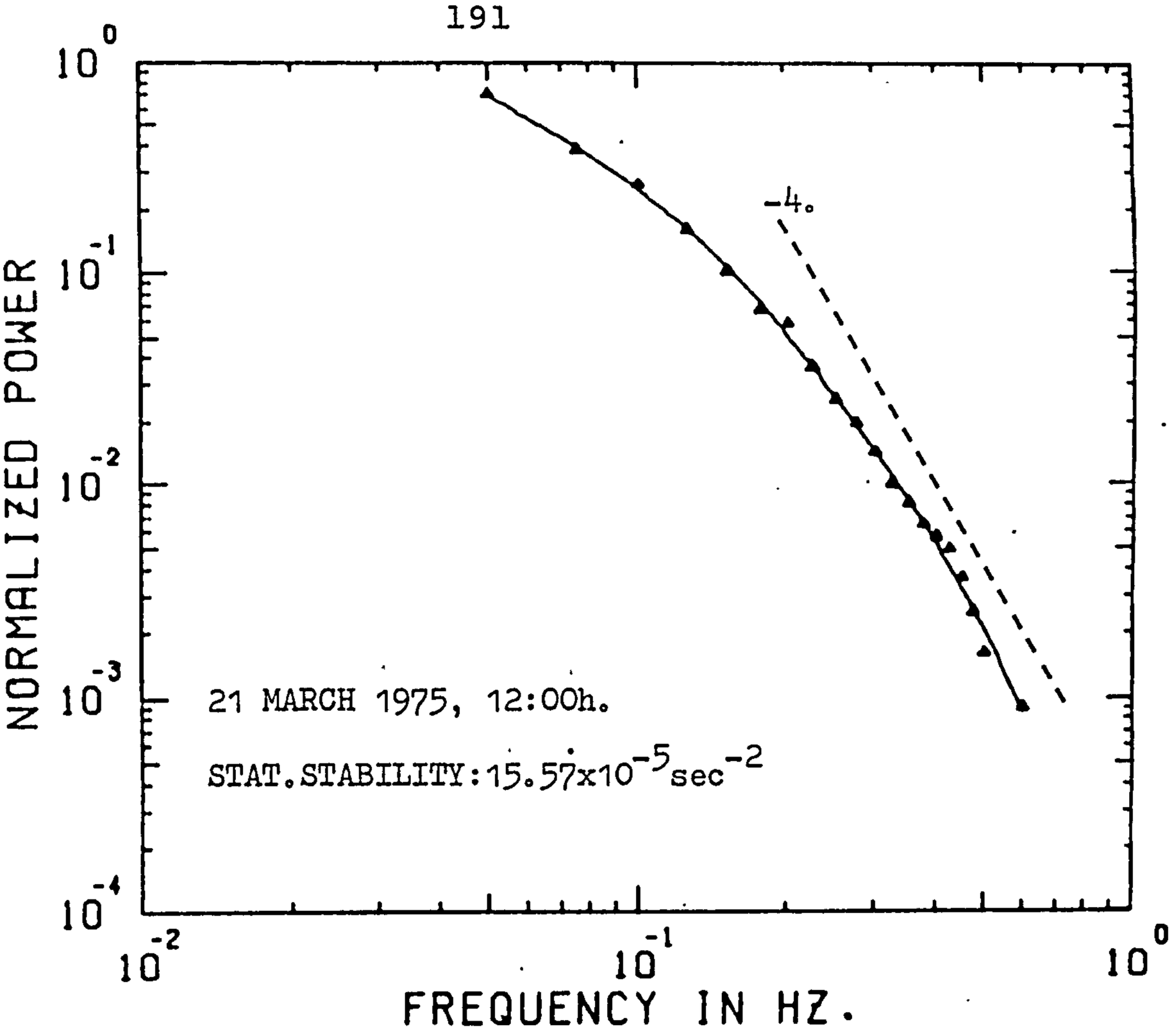
NORMALIZED POWER
10^{0}
10^{-1}
10^{-2}
10^{-3}
10^{-4}
-4.
21 MARCH 1975, 12:00h.
STAT.STABILITY: $15.57 \times 10^{-5} sec^{-2}$
10^{-2}
10^{-1}
10^{0}
FREQUENCY IN HZ.

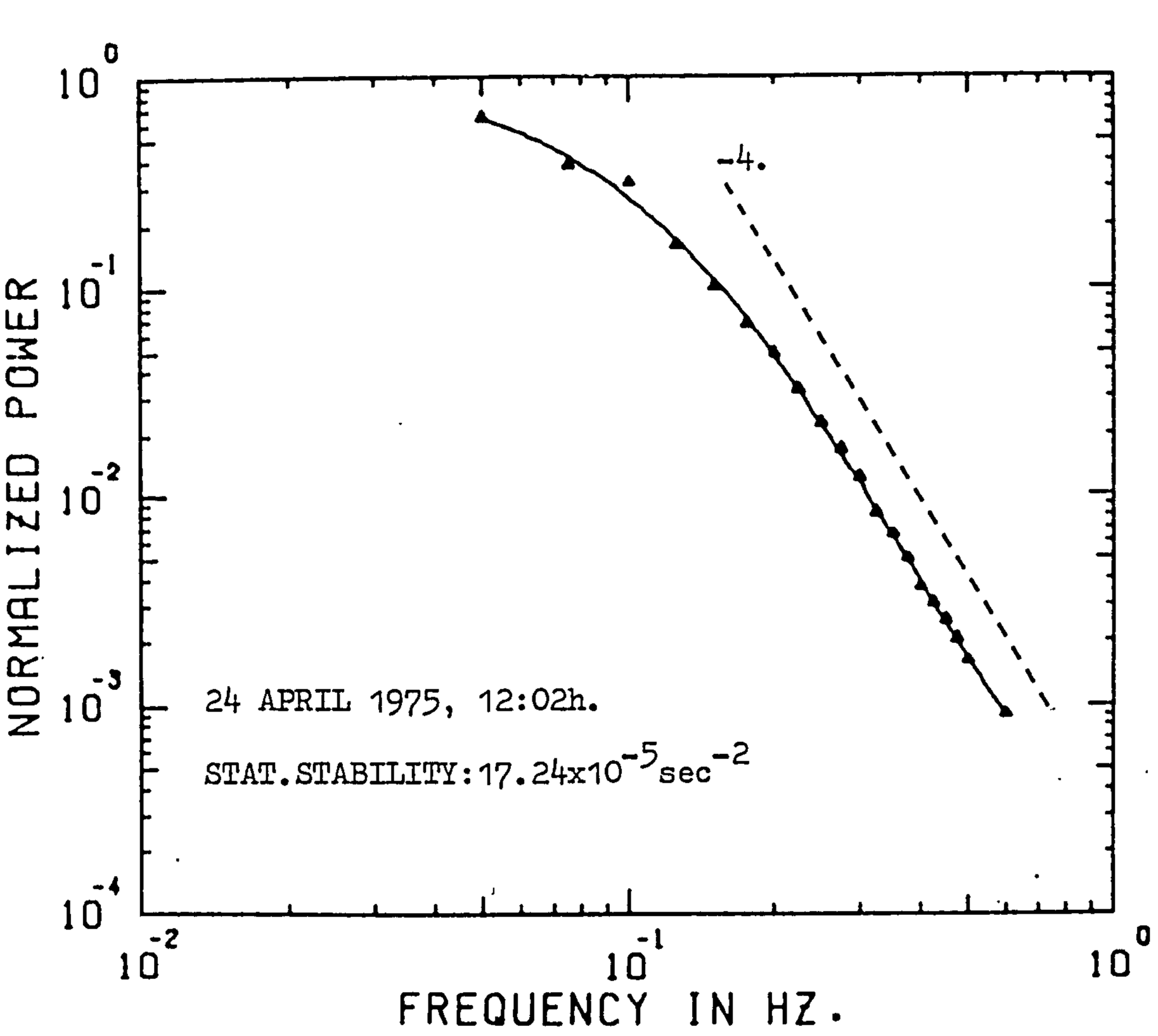
NORMALIZED POWER
10^{0}
10^{-1}
10^{-2}
10^{-3}
10^{-4}
-4.
24 APRIL 1975, 12:02h.
STAT.STABILITY: $17.24 \times 10^{-5} sec^{-2}$
10^{-2}
10^{-1}
10^{0}
FREQUENCY IN HZ.

FIGURE 5.25

from small to larger values, as frequency increases.

3. The exponent of the corresponding power spectral density function could be evaluated by measuring the slope of each logarithmic power spectrum. In the cases where a transition of the slope from small to large values occurred, the slope for the "high frequency" region of the spectrum was considered. The spectral exponents yielded in this way are marked on every plot.

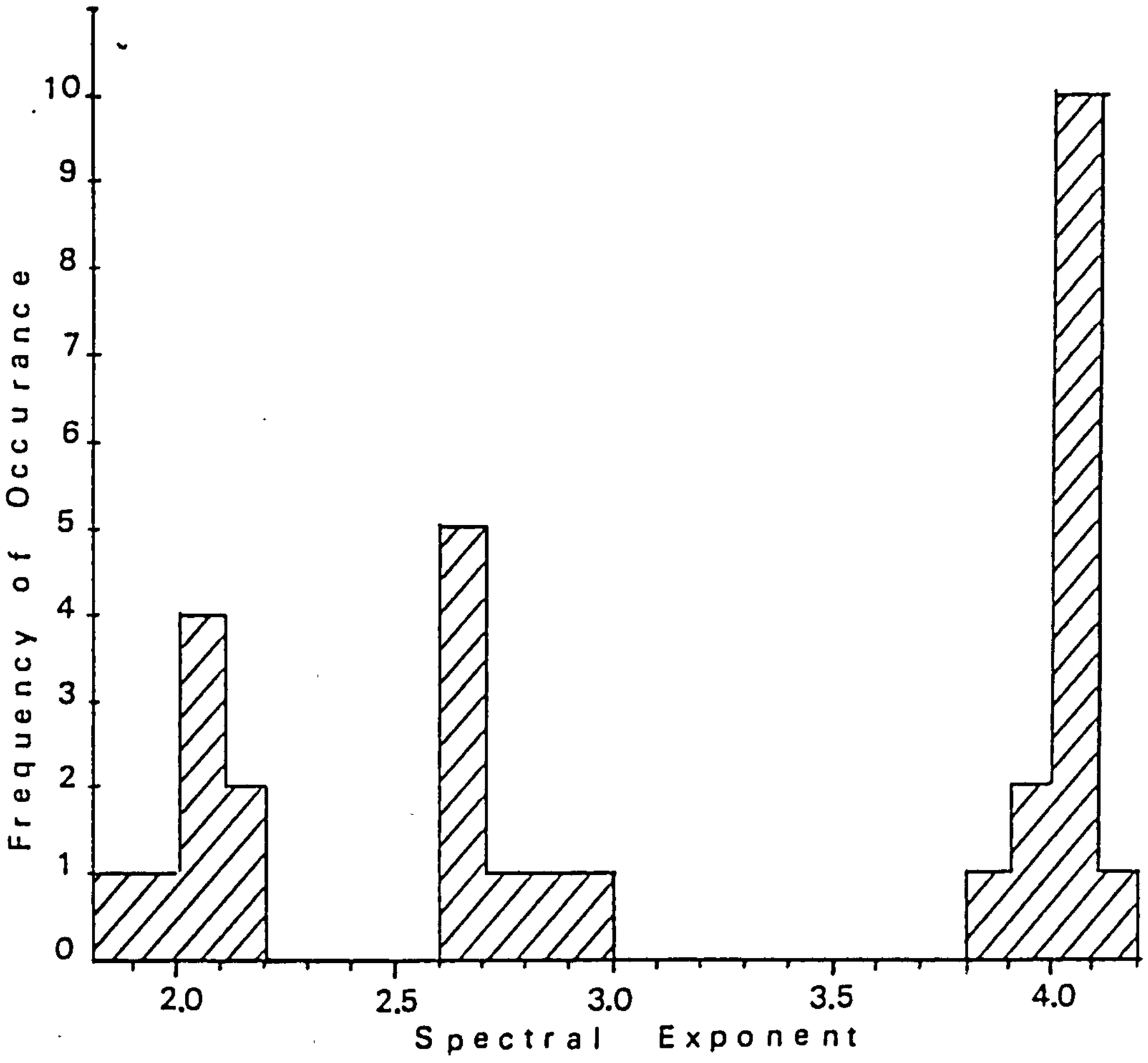

Fig. 5.26 Distribution of the spectral exponent n over its range of variation.

The values of the spectral exponents were found to vary between 1.8 and 4.1, which constitutes a rather wide range of variation. However, a closer examination of the spectral exponents revealed a concentration around the values 2.0, 2.67 and 4.0. This tendency is clearly shown in Fig. 5.26 which represents a histogramme of the frequency with which a spectral exponent attains a certain value in the range of its total variation. The values have been considered in intervals of 0.1.

From this histogramme, it can be seen that out of 30 power spectra of the "β-type" of fading, eight were characterised by a spectral exponent in the range 2.0 ± 0.2, another eight had an exponent in the range 2.7 ± 0.2 and fourteen had an exponent in the range 4.0 ± 0.2. None of the recorded power spectra was found to have an exponent outside these intervals.

5.5.2 Discussion

In Subsection 5.4.3, the "- 8/3" power law, governing the power spectral density function of the "α-type" of fading in the limiting case $U_n = 0$, had been attributed to a one-dimensional refractivity spectrum obeying a "- 5/3" power law. Similarly, the spectral exponents characterising the power spectra of the "β-type" of fading can be related to some models of atmospheric turbulence which have been extensively discussed in Sub-section 1.4.4. These models are briefly as follows:-

(a) The model of atmospheric turbulence under strong

thermal stratification, put forward by Shur[63] and developed by Lumley[70] and Tchen[73], suggesting a one-dimensional spectrum of turbulence obeying a "- 3" power law.

(b) The model proposed by Tchen[71] and Gisina[72] for the case when strong interaction occurs between mean and turbulent motion in regions of strong velocity and temperature gradients. In this model the one-dimensional spectrum of turbulence obeys a "- 1" power law.

(c) The more familiar "- 5/3" power law model of Kolmogorov[48] for atmospheric turbulence in the inertial range. This is the most universally accepted model[63,73] and it has been extensively used in theoretical investigations [49,97] for the description of the power spectrum of amplitude (or phase) fluctuations in line-of-sight propagation.

In this last case, Tatarski[49] has shown that the power spectrum of amplitude fluctuations, resulting from refractive index irregularities in the inertial range, must obey a "- 8/3" power law. Conversely, a one-dimensional refractivity spectrum obeying the "- 5/3" power law is responsible for an amplitude power spectrum obeying a "- 5/3 - 1" power law.

In fact, Tatarski's treatment of the problem of random amplitude fluctuations of a e.m. wave scattered in a turbulent atmosphere, can be easily extended to include other models of refractivity spectra. This does not require any modification in the mathematical formulation of the

problem, as described in[49] (pp. 259-264). The simple insertion of a one-dimensional refractivity spectrum obeying a "- n" power law would result in a "- (n + 1)" power law governing the amplitude power spectrum of the scattered e.m. wave.

Thus, for those models described in (a) and (b), the one-dimensional spectra of turbulence obeying a "- 3" and a "- 1" power law, would result in power spectra obeying "- 4" and "- 2" power laws respectively.

Fig. 5.26 shows that all the available power spectra of the "β-type" of fading were characterised by spectral exponents in the vicinity of "- 4", "- 8/3" and "- 2". This supports the above-mentioned hypothesis that the observed spectral exponents are a result of refractivity spectra obeying a "- 3", "- 5/3" and "- 1" power law respectively.

Since these spectral laws of atmospheric turbulence are considered to depend strongly on the thermal stratification of the atmosphere (see Subsection 1.4.4), the results available provided an opportunity to test this hypothesis even further. The available values of the fading power spectral exponents were plotted versus the static stability parameter characterising the lowest 1.5 km of the atmosphere for the times during which the corresponding signals had been received. The method of evaluation of the static stability parameter has been discussed in Section 4.1. Since upper air data is recorded by the Meteorological Station at Crawley only at 12.00 hours, spectral exponents from signals received at mid-day were used for this purpose.

This limited the number of spectral exponents to 22 out of the 30 cases of power spectra belonging to the "β-type" of fading. The resultant plot is shown in Fig. 5.27. It can

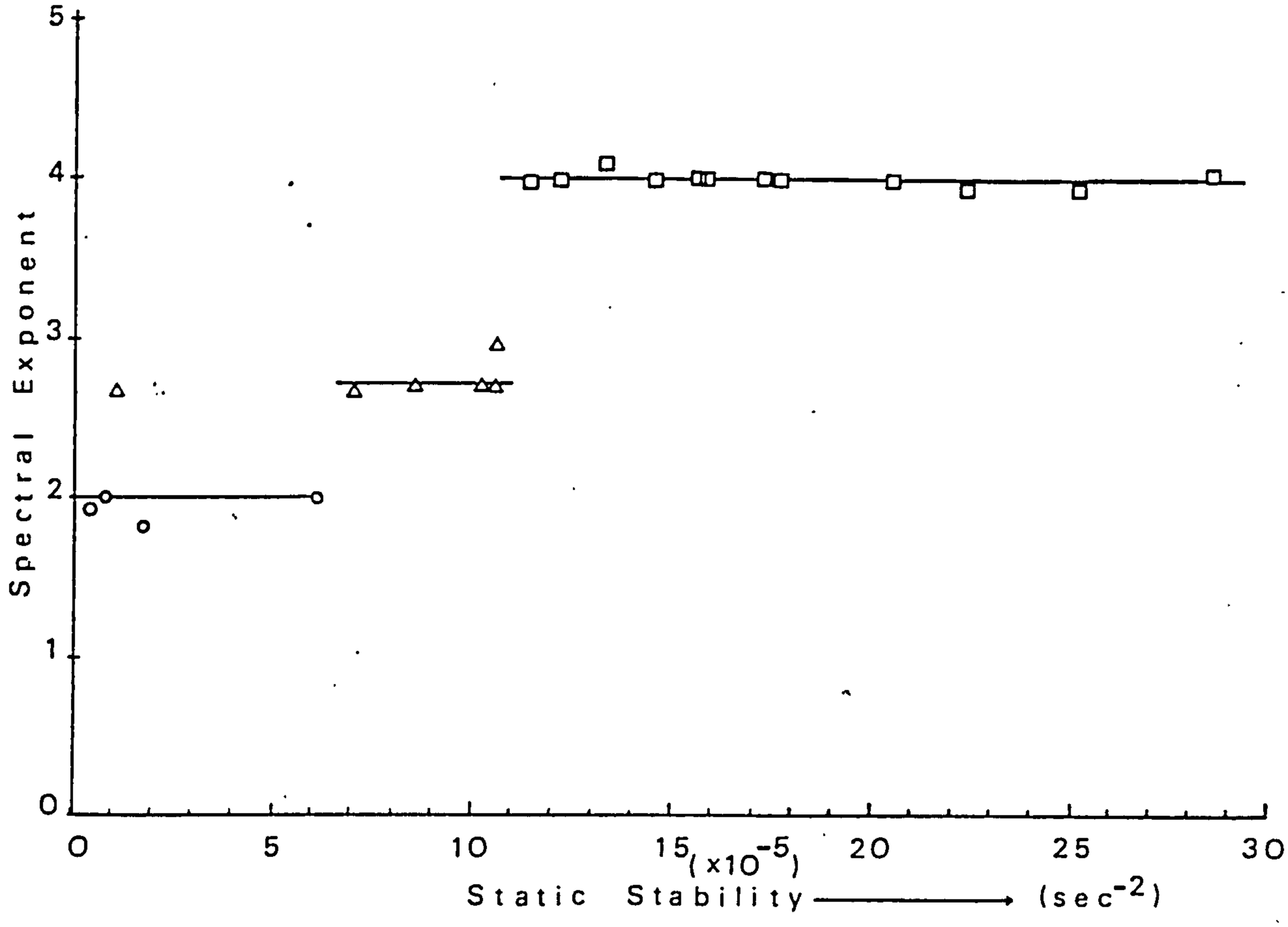

Fig. 5.27 The variation of spectral exponent n with static stability for the "β-type" of fading.

be seen that power spectral exponents with values in the vicinity of - 4 tend to occur for high static stabilities, i.e. under conditions of strong thermal stratification of the atmosphere. For such conditions the one-dimensional spectrum of atmospheric turbulence must obey a "- 3" power law according to the theoretical investigations of Shur[69],

Lumley[70] and Tchen[73]. That has also been confirmed by experimental measurements[63,65,66] (see Subsection 1.4.4).

As the static stability decreases, the values of the spectral exponent undergo a transition from - 4 to - 8/3 for static stabilities in the vicinity of 12×10^{-5} sec^{-2}. According to the hypothesis that the fading power spectral exponents depend on the spectral exponents of the atmospheric turbulence, this would indicate a transition of the atmospheric turbulence spectrum from a "- 3" to a "- 5/3" power law. Shur[63] has obtained spectra of vertical velocities in stratified regions of the atmosphere exhibiting such a transition from a "- 3" to a "- 5/3" spectral exponent. Through a theoretical treatment based on dimensional analysis, he concluded that the transition, for a given wave number, depends on the static stability parameter (see Subsection 1.4.4, Expressions 1.4.4e). Similar theoretical results have also been obtained by Lumley[70]. Further experimental evidence for this transition has been provided by Myrup[55] who reports that it usually occurs when the environmental stability changes from stable to near-neutral.

Weill, Aubrey et al[66] have measured the spectra of temperature fluctuations in the atmosphere and have found that spectral exponents in the vicinity of - 3 prevail under stable conditions whilst near neutral stratifications favour spectral exponents in the vicinity of - 5/3 or smaller.

For static stabilities close to zero (neutral stratifications) the fading spectral exponent appears to undergo another transition, this time from - 8/3 to - 2,

indicating one-dimensional spectra of atmospheric turbulence obeying a "- 1" power law. Such spectra have been measured in the atmosphere[64,65,66] and they have received a theoretical explanation by Gisina[72] and Tchen[71,73] based on the interaction between mean and turbulent motion (see Subsection 1.4.4). Such interaction is expected to take place in regions of strong temperature gradients where buoyancy forces provide energy not only to the large turbulent eddies but also to a whole range of scale sizes.

In general, the hypothesis that the fading power spectra obey inverse power laws determined by the spectra of turbulence in the propagation medium appears to be considerably supported by both experimental and theoretical investigations on atmospheric turbulence. As a result, the static stability parameter could be an important factor determining the functional form of the fading power spectra of the "β-type" of fading.

CHAPTER 6

SIMULATION IN THE LABORATORY: THE AIMS AND REALIZATION

6.1 Introduction

As already discussed in Chapter 2, a considerable amount of theoretical work has been dedicated to the interpretation of transhorizon propagation and its various characteristics. Atmospheric structures such as inversions acting as "ducts" or reflectors, turbulent eddies or "blobs", acting as scatterers have been considered to be of importance to transhorizon propagation through the troposphere. A large number of experiments have been also performed, in support of one theory or the other. Frequently, different investigators attribute similar propagation characteristics to different mechanisms. For example, "roller-top" fading ("type-β" in the present investigation), has been attributed by Kitchen and Richards[133] to interference from a few partially reflected field components, whereas Nicolis[134] attributes it to "ducting". Tatarski, a significant contributor to the theory of propagation by scattering, suggests[49]:-

"that the theoretically predicted dependence of "scatter loss" on transmitted frequency, is at variance with experimental evidence".

Similar discrepancies exist between the conclusions from other theories and the results obtained from the many experiments that have been conducted and the experience gained

from established commercial practice.

The accurate prediction of transhorizon tropospheric propagation characteristics for practical application, based on any specific theoretical work, is impossible. In the design of modern full-scale tropospheric radio systems, great reliance is still placed on empirical information which has been formulated from practical experience.

The obvious and most important difficulties arise from an incomplete understanding of the behaviour of the atmosphere, to the extent that even weather prediction is still unsatisfactory, and the real effects it has on a radio beam. In a full scale system the total atmospheric volume between the transmitter and receiver terminals is too large and of very complex structure as to defy any conclusive measurements which are within the abilities of the planning radio engineer. Furthermore, it is perhaps fortunate that man cannot exercise any degree of control over the behaviour of such an atmospheric volume. However, it may thus be argued that failure to effect any degree of control over such a region seriously inhibits the success of any concerted investigation into both its properties and behaviour and, therefore, its influence on a propagated radio-beam.

In contrast, any attempt at mathematical representation or modelling must, by the very nature of such an exercise, assume a number of parameters which may or may not be of significance. In this aspect, a mathematical model will be limited in its scope in much the same manner as any investigation conducted on a full-scale system by virtue of the complex spatial and temporal distribution of the properties of the

propagation medium.

The use of scaled models in fields such as aeronautical, civil or environmental engineering has hitherto proved of considerable value. These techniques have also been successfully used in the communications field for the purpose of investigating the properties and performance of aerial systems and arrays.

By developing these modelling techniques[136] to include optical aids and "wave sources", it is now possible to simulate most, if not all, the fading characteristics that are experienced on a tropospheric radio system in the laboratory. The advantages of such a technique are that the effects of an inhomogeneous gaseous medium on the path of an electro-magnetic wave, propagated as a conical beam, may be studied in a "controlled" environment whose overall properties may be related to those of a full-scale radio system. In addition, these same techniques may also be applied to studies of the diffraction effects of scaled natural obstacles and are to some extent supported by the Theorem of Similarity put forward by Sommerfeld[137]. A brief formulation of this Theorem is the following:-

"Let the distances between a diffracting object, the light source, and the observation plane be reduced by a factor K_1, then the diffraction pattern in the new plane of observation will be similar to the one in the previous plane if the dimensions of the diffracting object is reduced by a factor $K_2 = \sqrt{K_1}$, the wavelength of the light maintained constant".

This theorem can be extended to make the two reduction factors equal if the condition that the wavelength be kept constant is relaxed. Thus, if the wavelength is also reduced by a factor K_1, then $K_2 = K_1$ and a uniform linear scaling of all dimensions will result in a similar diffraction pattern.

A brief discussion on previous efforts to study specific radio communications problems by means of scaled models will be given in what follows.

6.2 Previous Work

Laboratory simulation in radio communications has been mainly practiced in the past for the investigation of microwave diffraction problems. In most cases[138,139,140], the investigators have considered regularly shaped diffracting objects like spheres, wedges and cones, being only approximately similar to real obstacles. In these investigations, no attempt was made to incorporate a simulation of atmospheric phenomena. However, attempts to simulate particular natural obstacles have been made more recently. Thus, Ridler[141] in 1972 studied the diffraction caused by a nearly conical volcanic mountain and Trivedi[142] in 1977 studied in detail the spatial distribution of the field diffracted by a hill ridge.

These two investigators have also incorporated elements of simulation of some atmospheric phenomena, namely, differential heating of the ground due to solar radiation and air flow over the diffracting obstacle. In both cases, the differential heating has been simulated by heating the aluminium-made diffracting obstacle from below by means of

electric resistors. Although in these two investigations the paths under simulation were line-of-sight obstructed paths and the primary subject of investigation was the diffraction pattern at the receiving plane, the fact that they report the presence of fading whenever atmospheric phenomena are simulated, makes them contributing works to the problem of transhorizon propagation modelling.

Very few attempts have been made up to now to simulate a transhorizon radio link in the laboratory. Burrows in[136] suggested for the first time in 1966 that transhorizon propagation characteristics, and particularly fading, can be reproduced in a laboratory model consisting of a laser beam propagated over a flat aluminium plate representing the earth's surface. There was a provision for creating a wide range of M profiles (the model was basically of the "flat earth" type). The receiver had been simulated by an aperture and a photosensitive detector. The propagation medium could be inspected in detail by Schlieren interferometer techniques which readily indicated the presence of air mass movement along the propagation path. This model had been used for the simulation of a real transhorizon link operating at a frequency of 900 MHz and extending over 500 km. Comparison between the records from both the model and full-scale links revealed a high degree of similarity for a wide range of meteorological conditions. Low speed wind tunnel techniques were used to simulate the effects of surface winds and turbulence. The author also stresses the importance of the near-surface activity in relation to the random variations, or fading, in light intensity at the receiving aperture.

From these investigations, it can be concluded that Burrows' guideline for the laboratory simulation of transhorizon propagation characteristics is the following:-

"An accurate simulation of the earth's atmosphere and its phenomena, can lead to the simulation of the effects of that atmosphere upon a propagated radio beam".

A different approach to the problem of modelling UHF transhorizon links in the laboratory was presented in 1968 by R. Post and D. Rost[143]. The authors describe another laboratory model where a laser beam is propagated over a Pyrex disc 24 inches wide and having a curvature of 18 feet. The field at the receiving plane is recorded on photographic film which consequently is scanned by a microphotometer. The laser light is scattered over the curvature of the disc by spherical glass beads dropped with varying spatial densities through the "common volume". The mean diameter of the scattering beads is 151 μ, i.e. 240 λ. The measured quantity is the ratio of scattered power to power in the central maximum of the transmitted beam, something analogous to the "scatter loss" in transhorizon propagation terms. The authors report that their results are similar to the predictions cited by Booker and Bettencourt[144]. Their work is essentially supporting the "scatter" theories of transhorizon propagation and no atmospheric phenomena except homogeneous and isotropic turbulence can be simulated. The only variations that can be introduced are through the size of the "common volume" and the size and spatial density of the scattering beads. The

fact that the reference index of the glass beads is quite different from that of the surrounding air has not been considered by the authors who, however, claim that their model "is not intended to simulate the earth's atmosphere but to simulate the effect of that atmosphere".

For the purpose of this investigation, the technique developed by Burrows has been adopted.

6.3 Aims of the Laboratory Simulation and Advantages of the Adopted Method

The aims of this laboratory simulation, seen in the light of the discussion presented in Section 6.1, can be summarized as follows:-

1. To model and simulate the full-scale ("prototype") radio-link.

2. To simulate and study, as accurately as possible, the properties and the phenomena of the real atmosphere; particularly the ones known to exist in the propagation medium of the "prototype" radio-link.

3. To reproduce in the laboratory model the same fading effects that have been observed and studied on the "prototype" radio-link.

4. To relate the general properties of the "model atmosphere" to those of the real atmosphere, which produced the same fading effects.

The method of laboratory simulation proposed by Burrows[136,145] was adopted for use in the present investigation since it offered the following advantages:-

(a) The ability to simulate various atmospheric effects such as winds, temperature gradients, mechanical and convective turbulence.

(b) Observability and controllability over the simulated atmospheric effects.

(c) Flexibility in monitoring the propagated light beam at any point on the receiving plane and simultaneously carrying out measurements of various simulated meteorological parameters.

6.4 Description of the Model

The experimental set-up consisted of three units: the actual model, a low-speed wind tunnel and a Schlieren interferometer. Plate 6.1 shows the model with the Schlieren system arranged for operation. In Plate 6.2, the model is shown as an integral part of the wind tunnel. Due to constructional difficulties, it was not made possible to operate the Schlieren system and the wind tunnel simultaneously. A detailed description of the principle of operation and the component parts of the model is given in the following section.

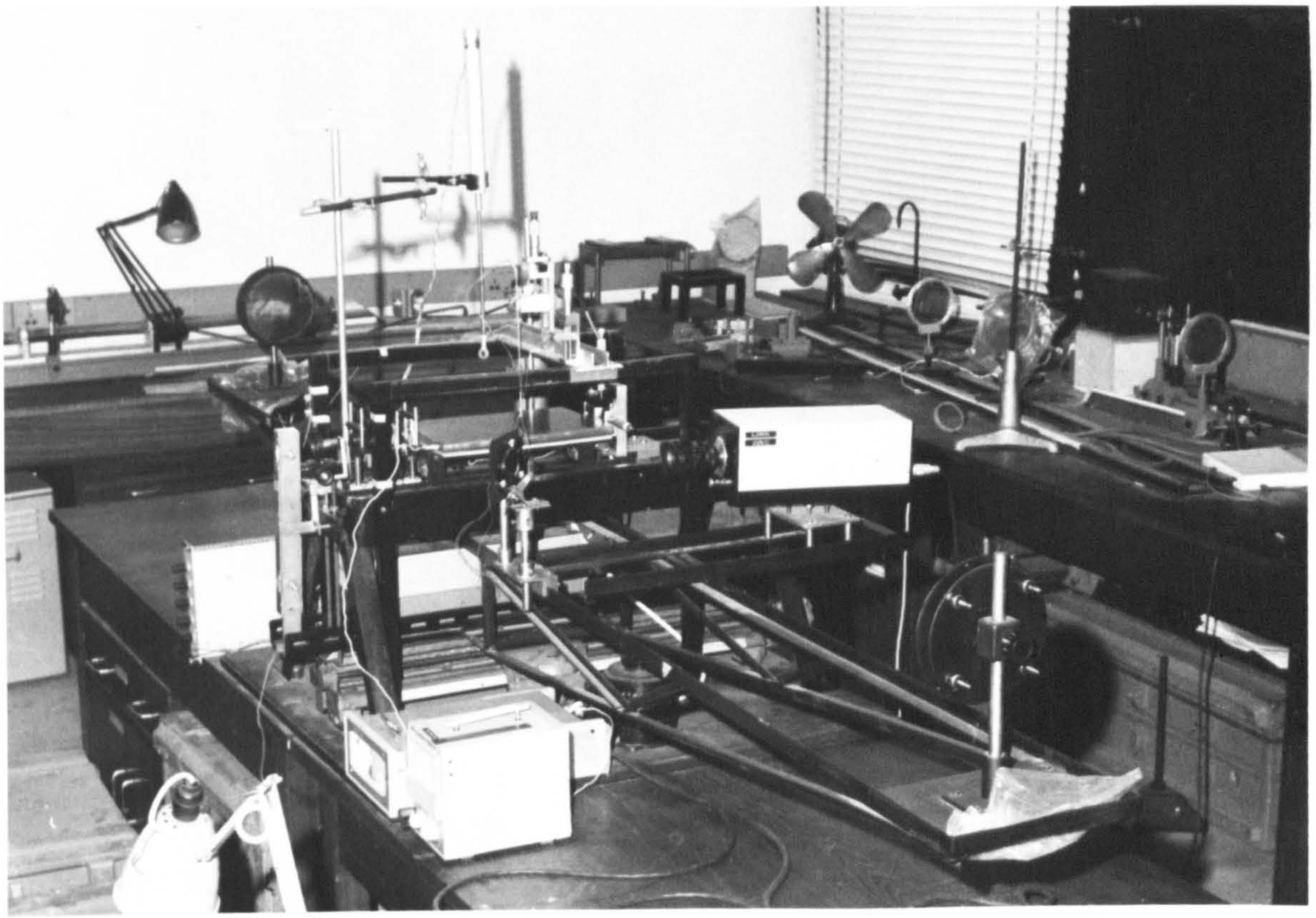

Plate 6.1

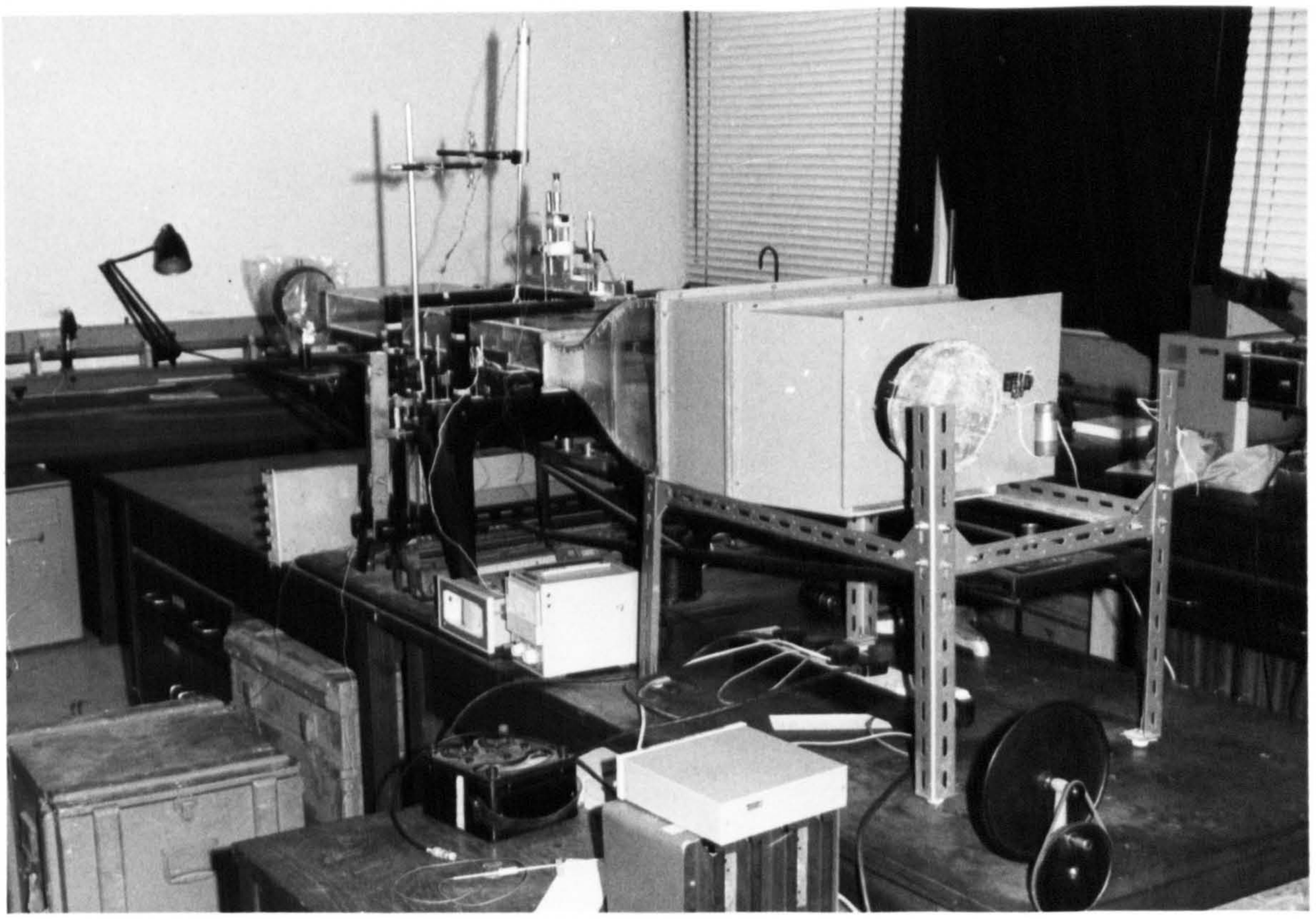

Plate 6.2

6.4.1 The Propagation Path - The Transmitter, The Receiver

The model consisted basically of a flat aluminium plate, which could be heated from below, over which a divergent laser beam is propagated.

The choice of aluminium to simulate the earth's surface was made because its reflection properties at optical frequencies are similar to those of a lossy dielectric and closely resemble the properties of ordinary terrain to UHF[142,146] Aluminium has a modulus of effective complex dielectric constant in the range of $10 < |\varepsilon| < 30$ at 5890 $\overset{o}{A}$ close to the range of normal soil dielectric constant at UHF.

The scale factor was derived from the ratio of the laser wavelength (6238 $\overset{o}{A}$) to the wavelength of the carrier wave of the prototype link. This scale factor was found to be 0.6328×10^{-6} m/0.333 m = 1.9×10^{-6} and thus permitted the reduction of the 142 km of the prototype radio-link path to a "model path" of 27 cm.

The aluminium plate simulating the earth's surface had a length of 27 cm, a width of 20 cm and was carefully milled and polished to reduce the effects of roughness to a minimum. For the purpose of creating a temperature gradient above the "path", the plate was heated from below by 8 heating elements of 40 W each. Layers of mica and asbestos were used for the electrical insulation of the heating system. The power for the heating was provided by a variac allowing control of the plate temperature. Provision was made for keeping the plate at a constant required temperature by the connection of an ETHER-TRANSITROL thermostat between the variac and the heating elements. The temperature of the plate

was sensed by the thermostat's probe which consisted of a NiCr-NiAl thermocouple inserted in a small cavity in the plate's body without actually touching the plate. It was decided that this would be the best way to sample the air temperature in the immediate vicinity of the plate without exposing the sensor to room draughts, etc.

The simulation of the transmitted radio beam was obtained from a He-Ne gas laser source together with a spatial filter and a series of lenses and apertures. A schematic diagram of this optical system is shown in Fig. 6.1.

The He-Ne laser (Fig. 6.1) was used as a source of monochromatic unpolarized light (λ = 6328 Å). The power output of the device was approximately 3 mW and the available light beam was in the form of a parallel beam with an approximate diameter of 1 mm. As the laser was placed underneath the model propagation path for space economy reasons, two right-angle deflecting prisms (I and II) were used to bring the laser beam at the right position. The light emerging from the second prism was then passed through a spatial filter consisting of a 20 x microscope objective focused of a 50 μ aperture. The purpose of the spatial filter was:-

(a) To create a secondary light source with a diameter much smaller than that of the original laser beam. Thus, the new source would have a diameter of 79 λ or approximately 20 times smaller than the diameter of the untapered laser beam ($\simeq$ 1600 λ). This would simulate better the prototype radio link where the aerial's diameter was 3.66 m or 11 λ.

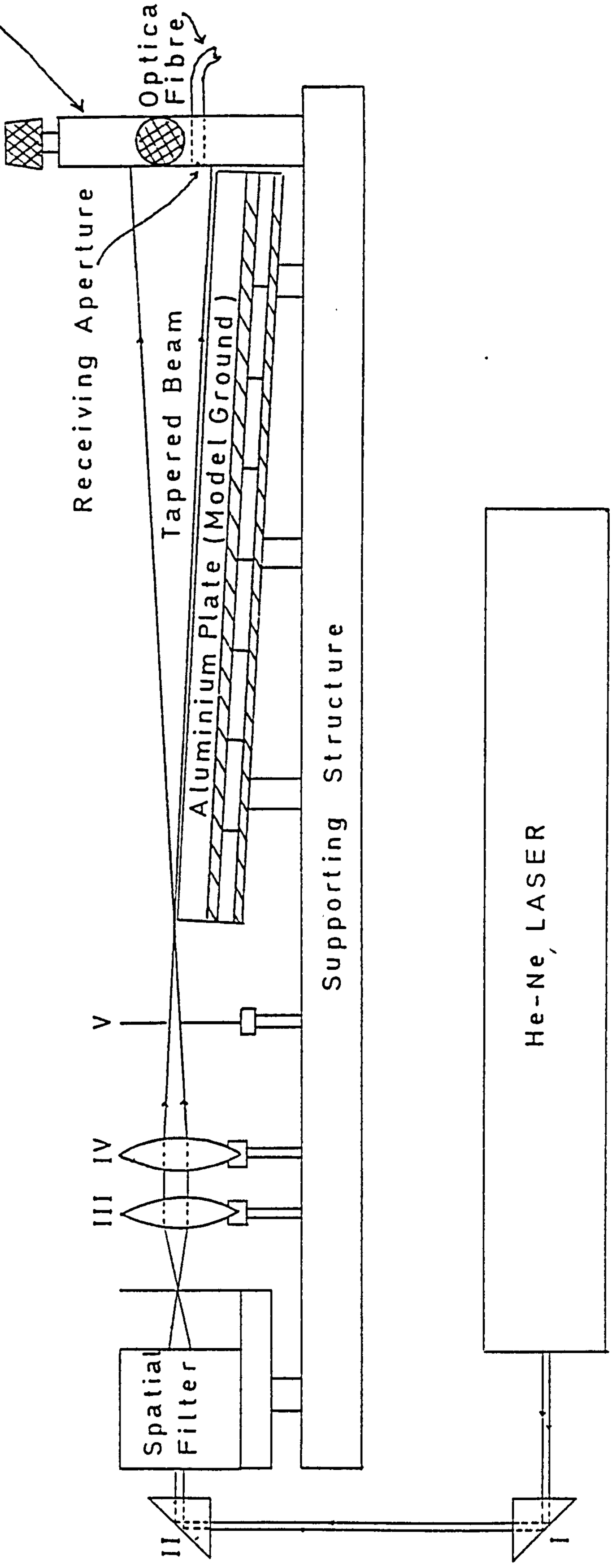

FIGURE 6.1: Schematic diagram of the Laboratory Model. (Vertical scale exaggerated).

(b) To eliminate secondary light beams created by reflections in the deflecting prisms and intensity irregularities in the periphery of the main beam.

(c) To create from the pencil light beam a broader divergent beam more similar to the radio beam transmitted by a directional "dish" type UHF aerial.

Further control upon the beam was provided by a combination of two convex lenses (III and IV in Fig. 6.1) of focal lengths 5 cm and an aperture (V) of 3 mm diameter.

By the combined adjustment of the two lenses and by repeated measurements of the light intensity on the receiving plane along the vertical direction, a light beam having a diameter of approximately 2.8 cm ± 0.1 cm was achieved.

The aperture (V) served for the purpose of eliminating unwanted side-lobes. This was achieved by positioning the aperture at a place between the lens (IV) and its focus in a way that the periphery of the aperture was coinciding with the first dark diffraction ring around the central lobe.

The whole system was adjusted so that the image of the 50 μ aperture, without the unwanted diffraction side-lobes, was formed just above the near edge of the aluminium plate and as close to the model ground as possible.

To avoid reflections from the ground, the beam was made to propagate with its lower boundary parallel to the plate's surface. That was achieved by tilting the aluminium

plate slightly downwards as shown in Fig. 6.1.

The receiving system was placed at the other end of the model path at a distance of 27 cm from the simulated transmitting aerial. It consisted of an aperture with a diameter of 25 μ, a photomultiplier and an optical fibre light guide conducting the light from the former to the latter. The type of the photomultiplier was EMI 9658 R with approximately 12% efficiency at red light wavelengths. Its output voltage was proportional to the intensity of the insident light and provided a direct measure of the received power. Its "dark current" was about 20 nA for a supply voltage of 1450 V at room temperature (20^{o}C). Its intensity-to-output characteristic was found to be linear over most of the operating range. The dynode chain circuit is shown in Fig. 6.2. The receiving aperture and one end of the light conducting optical fibre were mounted on a slide system shown in Fig. 6.3. The system consisted of a vertically movable frame A, within which a horizontal slide B, bearing the receiving aperture C, could be moved. In this way, the aperture could be moved in both the vertical and transverse directions in the receiving plane.

The displacement in the two directions could be controlled and measured by two micrometer screws D and E.

As in the prototype radio link the receiving aerial was standing 44 m above ground level, the receiving aperture in the model should stand: $44 \times 1.9 \times 10^{-6}$m = 84 μ above the model ground. The measurement of that distance by means of the vertical micrometer screw was possible but it was found difficult to define the micrometer's indication for

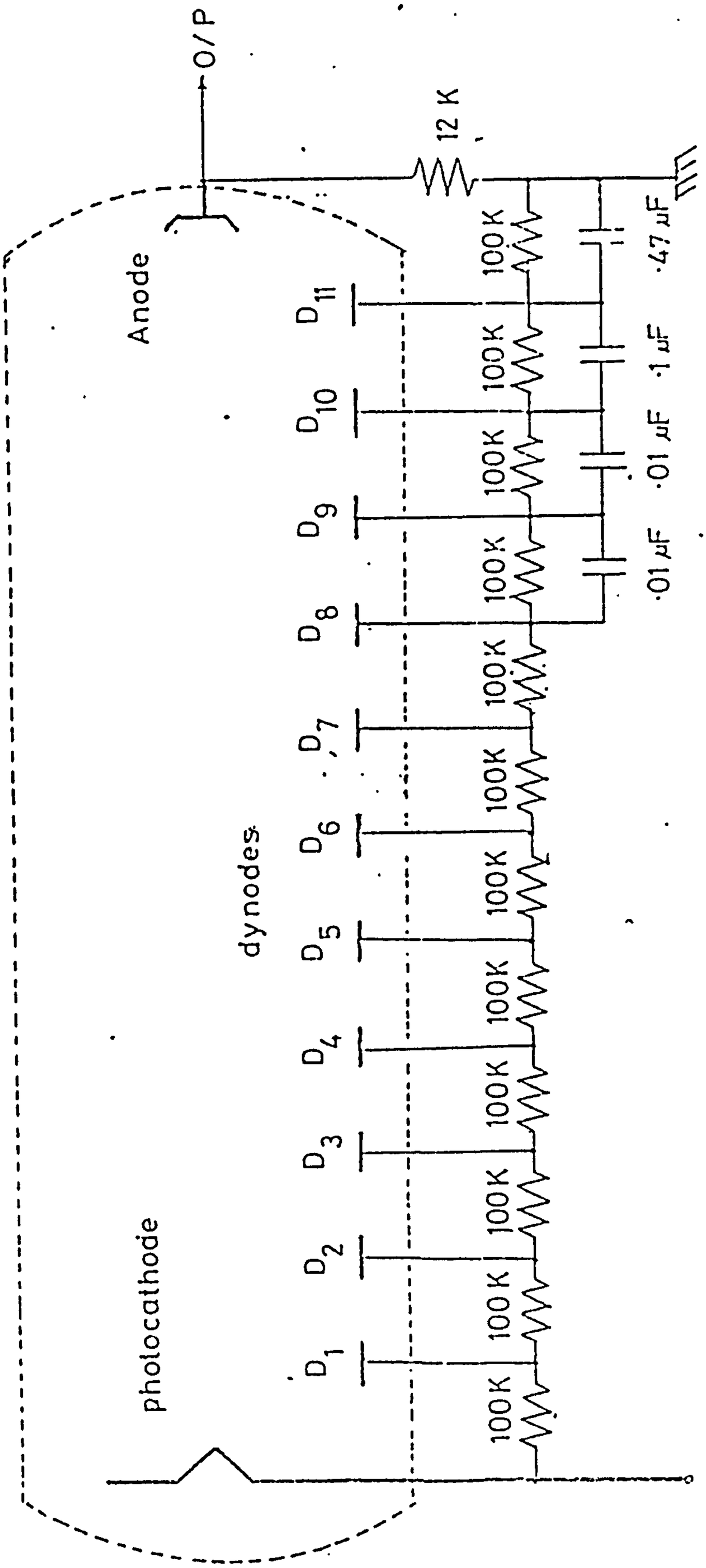

FIGURE 6.2: The Dynode chain circuit used with the E.M.I. 9658 R photomultiplier.

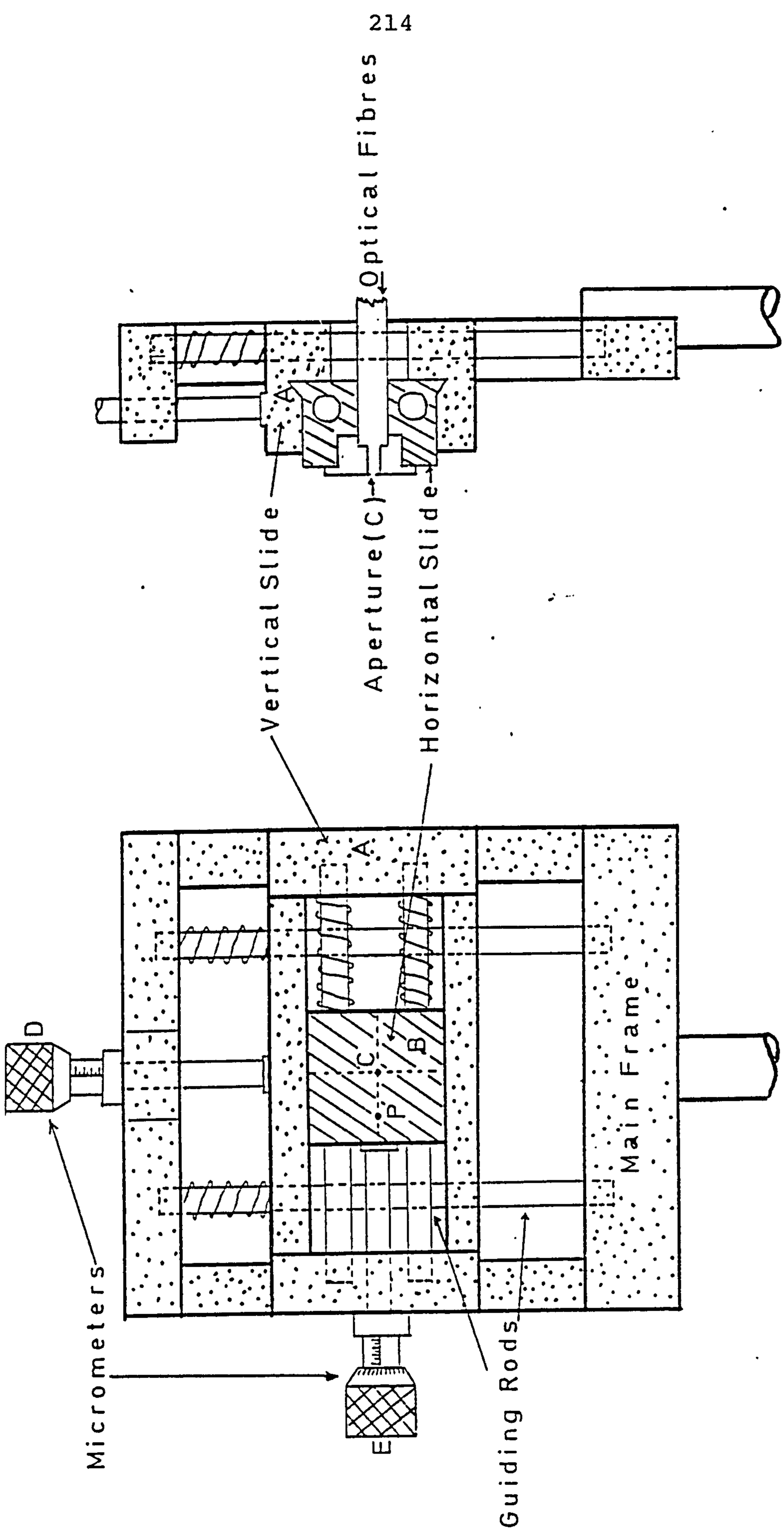

FIGURE 6.3: Slide - system for the horizontal and vertical displacement of the receiving aperture.

zero elevation of the aperture. To overcome this difficulty, a pin coated in insulating material was inserted in a hole P drilled in the horizontal slide B at the same level with the receiving aperture (see Fig. 6.3). The pin was connected to one of the poles of a d.c. battery and the other pole was connected to the aluminium plate simulating the ground. A small pilot-bulb was connected in this circuit. When the receiving aperture had a zero elevation the pin would touch the aluminium plate, close the circuit and the pilot-bulb would light. Then, the "zero elevation" indication of the micrometer screw could be taken and the aperture could be thereafter elevated at the appropriate height. This method proved extremely valuable since the "zero elevation" indication varied with the temperature of the model ground causing expansion of the plate.

Prior to any quantitative measurements, it was necessary to calibrate the photomultiplier and the accompanying recording apparatus to ensure that their combined response was linear for the range of light intensities likely to be involved in the experiment. For the calibration an arbitrary output voltage of 7 volts was taken as reference level. The calibration procedure is described in what follows.

The receiving aperture was located approximately on the axis of the diverging beam and then by means of the micrometer screw it was displaced off-axis downwards until the measured output was exactly 7 volts. Then a neutral filter with an attenuation coefficient of 2.2 dB was inserted into the beam and the output voltage, say V_1 volts,

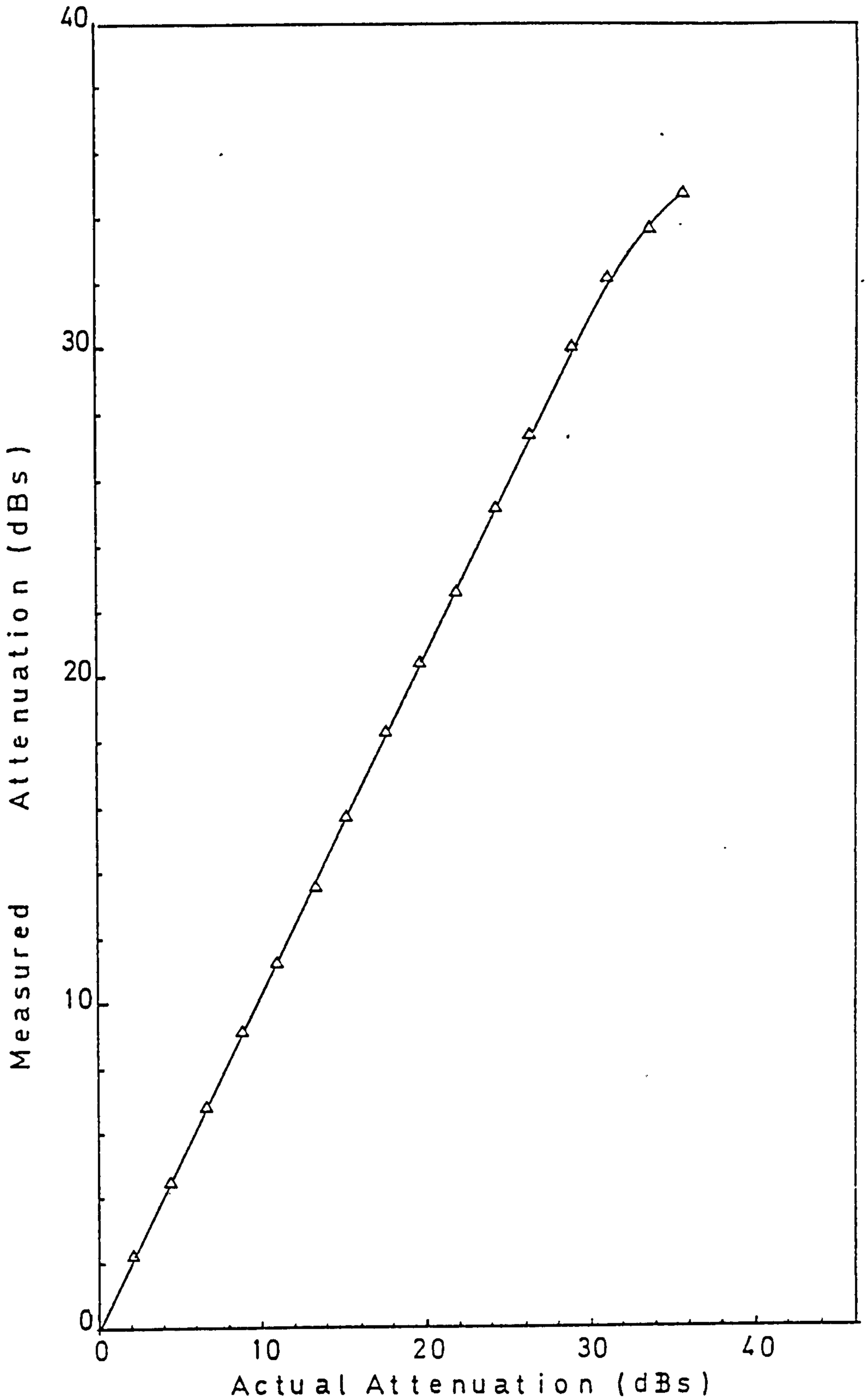

FIGURE 6.4: Calibration curve for the EMI 9658 R photomultiplier.

was measured. Then, the filter was removed and the receiving aperture was displaced further off-axis until the unattenuated beam produced an output voltage of V_1 volts. At that position the filter was introduced again and the beam was again attenuated by 2.2 dBs relative to the previous position and by 2.2 + 2.2 = 4.4 dBs relative to the initial position when the output voltage was 7 volts. For this attenuation the output voltage was, say V_2 volts. The filter was again removed and the aperture displaced further off-axis so that an output voltage of V_2 volts was achieved. This procedure was repeated several times and the resulting measurements produced the calibration curve shown in Fig. 6.4. It can be seen that for the region 0 to 30 dBs attenuation the response of the photomultiplier and the recording system was linear.

6.4.2 The Wind Tunnel: Dynamic Similarity, Description

As a part of the present investigation, the values of the simulated surface wind should be specified for which the results from the laboratory model would be similar to those obtained from the full-scale ("prototype") radio link. In Subsections 5.2.2 and 5.2.3, it was reported that only the normal to the path wind component was found to affect the fading spectrum of the received signal. It was, therefore, decided that only cross-path surface winds should be considered in the laboratory simulation experiment. These surface winds should be of controllable speed and of a low turbulence intensity and such air flows can be obtained only by means of a wind tunnel.

Before the construction of a suitable wind tunnel,

it was necessary to know, at least approximately, the range of wind speeds to be produced. The only indication as to what wind speeds were expected to be involved in the simulation experiment was provided by Burrows[145] who had successfully simulated atmospheric fading in the laboratory using air streams with speeds in the vicinity of 0.5 m/sec.

In most model investigations conducted in a wind tunnel, the conditions which must be satisfied, in order that the results obtained with the model are applicable to the prototype are: (a) Geometric Similarity and (b) Dynamic Similarity. In the present investigation, geometric similarity was achieved by scaling all dimensions of the model by a factor $K = 1.9 \times 10^{-6}$ equal to the ratio of the laser light wavelength to the wavelength of the UHF radio link.

It proved impossible to decide on a criterion for dynamic similarity as in theory, there is a host of dimensionless numbers whose equality ensures dynamic similarity, depending on the particular problem. Thus, equality of the Reynolds number in the model and in the prototype is necessary, when forces exerted on a body completely immersed in an incompressible fluid are of particular interest. As this criterion requires that:-

$$\left(\frac{U\ell}{\nu}\right)_{model} = \left(\frac{U\ell}{\nu}\right)_{prototype} \qquad (6.4.2a)$$

the wind speeds in the model must be many times greater than the ones in the prototype. In the present investigation that would amount to wind speeds approximately 2.10^5 times greater

than those encountered in the atmosphere. Moreover, the objective of the investigation was not to simulate the flow around an object and to measure forces exerted on it. Thus, the Reynolds number was not considered as a suitable criterion for dynamic similarity.

In the case of flows with a free surface or bodies floating in a fluid, equality of another dimensionless number ensures dynamic similarity. This is the Froude number defined as[147]:-

$$Fr = \frac{U^2}{gL}$$

where U is the velocity of the flow, L is a characteristic length of the flow or the floating body and g the gravitational constant.

This number provides a measure of the ratio of inertia forces to gravitational forces in the flow. The analogy between a body floating in a fluid and a buoyant plume "floating" or rising in the ambient air has led to the adoption of the Froude number as a criterion for similarity in the modelling of plumes[148]. In this case variations of density which are of primary importance in buoyancy must be included and Fr can be modified to include them in the following manner[149]:-

$$Fr = \frac{U^2}{g'L} \qquad \text{where now } g' = g\,\frac{\Delta\rho}{\rho_o} \qquad \rho = \text{density}$$

When density ratios are kept unchanged in the model

and in the prototype the condition for similarity in the modelling of plumes can be written(

$$\frac{U^2_{prototype}}{U^2_{model}} = \frac{L_{prototype}}{L_{model}} \qquad (6.4.2b)$$

and in this case, the flow speed in the model must be much less than that in the prototype.

C. K. Batchelor[150] has shown that for nearly ideal incompressible gases at low velocities which are thermally stratified, a Richardson number is the sole parameter governing the flow. For these conditions he assumes:-

$$\frac{\Delta\rho}{\rho_o} \simeq - \frac{\Delta T}{T_o}$$

where T is the temperature of the fluids.

Arya and Cermac[151], investigating problems of atmospheric shear flows and their laboratory simulation, use Batchelor's proposal for the simulation of such flows in the case of a thermally stratified atmosphere. Recognising the fact that the Richardson number defined in terms of gradients as in Equation (1.4.1d), is a local characteristic of the flow depending on the height and, therefore, not suitable for modelling purposes, they propose a "gross" Richardson number defined as:-

$$Ri_h = \frac{gh\ (T_h - T_o)}{T_a\ U_h^2} \qquad (6.4.2c)$$

where h is the thickness of the boundary layer (or equivalent layer in the wind tunnel), U_h and T_h are the values of velocity and temperature at the top of this layer, T_o is the surface temperature and T_a, the average temperature of the layer. Then, equivalence of Ri_h for the model and the prototype flows yield the following condition for similarity:-

$$\frac{U^2_{prototype}}{U^2_{model}} = \frac{h_{prot.}}{h_{mod.}} \quad \frac{(\Delta T/T_a)_{prot.}}{(\Delta T/T_a)_{mod.}} \qquad (6.4.2d)$$

It is worth noting that when temperature ratios are kept the same in the model and in the prototype the condition for similarity becomes the same as Equation (6.4.2b). This indicates that there is an analogy between Fr and Ri_h and this analogy becomes more apparent when Batchelor's assumption $\frac{\Delta\rho}{\rho} \simeq -\frac{\Delta T}{T}$ is taken into account. This assumption is rather correct for the atmosphere where air can be considered as a nearly ideal incompressible gas.

The above discussed concepts of similarity point out that either Fr or (equivalently) Ri_h should be used as a criterion for similarity in the present investigation. Indeed, the method of simulating the propagation medium would result in a thermally stratified model atmosphere with convective cells and thermal "bubbles" or plumes present. The adoption of such a criterion would suggest that the flow inside the model should occur at speeds much lower than the atmospheric winds under simulation.

As the general guideline of the present investigation was to avoid theoretical speculation, so prevalent with

dynamic similarity, a totally empirical method was finally adopted for determining the range of wind speeds the tunnel should produce. Nevertheless, all the previously mentioned concepts of dynamic similarity were kept in mind, to be used later for the interpretation of the experimental results.

The procedure used to determine the range of simulated wind speeds that would produce the right results in the model was the following.

Air streams of different speeds were blown across the laser beam by means of different fans. The model ground was at the same time heated from below. The signal received by the simulated "receiver" was then applied to the available SAICOR spectrum analyser and the resulting fading power spectra were observed.

It became immediately apparent that wind speeds in the range of the atmospheric winds were producing fading power spectra extending to frequencies much higher (up to 15 Hz) than the ones experienced in the radio link under simulation (up to 2 Hz). The speeds were gradually reduced until power spectra appeared in the range 0 to 2 Hz. The speeds required to produce these spectra were in the vicinity of 0.5 m/sec or lower, in agreement with the value suggested by Burrows in[145]. Thus, it was decided that the wind tunnel should be of the low speed type.

A description of the component parts of the wind tunnel, which was constructed in the workshop of e.m. Waves Group, will be given in what follows:-

(a) The Driving Unit. This was a three-blade Saucer

Fan made by ROTRON (Woodstock, New York) for the ventilation of large electronic equipment. It was chosen for its low weight (less than 1 kg), low level of vibrations and noise and its low friction rotation. It was power supplied by a variac which permitted a very good control of the revolution rate.

(b) The Diffuser. It was made of plywood and its function was to convert the kinetic energy of the air stream produced by the blades into pressure energy.

(c) One Gauze and two Honeycomb screens. The function of the gauze screen was to eliminate turbulence by the breaking down of large eddies created by the fan blades. The honeycomb screens, placed downstream of the gauze, would reduce the lateral components in the flow and, consequently, "straighten" the flow.

(d) The Contractor. The exact nature of turbulence changes produced by a contractor is not very certain[147]. Apart from the fact that it enables a low velocity to be maintained through the screens, there is evidence that it reduces the turbulent velocity components in the longitudinal direction. It was designed in the Fluid Mechanics Section of the Mechanical Engineering Department, Imperial College for a similar but rather larger wind tunnel. The original pattern-drawings were photographically reduced to the right size and then used for the construction of the contractor out of aluminium sheets.

(e) The Working Section. This was an air-duct of uniform rectangular cross section. The inner dimensions were 27 cm (length of the model propagation path) by 8 cm. Its length was 120 cm. The ceiling and the floor were made of plywood and the sides were made of perspex to allow viewing of the working area. As shown in Fig. 6.6, a part of the floor was left open so that the aluminium plate could fit in that position and become a part of the floor. Two semi-circular notches were cut on the sides of the working section at the positions shown in Fig. 6.6, allowing the laser beam to propagate unobstructed in a direction perpendicular to the flow inside the tunnel. The parts of the perspex sides adjacent to the heated aluminium plate were replaced by strips of asbestos to avoid deformation of melting of the perspex due to the high temperature.

With these arrangements, it became possible to have a constant air flow of controllable speed blowing across the propagation path of the laser beam.

Later it became apparent that for very low wind speeds, the flow could become intermittent due to the low rate of revolution of the fan blades. This problem was solved by placing a wire-mesh cover at the air inlet of the driving unit. By letting small pieces of porous paper to be sucked and stack on the mesh surface, the effective area of the air inlet could be reduced resulting in lower flow speeds without a reduction of the revolution rate of the driving unit.

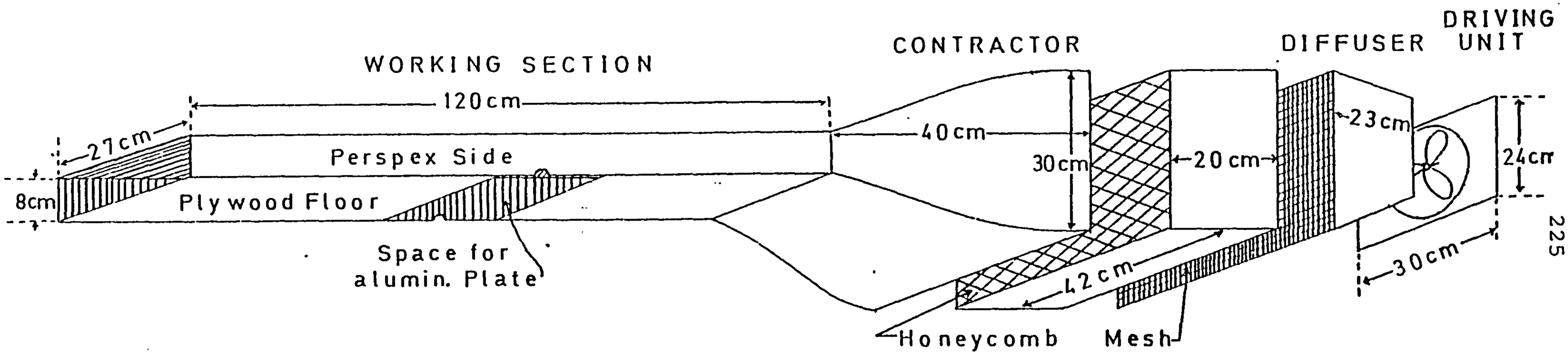

FIGURE 6.6: Schematic diagram of the Wind Tunnel and its component parts (to scale).

6.4.3 The Schlieren Interferometer

It was mentioned in Chapter 1 that for optical wavelengths the refractive index of atmospheric air is proportional to the pressure and inversely proportional to the air temperature, Equation (1.4.3z). In cases where the pressure is nearly constant, as in the low-speed flows in a laboratory environment, the refractive index depends only on the temperature of the air and observations of the refractivity field can lead to conclusions about the temperature field.

A method by which the refractivity field of a transparent material or a gas can be visually observed is the Schlieren method and the corresponding optical devices are known as Schlieren systems or interferometers. Detailed descriptions of such systems can be found in various sources (147,152).

Plate 6.3 shows the arrangement of the component parts of the interferometer used in this investigation and Fig. 6.7 is a schematic diagram showing the parts and their function. The monochromatic light source was a GROSSCOPE sodium lamp transmitting through a slit 2 cm long and approximately 1 mm wide (LS in Plate 6.3). The source was placed off the optical axis but on the focal plane of a spherical concave mirror having a diameter of 15 cm and a focal length of 150 cm. Thus, the reflected light had the form of a parallel beam. The axis of this beam was perpendicular to the major axis of the model ground and tangential to its surface as shown in Fig. 6.7. In this way, the lower half of the beam was intercepted by the model ground. The rest of the beam was incident upon a second mirror M_2 identical to the

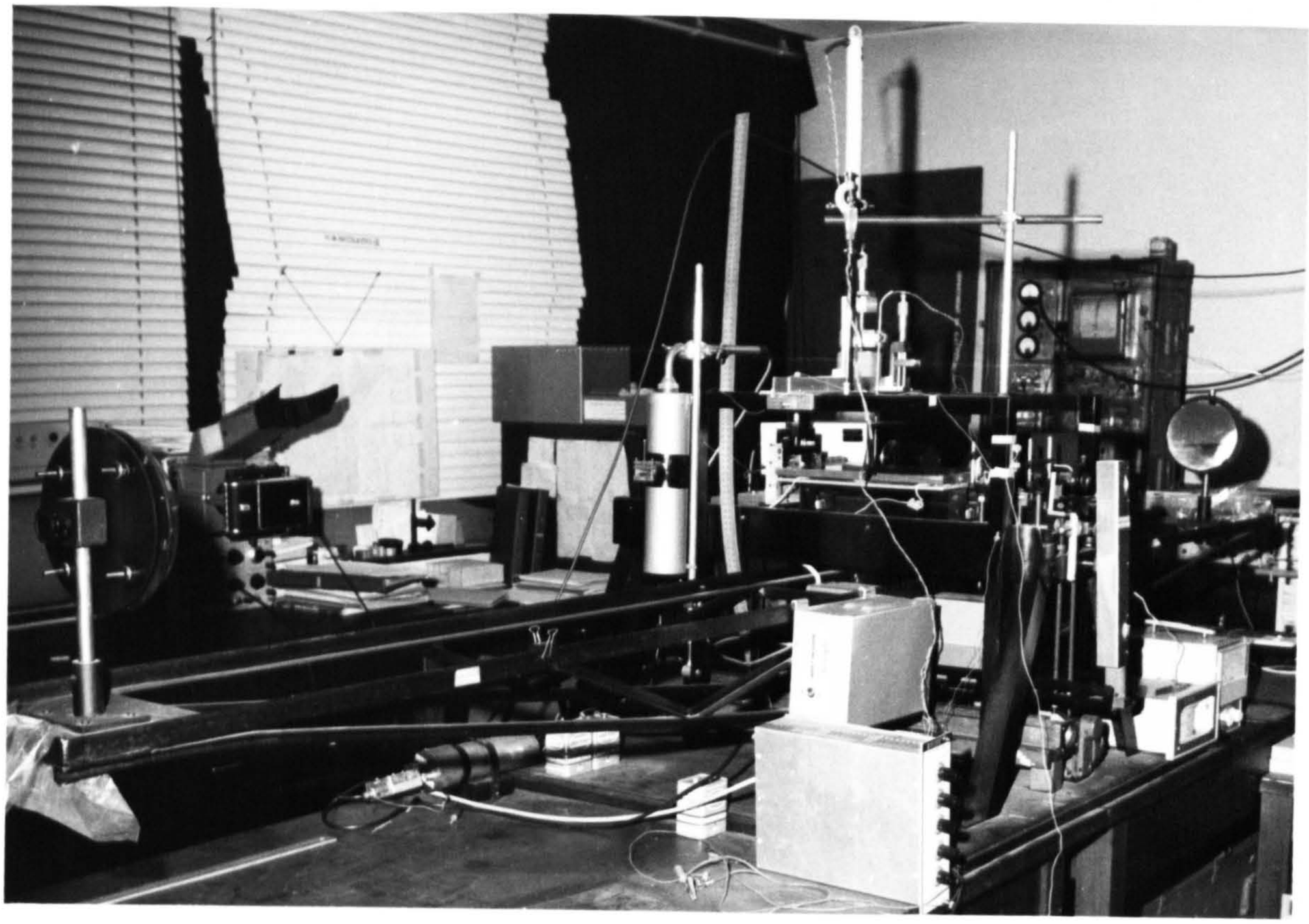

PLATE 6.3

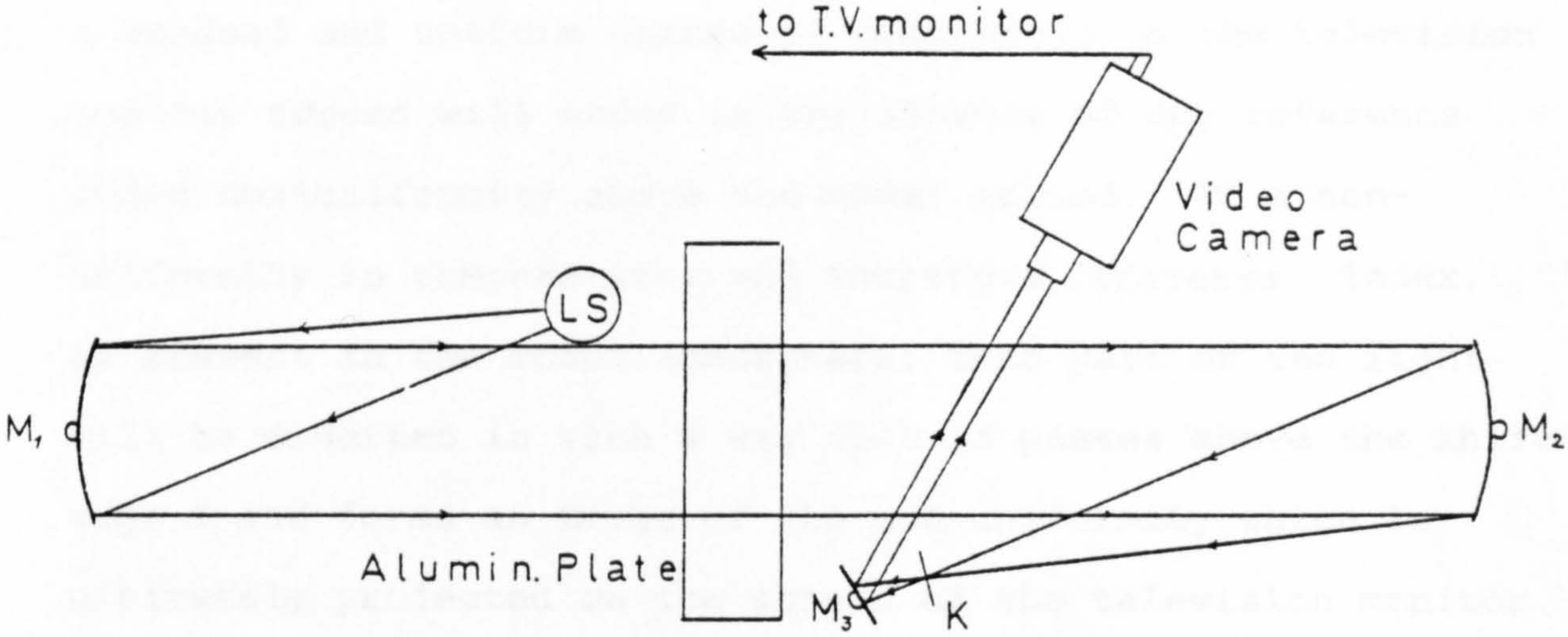

FIGURE 6.7: Schematic diagram showing the component parts of the Schlieren interferometer. LS: light source, M_1,M_2: convex mirrors, M_3: plane mirror, K: knife edge.

first one. The mirror M_2 was slightly tilted around its vertical axis so that it was focusing off the axis M_1 M_2 at the side opposite to the light source. A knife-edge cut-off K was placed at the focus F_2 of this mirror and it could be vertically moved to intercept totally or partially the light beam at this point. Beyond the focus F_2 a high quality flat mirror M_3 was placed which could reflect the image created by M_2 onto the objective lens of a video-camera C. The objective of this camera combined through the flat mirror M_3 with the concave mirror M_2 could be focused on the middle plane of the model. The received image was then continuously monitored on the screen of a television monitor connected to the video-camera.

As a result of the vertical movement of the knife-edge K, a position can be reached when part or all of the light arriving from the source will be cut off. In this case, a gradual and uniform change of brightness on the television monitor screen will occur in the absence of any reference index non-uniformity above the model ground. If a non-uniformity in temperature, and therefore reference index, is present in the model atmosphere, then part of the light will be diverted in such a way that it passes above the knife-edge K and forms an image of the non-uniformity which is ultimately projected on the screen of the television monitor. By means of the vertical movement of the knife-edge K, the sensitivity of the system can vary. When most of the light is cut off by K at the point F_2 only very strong gradients of reference index can divert the light rays sufficiently to pass over the knife-edge and give an image on the screen.

Schlieren systems are usually subject to astigmatism and coma. Astigmatism can be avoided to a large extent when the ratio of focal length to aperture exceeds about ten (i.e. f/diameter $\geqq$ 10). With the mirrors used in the described refractometer, this condition was fulfilled. Coma can be avoided when the component parts are arranged in a way that the light source and the knife-edge are on opposite sides of the axis of the two mirrors[147]. Again, provision had been taken for such an arrangement. Astigmatism was further reduced by placing the light-source LS, the knife-edge K and the heated aluminium plate in the same plane as the optical axis M_1 M_2.

The whole of the apparatus was firmly mounted on a special support with provision for the movement and adjustment of every single component. This support could move in a direction normal to the optical axis M_1 M_2 by means of a lead-screw system. In this way the whole of the model propagation path could be scanned.

The Schlieren interferometer provided a very effective means of continuous monitoring of the propagation medium above the heated model ground. It allowed inspection of the reference index inhomogeneities and recordings of the received light signal to be done simultaneously. Photographs of the television screen could be taken to serve as permanent records of the propagation medium. The whole system had the advantage of being a "passive" detector, not interfering with the properties of the "atmosphere" in the model.

6.5 Methods of Determining the Temperature and Velocity Profiles: Instruments, Calibrations

For point measurements of the temperature and velocity field in the propagation medium and, more important, for determining the vertical profiles of the same quantities, the following methods and instrumentation were used.

For temperature measurements, a calibrated electronic thermometer (CORMACK) was used with a NiCr-AlCr thermocouple probe. The probe could move vertically above the middle of the propagation path by means of a micrometer screw and it was placed inside the tunnel through a small hole in the ceiling.

A voltage output was available from the electronic thermometer and this was used to drive the Y axis circuit of a XY plotter (HEWLETT-PACKARD). The X voltage was provided by a displacement transducer following the vertical movement of the thermocouple probe. In this way temperature profiles above the middle of the path could be plotted for different ground temperatures and wind speeds.

The following method was used to displace the sensor vertically with a constant speed. One end of a piece of string was fixed on the thimble of the micrometer screw with sealing wax. The string was then rolled around the thimble about forty times. By pulling manually the free end of the string away from the thimble with a constant force the micrometer screw was made to rotate with a constant speed. This method would provide vertical displacements of up to 1 cm.

For the air flow measurements inside the wind tunnel

a hot-wire anemometer was used. This was a DISA Type 55D05 battery-operated instrument operating according to the constant-temperature principle. A bridge circuit and an amplifier keep the probe resistance and hence the probe temperature virtually constant. The anemometer measures the power delivered by the probe to the flowing medium in which it is placed. The sensor was a DISA 55A36 hot-wire probe, with a platinum plated tungsten wire 5 μ in diameter.

The instrument was calibrated against an inclined Pitot-static manometer in the following way. Since the anemometer was to be used to measure very low wind speeds, accurate calibration for the range of speeds 0 - 1 m/sec was required. This imposed some difficulties because Pitot-static manometers are rather insensitive in very low speeds. Nevertheless, this problem was solved by placing the hot-wire probe in the wide part of a wind tunnel contractor and the manometer tubes in the working part of the tunnel. The contraction ratio of this particular wind tunnel was 8.7, thus wind speeds experienced by the hot-wire probe were 8.7 times smaller than the ones measured by the manometer.

The inclination angle of the manometer was $\phi = 20^{o}$ and it is known[147] that the velocity of an air stream in ft/sec measured by a Pitot-static manometer under standard conditions is:-

$$U_m = 66.15 \sqrt{h \,.\, \sin \phi \,.\, \rho} \qquad \text{(ft/sec)}$$

where h is the Pitot-static difference in inches and ρ is the density of the fluid in the manometer. In this particular

case, ρ = 0.8 g/ml and:-

$$U_m = 20.176 \sqrt{0.8 \cdot \sin \phi \cdot h(\text{inches})} = 10.57 \sqrt{h(\text{inches})} \quad \text{m/sec}$$

Taking into account the contraction ratio of the wind tunnel, the flow speed measured by the anemometer should be:-

$$U_a = \frac{U_m}{8.7} = 1.215 \sqrt{h(\text{inches})} \quad \text{m/sec}$$

With the anemometer output connected to a galvanometer, the calibration curve shown in Fig. 6.8 was plotted, showing the flow speed in m/sec^{-1} versus anemometer output voltage. The effect of temperature upon the hot-wire resistance had been taken into account according to the manufacturer's specifications.

For vertical scannings of the flow regime inside the wind tunnel, the anemometer probe could be displaced vertically by means of a micrometer screw through a hole in the ceiling of the tunnel. Profiles of wind speed versus height could be measured by the same method as for temperature profiles, involving a displacement transducer and rotating the micrometer thimble by means of a thread.

As temperature fluctuations in the gaseous medium could affect the anemometer readings in an unpredictable way, the hot-wire probe was not mounted right above the heated model ground but it was placed a small distance upwind of it, in a convection-free region of the working part of the tunnel.

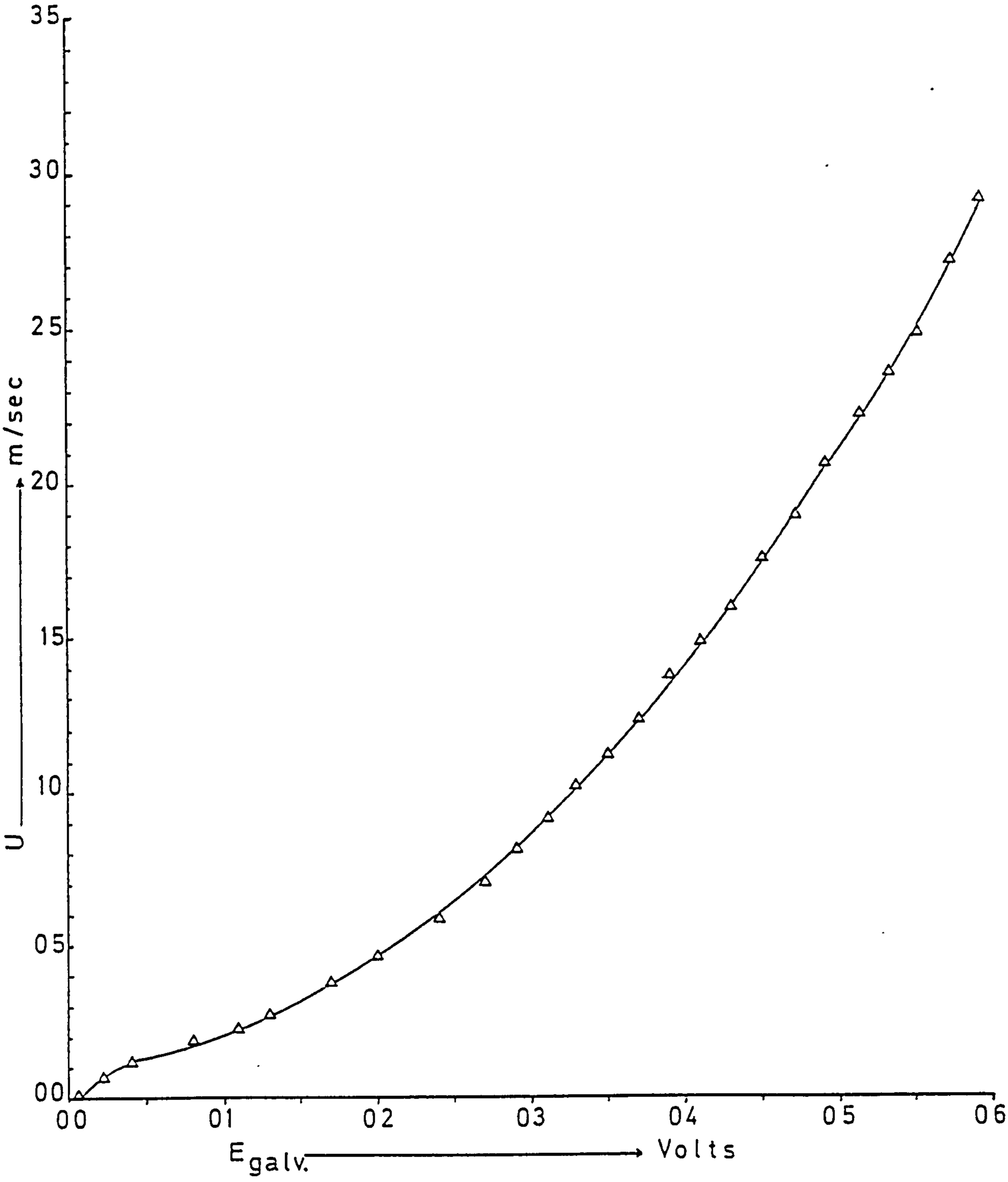

FIGURE 6.8: Calibration curve for the DISA 55A36 hot - wire Anemometer.

6.6 Data Recording and Processing

As the results obtained from the laboratory model were to be compared quantitatively with those obtained from the prototype radio link, it was considered appropriate to use exactly the same method for data recording and processing. This would ensure that fortuitous similarities or differences between the two sets of results would not be introduced due to a change in the recording method, equipment and computational procedure.

Thus, the voltage output from the photomultiplier dynode was applied to the same recording system as in the case of the voltage output from the radio-receiver. A detailed description of all the recording apparatus together with a block diagram (Fig. 3.5) has been given in Section 3.3. The only difference is that in the case of the model the DC amplifier was operating with a constant gain of 50 instead of 10 as in the case of the radio-link recordings. However, the signal was sampled with a rate of 5 samples/sec, encoded and recorded in digital form on paper-tape in a method identical to the one described in Section 3.3

For the processing of the digital data in the CDC 6400 Computer Unit of Imperial College, the procedure already described in Subsection 4.2.2 was employed. Thus, the routine DATPOW (Appendix III) was used for the estimation and plotting of the fading power spectrum, as in the case of the prototype radio-link. This routine incorporated the subroutines: REGRE, for the prewhitening of the Digital Data; TAPER, for the application of a Hamming Data window; FASTF, for the Fourier transformation. The spectral estimates were obtained

by squaring and adding together the real and imaginary parts of the FASTF output. These estimates were then smoothed and normalized to the maximum value. Thence, the Power Spectrum could be plotted either in linear axes, by means of the subroutine POWPLO, or in logarithmic axes by means of the subroutine LOGPLO (see Appendix III).

CHAPTER 7

SIMULATION IN THE LABORATORY. EXPERIMENTAL INVESTIGATION

In using a laboratory model technique as an aid in the study of the influence of the atmosphere on a radio beam, with the objectives as outlined in Sections 6.2 and 6.3, it is necessary to conduct two quite different investigations.

1. To establish that within a sealed model, which has been constructed to represent a given full-scale radio system, it is possible to affect suitable variations of the physical properties of the gaseous or "atmospheric" medium under controlled conditions. The ranges of these variations in parameters such as temperature, temperature gradient, surface wind speed, etc. are required to be such that the variations in the resultant refractive index (and its gradient) produces similar effects on the model "radio-beam" to those which occur in the full scale system.

2. To reproduce and simulate, as accurately as possible, the same fading characteristics on the model system as those observed on the full scale system. The controlled conditions in the model "atmosphere" are then to be related to those meteorological conditions which prevail on the full scale ("prototype") system when the fading characteristics under consideration are observed.

7.1 The Propagation Medium

The propagation medium in the laboratory model was studied in three different ways:-

(a) Vertical soundings of temperature were performed above the middle of the propagation path by means of an electronic thermometer used as described in Section 6.5. From the resulting temperature profiles and by employing the relationship:-

$$N = - \frac{77.6}{T} \cdot p$$

where T is the absolute temperature and p is the atmospheric pressure in mbars., the corresponding refractive index profiles could be deduced.

(b) The continuous changes in the refractive index properties of the propagation medium were monitored by means of the schlieren system and continuously displayed on the television screen. Any special features of its activity could be studied in detail from photographs which were obtainable from the screen image.

(c) Vertical soundings of the flow above the propagation path were obtained by means of the hot-wire anemometer. This was done with the model ground unheated, so that temperature fluctuations would not alter the readings of the anemometer. The velocity profiles above the middle of

the propagation path were afterwards used to extrapolate the wind speed very close to the model ground for given free-stream velocities.

The measurements and observations obtained by these three methods will be extensively discussed in the following subsections.

7.1.1 Temperature and Refractive Index Profiles

Vertical soundings of the temperature, performed in the way described in Section 6.5, produced the profiles shown in Figs. 7.1 - 7.4. The method of displacing the thermocouple probe vertically with constant speed makes the soundings equivalent, if not more accurate, to similar temperature soundings of the real atmosphere performed by radiosondes or free ascending balloons. The vertical extent of these soundings was approximately 1 cm so that it covered the vertical extent of the diverging laser beam at the middle of the path. Fig. 7.1 shows the temperature profile for a model ground temperature of 60^{o}C, an ambient temperature of 23^{o}C and in the absence of any air flow in the tunnel. It can be seen that a negative average temperature gradient persists in the propagation medium. This average gradient is not constant throughout the boundary layer but changes value for different depths. Thus, very close to the ground a very steep gradient persists with a value around - 25^{o}C/mm. This is the region where heating of the air takes place rather by conduction than convection.

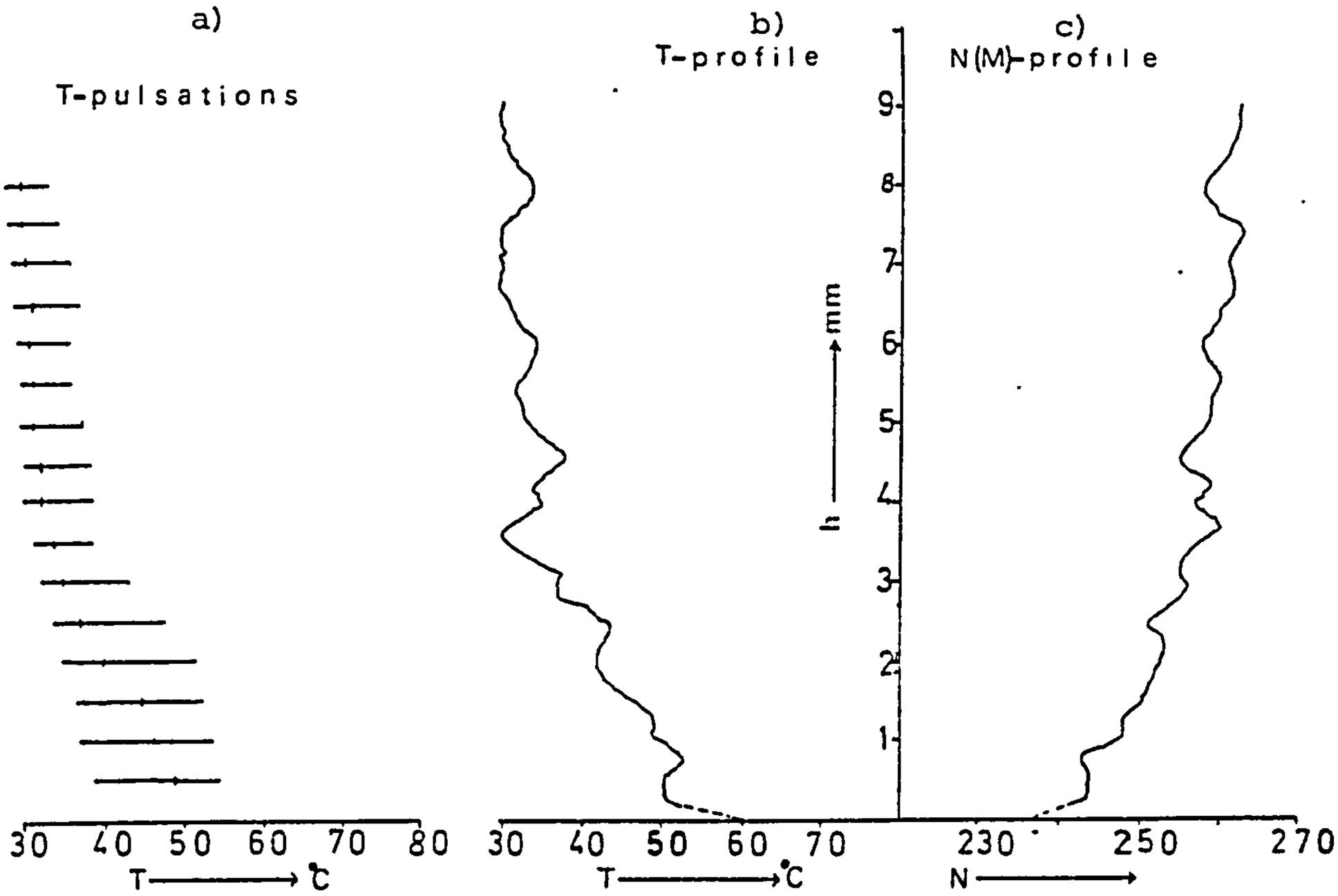

FIGURE 7.1: Vertical profiles of: temperature pulsations (a), temperature (b), and refr. index (c) for a ground-plane temperature of 60 °C and zero free-stream velocity.

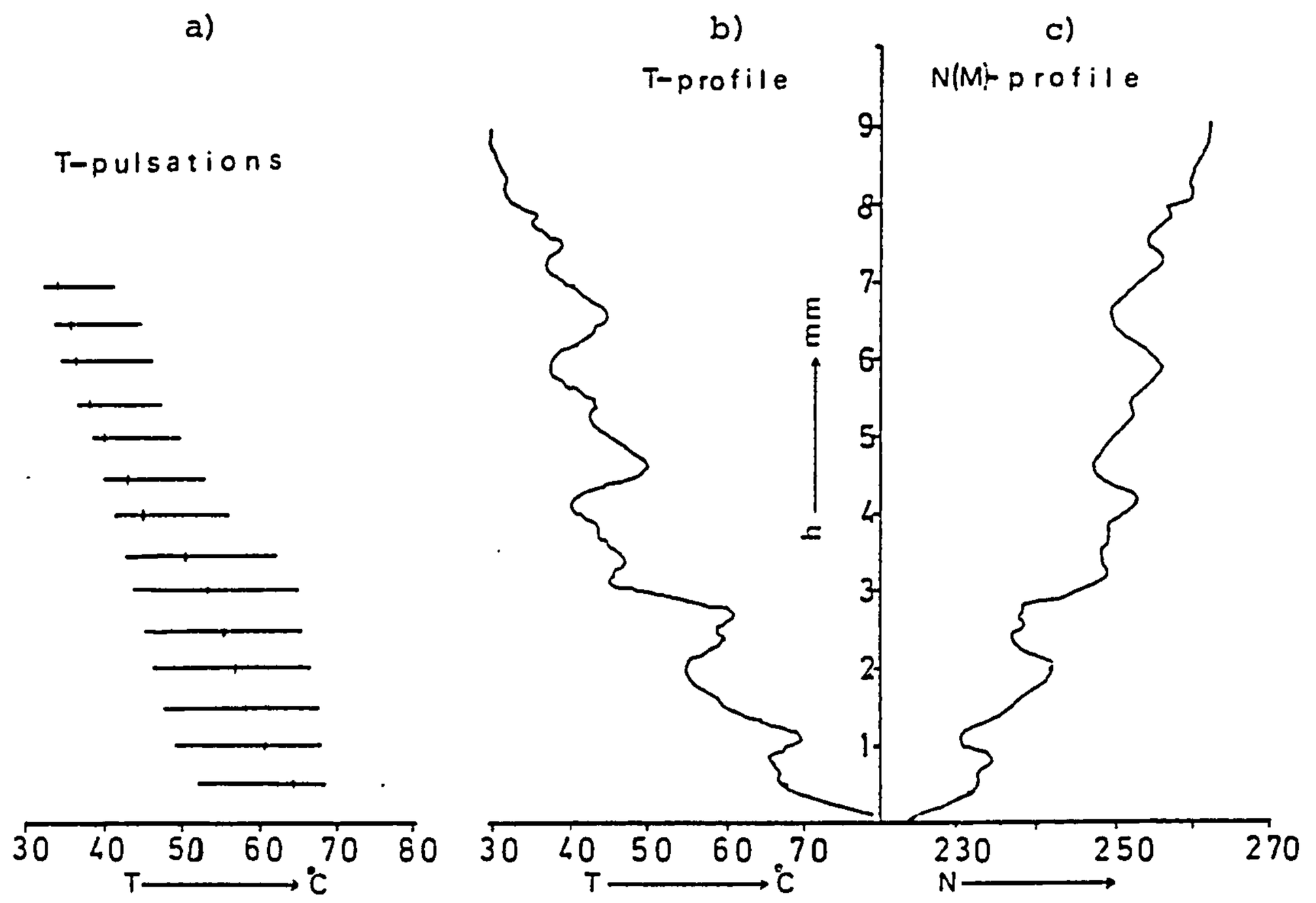

FIGURE 7.2: Same as above, for a ground-plane temperature of 80 °C and zero free-stream velocity.

Right above this region the gradient falls to values of around - 6°C/mm where mixing due to convection is expected to occur. Further up the gradient rises again to values of - 10°C/mm and this marks the region where a transition possibly occurs from persistent organized convection to random convective turbulence due to convective elements which detach themselves from the ground and rise under the buoyant forces. Even higher, the gradient falls again to small values of about - 1°C/mm and in this region, the temperature gradient seems to be maintained by the rising convective elements ("bubbles").

Upon this average distribution of temperature with height, random fluctuations are superimposed which are shown in Fig. 7.1. These fluctuations are possibly due to rising "bubbles" and descending cold volumes of air. They give rise to continuous variations of the average temperature gradient and they are responsible for local temperature inversions. These inversions can be as strong as + 10°C/mm and they occur mainly in the layer from 2 - 4 mm where most of the convective "mixing" occurs. The rising "bubbles" seem to have a vertical extent of about 1 - 2 mm but they are probably larger than that and the apparent "contraction" in their vertical dimensions is due to the fact that they rise faster than the temperature probe.

A better understanding of the motion of convective elements is gained by studying the temperature pulsations (T-pulsations) at different heights. These pulsations were recorded by placing the thermocouple probe at a certain

height and recording the temperature vs time at this point. The recording was done on a MINI-WRITER hot-pen recorder with a fast response and a speed of 2 mm/sec. Records of 30 seconds were used for determining the mean value of temperature at the point of sampling and the positive and negative pulsations of temperature relative to the mean level. The estimation was easily done by simple inspection of the time records.

These T-pulsation recordings (see Figs. 7.1 to 7.4, Section a) reveal the nature of the temperature fluctuations more clearly. Thus, from Fig. 7.1a it can be seen that close to the heated ground plane the temperature pulsations are predominantly "cold". This means that "pockets" of cold air are present in this otherwise "hot" layer of air. These cold "pockets" can be attributed to descending cold air and point towards an organised circulation similar to that occurring inside thermal cells. As it was previously discussed in Subsection 1.4.2B, such formations are a common feature of the atmospheric boundary layer.

In the region of convective "mixing" there seems to be a balance between cold and hot pulsations, whereas, further up the pulsations appear to be predominantly "hot". These can be attributed to ascending volumes of hot air in the form of "bubbles" and again, they are a common feature of the real atmosphere (see Subsection 1.4.2A).

Figs. 7.2a and b show the temperature-profile (T-profile) and the corresponding T-pulsation profile for a ground temperature of 80^{o}C and all other conditions as previously. It can be seen that the average temperature

gradients are now intensified. More specifically, in the "conduction layer" right above the ground the average T-gradient is almost - 30°C/mm. In the region where convective activity is expected to occur, the average gradient is - 8°C/mm and the T-pulsations are mainly "cold biased" due to the possible convective circulation.

The next higher region is marked by a steeper gradient and a balance between cold and hot pulsations indicating the intensive mixing that occurs in this region. The whole activity in the model "atmosphere" is intensified and the vertical extent of the different regions ("conductive", "convective", etc.) is increased as a result of the increased temperature of the model ground plane. A comparison of Fig. 7.1 and Fig. 7.2 (Sections a and b) provides a good example of the control that can be exerted upon this activity only by means of varying the ground plane temperature.

Figs. 7.3a and b show the temperature distribution for a ground temperature of 80°C, an ambient temperature of 23°C and an air flow of 0.2 m/sec above the heated ground. In this case, the temperature gradients near the ground are intensified to values of - 60°C/mm in the conduction layer and of - 13°C/mm in the higher region. Cold T-pulsations in this region still persist, showing the presence of possible circulation, but their magnitudes are slightly reduced compared with the previous cases.

The profiles shown in Figs. 7.4a and b show the temperature field under the previous conditions of heating and in the presence of a free-stream velocity of 0.5 m/sec

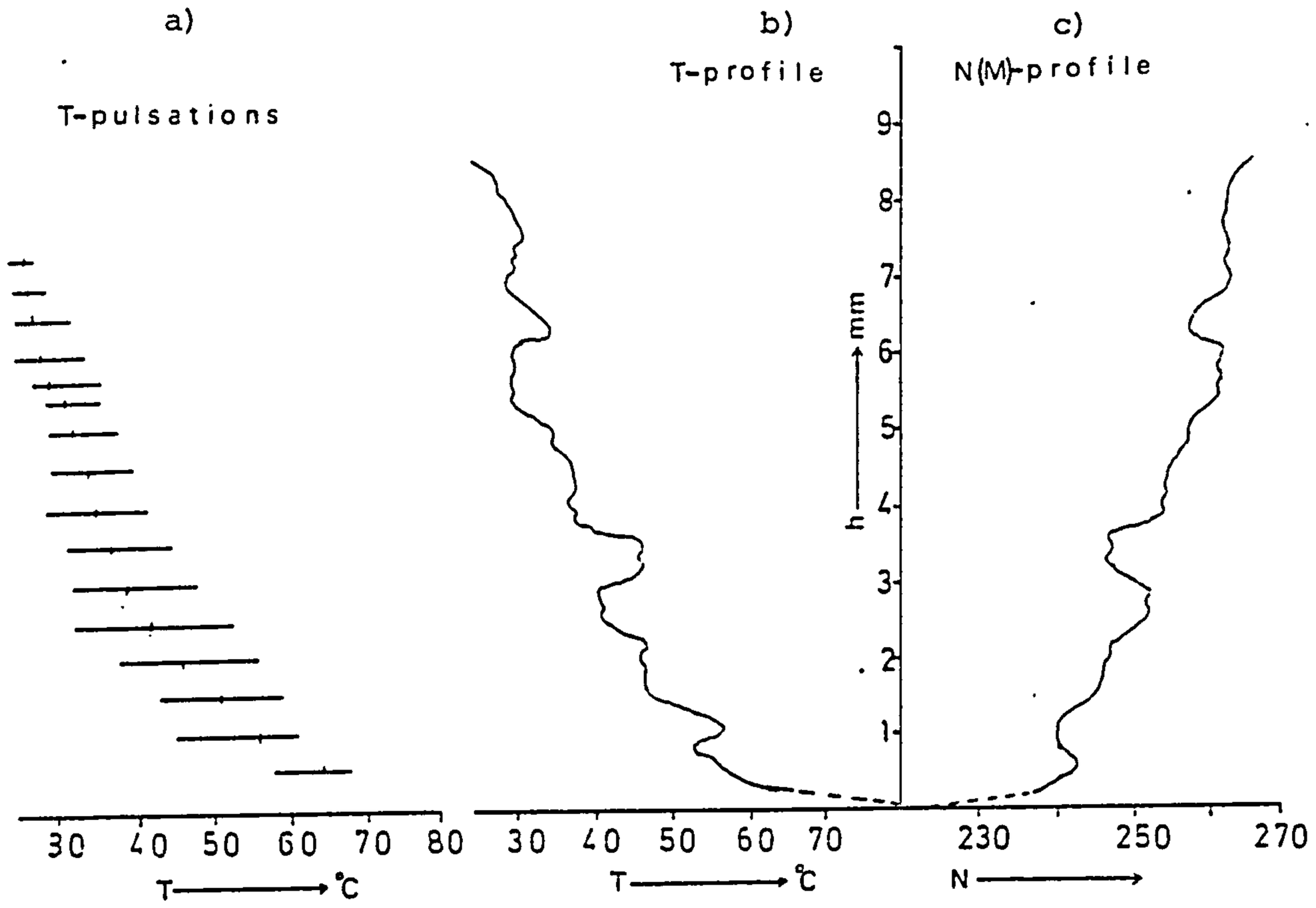

FIGURE 7.3: Vertical profiles of: temperature pulsations (a), temperature (b) and refr. index (c) for a ground-plane temperature of 80 °C and a free-stream velocity of 0.2 . m/sec.

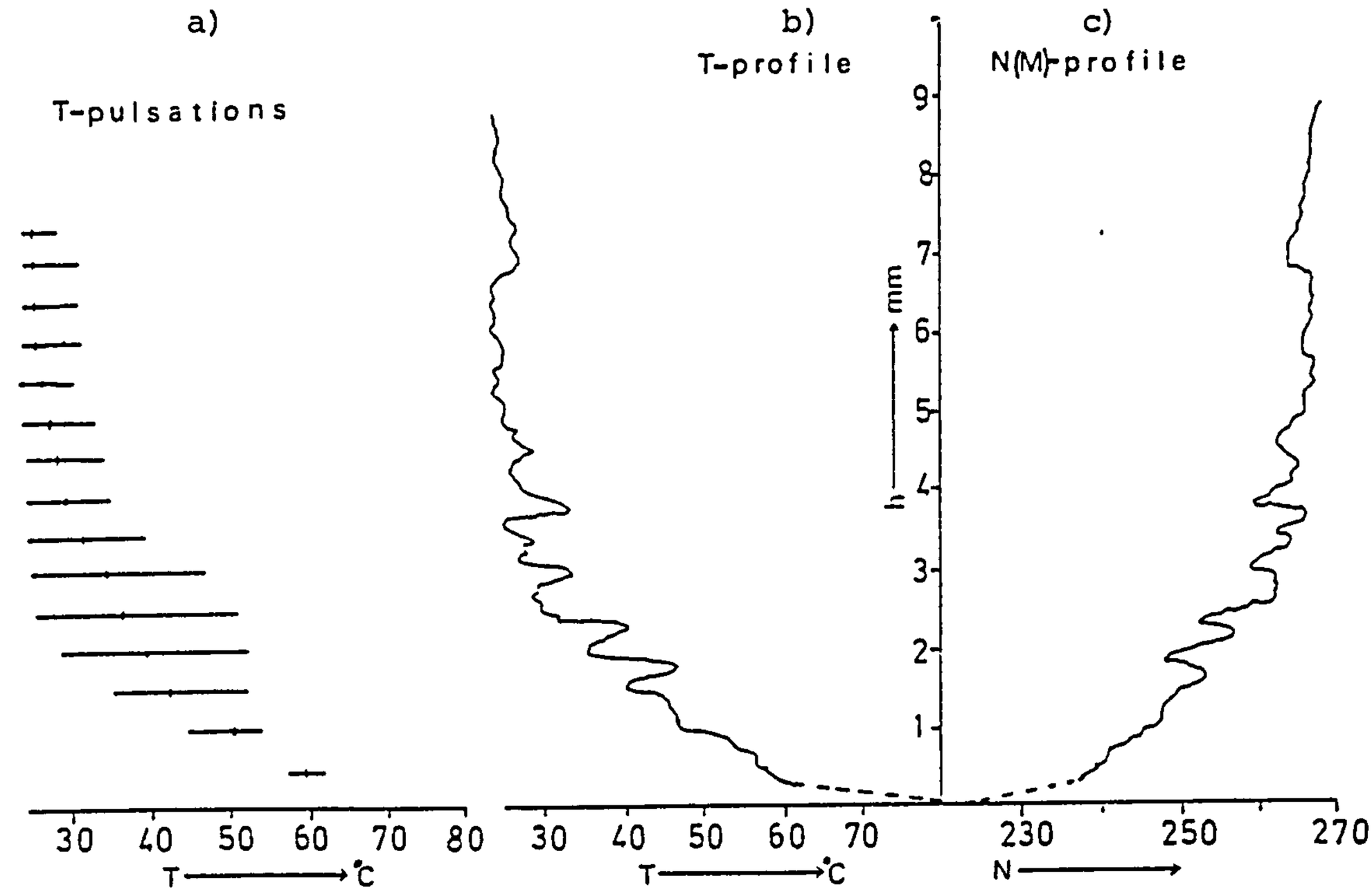

FIGURE 7.4: Same as above, for a ground-plane temperature of 80 °C and a free-stream velocity of 0.5 m/sec.

in the wind tunnel. Under these conditions, the flow-regime is that of "forced convection"[153] and the temperature profile is expected to be similar to the wind velocity profile. The average T-gradient in the "conduction layer" is around - 60°C/mm and it becomes less and less steep with increasing height. The fact that very small T-pulsations, equally "cold" and "hot", have been recorded in the proximity of the ground plane possibly indicates that the formation of any organized activity is now inhibited by the presence of wind shear. This is a well known fact for the real atmosphere and has been already discussed in Subsection 1.4.2B. The region of possible organized activity seems to have been replaced by a strongly unstable thermal layer where disorganized thermal turbulence prevails as suggested by Batchelor[29]. This turbulence appears in the T-profile (see Fig. 7.4b) as thin regions of intense negative and positive temperature gradients and in the case of a temperature sounding of the real atmosphere by means of a sonde, could be easily interpreted as "feuillets" due to thermal stratification.

The vertical distribution of refractive index in the four previously discussed cases is shown in Section c of Figs. 7.1 - 7.4. Under the designation: N(M)-profile. This designation has been chosen because the model is a "flat earth" one and, therefore, the actual coindex of refraction N must represent the modified refractive index M in a real atmosphere. The fact that the refractive index in the model atmosphere increases with height serves the purpose of

simulation because in the real atmosphere M is also an increasing function of height.

As already mentioned the N(M)-profiles have been derived from the T-profiles by means of the relationship (1.4.3z) giving the coindex of refraction N for optical wavelengths as a function of temperature and pressure. The average pressure at the time of the measurements was approximately 1020 mbars and this value has been substituted in (1.4.3z).

A common feature in all four N(M)-profiles shown in Figs. 7.1 - 7.4 (Section c) is the very steep positive gradient in the first 0.5 mm above the model ground. The value of this gradient is about 25 N units/mm in the first case (ground temperature: 60^{o}C) and about 30 N units/mm in the second case (ground temperature: 80^{o}C). Taking into consideration the scaling factor of the model (1.9×10^{-6}) and the fact that N-profiles in the model simulate M-profiles in the real atmosphere, the above-mentioned values correspond to gradients of approximately 50 M-units/km and 60 M-units/km respectively. These values are not unrealistic for the real atmosphere and represent slightly sub-refractive conditions. Indeed, average values of 120 M-units/km for a temperature climate in the month of May have been reported by Bean and Dutton[82]. The values of refractive index gradient encountered in the "conduction layer" for the two "windy" cases is approximately - 47 N-units/mm and this would correspond to approximately 95 M-units/km for a real atmosphere, a value rather close to the ones reported in[82].

As the altitude from the heated ground increases,

other features are encountered which also bear similarity to the real atmosphere. Thus, for the model under "calm" conditions, refractive index inversions exist with a vertical extent of 0.5 - 1 mm and magnitude reaching 6 - 7 N-units. These dimensions correspond to 250 - 500 m in the real atmosphere and inversions of such vertical extent and even larger magnitude (reaching 45 N-units) have been reported to exist under light wind conditions[61,154]. The smaller scale but rather intense refractive index fluctuations under "windy" conditions (see Fig. 7.4c) also agree with observations in the real atmosphere. Thus Crain[154] reports the presence of such fine structure refractive index fluctuations for altitudes of 2 - 3 km but also for much lower altitudes of 500 - 1000 m. Gossard[57] has measured by microwave refractometer large refractive index variances at altitudes of 500 and 1200 m. Similar results have been obtained by Lane[62] during refractometer soundings, in one case strong refractive index fluctuations at altitudes of 600 - 900 m coincided with the presence of strong wind shear in this layer. In another case, strong small scale N-fluctuations were occurring under temperature inversions. Usually such inversions at day-time mark the top of a so-called "convective layer".

7.1.2 The Refractivity Field as Revealed by the Schlieren Interferometer

As already mentioned in Subsection 6.4.4, the schlieren interferometer provided a means of visual monitoring of the refractivity field above the heated ground plane. Photographs

Plate 7.1

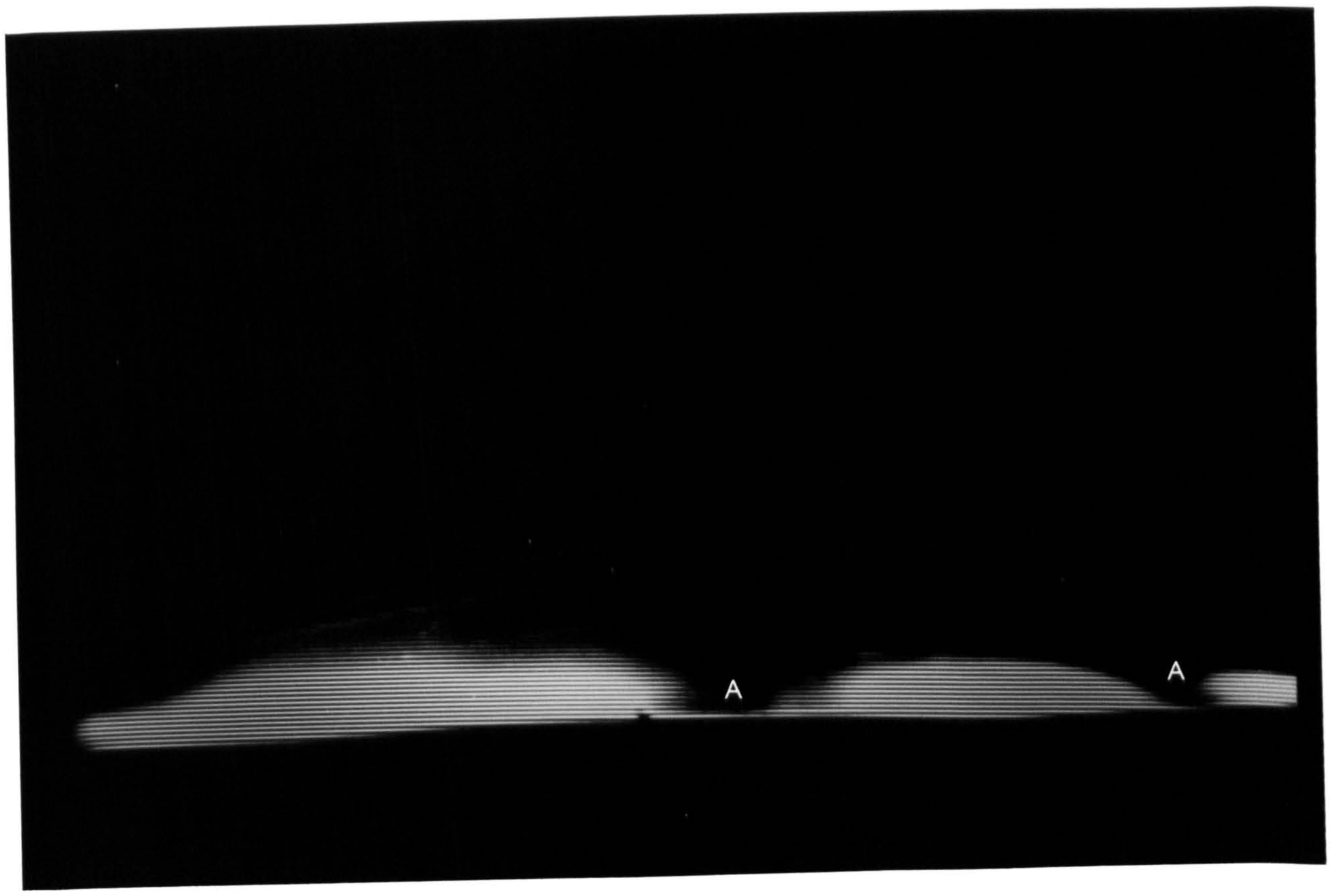

Plate 7.2

of the television screen could be taken and used as instantaneous records of the activity occurring in the model propagation medium. Much of this activity is, of course, due largely to convective motion above the heated ground plane. Plates 7.1 to 7.4 are examples of such photographs which have been taken under different conditions of ground heating and system sensitivity.

In Plate 7.1 there is some evidence of organized structures immediately above the ground plane which is maintained at a temperature of approximately 60^{o}C (the ambient temperature was 21^{o}C). These structures appear as extensive regions of strong vertical refractive index gradient separated by a small region of no appreciable refractive index gradient (region A in Plate 7.1).

The same type of activity appears in Plate 7.2 which is a photograph of the screen taken with the ground plane at a temperature of 70^{o}C. The regions of strong refractive index gradient appear with their vertical extent slightly increased, whilst their horizontal dimensions are reduced. In this photograph two regions of low refractive index gradient (region A) can be seen in the form of slanting "tongues" or "pockets". These regions can be identified as cold air "pockets" from the fact that no considerable refractive index (temperature) gradient exists between them and the colder air far above the heated ground plane.

Plate 7.3 shows the activity above the ground plane maintained at a temperature of 90^{o}C. The rather organized structures observed in the previous two cases have now been

Plate 7.3

Plate 7.4

replaced by a deeper region of strong refractive index (temperature) gradient with a "wave-like" upper boundary. Smaller scale variations in refractive index gradient are embedded in this boundary (regions B).

The photograph shown in Plate 7.4 has been taken with the heating conditions the same as previously but with the sensitivity of the schlieren refractometer increased, so that regions of weaker refractive index (temperature) gradients are now visible. Smaller scale fluctuations of refractive index gradient can now be seen to occur in the upper region of the model "boundary layer".

Given the conditions under which the above-discussed photographs have been taken (heating of a gaseous medium from below), most of the heat is transferred from the heated ground plane to the atmospheric air by convection. This is expected to give rise to various formations such as organized convective cells and/or "bubbles" depending upon the thermal stability of the gaseous medium.

The organized structures shown in Plates 7.1 and 7.2 can well be the result of organized convection in the proximity of the heated ground plane. Further evidence that the dark regions of small refractive index gradient are cold air "pockets" was provided by placing the probe of the electronic thermometer in the region of this activity. Each time the probe was coinciding with such a "pocket", and this could easily be checked from the schlieren image, a "cold" temperature pulsation was recorded by the thermometer. This fact pointed towards a circulation with ascending cold

air volumes, known to occur in organized convection. Another interesting feature of the sort of activity seen in Plates 7.1 and 7.2, is the ratio of the horizontal dimensions of the regions with a strong refractive index gradient to their vertical dimensions. This ratio was found to be between 6.5 and 7 and is in agreement with observations from the real atmosphere carried out by Fitzjarrold[155,156] by means of an acoustic sounder detecting thermal cells under slightly unstable conditions.

The replacement of these organized structures by a spatially and temporally random distribution of refractive index gradient, seen in Plates 7.3 and 7.4, when the ground plane temperature is increased, points towards a transition from organized convection to random "thermal turbulence". Batchelor[29] suggests that such a transition is expected when the Rayleigh number exceeds a value around 50000, i.e. when the vertical temperature gradient exceeds a certain critical value.

7.1.3 Study of the Velocity Field in the Model Propagation Medium

The effect of the mean surface wind upon the fading spectrum of the received signal was the subject of extensive investigation in the case of the full-scale ("prototype") transhorizon radio-link (Section 5.3).

The range of wind speeds considered in the prototype radio-link investigation were measured at Meteorological Office stations at a height of 10 m above the ground. Since

this height corresponds to approximately 20 μ in the model, there are very considerable difficulties in determining stream velocities at such a distance from a boundary, even with the aid of a very sensitive hot-wire anemometer. First, this distance is difficult to measure and second, the extremely low wind speeds at such a distance from the plate could not be accurately measured by the hot-wire anemometer, since the presence of temperature fluctuations due to the ground heating would seriously affect any measurements of stream velocity in this region.

To overcome these difficulties, the following method of measurement was adopted:-

1. The air velocity was measured by means of the hot-wire anemometer at different heights above the ground plane in the range from 2.5 cm to 0.5 mm for various free-stream velocities with the ground plane at ambient temperature.

2. From these measurements, the velocity profiles were deduced for the specific free-stream velocities and for heights from 2.5 cm to 0.5 mm above the unheated plate.

3. An analytic expression for the vertical distribution of wind velocity was found, which would fit the experimentally deduced wind profiles. From this expression, the wind velocity at a height of 20 μ

above the plate could be found by extrapolation. The only parameter of this analytic expression was the free-stream velocity.

4. Free-stream velocities during the simulation experiments were not measured above the heated plate but at a certain distance upwind and above the wooden floor of the wind tunnel. This region of the working part of the tunnel was free of temperature fluctuations.

Preliminary vertical "soundings" of the propagation medium above the plate had revealed the presence of a boundary layer for free stream velocities in the range of 20 - 50 cm/sec. This boundary layer appeared to be "weakly" turbulent as it can be seen from the wind profiles in Figs. 7.5a and b which are of qualitative interest only. For the

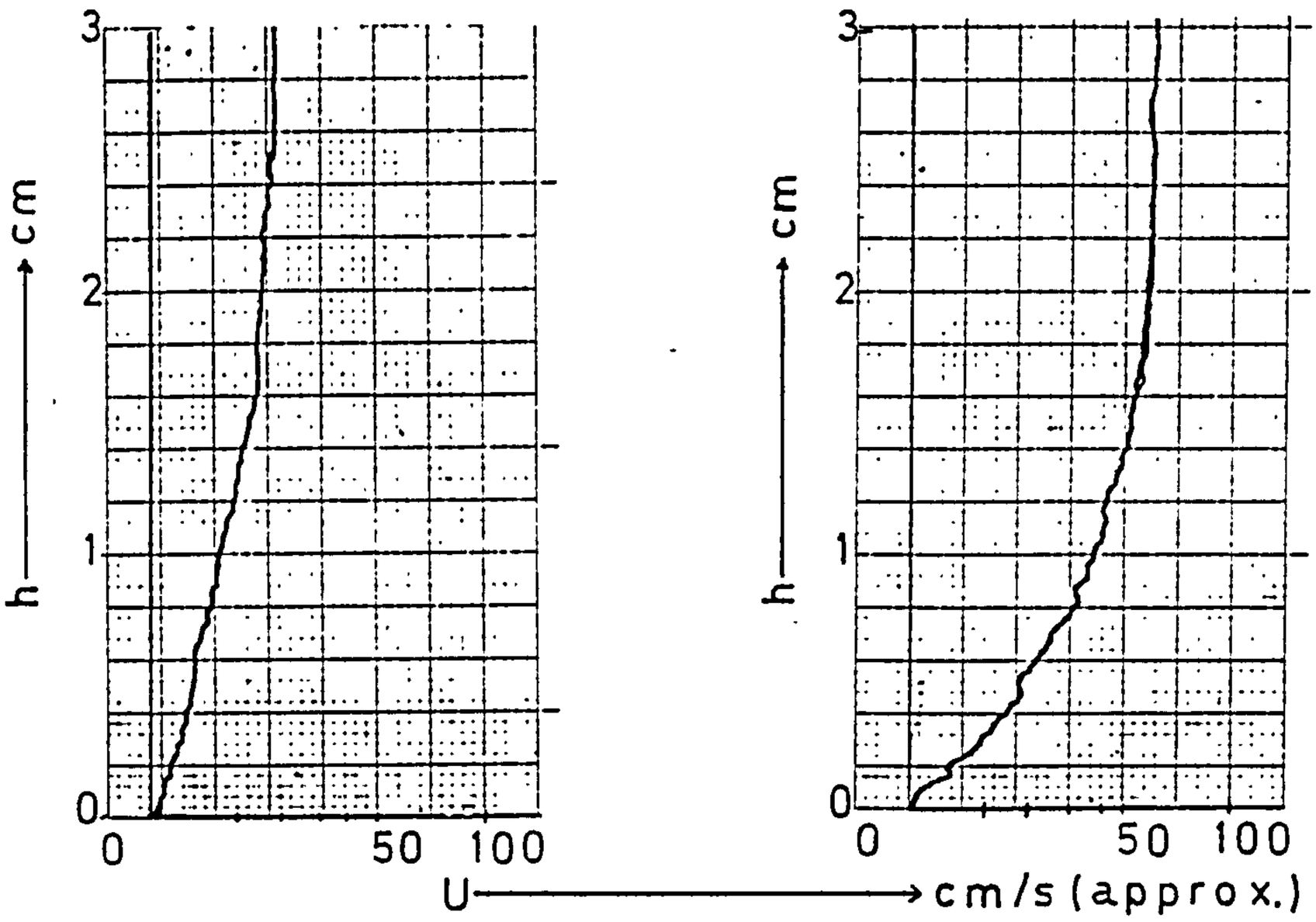

Figure 7.5

quantitative determination of the vertical wind velocity distribution the hot-wire probe was placed at different heights above the cold plate and the mean value of wind speed was measured at this height for different free-stream velocities by means of an rms voltmeter and the calibration curve of Fig. 6.8. An rms instrument was chosen because it would tend to "smooth-out" fluctuations and give a more accurate measure of the mean speed of air. The vertical distribution of wind velocity measured in this way is shown in Figs. 7.6a, b, c and d and Figs. 7.7a and b for different free-stream velocities. The presence of a boundary layer is clearly shown and the depth δ of this layer, for which the mean velocity starts dropping below its free-stream value, could be graphically determined.

The development of a natural boundary layer above a flat plate placed in an air stream at zero incidence has been throughly investigated by fluid mechanicists. It has been found[153] that the thickness δ of the boundary layer is inversely proportional to the square root of the Reynolds number of the free-stream flow, i.e.:-

$$\delta \sim \frac{1}{\sqrt{Re}} = \frac{1}{\sqrt{\frac{U_\infty \cdot x}{\nu}}} \qquad (7.1.3a)$$

where U_∞ is the free-stream velocity, ν is the kinematic viscosity ($\simeq$ 0.15 stokes for air at a temperature of 20^{o}C and a pressure of 1 atm.) and x is the distance of the point of measurement from the "leading edge" of the flat plate. In

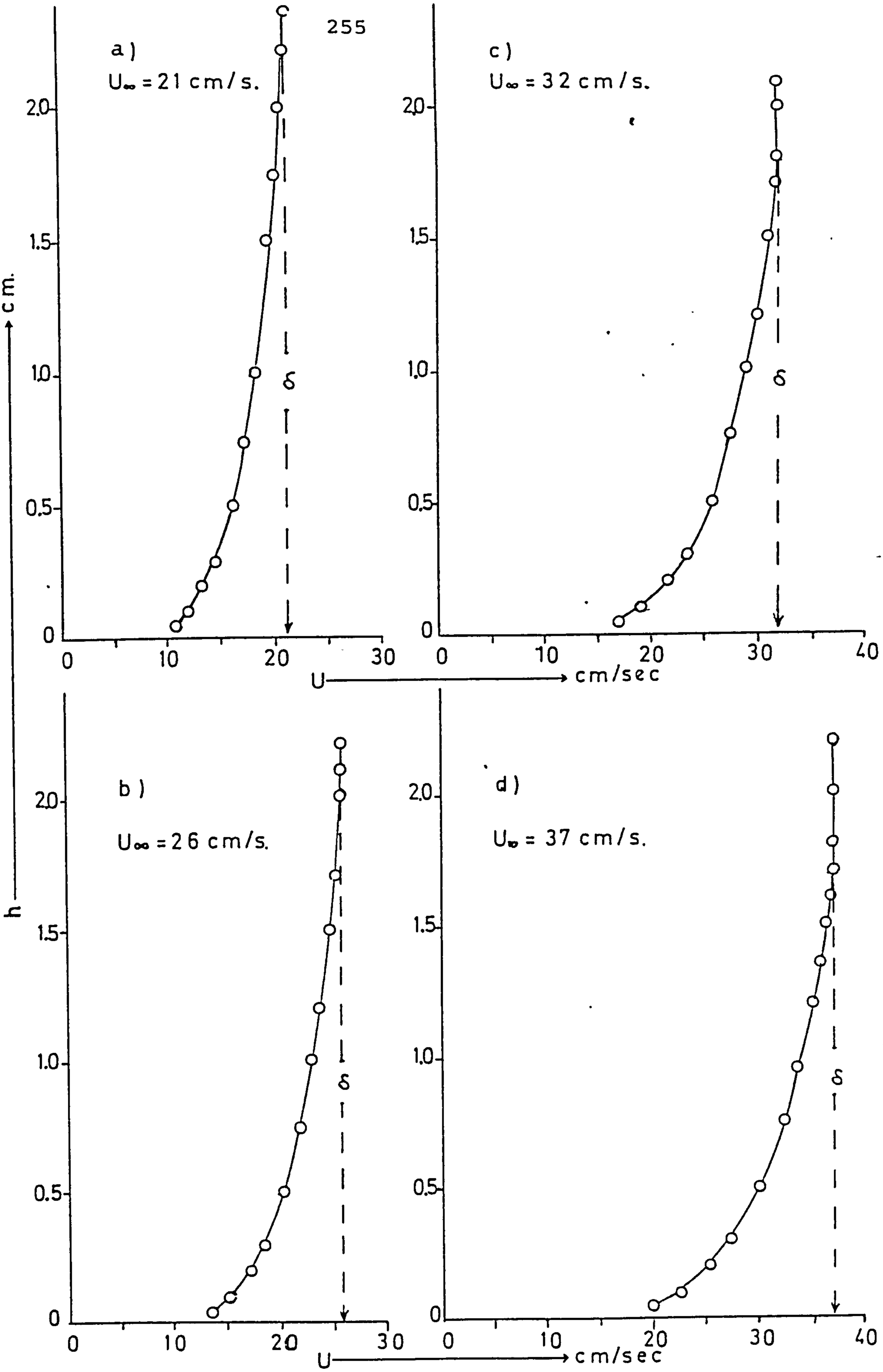

FIGURE 7.6: Velocity profiles above the Model ground-plane for various free-stream velocities.

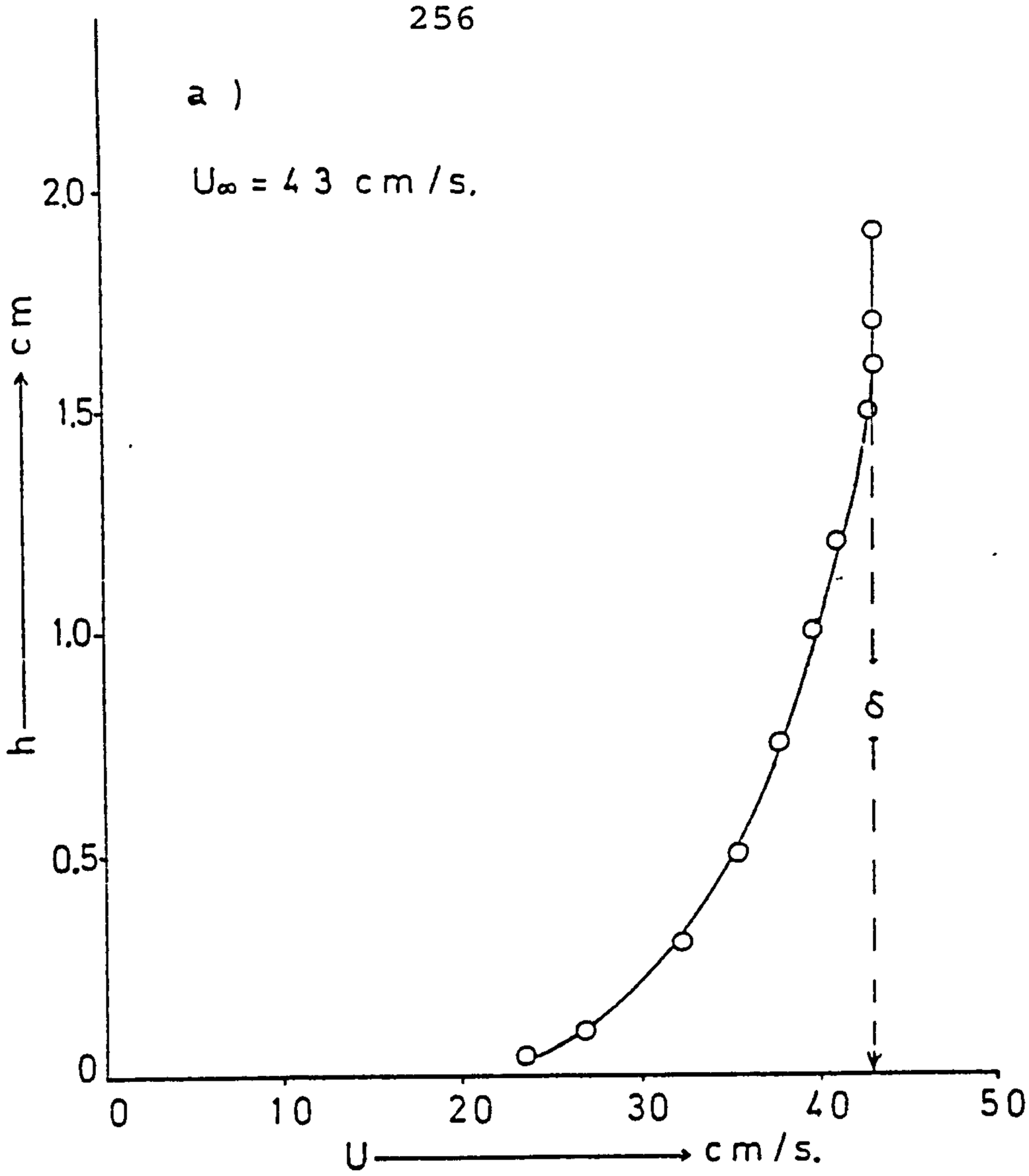

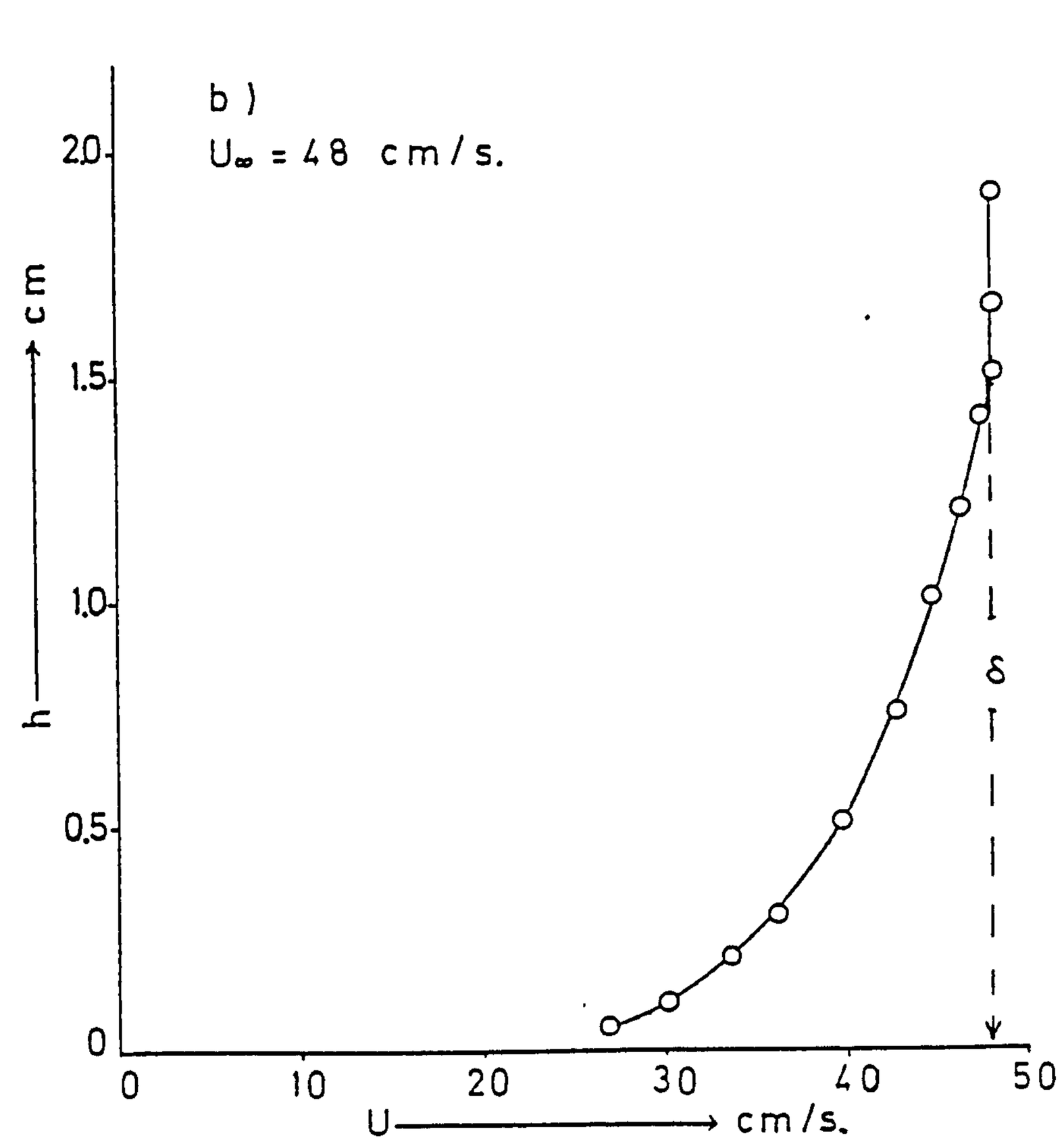

FIGURE 7.7: Velocity profiles above the Model ground-plane for various free-stream velocities.

this case the leading edge was at the entry of the working section of the tunnel, where a very shallow escarpment had been deliberately created at joining the floor of the working section with the contractor of the tunnel.

The distance x between this "leading edge" of the floor and the middle of the aluminium plate was 40 cm. From Figs. 7.6 and 7.7 it can be seen that for the free-stream velocities involved, the measured boundary layer thicknesses δ^* satisfied the condition (7.1.3a) quite accurately (the actual values are listed in Table 7.1).

In determining an analytical expression for the vertical distribution of velocity above a plate, Schlichting in[153] concludes that for the case of a fully developed turbulent boundary layer above a flat plate at zero incidence, the vertical distribution of velocity can be given by the general expression:-

$$\frac{U}{U_\infty} = \left(\frac{h}{\delta}\right)^{1/n} \qquad (7.1.3b)$$

where h is the height above the plate, U_∞ is the free-stream velocity and U the mean horizontal velocity in the direction of the flow at the height h. He suggests that $n = 7$ for $Re > 5 \times 10^5$. This is for the ideal case of a flat plate in a flow with a laminar approach and practically no upper boundary (wind tunnel producing 100% laminar flow and a ceiling very far from the floor). In the present investigation the ceiling of the working section was only 8 cm above the floor. From this point of view the flow was

rather similar to a flow in a smooth pipe with a rectangular cross-section. The values of Re were in the range of 5.6×10^3 to 1.3×10^4 for the free-stream velocities involved. Schlichting[153], referring to experimental work carried out by Nicuradse[157], mentions that velocity profiles in smooth pipes of various cross-sections were found to obey the law given by (7.1.3b) with the exponent n varying from n = 6, for $Re = 4 \times 10^3$, to n = 10 for $Re = 3.2 \times 10^6$. This indicated that a similar law could possibly express analytically the velocity profiles shown in Figs. 7.6 and 7.7.

To verify this assumption values of U_m/U_∞ were plotted against the corresponding values of h/δ, with both axes logarithmic, for all the cases shown in Figs. 7.6 and 7.7. In this manner, the exponent n could be derived from the slope of the graph (U_m/U_∞) vs (h/δ). As it can be easily shown from the expression (7.1.3b):-

$$\left(\frac{U_m}{U_\infty}\right) = \left(\frac{h}{\delta}\right)^{1/n} \rightarrow \frac{1}{n} = \log\left(\frac{U_m}{U_\infty}\right) \,/\, \log\left(\frac{h}{\delta}\right) \qquad (7.1.3c)$$

Such a graph is shown in Fig. 7.8 and the linearity between the quantities $\log(U_m/U_\infty)$ and $\log(h/\delta)$ can be clearly seen. From this graph and the expression (7.1.3c) the value of n was found to be n = 5.8, a value close to the value 6 suggested by Nicuradse[157] for $Re \simeq 10^4$.

Thus, the final analytical expression, describing the velocity profiles in the propagation medium, was found to be:-

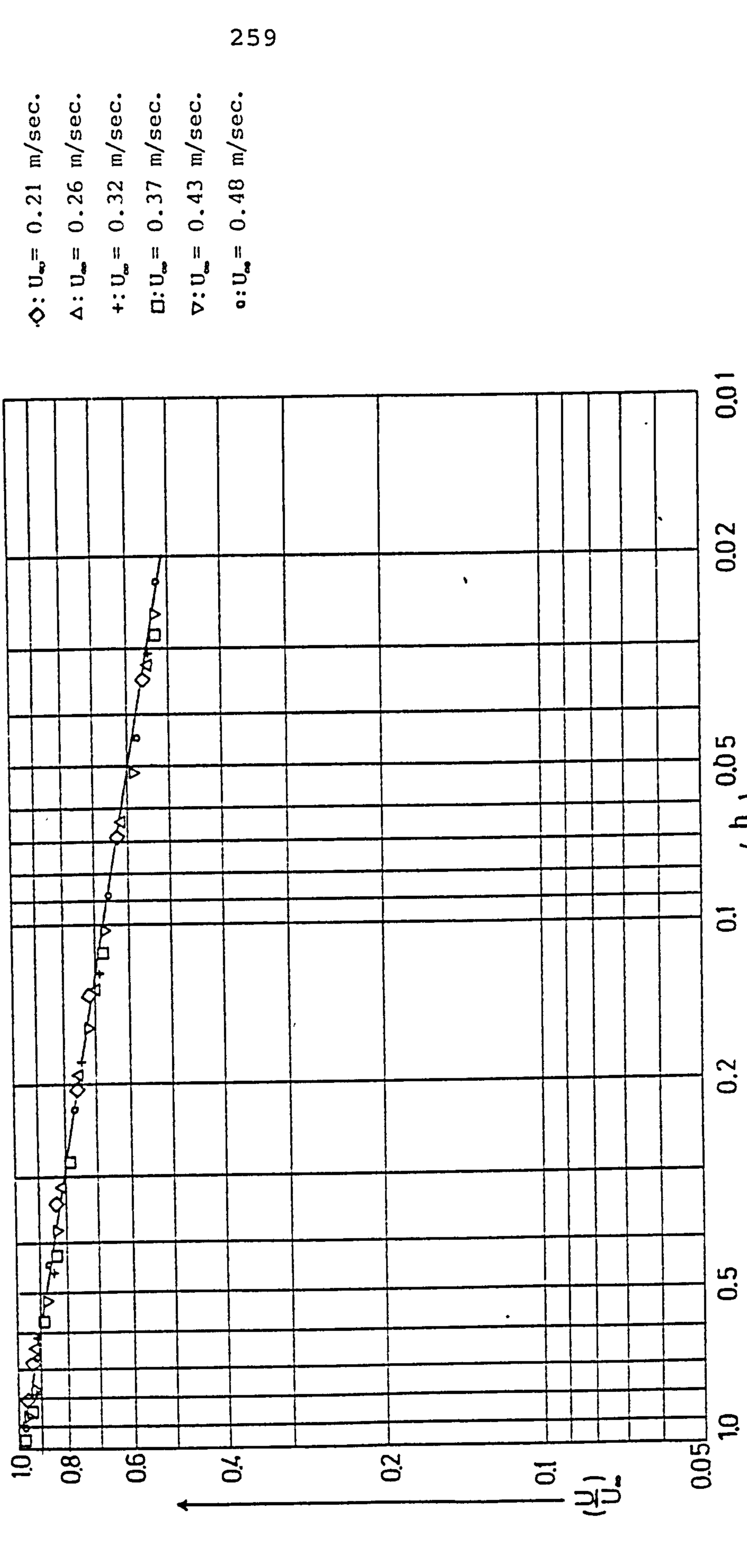

FIGURE 7.8: Graph for the determination of the exponent 1/n in the expression (7.1.3 b).

$$\frac{U_m}{U_\infty} = \left(\frac{h}{\delta}\right)^{1/5.8} \qquad (7.1.3d)$$

From this expression and for the values of δ found experimentally from the graphs in Figs. 7.6 and 7.7, the values of U_m at a height of h = 20 μ were found by extrapolation to be as in Table 7.1.

TABLE 7.1

δ (cm) (measured)	U_∞ (cm/sec) (measured)	U_m (cm/sec) (extrapolated)
2.23	21	6.2
1.98	26	7.9
1.78	32	9.9
1.63	37	11.6
1.56	43	13.6
1.47	48	15.4

7.2 Qualitative Simulation of the Two Types of Fading

The fast records (3.5 mins length) received on the prototype radio-link were characterized by two distinct types of fading. These types of fading were classified into "α-type" and "β-type" and were referred to as such throughout Chapter 5. Their special characteristics, the conditions under which they occur and the propagation mechanisms with which they have been associated, have been discussed in Subsection 5.2.1.

Since a very large proportion of the fading characteristics from the prototype radio-link could be classified into these two categories, the laboratory simulation was initially directed towards reproducing these particular types of fading.

7.2.1 Experimental Results

The "α-type" of fading was found to be favoured by "windy" conditions and nearly neutral or negative static stability of the atmosphere (large temperature lapse rates). This suggested that similar conditions should be simulated in the model propagation medium. The model ground plane was, therefore, heated to a temperature of 80^{o}C (the ambient temperature was 23^{o}C), so that high temperature gradients would be established immediately above the ground plane. Then, air streams of U_{∞} = 0.3, 0.4, 0.5 and 0.6 m/sec were established in the wind tunnel and the received signal was recorded on paper tape for 3.5 mins in each case. The records were submitted to the CDC 6400 computer and processed by the programme DATTAP (see Appendix III) giving the received signal vs time record in normalized axis. The four records were visually inspected on a VIDEO terminal and it was found that the fading in all of them had qualitative similarities with the fading of the "α-type" received on the prototype radio-link. A hard-copy of one of them, plotted by the KINGMATIC system, is shown in Fig. 7.9a and can be compared with a similar record from the prototype radio-link (Fig. 7.9b). The conditions under which the two signals have been received are also shown in Fig. 7.9. The temperature

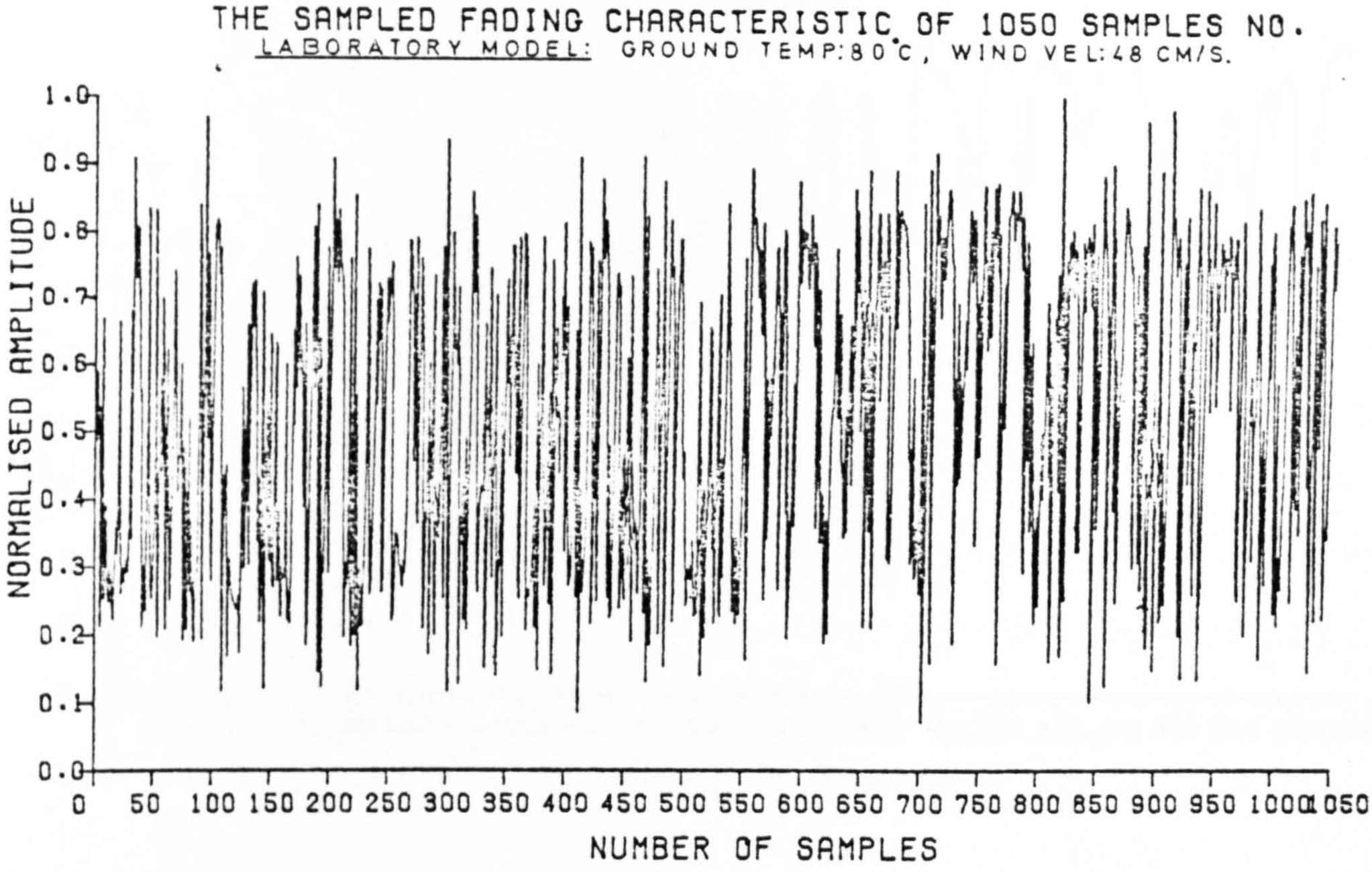

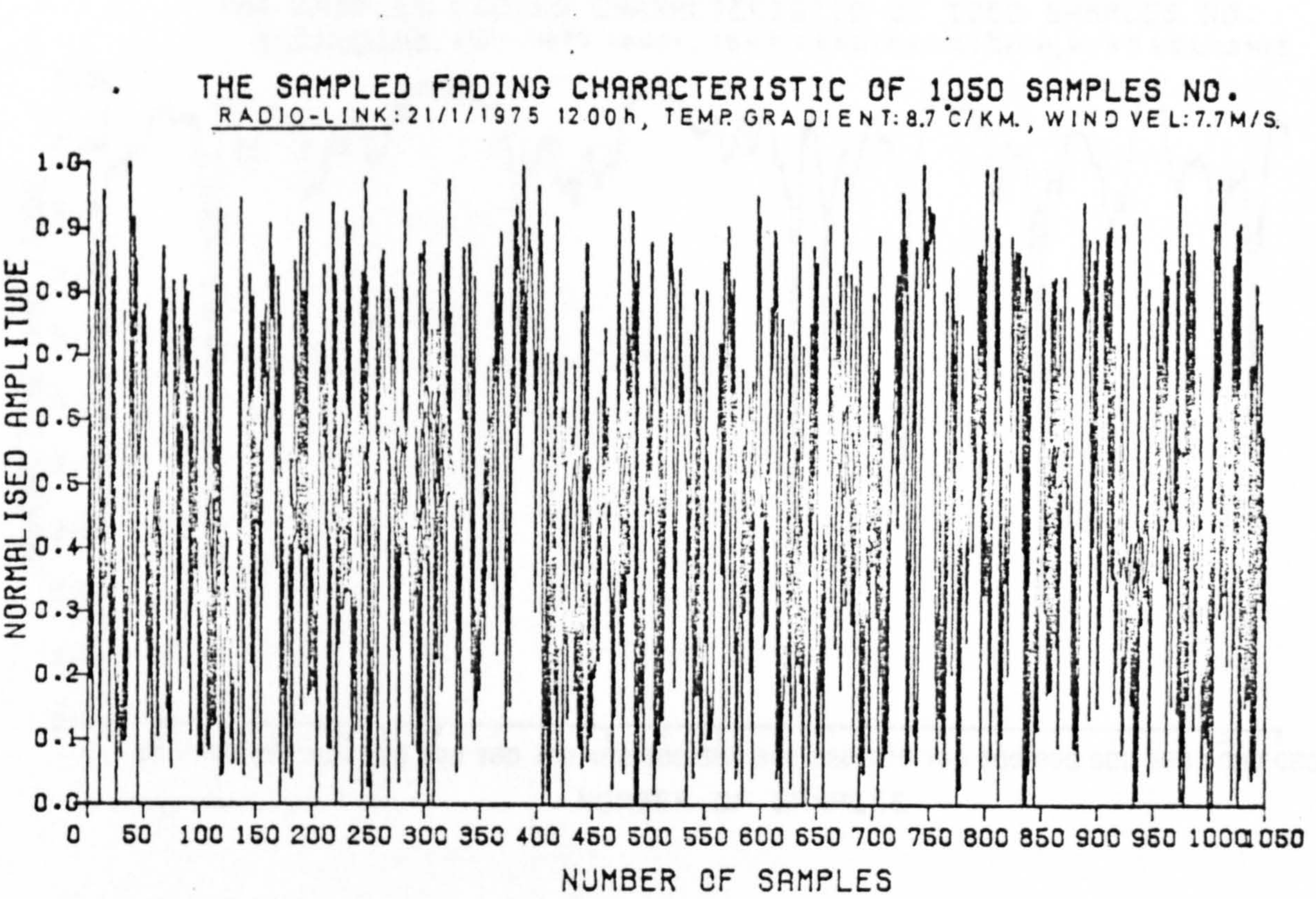

FIGURE 7.9: An example from the qualitative simulation of the "α-type" of fading in the Laboratory. (Record length: 3.5 mins.)

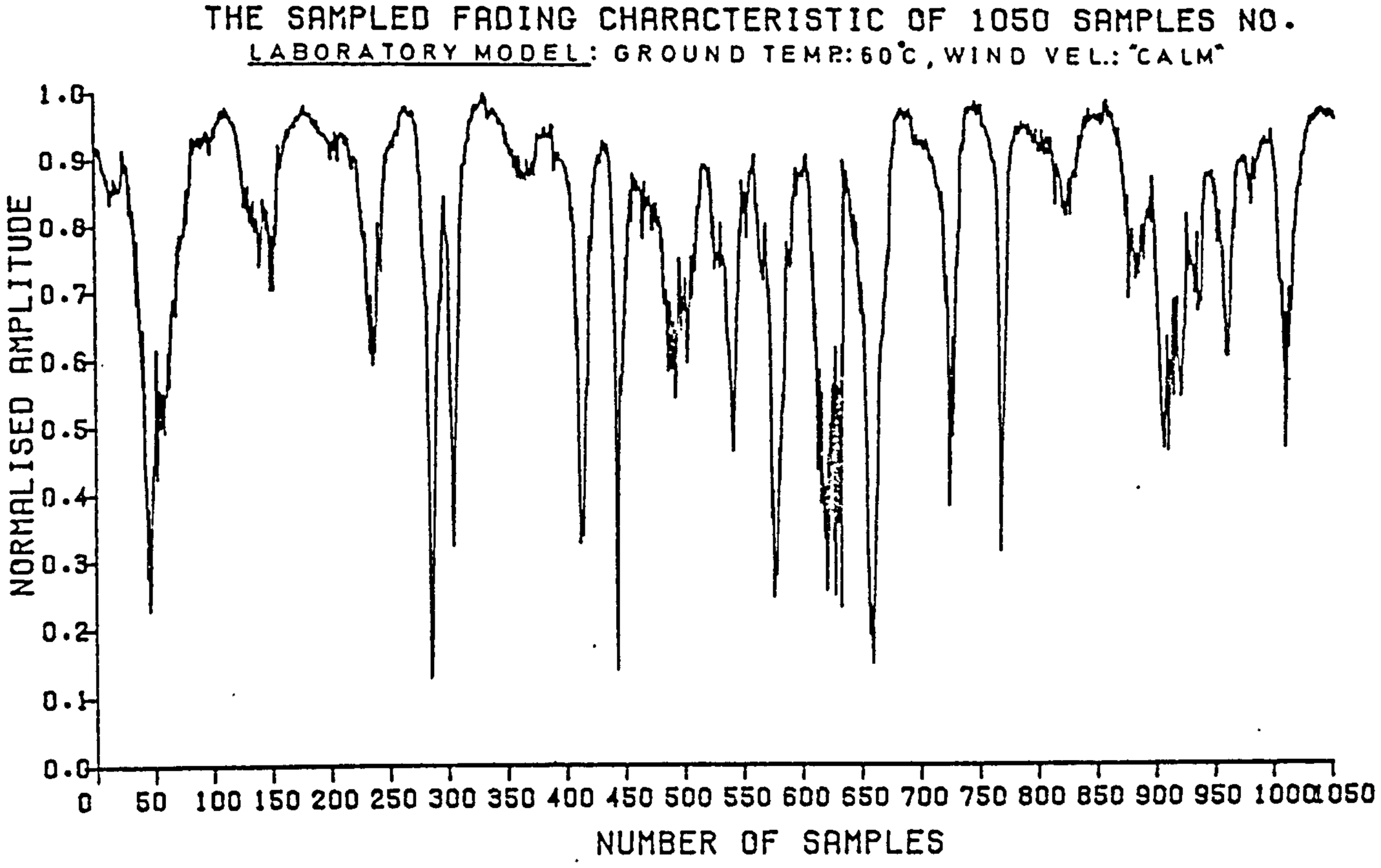

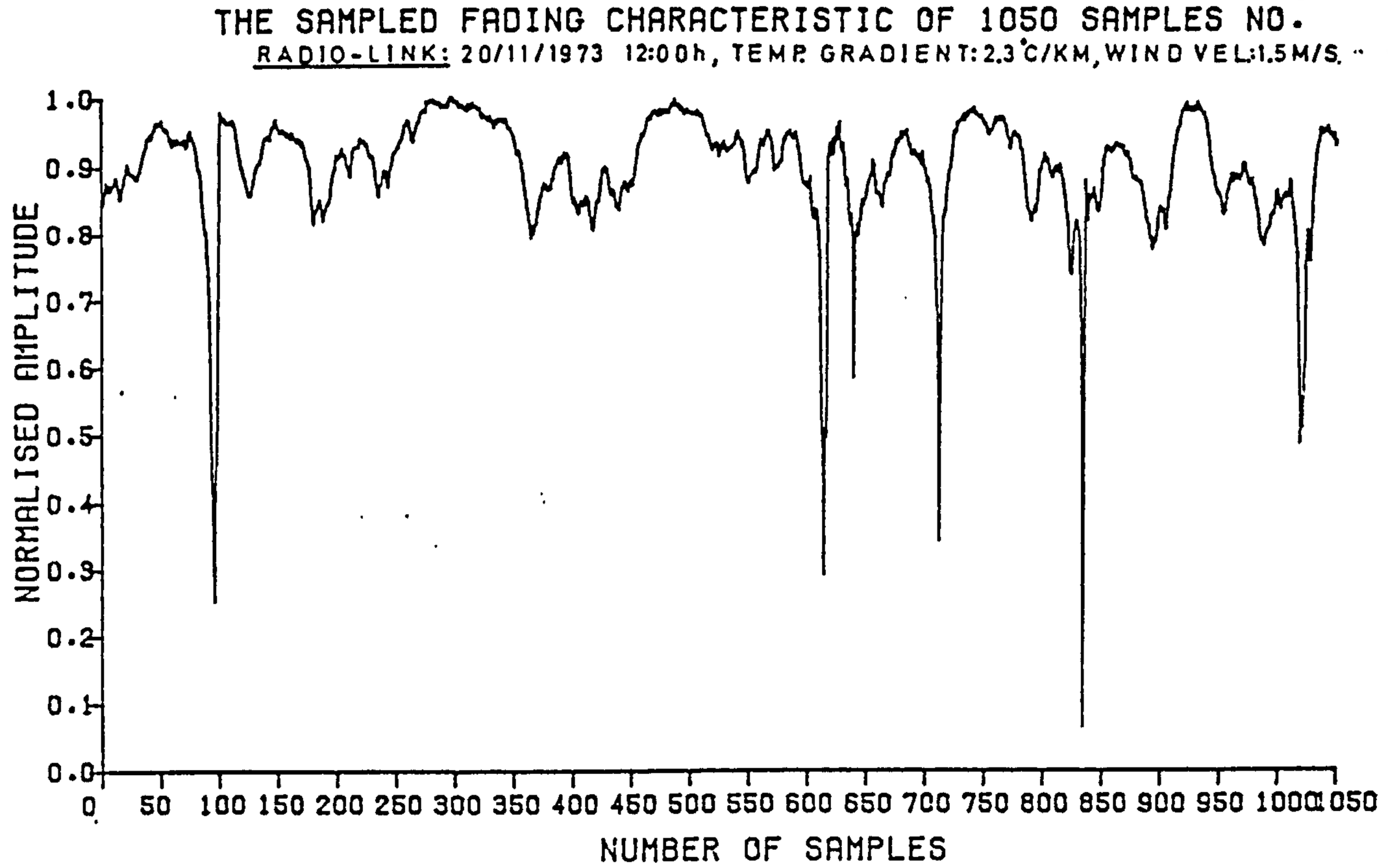

FIGURE 7.10: An example from the qualitative simulation of the "β-type" of fading in the Laboratory. (Record length: 3.5 mins.)

and refractive index profiles for this particular record are similar to those shown in Fig. 7.4 and have been already discussed in Subsection 7.1.1.

The "β-type" of fading had been recorded on the radio-link under conditions of light surface wind and high static stability (small temperature lapse rates). To simulate these conditions in the model, no air flow was established in the propagation medium and the ground was heated at a temperature of 60°C. The temperature and refractive index profiles under such conditions have been shown in Fig. 7.1 and discussed in Subsection 7.1.1.

Fig. 7.10a shows an example of the received signal recorded under these conditions and Fig. 7.10b shows a typical record of "β-type" of fading received on the proto-type radio-link. The qualitative similarities between the two are obvious, although the record from the laboratory model exhibits a slightly faster fading. Also, localized periods of very fast fading are present probably due to dust particles crossing the light beam or to vibrations of the building.

A possible explanation of the propagation mechanisms responsible for the two types of fading in the model, will be discussed in the following subsection.

7.2.2 Discussion

The conditions under which the "α-type" of fading was recorded in the model were already discussed in Subsection 7.1.1. The profiles of temperature and refractive index were also shown in Figs. 7.4b and c. It had been observed that a

strong positive refractive index gradient was present in the lowest region of the medium which was rather homogeneous (a few weak T-pulsations). Above that region an additional region of intense thermal turbulence existed with very strong negative and positive refractive index gradients present.

A schematic representation of a possible propagation mechanism in this case is shown in Fig. 7.11a. Under the influence of the strong positive refractive index gradient a ray transmitted from T in a direction parallel to the ground, will curve upwards with a radius of curvature: $\frac{1}{R} = -\frac{dn}{dz}$ (see Section 2.1). This ray may well miss the receiving point R, and if this case represents the lower boundary of the transmitted light beam, the whole of the beam could be assumed to miss the receiver R. However, the presence of small scale thermal turbulence above the region of high refractive index gradient may give rise to scattering towards the receiver R. The resultant constructive or destructive interference between the many scattered components will give rise to a rapidly fluctuating field at the point R, similar to that encountered in the "α-type" of fading.

The conditions favouring the "β-type" of fading in the model were also discussed in Subsection 7.1.1 with the corresponding T and N-profiles shown in Fig. 7.1. In this case, the region in the vicinity of the ground was characterized by a strong positive gradient of refractive index and, also, by "cold biased" temperature pulsations which, by means of the schlieren system and the electronic thermometer, were identified as "pockets" of cold air moving in the circulation near the ground plane. These cold air "pockets" are expected

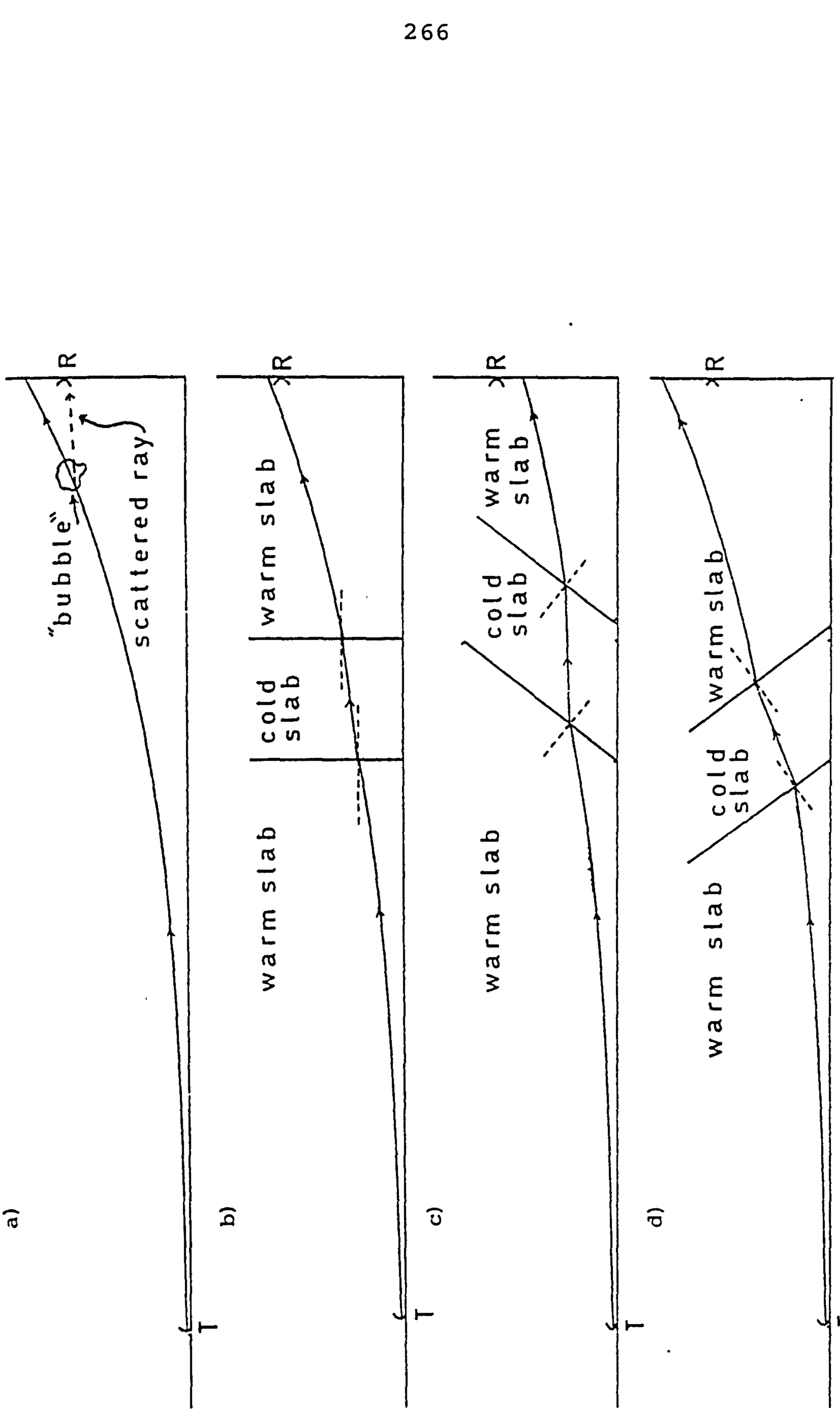

FIGURE 7.11: The path of a ray propagated in: (a) a medium with a positive refr. index gradient, (b) the same medium,having alternative "warm" and "cold" slabs, (c)&(d) when the "cold" slabs are slanting.

to have a higher refractive index than the adjacent regions of warm air and if they are represented as vertical "slabs" of cold air between "slabs" of warm air, the effect they would have upon a ray initially launched in a direction parallel to the ground is shown in Fig. 7.11b. It can be seen that the vertical distance between the receiving aperture (or aerial) R and the propagated ray is reduced compared with the case shown in Fig. 7.11a where no such "cold slabs" are present. However, the cold air pockets shown in Plates 7.1 and 7.2 appear to be slanting with respect to the ground plane. If this is taken into account, then the situation may be modified into that shown in Fig. 7.11c and/or Fig. 7.11d. In the former case the "cold air slab" is bent towards the receiver R and the same ray is now incident upon the plane of reception below the receiving aperture R. If this ray represents the lower boundary of the transmitted beam, then the receiver R is "illuminated" by the beam. Conversely, if the "cold air slab" is bent towards the transmitter T (Fig. 7.11d), then the whole of the beam may miss the receiving aperture R.

Visual observation of these cold air pockets (or "slabs") by means of the schlieren interferometer revealed that their motion, bending and evolution was relatively slow but, nevertheless, random. In the light of this observation and based on the previous discussion, the slow "β-type" of fading can possibly be attributed to a "beam wandering" mechanism due to the combined action of successive "warm" and "cold" slabs having a high and a low refractive index gradient respectively.

7.3 Simulation of the Effect of the Surface Wind Upon the Fading Power Spectrum

In Subsection 5.2.2 the influence of the surface wind upon the fading spectrum of the received signal was investigated for the case of the prototype radio-link. It was concluded that an increasing surface wind is causing "spread" of the fading spectrum towards higher frequencies. This effect was found to be mainly due to the normal-to-the-path wind component, whereas the longitudinal component did not seem to affect the fading spectrum in any particular way.

Another effect, observed on the prototype radio-link and discussed in Subsection 5.2.4, is that the surface wind was found to affect only the spectrum of the "α-type" of fading, whereas the fading spectra of the "β-type" did not seem to be consistently affected.

Section 5.4 was dedicated to a more quantitative investigation of the effect of the normal-to-the-path component of the surface wind upon the power spectrum of the "α-type" of fading. It was finally concluded that the power spectral density function can be expressed analytically by an inverse power law of the form: $P(f) \sim f^{-n}$ and that n was dependent on the normal-to-the-path component of the surface wind. An empirical relationship of the form: $1/n = 0.366 + 0.131\ U_n$, where U_n is the normal-to-the-path wind component in knots, was found to describe adequately this dependence.

It was decided that this effect could be adequately simulated on the laboratory model after encouraging on-line observations had been made by means of the Real-Time Spectrum Analyzer (SAI-51). These observations had revealed that very

low free-stream velocities in the wind tunnel, in the range 0.2 - 0.5 m/sec, could result in fading power spectra similar to those received on the prototype radio-link. The experimental results of this simulation experiment will be given, together with a discussion on their similarity to the results obtained on the prototype radio-link, in the following section.

7.3.1 Experimental Results

The aim of this experiment was to reproduce fading power spectra on the laboratory model, which would be, as precisely as possible, similar to those obtained on the prototype radio-link under various surface winds. The only parameter to be changed in the model propagation medium should be the free-stream wind speed. The procedure followed for this purpose was the following.

1. A "gross" temperature gradient of $40^{o}C/cm$ was established in the propagation medium and was kept constant throughout the measurements.

2. The received light signal was processed on the real-time Spectrum Analyzer and the fading power spectrum, integrated over a period of 160 sec, was displayed on a cathode ray oscilloscope. A transparent overlay was placed on the oscilloscope screen on which a prototype "smooth" power spectrum was drawn. These "prototypes" were taken from Fig. 5.9, where power spectral density functions are shown, known to represent fading spectra received on the radio-link

under specific conditions of surface wind.

3. The free-stream wind velocity in the tunnel was varied until the integrated power spectrum on the oscilloscope screen was as similar as possible to the "prototype" one. Then, the received signal was recorded in digital form on paper tape for 3.5 mins and at the same time, the free-stream velocity in the wind tunnel was measured by the hot-wire anemometer. To increase the reliability of the results this procedure was repeated four times for each "prototype" power spectrum.

4. The four records were processed on a CDC 6400 computer unit with the programme DATPOW giving the normalized spectral estimates of each original time-series. These spectral estimates were further averaged in the frequency domain (see Subsection 4.2.2) so that finally 30 estimates from each record were available for plotting. Then, the four sets of estimates were fitted by a least-square polynomial of the 5th degree (subroutine E02ABF) to provide a curve representing all four power spectra. Finally, the four sets of spectral estimates together with the best-fitting curve were plotted on logarithmic scales by means of the subroutine LOGPLO.

5. The whole procedure was repeated for six different "prototype" power spectra, corresponding to normal-

to-the-path surface winds U_n of 16, 14, 12, 10, 8 and 6 knots.

For the simulation of the 6 knot case, the free-stream wind speed in the tunnel should be around 0.21 m/sec. As the readings of the hot-wire anemometer would become unreliable for lower wind speeds, it was decided that "prototype" cases corresponding to U_n < 6 knots should be excluded.

Each of Figs. 7.12 - 7.17 shows a computer plot of the results from the simulation of each "prototype" power spectrum. The spectral estimates of each of the four trials are shown together with the best-fitting curve which represents the average fading power spectrum. The free-stream wind speeds for each of the trials and their average can be also found on every plot. It can be seen that although the fitted least-square polynomials were of the 5th degree, allowing ample flexibility, the best-fitting curves on logarithmic axes are linear for most of the frequency range. This indicates that the fading power spectra can be analytically described by an inverse-power law of the form: $P(f) \sim f^{-n}$, as in the case of the prototype radio-link (see Subsection 5.4.2).

The effect of the free-stream wind speed U_∞ upon the spectral exponent n can be clearly seen in Fig. 7.18 where all the fading power spectra, as represented by the best-fitting curves, are plotted on the same graph with U_∞ as a parameter.

The spectral exponents n were easily estimated from

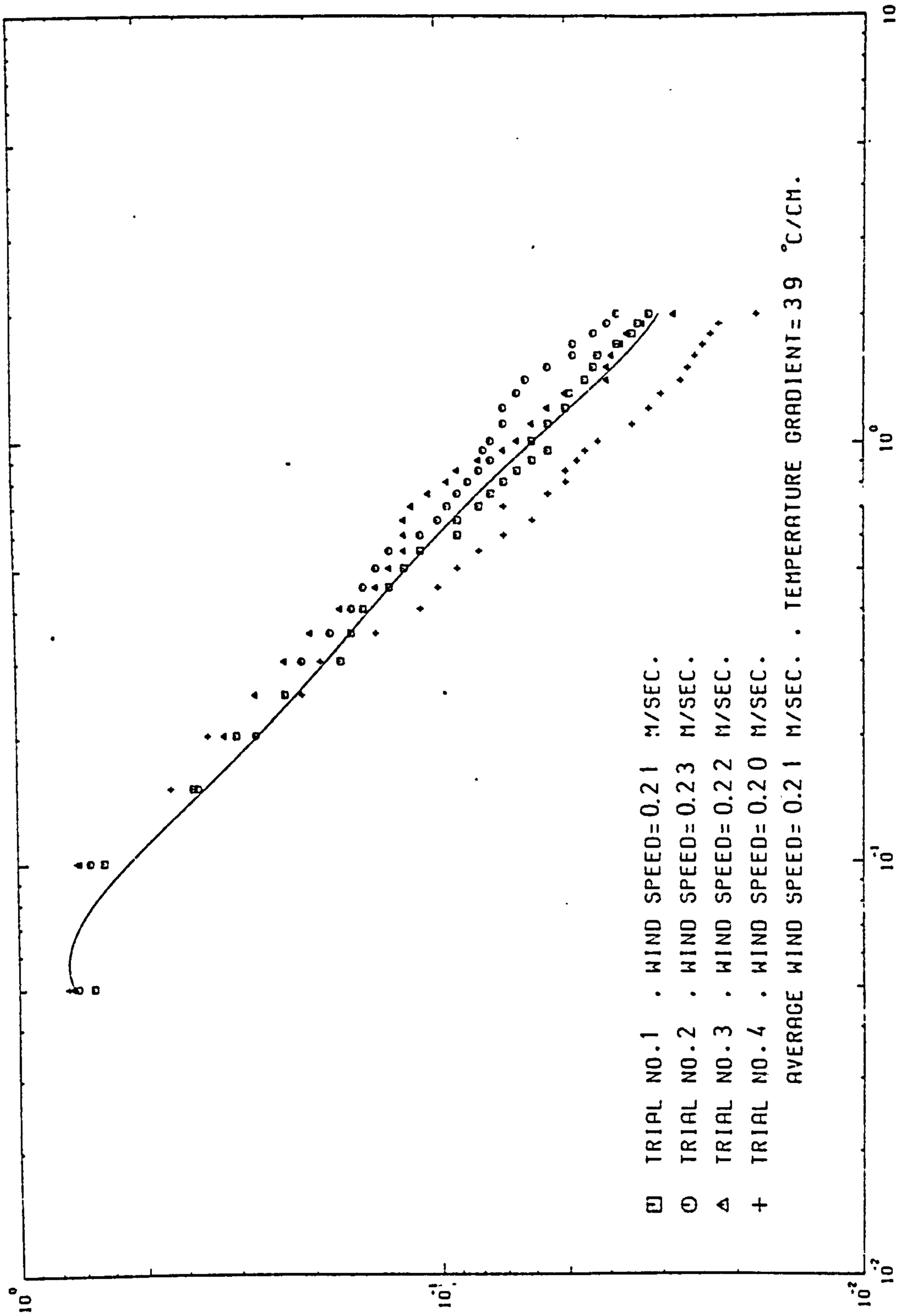
NORMALIZED POWER
FREQUENCY IN HZ.
TEMPERATURE GRADIENT=39 °C/CM.
TRIAL NO.1 . WIND SPEED=0.21 M/SEC.
TRIAL NO.2 . WIND SPEED=0.23 M/SEC.
TRIAL NO.3 . WIND SPEED=0.22 M/SEC.
TRIAL NO.4 . WIND SPEED=0.20 M/SEC.
AVERAGE WIND SPEED=0.21 M/SEC. . T

FIGURE 7.12

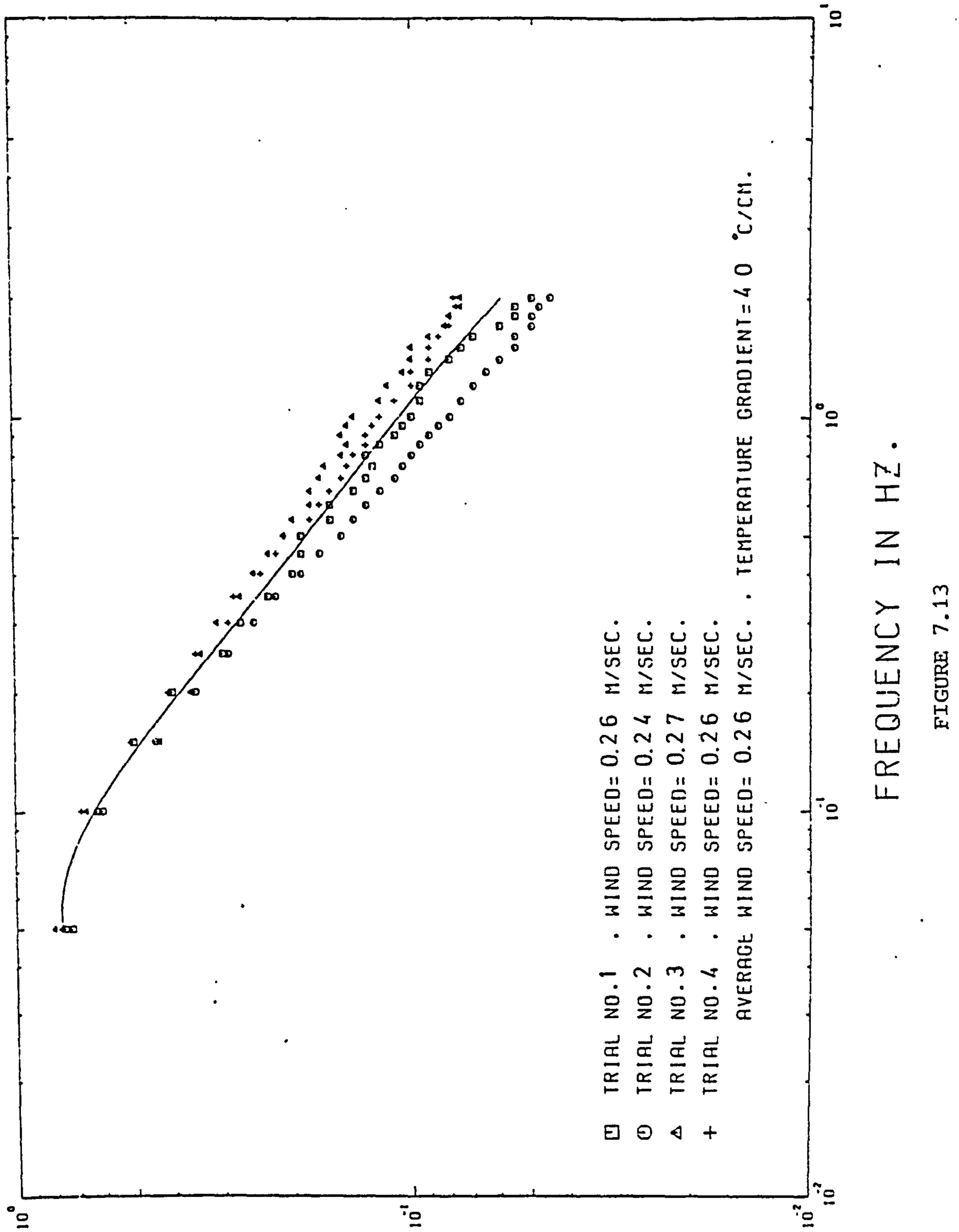
NORMALIZED POWER
FREQUENCY IN HZ.
TRIAL NO.1 . WIND SPEED= 0.26 M/SEC.
TRIAL NO.2 . WIND SPEED= 0.24 M/SEC.
TRIAL NO.3 . WIND SPEED= 0.27 M/SEC.
TRIAL NO.4 . WIND SPEED= 0.26 M/SEC.
AVERAGE WIND SPEED= 0.26 M/SEC. . TEMPERATURE GRADIENT=4.0 °C/CM.

FIGURE 7.13

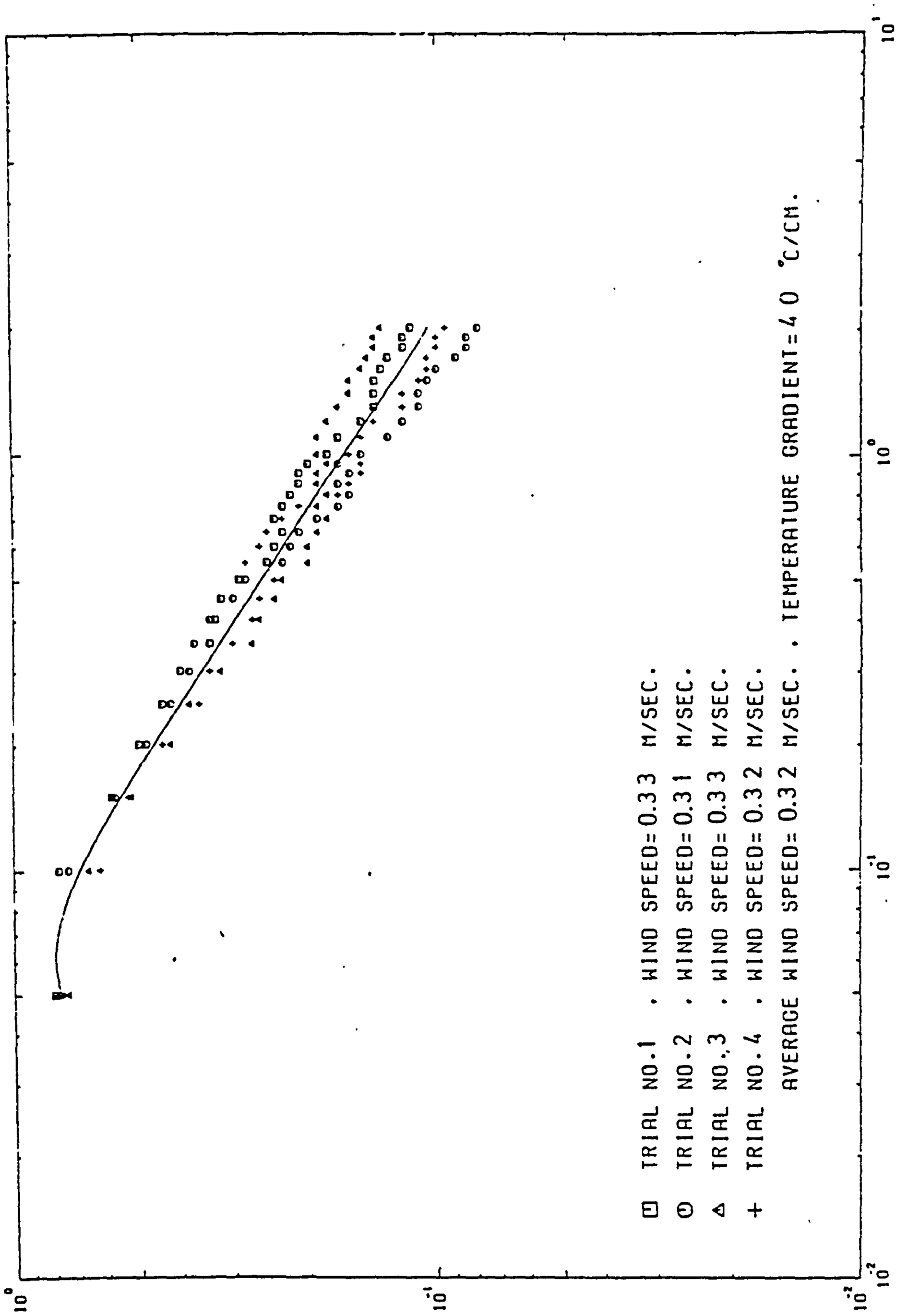
NORMALIZED POWER
FREQUENCY IN HZ.
TRIAL NO.1 . WIND SPEED= 0.33 M/SEC. . TEMPERATURE GRADIENT= 4.0 °C/CM.
TRIAL NO.2 . WIND SPEED= 0.31 M/SEC.
TRIAL NO.3 . WIND SPEED= 0.33 M/SEC.
TRIAL NO.4 . WIND SPEED= 0.32 M/SEC.
AVERAGE WIND SPEED= 0.32 M/SEC.

FIGURE 7.14

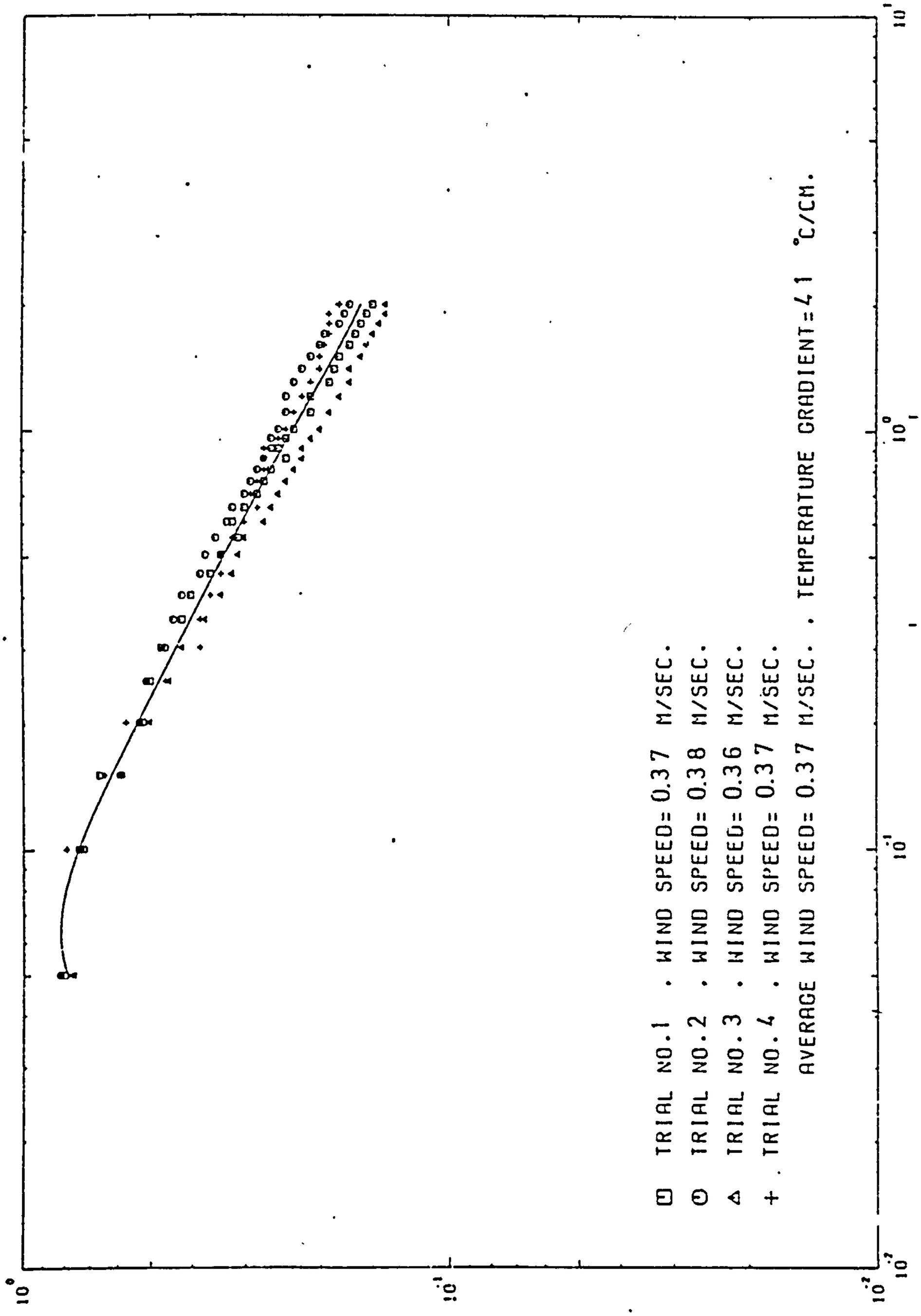
□ TRIAL NO.1 . WIND SPEED= 0.37 M/SEC.
○ TRIAL NO.2 . WIND SPEED= 0.38 M/SEC.
△ TRIAL NO.3 . WIND SPEED= 0.36 M/SEC.
+ TRIAL NO.4 . WIND SPEED= 0.37 M/SEC.
AVERAGE WIND SPEED= 0.37 M/SEC. . TEMPERATURE GRADIENT=41 °C/CM.
NORMALIZED POWER
FREQUENCY IN HZ.
10^0
10^-1
10^-2
10^1

FIGURE 7.15

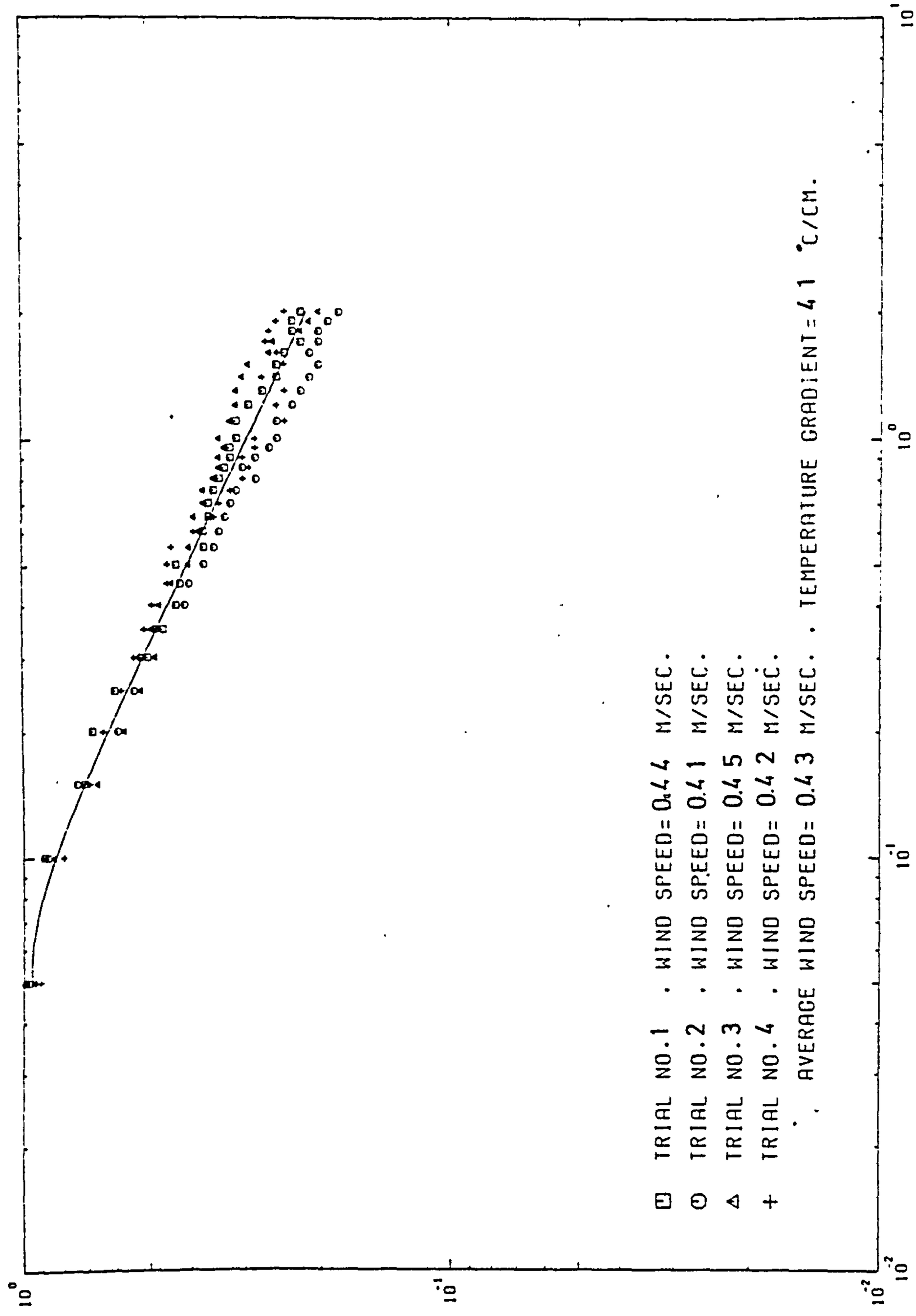
NORMALIZED POWER
FREQUENCY IN HZ.
□ TRIAL NO.1 . WIND SPEED= 0.44 M/SEC.
○ TRIAL NO.2 . WIND SPEED= 0.41 M/SEC.
△ TRIAL NO.3 . WIND SPEED= 0.45 M/SEC.
+ TRIAL NO.4 . WIND SPEED= 0.42 M/SEC.
AVERAGE WIND SPEED= 0.43 M/SEC.
. . . TEMPERATURE GRADIENT= 41 °C/CM.
10^0
10^-1
10^-2
10^1

FIGURE 7.16

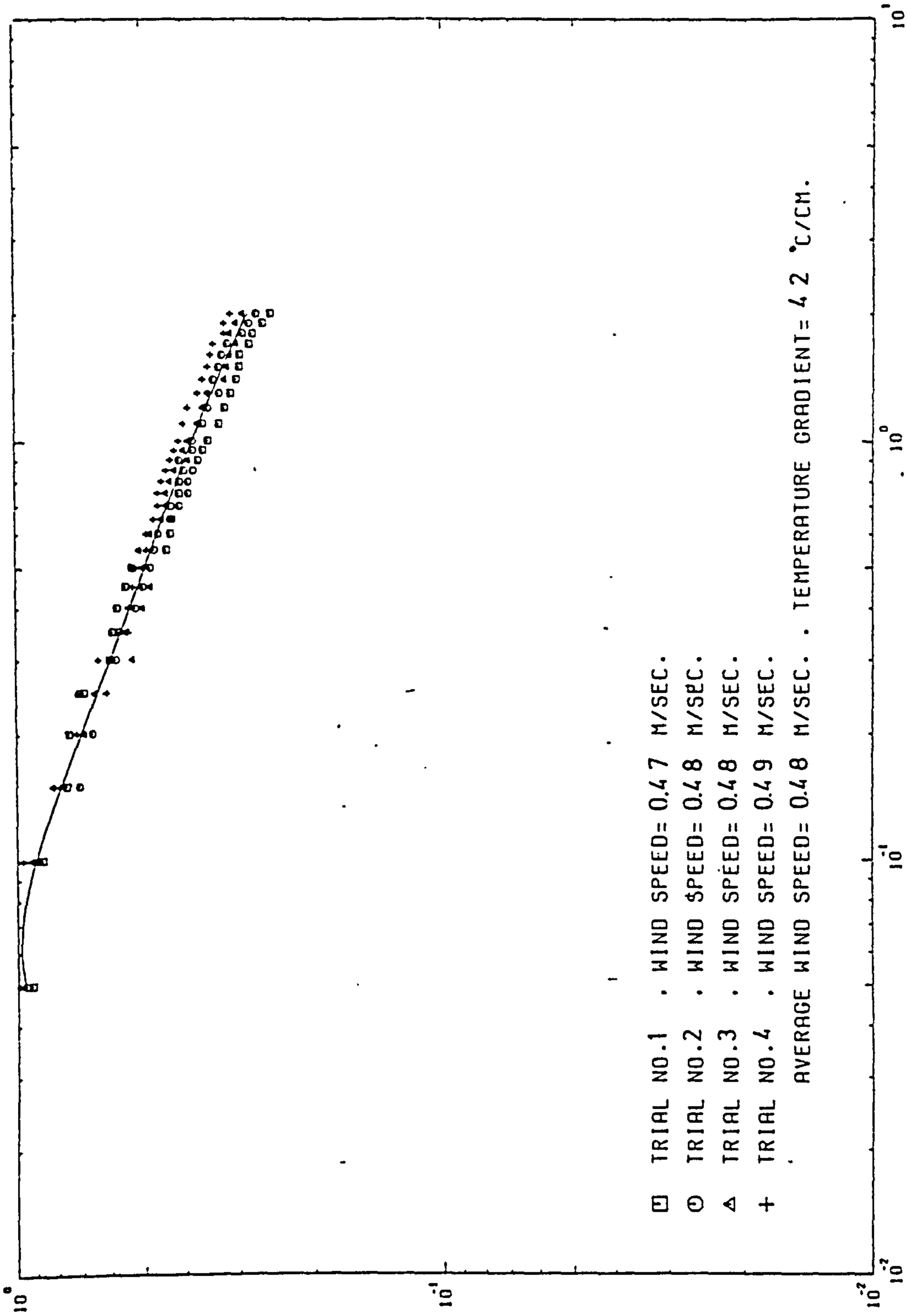
FREQUENCY IN HZ.
NORMALIZED POWER
TRIAL NO.1 . WIND SPEED= 0.47 M/SEC. . TEMPERATURE GRADIENT= 4.2 °C/CM.
TRIAL NO.2 . WIND SPEED= 0.48 M/SEC.
TRIAL NO.3 . WIND SPEED= 0.48 M/SEC.
TRIAL NO.4 . WIND SPEED= 0.49 M/SEC.
AVERAGE WIND SPEED= 0.48 M/SEC.

FIGURE 7.17

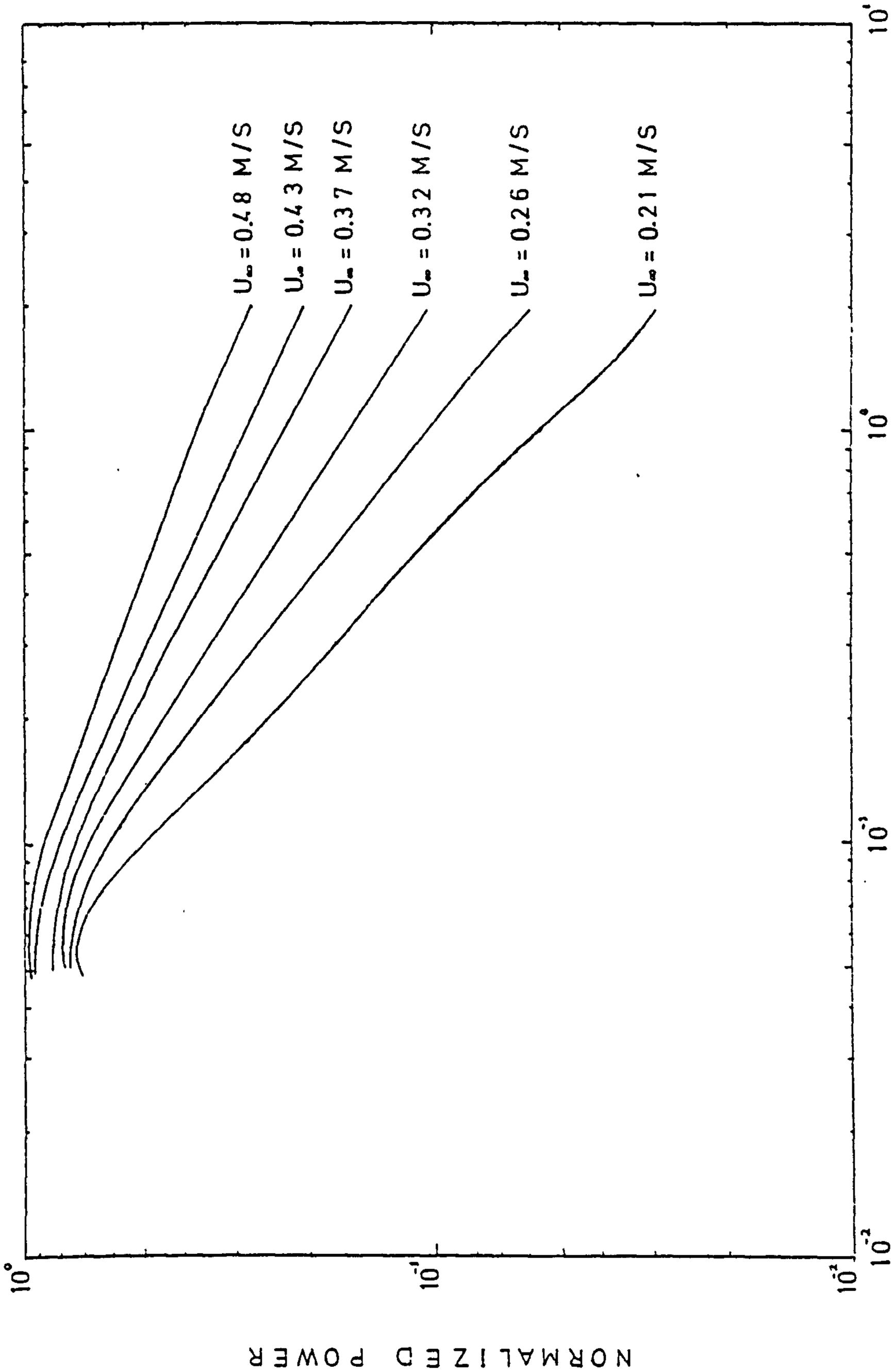

FIGURE 7.18: The effect of increasing U_∞ upon the logarithmic Power Spectra of the simulated "α-type" of fading.

the slope of the logarithmic spectra. Their values together with the corresponding free-stream velocities U_∞ are listed in Table 7.2.

TABLE 7.2

n	U_∞ (m/sec)
0.40	0.48
0.46	0.43
0.52	0.37
0.62	0.32
0.78	0.26
0.94	0.21

The similarity between these results and the results from the same investigation on the prototype radio-link will be discussed in the following subsection.

7.3.2 Discussion

The results from the laboratory simulation listed in Table 7.2 cannot be directly compared with the results from the prototype radio-link, listed in Table 5.8 for one main reason.

The normal-to-the-path wind speeds in the radio-link were surface values measured at a standard height of 10 m from the ground whereas, the wind speeds in Table 7.2 are free-stream wind speeds measured at a height of 3.5 cm above the model ground (a distance corresponding to stratospheric

altitudes in the real atmosphere).

However, the investigation of the velocity field in the laboratory model (see Subsection 7.1.3) made possible the estimation of the wind speed U_m at a scaled "standard anemometer height" of 20 μ above the model ground for the free-stream velocities involved in the simulation experiment (Table 7.1).

Table 7.3 contains the values of the spectral exponent n and the corresponding values of the normal-to-the-path wind speed U_n for the radio-link. It also contains the values of n from the simulation experiment and the corresponding wind speeds at the scaled "standard anemometer height".

TABLE 7.3

RADIO-LINK		LABORATORY MODEL		K_D
n	U_n (m/sec)	n	U_n (m/sec)	
0.392	8.2	0.400	0.154	53.2
0.459	7.2	0.462	0.136	52.8
0.513	6.2	0.520	0.116	53.5
0.614	5.1	0.620	0.099	52.6
0.786	4.1	0.781	0.079	52.0
0.876	3.1	0.938	0.062	50.1

It can be seen that the values of n obtained from the laboratory simulation are very close to the ones obtained from the radio-link. This was hardly surprising, as special care

had been taken so that the fading spectra from the model would be similar to those obtained from the prototype radio-link. Of special interest in Table 7.3 is the ratio $U_n : U_m \doteq K_D$ between the normal-to-the-path surface winds in the prototype and the respective values of wind speed at a height of 20 μ in the model. This ratio is almost constant with an average value of 52.4 and provides a "dynamic similarity" factor for the scaling of wind speeds in the laboratory model.

As already discussed in Subsection 6.4.2, a condition for dynamic similarity which results in model wind speeds much smaller than those in the prototype, is the equality of the Froude numbers in the model and in the prototype or, equivalently, the equality of "gross" Richardsons numbers. Both of these dimensionless numbers are used as dynamic similarity criteria in cases of flow in thermally stratified fluids where buoyancy effects are predominant[148,149,151].

Unfortunately, the records from the prototype radio-link had been collected under a variety of meteorological conditions for which data were somewhat restricted and did not permit a consistent estimation of Ri_g in the real atmosphere. Thus, a quantitative confirmation of the assumption that the equality of Ri_g was the criterion for dynamic similarity between model and prototype, was not possible. However, the obtained results indicate that a "buoyancy governed" model propagation medium can readily reproduce effects known to occur in the prototype radio-link.

7.4 Investigation of the Effect of Temperature Gradient Upon the Fading Power Spectrum

Measurements on the prototype radio-link had revealed (Section 5.3) that decreasing static stability, i.e. increasing temperature lapse rate, was causing an increase in the "spread" of the fading power spectrum towards higher frequencies. This effect had been better demonstrated after the available fading spectra had been divided into three categories according to the mean surface wind velocity prevailing at the time of the recordings. Thus, the fading spectra were classified into three groups corresponding to the three wind velocity ranges: 1 to 6 knots, 6 to 12 knots and 12 to 18 knots. This was considered an effective way of eliminating the effect of very diverse wind velocities without decreasing very much the number of available fading spectra in each group.

After this classification, simple correlation tests revealed a very significant negative correlation existing between spectrum "spread" and static stability parameter, for each group of measurements. A plausible explanation for this effect had been given in Section 5.3 but it was thought that the investigation of the effect by means of the laboratory model would contribute to its better understanding.

7.4.1 Experimental Results

For the experimental investigation of the effect of the temperature gradient upon the fading spectrum the following procedure was used.

A constant free stream velocity of 0.26 m/sec was

established in the wind tunnel and three different temperature gradients of 20, 30 and 42°C/cm were created by heating the model ground at 50, 60 and 70°C respectively. The temperature gradients were estimates resulting from measurements of the ground temperature and the temperature at a height of 1 cm from the ground. The former were taken by means of the ETHER-TRANSITROL electronic thermostat-thermometer and the latter by means of the CORMACK electronic thermometer.

Under each of these conditions, the received light signal was recorded for 3.5 mins on paper tape and subsequently processed by computer (program DATPOW) for the estimation and plotting of the fading spectrum. The resulting three fading spectra are shown in Fig. 7.19 with the corresponding conditions of wind and temperature gradient indicated on the graph. It would appear that an increase in the temperature gradient, corresponding to a decrease in static stability, brings about an increase of the spectrum "spread" towards higher frequencies.

The same procedure was repeated for another free-stream velocity of 0.37 m/sec and for temperature gradients of 21, 30 and 40°C (almost the same as before). The resulting fading spectra are shown in Fig. 7.20. Again, the effect of increasing temperature gradient upon the fading spectrum is to cause a "spread" towards higher frequencies.

7.4.2 Discussion

From the results shown in Figs. 7.19 - 20, it becomes evident that the fading spectrum is not solely affected by the wind velocity in the propagation medium. Another

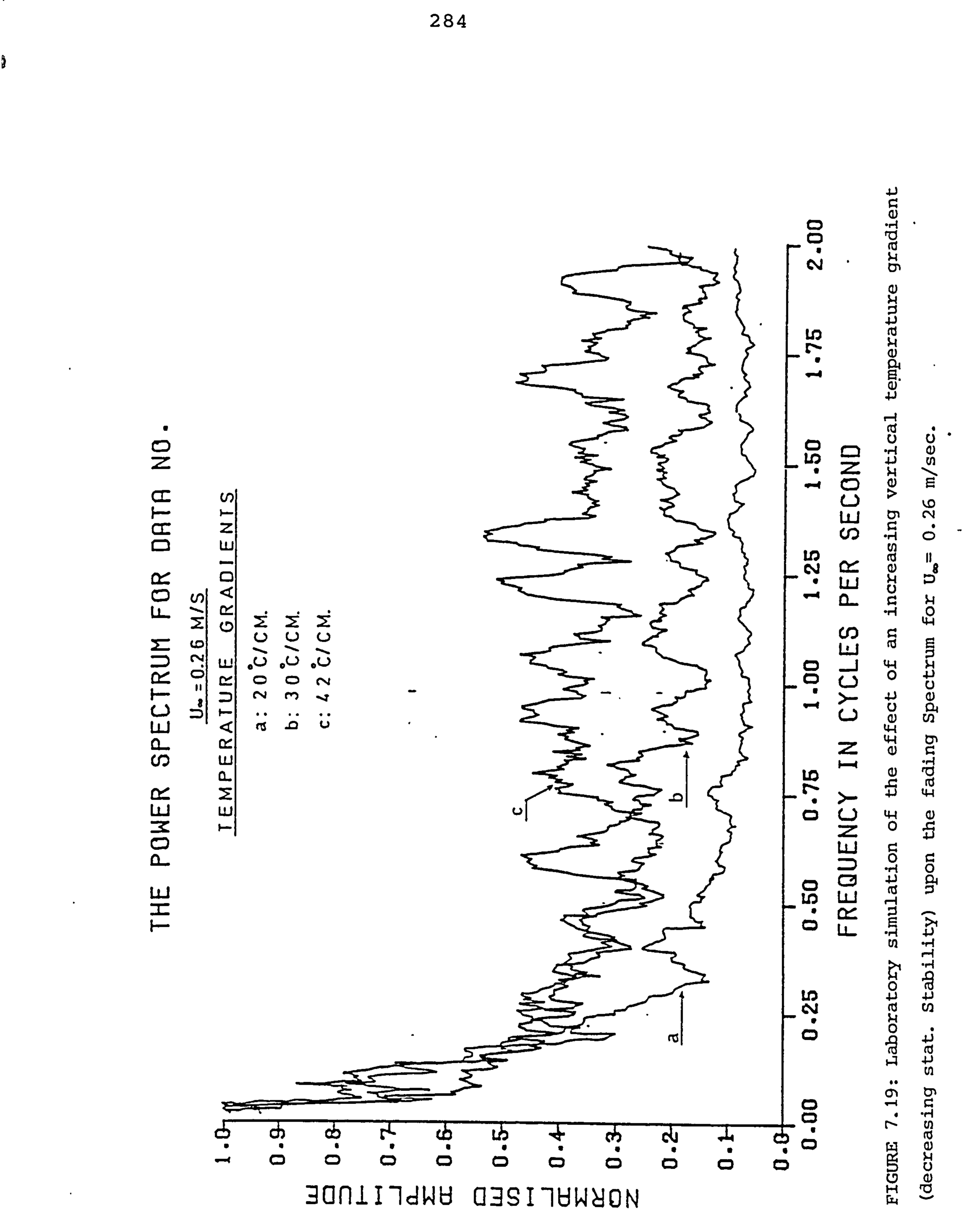

FIGURE 7.19: Laboratory simulation of the effect of an increasing vertical temperature gradient (decreasing stat. Stability) upon the fading Spectrum for U_∞= 0.26 m/sec.

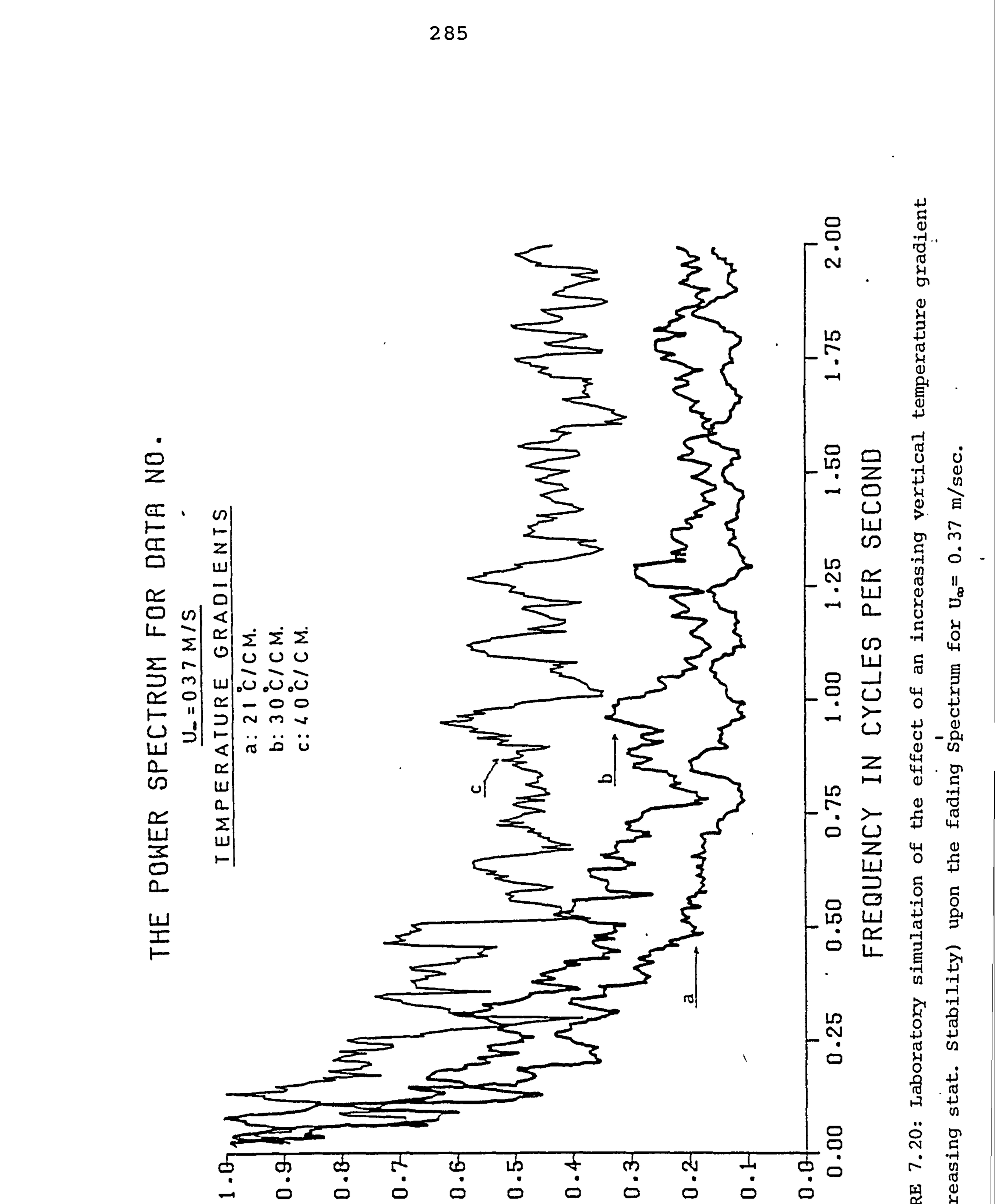

FIGURE 7.20: Laboratory simulation of the effect of an increasing vertical temperature gradient (decreasing stat. Stability) upon the fading Spectrum for U_∞= 0.37 m/sec.

parameter that can cause considerable "spread" of the spectrum towards higher frequencies is the vertical temperature gradient (or lapse rate). Thus, for the same wind velocity an increasing temperature gradient is causing more rapid fluctuations of the received light signal.

This effect had been also experienced on the prototype radio-link, where fading spectra received under the same or contiguous conditions of surface wind could differ considerably depending on the static stability (i.e. temperature lapse rate) at the time of recording. The tendency was for more rapid fading to occur under conditions of small positive or negative static stability, i.e. under strong lapse rate conditions. The effect had been interpreted in Section 5.3 as a result of the suppression of small scale scattering "blobs", contributing to fast fading, by a thermally stable atmosphere (weak lapse rates) and also by the interaction between mechanical and convective turbulence in the case of strong winds and strong lapse rates. In the latter case, due to the increased instability of the atmosphere, convective turbulence is added to the mechanical one and the production of small scale scattering "blobs" is enhanced, thus favouring the presence of fast-fading in the received signal.

In view of the observations of the propagation medium in the laboratory model, this interpretation seems to be correct. Indeed, conditions of strong wind and strong lapse rate simulated in the model (see Subsection 7.1.1) were found to favour the formation of intense small scale irregularities of refractive index in the propagation medium as it can be

seen from Fig. 7.4.

However, an increase of the temperature lapse rate has been found to cause some additional effects in the model propagation medium which could account for the "spread" of the fading spectrum towards higher frequencies. These effects might be summarized as follows.

An increase in ground heating temperature, not only increased the overall temperature lapse rate but also intensified all "local" temperature gradients and mainly that in the proximity of the model ground plane (conduction region). As a result, a light beam, launched from the vicinity of the ground plane, would tend to curve more upwards and away from the receiving aperture.

Under these conditions, the received field would be mainly due to "scattering" from the intense small scale refractive index inhomogeneities. This mechanism is obviously more prone to fast fading than a quasi-line-of-sight one.

This effect could well occur in the real atmosphere and would result in an "effective" decrease of the k-value ("effective" earth radius factor), as in sub-standard refractive conditions. Under such conditions, the main propagation mechanism is probably "scattering" with relatively large scattering angles. Thus, small inhomogeneities would contribute more to the received signal and rapid fading due to random interference would be favoured.

Another effect caused by strong temperature gradients in both the model propagation medium and in the real atmosphere, is the decrease of static stability. Under unstable conditions, scattering "blobs" of convective origin

would tend to rise much faster through the "common volume" under the influence of buoyancy forces. This, in fact, corresponds to an increase of the vertical component W of the velocity field in the propagation medium. Since W is a normal-to-the-propagation path wind component, it is expected to contribute to rapid fading according to the findings reported in Subsection 5.2.2 and Section 7.3.

A large increase in temperature gradient in the model propagation medium eventually leads to a replacement of any organized convective activity by random convective turbulence. In the case of organized convective activity persisting above the ground, the propagation mechanism could be the one described in Subsection 7.2.2 as "beam wandering" and possibly responsible for the "β-type" (slow) fading. The replacement of this activity by random convective turbulence, brought about by strong temperature gradients, would result in a transition to a purely "scatter" mechanism most probably responsible for the more rapid "α-type" of fading.

It is very likely that all of these processes contribute simultaneously, with a varying degree of importance, to the effect of vertical temperature gradient upon the fading spectrum of the received light (or radio) signal.

CHAPTER 8

CONCLUSIONS AND SUGGESTIONS FOR FUTURE WORK

The results of a fairly comprehensive investigation on the performance of a transhorizon radio-link, operating at a frequency of 900 MHz, have been presented together with the simulated results obtained from a laboratory scale-model of the link.

Whilst it is recognised that the characteristics of the "atmosphere" in the laboratory model do not necessarily completely represent those of the real atmosphere, the aid provided by the model in respect of studies concerned with the effect of the more dominant features of the lower troposphere on a radio-link has been invaluable. Indeed, many of the results obtained from the laboratory model could not be obtained from a full scale propagation path because of the magnitude and cost of such an exercise.

A number of conclusions may be drawn from this investigation. These are listed in the following section.

8.1 Conclusions

1. The long-term study of the received signal median level on a monthly and annual basis revealed significant correlations between the monthly averages of some meteorological parameters and the monthly average median signal level. For example, monthly average surface wind was found to be negatively correlated with the monthly median level, whilst the monthly relative sunshine was

positively correlated with the same quantity. This suggests that the "worst month" of the year, in propagation terms and for the particular radio system, is that month which is characterised by the strongest surface winds and the least insolation.

2. The same long-term investigation also revealed that severe transmission losses can be expected during the passage of a cold front over the propagation path.

3. All the fading characteristics recorded could, with very few exceptions, be readily classified into two categories, α- and β-type of fading. The former was found to be strongly affected by the surface wind, especially its normal to the propagation path component U_n, whilst the latter was not found to be affected by the near-ground wind activity in any particular manner.

4. An increase in the surface wind component (U_n) caused a "spread" of the α-type of fading spectrum towards higher frequencies. This effect was quantitatively studied, using spectra from 92 α-type cases. An empirical expression was established relating the fading power spectral density to surface wind component U_n, having the form:-

$$P(f) \sim \left[\frac{f}{f_m}\right]^{-\frac{1}{0.366 + 0.131 \cdot U_n}} \qquad (U_n \text{ in knots})$$

where f_m is the frequency for which $P(f)$ attains its maximum.

For U_n = 0 (zero mean surface wind across the propagation path) this empirical expression takes the form:-

$$P(f) \sim \left[\frac{f}{f_m}\right]^{-2.73} \cong \left[\frac{f}{f_m}\right]^{-8/3}$$

Thus, for the particular case when U_n = 0, the dependence of the power spectral density upon frequency was found to be in agreement with Tatarski's theoretical expression concerning the frequency power spectrum of amplitude (or phase) fluctuations experienced in line-of-sight propagation. This implies that the mechanism responsible for the α-type of fading is possibly similar to that which causes signal fluctuations in line-of-sight radio-links.

5. The static stability in the lower 1.5 km of the atmosphere was another parameter found to affect the spectrum of both types of fading. Decreasing static stability was found to cause a "spread" of the fading spectrum towards higher frequencies. In the case of the β-type of fading, the static stability appeared to govern the power spectral density function which was found to be of the form:-

$$P(f) \sim f^{-n}$$

The exponent n appeared to undergo a transition from - 2 to - 8/3 and hence to - 4 when the static stability was increasing.

From recently available theoretical and experimental

work concerning the influence of thermal stratification upon the spectra of atmospheric turbulence, this effect might be interpreted as a result of refractivity spectra obeying a - 1 "- 5/3" or "- 3" power laws in the range of wave numbers responsible for the β-type of fading.

6. In recognising that the laboratory model had already been shown to offer facilities for simulating all types of fading, particular attention was given to the simulation of both the "α" and "β" types that were obtained from the full-scale system under investigation. In particular, the simulation of the "α-type" of fading for a range of different cross-path surface wind velocity components (U_n) yielded a scale reduction factor of approximately 52 between the components experienced on the full-scale model and those required to produce the same fading power spectra on the model system. This reduction of "dynamic similarity" factor of 52 is in close agreement with the value first obtained by Burrows[145] in the first model of this type which was related to a totally different full-scale trans-horizon system.

7. In the study on the effects of changing the static stability of the model "atmosphere", it has been shown that when the near-surface static stability is reduced (increasing vertical temperature gradient) the "spread" of the resultant fading spectra increases towards the higher frequency regions. Under these conditions it was found that increasing the near-surface vertical temperature gradient created more intense

random thermal turbulence in the region and which was responsible for the faster fluctuations in the "received signal".

8. The investigations that have been carried out on both the full-scale radio system and the laboratory model have revealed that the near ground atmospheric activity is of primary importance in the performance of a transhorizon radio system. This is a feature which has been rather neglected in the past when most of the theoretical and experimental work was directed towards the investigation of atmospheric effects in mid-tropospheric altitudes.

Clearly, these conclusions suggest that the near-surface activity of the lower atmosphere should be the subject of further investigation, particularly with respect to its effect on a radio-beam. Some suggestions for additional work in this area are given in the following section.

8.2 Suggestions for Future Work

In the light of the conclusions drawn from the present investigation, it is suggested that further research is required in studying the effects of the near-ground activity upon both full-scale and simulated transhorizon radio-links. Such studies could be accomplished by simultaneous measurements of propagation characteristics (transmission loss, fading, etc.) and meteorological parameters in the proximity of the ground. Radar or acoustic sounder observations of the near-ground activity at the same

time could reveal more of its importance in transhorizon propagation.

Future research on laboratory simulation may be extended to include both the effects of the propagation medium and of the underlying terrain. In this respect, the experience gained from the present investigation could be combined with the works of Trivedi[142], Ridler[141] and King[139], concerning the laboratory simulation of diffraction effects due to the terrain structure.

REFERENCES

1. H. R. BYERS: "Synoptic and Aeronautical Meteorology". McGraw Hill, New York, 1937.

2. A. MONIN: "Weather Forecasting as a Problem in Physics". The M.I.T. Press, Cambridge, Mass. and London, 1972.

3. J. VAN MIEGHEM: "Atmospheric Energetics". Clarendon Press, Oxford, 1973.

4. J. VAN DER HOVEN: "Power Spectrum of Horizontal Wind Speed in the Frequency range from 0.0007 to 900 Cycles per Hour". J. Meteorology, Vol. 14, pp. 160-164, 1957.

5. HANS PANOFSKY: "Spectra of atmospheric variables in the boundary layer". Radio Sci., Vol. 4, pp. 1101-1109, 1969.

6. P. B. MacCREADY: "Structure of Atmospheric Turbulence". J. Meteorology, Vol. 10, pp. 434-449, 1953.

7. W. G. BURROWS: "VHF Radio wave propagation in the Troposphere". Intertext Books, London, 1968.

8. D. LIVINGSTON: "The Physics of Microwave Propagation". Prentice-Hall, New Jersey, 1970.

9. D. KERR: "Propagation of Short Radio waves". Dover Publications, New York, 1951.

10. P. DEBYE: "Polar Molecules". Chemical Catalogue Co., New York, 1929.

11. E. K. SMITH and S. WEINTRAUB: "The constants in the equation for atmospheric refractive index at radio frequencies". Proc. IRE, Vol. 41, pp. 1035-1037, 1953.

12. F. DU CASTEL: "Tropospheric Radiowave Propagation beyond the Horizon". Pergamon Press, London, 1966.

13. C.C.I.R. Recommendations, Rec. No. 309, Los Angeles, 1959.

14. G. J. TAYLOR: "Some early ideas about turbulence". J. Fluid Mechanics, Vol. 41, pp. 3-11, 1970.

15. J. L. LUMLEY and H. PANOFSKY: "The Structure of Atmospheric Turbulence". John Wiley & Sons, New York, 1964.

16. V. A. BELINSKII: "Dynamic Meteorology". The Israel Program for Scientific Translations, Jerusalem, 1961.

17. L. F. RICHARDSON: "The supply of energy from and to atmospheric eddies". Proc. Roy. Soc., Vol. 97, pp. 354-373, 1920.

18. H. B. PRIESTLEY: "Convection from a large horizontal surface". Austral. J. Phys., Vol. 7, pp. 312-323, 1954.

19. T. K. ELLISON and J. S. TURNER: "Mixing of dense fluid in a turbulent pipe flow". Parts 1-2, J. Fluid Mech., Vol. 8, pp. 514-544, 1960.

20. C. H. PRIESTLEY: "Turbulent transfer in the lower Atmosphere". University of Chicago Press, Chicago, 1964.

21. J. PROUDMAN: "Dynamical Oceanography". Methuen, London, 1957.

22. R. S. SCORER: "The nature of convection as revealed by soaring birds and dragonflies". Quart. J. Roy. Met. Soc., Vol. 80, pp. 68-77, 1954.

23. R. C. RAINEY: "Some observations of flying locusts and atmospheric turbulence in Eastern Africa". Quart. J. Roy. Met. Soc., Vol. 84, pp. 334-354, 1958.

24. A. WELCH, L. WELCH and F. G. IRVING: "The Soaring Pilot". London: John Murray, 1955.

25. R. S. SCORER and F. H. LUDLAM: "Bubble theory of penetrative convection". Quart. J. Roy. Met. Soc., Vol. 79, pp. 94-103, 1953.

26. J. S. MALKUS and R. S. SCORER: "The erosion of cumulus towers". J. Meteorol., Vol. 12, pp. 43-57, 1955.

27. C. H. PRIESTLEY: "Free and forced convection in the atmosphere near the ground". Quart. J. Roy. Met. Soc., Vol. 81, pp. 139-143, 1955.

28. R. S. SCORER and C. RONNE: "Experiment with convective bubbles". Weather, No. 11. pp. 151-154, 1956.

29. K. G. BATCHELOR: "Heat convection and buoyancy effects in fluids". Quart. J. Roy. Met. Soc., Vol. 80, pp. 339-358, 1954.

30. J. LEVINE: "Spherical vortex theory of bubble-like motion in cumulus clouds". J. Meteorol., Vol. 16, pp. 653-662, 1959.

31. BETSY WOODWARD: "The motion in and around isolated thermals". Quart. J. Roy. Met. Soc., Vol. 85, pp. 144-151, 1959.

32. Yu. CHERNOV: "Investigation of Ascending Streams by means of Gliders". Trudy Ts AO, No. 63, pp. 87-98, 1965.

33. N. I. WULFSON: "Investigation of Convective motion in the free Atmosphere". Izd. Akad. Nauk USSR, 1961.

34. K. HARDY and H. OTTERSTEN: "Radar investigation of Convective patterns in the clear Atmosphere". J. Atm. Sci., Vol. 26, pp. 666-672, 1969.

35. T. G. KONRAD: "The dynamics of the convective process in the clear air as seen by Radar". 14th Radar Meteorology Conference, Tucson, Arizona, pp. 57-60, 1970.

36. J. TELFORD: "A Plume theory for the Convective field in clear Air". J. Atm. Sci., Vol. 29, pp. 128-134, 1972.

37. A. S. FRISCH, R. B. CHADWICK et al: "Observations of Boundary Layer Convection Cells, measured by Dual-Doppler Radar and echosonde, and by microbarograph array". Boundary Layer Meteorol., Vol. 10, pp. 55-68, 1976.

38. W. T. CRONENWETT, G. B. WALKER and R. L. INMAN: "Acoustic Sounding of Meteorological Phenomena in the Planetary Boundary Layer". J. Appl. Met., Vol. 11, pp. 1351-1358, 1972.

39. H. D. PARRY, M. J. SANDERS et al: "Operational Applications of a Pure Acoustic Sounding System". J. Appl. Met., Vol. 14, pp. 67-77, 1975.

40. F. F. HALL, J. G. EDINGER and W. D. NEFF: "Convective Plumes in the Planetary Boundary Layer, Investigated with an Acoustic Echo Sounder". J. Appl. Met., Vol. 14, pp. 513-523, 1975.

41. D. N. ASIMACOPOULOS, R. S. COLE et al: "A Quantitative comparison between Acoustic Sounder returns and the direct measurement of Atmospheric Temperature Fluctuations". Boundary Layer Met., Vol. 10, pp. 137-147, 1976.

42. J. F. CROFT: "The convective regime and temperature distribution above a horizontal heated surface". Quart. J. Roy. Met. Soc., Vol. 84, pp. 418-427, 1958.

43. A. PELLEW and R. V. SOUTHWELL: "On maintained convective motion in a fluid heated from below". Proc. Roy. Soc., A, Vol. 176, pp. 312-343, 1940.

44. H. OTTERSTEN: "Atmospheric structure and radar backscattering in clear air". Radio Sci., Vol. 4, pp. 1179-1193, 1969.

45. K. R. HARDY and K. M. GLOVER: "Twenty-four hour history of radar angel activity at three wavelengths". Proc. 12th Conf. Rad. Meteor., Amer. Met. Soc., Boston, Mass., pp. 269-274, 1966.

46. G. I. TAYLOR: "Statistical Theory of Turbulence". Parts 1-4, Proc. Roy. Soc., Vol. 151, pp. 421-478, 1935.

47. G. I. TAYLOR: "The Spectrum of Turbulence". Proc. Roy. Soc., Vol. 164, pp. 476-490, 1938.

48. A. N. KOLMOGOROV: "The Local Structure of Turbulence in Incompressible Viscous Fluid for Very Large Reynolds Numbers" and "On Degeneration of Isotropic Turbulence in an Incompressible Viscous Liquid". Turbulence: Classic Papers on Statistical Theory, Interscience Publishers Inc., New York, pp. 151-158, 1961.

49. V. I. TATARSKII: "The effects of the Turbulent Atmosphere on Wave Propagation". Israel Program for Scientific Translations, Jerusalem, 1971.

50. H. OTTERSTEN: "Mean vertical gradient of potential refractive index in turbulent mixing and radar detection of CAT". Radio Sci., Vol 4, pp. 1247-1249, 1969.

51. L. R. TSVANG, S. L. ZUBKOVSKII et al: "Measurements of some properties of turbulence in the lowest 300 m. of the Atmosphere". Bull. Acad. Sci. USSR, Geoph. Ser., No. 5, pp. 475-481, (English translation), 1963.

52. A. BURNS: "Power Spectra of Low-Level Atmospheric Turbulence Measured from an Aircraft". Ministry of Aviation, London CP 733, 1964.

53. B. M. KOPROV: "Spectra of turbulent fluctuations of the vertical wind-velocity component in the boundary layer under conditions of developed convection". Bull. Acad. Sci. USSR, Ser. Atmosph. and Ocean. Phys., Vol. 1, pp. 1151-1159, 1965.

54. N. Z. PINUS and L. V. SHCHERBAKOVA: "The structure of the wind velocity field in a thermally stratified Atmosphere". Bull. Acad. Sci. USSR, Ser. Atmosph. and Ocean Phys., Vol. 2, pp. 696-700, 1966.

55. L. O. MYRUD: "Atmospheric Measurements of the Buoyant Subrange of Turbulence". J. Atm. Phys., Vol. 25, pp. 1160-1164, 1968.

56. N. K. VINNICHENKO and J. A. DUTTON: "Empirical studies of atmospheric structure and spectra in the free atmosphere". Radio Sci., Vol. 12, pp. 1115-1126, 1969.

57. E. E. GOSSARD: "Spectra of Atmospheric Scalars". J. Geophys. Res., Vol. 65, pp. 3339-3351, 1960.

58. L. R. TSVANG: "Some characteristics of the spectra of temperature pulsations in the Boundary Layer of the Atmosphere". Bull. Acad. Sci. USSR, Geoph. Ser., No. 10, pp. 961-965, (English translation), 1963.

59. H. PANOFSKY: "The spectrum of temperature". Radio Sci., Vol. 4, pp. 1143-1146, 1969.

60. L. G. ELAGINA: "Measurement of the frequency spectra of pulsations in absolute humidity in the near ground layer of the atmosphere". Bull. Acad. Sci. USSR, Geophys. Ser., No. 12, pp. 1133-1137, (English translation), 1963.

61. J. A. LANE: "Small-scale variations of radio refractive index in the troposphere". Proc. IEE, Vol. 115, pp. 1227-1239, 1968.

62. J. A. LANE: "Some aspects of the fine structure of elevated layers in the troposphere". Radio Sci., Vol. 4, pp. 1111-1114, 1969.

63. G. N. SHUR: "Experimental investigations of the Energy Spectrum of Atmospheric Turbulence". Trudy TsAO, No. 43, pp. 79-90, (Translated as AID Rept. T-63-55, Aerospace Info., Library of Congress), 1962.

64. E. PLATE and S. P. ARYA: "Turbulence spectra in a stably stratified boundary layer". Radio Sci., Vol. 4, pp. 1163-1168, 1969.

65. G. FICHTL and D. CAMP: "Spectral structure of tropospheric vertical temperature profiles". J. Geoph. Res., Vol. 78, pp. 6218-6223, 1973.

66. A. WEILL, M. AUBREY and F. BAUDIN: "A study of temperature fluctuations in the atmospheric boundary layer". Boundary Layer Meteor., Vol. 10, pp. 337-346, 1976.

67. R. BOLGIANO Jr.: "Turbulent Spectra in a Stably Stratified Atmosphere". J. Geoph. Res., Vol. 64, pp. 2226-2229, 1959.

68. R. BOLGIANO Jr.: "Structure of Turbulence in Stratified Media". J. Geophys. Res., Vol. 67, pp. 3015-3023, 1962.

69. A. S. MONIN: "On the turbulence spectrum in a thermally stratified atmosphere". Bull. Acad. Sci., USSR, Geoph. Ser., No. 2, pp. 266-270, (English translation), 1962.

70. J. L. LUMLEY: "The Spectrum of Nearly Inertial Turbulence in a Stably Stratified Fluid". J. Atmosph. Sci., Vol. 21, pp. 99-102, 1964.

71. C. M. TCHEN: "On the spectrum of energy in turbulent shear flow". J. Res. Nat. Bur. Stand., Vol. 50,. No. 1, 1953.

72. F. A. GISINA: "The effect of mean velocity and temperature gradients of the spectral characteristics of turbulence". Bull. Acad. Sci. USSR, Ser. Atmosph. and Ocean. Phys., Vol. 2, pp. 487-491, (English translation), 1966.

73. C. M. TCHEN: "Cascade theory of turbulence in a stratified medium". Tellus XXVII, 1, pp. 1-13, 1975.

74. S. L. ZUBKOVSKII: "An experimental investigation of the spectra of pulsations in vertical wind component of the wind velocity in the free atmosphere". Bull. Acad. Sci. USSR, Ser. Atm. and Ocean. Phys., No. 8, pp. 782-784, (English translation), 1963.

75. J. C. SCHELLING, C. R. BURROWS and E. G. FERREL: "Ultra short wave propagation". Proc, IRE, Vol. 21, pp. 427-463, 1933.

76. B. R. BEAN: "The geographical and height distributions of the gradient of refractive index". Proc. IRE, Vol. 41, pp. 549-550, 1953.

77. B. R. BEAN and F. M. MEANEY: "Some applications of the monthly median refractivity gradient in tropospheric propagation". Proc. IRE, Vol. 43, pp. 1419-1431, 1955.

78. K. A. NORTON, P. L. RICE and L. E. VOGLER: "Use of angular distance in estimating transmission loss and fading range for propagation through a turbulent atmosphere over irregular terrain". Proc. IRE, Vol. 43, pp. 1488-1526, 1955.

79. B. R. BEAN and G. D. THAYER: "On models of the atmospheric radio refractive index". Proc. IRE, Vol. 47, pp. 740-755, 1959.

80. B. R. BEAN: "Atmospheric bending of radio waves". Electromagnetic Wave Propagation, Academic Press, London and New York, p. 163, 1960.

81. H. G. BOOKER and W. WALKINSHAW: "The mode theory of tropospheric refraction and its relation to wave guides and diffraction". Meteorological Factors in Radio Wave Propagation, pp. 80-127, The Physical Society of London, 1946.

82. B. R. BEAN and E. J. DUTTON: "Radio Meteorology". National Bureau of Standards Monograph 92, pp. 132-163, 1966.

83. A. PICQUENARD: "Radio Wave Propagation". Philips Technical Library, Macmillan, 1974.

84. J. FEINSTEIN: "Tropospheric propagation beyond the horizon". J. Appl. Phys., Vol. 22, pp. 1292-1293, 1951.

85. H. T. FRIIS, A. B. CRAWFORD and D. C. HOGG: "A reflection theory for propagation beyond the horizon". Bell Syst. Tech. J., Vol. 36, pp. 627-644, 1957.

86. F. du CASTEL, P. MISME et al: "Refléxion partielles dans l'atmosphère et propagation à grand distance". Ann. Téléc., Vol. 13, pp. 209-219, 1958.

87. F. du CASTEL, P. MISME et al: "On the role of the process of reflection in radio wave propagation". J. Res. Nat. Bur. Stand., Vol. 66-D, pp. 273-284, 1962.

88. J. K. S. JOWETT: "The measurement and prediction of VHF tropospheric field strenghts at distances beyond the horizon". Proc. IEE, Vol. 105, Part B, Suppl. 8, Symposium on long-distance Propagation above 30 Mc/s, pp. 91-96, 1958.

89. P. A. MATTHEWS and S. DUFU: "The effect of Reflecting Layers in the Troposphere on Transhorizon Propagation". IEE Conference, Publication No. 48, Tropospheric Wave Propagation, pp. 22-29, 1968.

90. H. G. BOOKER and W. E. GORDON: "A theory of radio scattering in the troposphere". Proc. IRE, Vol. 38, pp. 401-412, 1950.

91. E. C. S. MEGAW: "Scattering of electromagnetic waves by atmospheric turbulence". Nature, Vol. 166, pp. 1100-1104, 1950.

92. C. L. PEKERIS: "Note on scattering in an inhomogeneous medium". Phys. Rev., Vol. 71, pp. 268-269, 1947.

93. G. K. BATCHELOR: "The scattering of radio waves in the atmosphere by turbulent fluctuations in refractive index". School of Elec. Eng., Cornell University, Res. Rep. EE 262, 1955.

94. R. A. SILVERMAN: "Turbulent mixing theory applied to radio scattering". J. Appl. Phys., Vol. 27, pp. 699-705, 1956.

95. R. A. SILVERMAN: "Fading of radio waves scattered by dielectric turbulence". J. Appl. Phys., Vol. 28, pp. 506-511, 1957.

96. E. C. S. MEGAW: "Fundamental radio scatter propagation theory". Proc. IEE, Vol. 104, Monograph No. 236 R, pp. 441-455, 1957.

97. V. I. TATARSKI: "Wave Propagation in a Turbulent Medium". Dover Publications, New York, 1961.

98. F. VILLARS and V. F. WEISSKOPF: "The scattering of electromagnetic waves by turbulent atmospheric fluctuations". Phys. Rev., Vol. 94, pp. 232, 1954.

99. R. BOLGIANO Jr.: "The role of turbulent mixing in scatter propagation". IRE Trans. Ant. Prop., Vol. A-P 6, pp. 161-168, 1958.

100. A. D. WHEELON: "Spectrum of turbulent fluctuations produced by convective mixing of gradients". Phys. Rev., Vol. 105, pp. 1706-1710, 1957.

101. H. STARAS and A. D. WHEELON: "Theoretical research on tropospheric Scatter propagation in the United States, 1954-1957". IRE Trans. Ant. Prop. Vol. A-P 7, pp. 80-87, 1959.

102. A. WHEELON: "Near-field corrections to line-of-sight propagation". Proc. IRE, Vol. 43, pp. 1459-1466, 1955.

103. A. WHEELON: "Radio wave scattering by tropospheric irregularities". J. Res. Nat. Bureau of Stand., Vol. 63D, pp. 205-233, 1959.

104. M. A. JOHNSON: "A review of tropospheric scatter propagation theory and its application to experiment". Proc. IEE, Vol. 105, Part B, Suppl. 8, Symposium on long-distance propagation above 30 Mc/s, pp. 165-176, 1958.

105. F. N. EDWARDS: "An analysis of Airborne measurements of tropospheric Index of refraction fluctuations". Statistical Methods in Radio Wave Propagation, Pergamon Press, Symposium Publications Division, 1960.

106. F. VILLARS and V. F. WEISSKOPF: "On the scattering of radio waves by turbulent fluctuations of the atmosphere". Proc. IRE, Vol. 43, pp. 1232-1239, 1955.

107. R. BOLGIANO Jr.: "Wavelength dependence in trans-horizon propagation". Proc. IRE, Vol. 47, p. 331, 1959.

108. J. H. CHISHOLM, P. A. PORTMANN et al: "Investigations of angular scattering and multipath properties of tropospheric propagation of short radio waves beyond the horizon". Proc. IRE, Vol. 43, pp. 1317-1335, 1955.

109. M. HIRAI, K. NISHIKORI et al: "Studies in UHF overland propagation beyond the horizon". J. Radio Res. Labs. (Japan), Vol. 7, pp. 137-176, 1960.

110. N. R. ORTWEIN, R. U. HOPKINS and J. E. POHL: "Properties of tropospheric scattered fields". Proc. IRE, Vol. 49, pp. 788-802, 1961.

111. F. EKLUND and S. WICKERTS: "Wavelength dependence of microwave propagation far beyond the horizon". Radio Sci., Vol. 3, pp. 1066-1074, 1968.

112. A. CRAWFORD, D. C. HOGG and W. H. KUMMER: "Studies in tropospheric propagation beyond the horizon". Bell. Syste. Techn. J., Vol. 38, pp. 1067-1178, 1959.

113. S. O. RICE: "Statistical fluctuations of radio field strength far beyond the horizon". Proc. IRE, Vol. 41, pp. 274-282, 1953.

114. L. FEHLHABER and J. GROSSKOPF: "Das elektromagnetische Feld am Empfangsort einer troposphärischen Scatterstrecke. I. Die Eigenschaften des Empfangsfeldes und ihre Messung". Nachr. Techn. A., Vol. 20, pp. 511-520, 1967.

115. L. FEHLHABER and J. GROSSKOPF: "Das elektromagnetische Feld am Empfangsort einer troposphärischen Scattertrecke, II. Die Struktur der Dielektrizitätskonstanten im gemeinsamen Volumen und ihre Wirkungen auf das Empfangsfeld bei Frequenzen über 1000 MHz". Nachr. Techn. Z., Vol. 20, pp. 649-657, 1967.

116. I. S. GRADSHTEYN and I. M. RYZHIK: "Table of Integral Series and Products". Academic Press, New York, 1965.

117. J. D. KRAUS: "Antennas". McGraw-Hill Book Co., New York, 1950.

118. J. S. BENDAT and A. PIERSOL: "Random Data: Analysis and Measurement Procedures". John Wiley & Sons Inc., New York, 1971.

119. R. K. OTNES and L. ENOCHSON: "Digital Time Series Analysis". John Wiley & Sons, New York, 1972.

120. A. PAPOULIS: "The Fourier Integral and its Applications". McGraw-Hill, New York, 1962.

121. G. D. BERGLAND: "A guided tour of the fast Fourier transform". IEEE Spectrum, Vol. 6, pp. 41-52, 1969.

122. P. J. RICHARDS: "Computing reliable power spectra". IEEE Spectrum, Vol. 4, pp. 83-90, 1967.

123. R. W. RAMIREZ: "The FFT: Fundamentals and Concepts". Published by TEKTRONICS Inc., Beaverton, Oregon, U.S.A., 1975.

124. D. M. MONRO: "Real Discrete Fast Fourier Transform". Statistical Algorithms, App. Statistics, Vol. 25, No. 2, pp. 166-172, 1976.

125. D. M. MONRO: "Complex Discrete Fast Fourier Transform". Statistical Algorithms, Appl. Statistics, Vol. 24, No. 1, pp. 153-160, 1975.

126. K. W. SMILLIE: "An Introduction to Regression and Correlation". Academic Press, London and New York, 1966.

127. A. C. STICKLAND and R. L. SMITH-ROSE: "Centimetre Wave Propagation over Land. A preliminary study of the Field Strength records between March and September, 1943". Meteorological Factors in Radio Wave Propagation, The Physical Society of London, 1946.

128. K. BULLINGTON, W. J. INKSTER and A. L. DURKEE: "Results of propagation Tests at 505 mc and 4.090 mc on Beyond-Horizon Paths". Proc. of the IRE, Vol. 43, pp. 1306-1316, 1955.

129. P. C. BELATINI: "Inadequacy of scatter mechanisms in tropospheric radio propagation". Nature, Vol. 184, 14th November, 1959.

130. W. G. BURROWS: "EM wave proagation in an inhomogeneous medium - A laboratory study". Proc. of AGARD/NATO, Conference on aspects of em wave scattering in Radio-Communications, Cambridge, Mass., October, 1977.

131. B. C. ANGELL, J. B. FOOT et al: "Propagation Measurements at 3480 Mc/s over a 173-Mile Path". Proc. IEE, Vol. 5, Suppl. 8, pp. 128-142, 1958.

132. G. C. RIDER: "Some Tropospheric Scatter Propagation Measurements and Tests of Aerial Siting Conditions at 858 Mc/s". Proc. IEE, Vol. 15, Suppl. 8, pp. 143-152, 1958.

133. F. A. KITCHENS, E. G. RICHARDS and I. J. RICHMOND: "Some Investigations on Metre-Wave Radio Propagation in the Transhorizon Region". Proc. IEE, Vol. 5, Suppl. 8, pp. 106-116, 1958.

134. J. S. NICOLIS: "Systematic Long-Term Duct Propagation Conditions Over a VHF Overhorizon Path Between Greece and Italy". IEEE Trans. Ant. and Prop., Vol. AP-15, No. 2, pp. 264-268, 1967.

135. R. W. LEE and J. C. HARP: "Weak Scattering in Random Media, with Applications to Remote Probing". Proc. of the IEEE, Vol. 57, No. 4. pp. 375-406, 1969.

136. W. G. BURROWS: "Study of the propagation Characteristics of a tropospheric radio link by the use of a laboratory model". Electronics Letters, Vol. 2, No. 9, pp. 325, 1966.

137. A. SOMMERFELD: "Optics". Academic Press, New York, 1954.

138. M. P. BACHYNSKI: "Scale model investigations of em wave propagation over natural obstacles". RCA Rev., Vol. 24, No. 1, pp. 105-144, 1963.

139. R. W. KING: "Diffraction of Electromagnetic Waves by Irregular Terrain". Ph.D. Thesis, University of London, 1972.

140. C. BOUTLAS: "Considerations relating to the Planning and Performance of Microwave Links". M. Phil. Thesis, University of London, 1974.

141. J. D. RIDLER: "Diffraction of electromagnetic waves by mountains". M. Phil. Thesis, University of London, 1972.

142. A. I. TRIVEDI: "Propagation of radio waves over natural obstacles". M. Phil. Thesis, University of London, 1977.

143. R. E. POST and D. F. ROST: "Modelling UHF Trans-horizon Scatter Propagation". IEEE Trans., Ant. and Prop., Vol. AP-16, pp. 612-613, 1968.

144. H. G. BOOKER and J. T. BETTENÇOURT: "Theory of radio transmission by tropospheric scattering using very narrow beams". Proc. IRE, Vol. 43, pp. 281-290, 1955.

145. W. G. BURROWS: "A study of the effects of Troposphere Air Mass movements on the fading characteristics of UHF transmissions by the use of a laboratory model". Proc. AGARD/NATO (EPC), Symposium on Tropospheric Radio Wave Propagation, Dusseldorf, September, 1970.

146. K. HACKING: "UHF Propagation over rounded hills". Proc. IEE, Vol. 117, No. 3, pp. 499-511, 1970.

147. R. C. PANKHURST: "Wind-Tunnel Technique". Sir Isaac Pitman & Sons Ltd., London, 1952.

148. G. A. BRIGGS: "Plume Rise". US Atomic Energy Commission, Division of Technical Information, 1969.

149. J. S. TURNER: "Buoyancy Effects in Fluids". Cambridge University Press, 1973.

150. G. K. BATCHELOR: "The conditions for dynamic similarities of motions of a frictionless perfect-gas atmosphere". Quart. J. Roy. Met. Soc., Vol. 79, pp. 224-235, 1953.

151. J. E. CHERMAK and P. S. ARYA: "Problems of atmospheric shear flows and their laboratory simulation". Aerodynamics of Atmospheric Shear Flows, AGARD Conf. Proc. No. 48, Paris, France, February, 1970.

152. A. S. DUBOVIK: "Photographic Recording of High Speed Processes". Pergamon Press, London, 1968.

153. H. SCHLICHTING: "Boundary Layer Theory". McGraw-Hill Book Co., 1960.

154. C. M. CRAIN: "Surrey of airborne refractometer measurements". Proc. IRE, Vol. 43, pp. 1405-1414, 1955.

155. D. E. FITZJARRALD: "A field observation of atmospheric free convection". J. Appl. Met., Vol. 15, pp. 259-263, 1976.

156. D. E. FITZJARRALD: "Horizontal scales of motion in atmospheric free convection observed during the GATE experiment". J. Appl. Met., Vol. 17, pp. 213-221, 1978.

157. J. NICURADSE: "Gesetzmässigkeit der turbulenten Strömung in glatten Rohen". Forschungsheft 356, 1932.

APPENDIX I

THE CURVATURE OF RADIO RAYS PROPAGATED IN A MEDIUM WITH A NEGATIVE REFRACTIVE INDEX GRADIENT

Consider a wave front moving from the position AB to A´B´ along the propagated ray path, as shown in the figure below:-

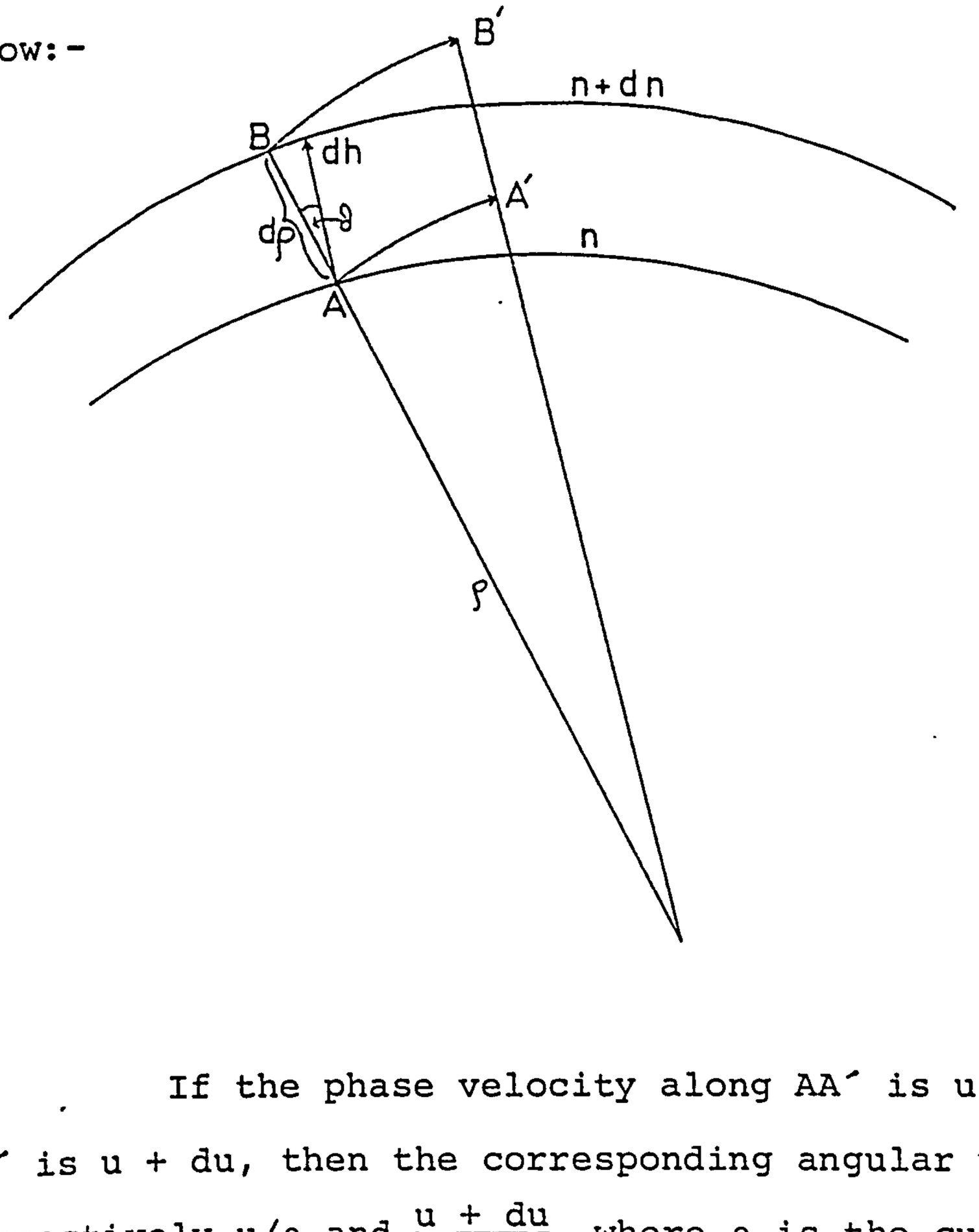

If the phase velocity along AA´ is u and along BB´ is u + du, then the corresponding angular velocities are respectively u/ρ and $\frac{u + du}{\rho + d\rho}$, where ρ is the curvature radius (arc AA´).

These angular velocities are equal, thus:-

$$\frac{u}{\rho} = \frac{U + dU}{\rho + d\rho} \qquad (I.1)$$

From (I-1):-

$$\frac{du}{u} = \frac{d\rho}{\rho} \qquad (I.2)$$

Taking into account that U = c/n, where c is the velocity of light in vacuo and n the refractive index, one obtains:-

$$\frac{du}{u} = - \frac{dn}{n} \qquad (I.3)$$

Combination of (I.2) and (I.3) yields:-

$$\frac{1}{\rho} = - \frac{1}{n} \frac{dn}{d\rho} \qquad (I.4)$$

If the angle between the ray path and the surface of constant refractive index is θ, then $dh = d\rho \cdot \cos \theta$ and:-

$$\frac{1}{\rho} = - \frac{1}{n} \frac{dn}{dh} \cos \theta \qquad (I.5)$$

This is the general expression giving the radius of curvature ρ as a function of the refractive index gradient dn/dh.

APPENDIX II

DERIVATION OF THE WAVE EQUATION FOR THE SCATTERED ELECTRIC FIELD

The wave equation, derived from Maxwell's equations for an inhomogeneous medium, gives for the electric vector $\vec{E}(101,102)$:-

$$\nabla^2 \vec{E} - \frac{1}{c^2} \frac{\partial^2}{\partial t^2} (\varepsilon \cdot \vec{E}) = - \vec{\nabla} \left[\frac{1}{\varepsilon} \vec{E} \cdot \vec{\nabla}\varepsilon \right] \qquad \text{(II.1)}$$

where ε is the dielectric constant of the medium. Since the field oscillates much more rapidly than the dielectric constant, the time derivatives operate mainly on $\vec{E}$. Expressing the dielectric constant as the sum of a mean and a fluctuating part: $\varepsilon = \langle\varepsilon\rangle + \delta\varepsilon$ and assuming that $\langle\varepsilon\rangle \simeq 1$, (II.1) can be written as:-

$$\nabla^2 \vec{E} - \frac{1}{c^2} (1 + \delta\varepsilon) \frac{\partial^2}{\partial t^2} \vec{E} = - \vec{\nabla} \left[\vec{E} \cdot \vec{\nabla} \ln (1 + \delta\varepsilon) \right] \qquad \text{(II.2)}$$

Taking $\ln (1 + \delta\varepsilon) \simeq \delta\varepsilon$ [49] and considering the harmonic time dependence of the electric field, (II.2) can be written:-

$$\left[\nabla^2 + k^2 (1 + \delta\varepsilon) \right] \vec{E} = - \vec{\nabla} \left[\vec{E} \cdot \vec{\nabla} (\delta\varepsilon) \right] \qquad \text{(II.3)}$$

Hence:-

$$(\nabla^2 + k^2) \vec{E} = k^2 \cdot \delta\varepsilon \cdot \vec{E} - \vec{\nabla} \left[\vec{E} \cdot \vec{\nabla} (\delta\varepsilon) \right] \qquad \text{(II.4)}$$

Let $\vec{E} = \vec{E}_o + \vec{E}_s$, where $\vec{E}_o$ is the unperturbed electric field and $\vec{E}_s$ the scattered field proportional to the fluctuations of the dielectric constant $\delta\varepsilon$, then (II.4) can be written:-

$$(\nabla^2 + k^2)\ (\vec{E}_o + \vec{E}_s) = - k^2 \ .\ \delta\varepsilon\ (\vec{E}_o + \vec{E}_s) -$$

$$- \vec{\nabla} \left[(\vec{E}_o + \vec{E}_s) \ .\ \vec{\nabla}\delta\varepsilon \right] \qquad \text{(II.5)}$$

Noting that $\nabla^2\vec{E}_o + k^2\ \vec{E}_o = o$[49], (II.5) becomes:-

$$(\nabla^2 + k^2)\ \vec{E}_s = - k^2\delta\varepsilon\ \vec{E}_o - k^2 \ .\ \delta\varepsilon \ .\ \vec{E}_s -$$

$$- \vec{\nabla}\ (\vec{E}_o \ .\ \vec{\nabla}\delta\varepsilon) - \vec{\nabla}\ (\vec{E}_s \ .\ \delta\varepsilon) \qquad \text{(II.6)}$$

Noting that the product $\vec{E}_s \ .\ \delta\varepsilon$ is proportional to $(\delta\varepsilon)^2$ (because $\vec{E}_s \sim \delta\varepsilon$) and, therefore, very small, the expression (II.6) may be written:-

$$(\nabla^2 + k^2)\ \vec{E}_s = - k^2\delta\varepsilon \ .\ \vec{E}_o - \vec{\nabla}\ (\vec{E}_o \ .\ \vec{\nabla}\delta\varepsilon) \qquad \text{(II.7)}$$

The term $\vec{\nabla}\ (\vec{E}_o \ .\ \vec{\nabla}\delta\varepsilon)$ can be written:-

$$\nabla^2 \left(\vec{E}_o \cdot \frac{\delta\varepsilon}{\ell_o} \right)$$

where ℓ_o is the correlation radius of the dielectric constant fluctuations, then:-

$$\nabla^2 \left(\vec{E}_o \cdot \frac{\delta\varepsilon}{\ell_o} \right) = \frac{1}{\ell_o} (\vec{\nabla} \cdot \delta\varepsilon) \cdot \vec{E}_o + \frac{\delta\varepsilon}{\ell_o} \vec{\nabla} \vec{E}_o =$$

$$= \frac{1}{\ell^2} \delta\varepsilon \cdot \vec{E}_o + \frac{\delta\varepsilon}{\ell_o} \vec{\nabla} \cdot \vec{E}_o$$

and because $\vec{E}_o$ satisfies the condition $\vec{\nabla} \vec{E}_o = 0$ (absence of electric sources in the scattering volume), the term $\nabla^2 (\vec{E}_o \cdot \vec{\nabla}\delta\varepsilon)$ is of the order $\frac{1}{\ell_o^2} \delta\varepsilon \cdot \vec{E}_o$. If $\lambda << \ell_o$, then:-

$$k^2 \delta\varepsilon \cdot \vec{E}_o = \frac{4\pi^2}{\lambda^2} \delta\varepsilon \cdot \vec{E}_o >> \frac{1}{\ell_o^2} \delta\varepsilon \vec{E}_o$$

and the last term in (II.7) can be also dropped, thus giving:-

$$(\nabla^2 + k^2) \vec{E}_s = - k^2 \delta\varepsilon \cdot \vec{E}_o \qquad \text{(II.8)}$$

APPENDIX III

DETERMINATION OF THE STATIC STABILITY IN THE ATMOSPHERIC LAYER BETWEEN GROUND AND 850 mb LEVEL BY MEANS OF A TEPHIGRAM

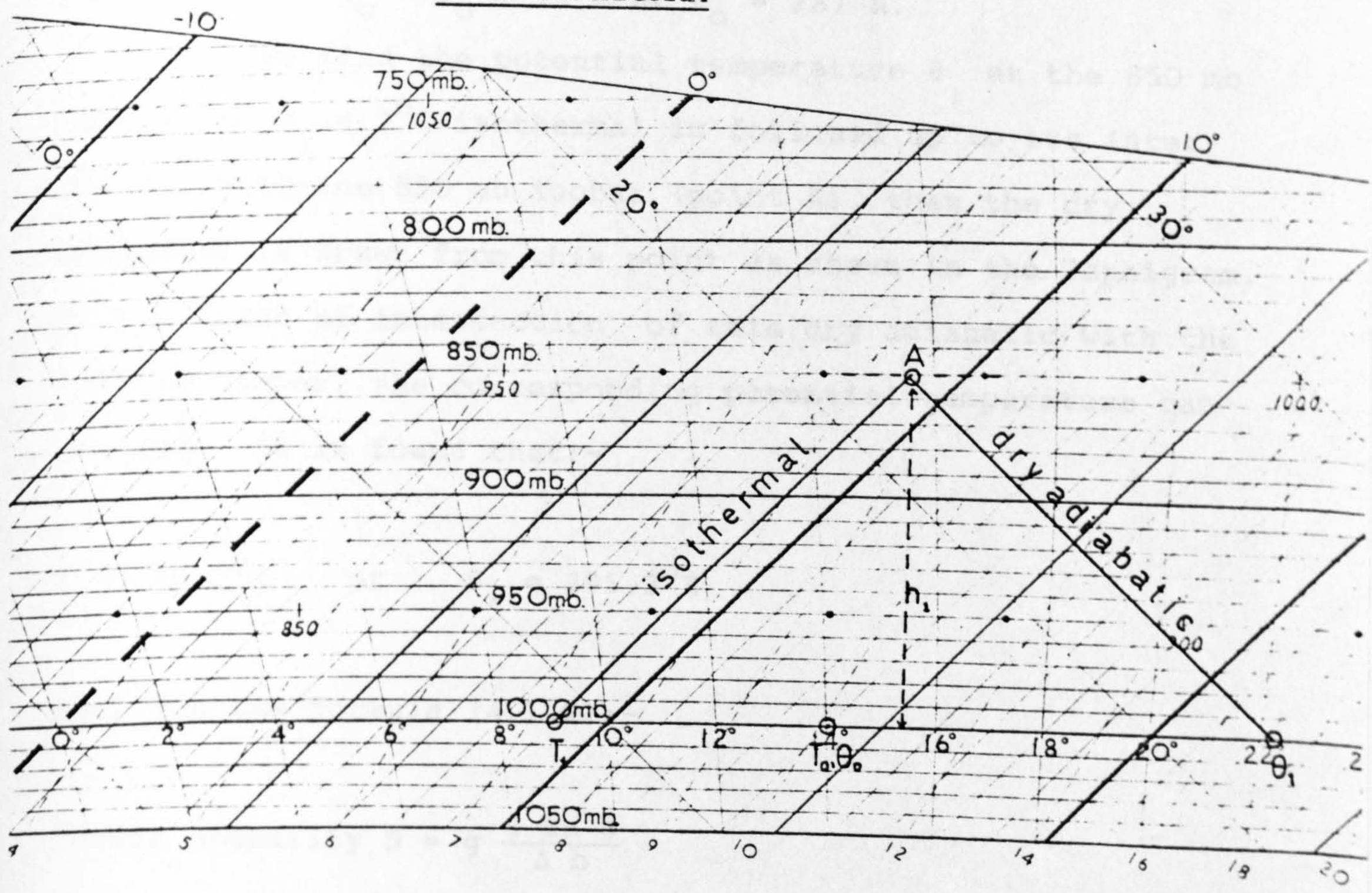

TEPHIGRAM

EXPLANATIONS

1. The basic co-ordinates are temperature and entropy.

2. ISOTHERMALS are straight lines running diagonally upwards from left to right.

3. ISENTROPES are also DRY ADIABATICS and lines of constant potential temperature. They run diagonally upwards from right to left, and are designated by the dry-bulb temperature, which is the temperature at the point of intersection with the 1000 mb. isobar.

4. ISOBARS are slightly curved and nearly horizontal lines. The heights in feet and metres which correspond to their respective pressures in the I.C.A.O. Standard Atmosphere are printed along the left-hand edge of the diagram.

On 24th April, 1975 at 12.00 h the Daily Aerological Record reported for the meteorological station at Crawley:-

Ground Temperature T_o = 14°C

Temperature at 850 mb level T_1 = 9°C

Height of the 850 mb isobar h_1 = 1619m

The potential temperature at ground level can be considered, with negligible error, as equal to the ambient temperature: $\theta_o \simeq T_o = 14^oC$ or $\theta_o = 287^oK$.

To find the potential temperature θ_1 at the 850 mb level, the $T_1 = 9^oC$ isothermal is followed up to its intersection with the 850 mb isobar (point A), then the dry adiabatic is drawn from this point as shown in the Tephigram. At the point of intersection of this dry adiabatic with the 1000 mb isobar, the corresponding potential temperature can be read. It is found that:-

$\theta_1 = 22.3^oC$ or $\theta_1 = 295.3^oK$

Applying the formula (4.1.2):-

$$\text{Static stability } S = g \frac{\Delta \ln \theta}{\Delta h}$$

for $\Delta \ln \theta = \ln \theta_1 - \ln \theta_o$ and $\Delta h = h_1$, the static stability in the atmospheric layer under consideration is found to be $S = 17.24 \times 10^{-5} \text{ sec}^{-2}$.

APPENDIX IV

LIST OF COMPUTER PROGRAMS AND SUBROUTINES

```
      PROGRAM DATTAP(TAPE5.OUTPUT.TAPE6=OUTPUT.TAPE62)                          DATTAP     2
      DIMENSION TROPO(1050).XDATA(10)                                           DATTAP     3
      CALL START(2)                                                             DATTAP     4
      CALL PEN(1)                                                               DATTAP     5
      NP=1050                                                                   DATTAP     6
      NOP=0                                                                     DATTAP     7
C                                                                               DATTAP     8
C  THIS IS THE MAIN ROUTINE TO PREPARE THE TROPO DATA FOR THE CALCOMP PL        DATTAP     9
C  PREPARE ARRAY TO STORE DATA                                                  DATTAP    10
C CLEAR ARRAY TROPO                                                             DATTAP    11
      DO 10 K=1.1050                                                            DATTAP    12
   10 TROPO(K)=0.0                                                              DATTAP    13
C                                                                               DATTAP    14
C READ ALL THE DATA INTO TROPO                                                  DATTAP    15
      DO 11 I=1.1041.10                                                         DATTAP    16
      J=I+9                                                                     DATTAP    17
      READ (5.100) XDATA                                                        DATTAP    18
  100 FORMAT (F5.3.2X)                                                          DATTAP    19
      L=0                                                                       DATTAP    20
      DO 12 K=I.J                                                               DATTAP    21
      L=L+1                                                                     DATTAP    22
      TROPO(K)=XDATA(L)                                                         DATTAP    23
   12 CONTINUE                                                                  DATTAP    24
   11 CONTINUE                                                                  DATTAP    25
C                                                                               DATTAP    26
C FIND THE MAX ELEMENT IN THE TROPO DATA                                        DATTAP    27
      BIG=TROPO(1)                                                              DATTAP    28
      DO 13 K=2.1050                                                            DATTAP    29
      IF (TROPO(K).GT.BIG) BIG=TROPO(K)                                         DATTAP    30
   13 CONTINUE                                                                  DATTAP    31
      WRITE (6.200) BIG                                                         DATTAP    32
  200 FORMAT (1H0.23H MAX ELEMENT EQUALS     .F5.3)                             DATTAP    33
C                                                                               DATTAP    34
C NORMALISING THE TROPO DATA TO THE MAX ELEMENT                                 DATTAP    35
      DO 14 K=1.1050                                                            DATTAP    36
   14 TROPO(K)=TROPO(K)/BIG                                                     DATTAP    37
C                                                                               DATTAP    38
C CALL THE CALCOMP SUBROUTINE                                                   DATTAP    39
      CALL ARYPLO (TROPO.NP.NOP)                                                DATTAP    40
C                                                                               DATTAP    41
C TO END PLOT                                                                   DATTAP    42
      CALL ENPLOT (10.5)                                                        DATTAP    43
      STOP                                                                      DATTAP    44
      END                                                                       DATTAP    45
```

```
      SUBROUTINE ARYPLO (TROPO,NP,NOP)                                  ARYPLO     2
C THIS IS A SUBROUTINE TO PLOT THE SAMPLED TROPO DATA                   ARYPLO     3
      DIMENSION TROPO(NP)                                               ARYPLO     4
C TO ESTABLISH PAGE ORIGIN                                              ARYPLO     5
C                                                                       ARYPLO     6
      NOPY=1+NOP-3*(NOP/3)                                              ARYPLO     7
      IF (NOP.EQ.0) GO TO 500                                           ARYPLO     8
      IF (NOPY.EQ.1) GO TO 502                                          ARYPLO     9
      GO TO 501                                                         ARYPLO    10
  500 CALL PLOT (0.0,1.0,3)                                             ARYPLO    11
      CALL PLOT (0.0,1.0,-1)                                            ARYPLO    12
      GO TO 503                                                         ARYPLO    13
  501 CALL PLOT (0.0,9.0,3)                                             ARYPLO    14
      CALL PLOT (0.0,9.0,-1)                                            ARYPLO    15
      GO TO 503                                                         ARYPLO    16
  502 CALL PLOT (10.5,-18.0,3)                                          ARYPLO    17
      CALL PLOT (10.5,-18.0,-1)                                         ARYPLO    18
  503 NOP=NOP+1                                                         ARYPLO    19
C                                                                       ARYPLO    20
C TO DRAW A RECTANGLE 8 BY 10 INCHES.                                   ARYPLO    21
      CALL PLOT (0.0,8.0,2)                                             ARYPLO    22
      CALL PLOT (10.0,8.0,2)                                            ARYPLO    23
      CALL PLOT (10.0,0.0,2)                                            ARYPLO    24
      CALL PLOT (0.0,0.0,2)                                             ARYPLO    25
C                                                                       ARYPLO    26
C TO DRAW AXES WITH ORIGIN AT 0.75,1.0                                  ARYPLO    27
      CALL PLOT (0.75,6.0,3)                                            ARYPLO    28
      CALL PLOT (0.75,1.0,2)                                            ARYPLO    29
      CALL PLOT (9.75,1.0,2)                                            ARYPLO    30
C                                                                       ARYPLO    31
C TO SCALE AND MARK THE OX AXIS                                         ARYPLO    32
C TO MARK OFF THE OX AXIS IN STEPS OF 50                                ARYPLO    33
C                                                                       ARYPLO    34
      XINT=9.0/1050.0                                                   ARYPLO    35
      DO 15 K=1,1051,50                                                 ARYPLO    36
      SP=K-1                                                            ARYPLO    37
      XMARK=XINT*SP                                                     ARYPLO    38
      CALL PLOT (0.75+XMARK,1.0,3)                                      ARYPLO    39
      CALL PLOT (0.75+XMARK,0.9,2)                                      ARYPLO    40
      CALL NUMBER (XMARK+0.6,1.0,7.0,12,SP,0.0,-1)                      ARYPLO    41
   15 CONTINUE                                                          ARYPLO    42
C                                                                       ARYPLO    43
C TO SCALE AND MARK OY AXIS                                             ARYPLO    44
      DO 25 K=1,11                                                      ARYPLO    45
      SP=K-1                                                            ARYPLO    46
      ORDN=0.10*SP                                                      ARYPLO    47
      YMARK=1.0+0.5*SP                                                  ARYPLO    48
      CALL PLOT (0.75,YMARK,3)                                          ARYPLO    49
      CALL PLOT (0.65,YMARK,2)                                          ARYPLO    50
      CALL NUMBER (0.36,YMARK-0.05,0.12,ORDN,0.0,1)                     ARYPLO    51
   25 CONTINUE                                                          ARYPLO    52
C                                                                       ARYPLO    53
C TO PLOT THE FADING CHARACTERISTIC OF THE DATA SAMPLES                 ARYPLO    54
      Y1=1.0+5.0*TROPO(1)                                               ARYPLO    55
      XINT=9.0/1050.0                                                   ARYPLO    56
      CALL PLOT (0.75+XINT,Y1,3)                                        ARYPLO    57
      DO 17 K=2,NP                                                      ARYPLO    58
      RN=K                                                              ARYPLO    59
      XN=0.75+XINT*RN                                                   ARYPLO    60
      YN=1.0+5.0*TROPO(K)                                               ARYPLO    61
      CALL PLOT (XN,YN,2)                                               ARYPLO    62
   17 CONTINUE                                                          ARYPLO    63
C                                                                       ARYPLO    64
C DRAW TITLE AND LABEL AXES                                             ARYPLO    65
      CALL SYMBOL (1.6,6.5,0.15,53HTHE SAMPLED FADING CHARACTERISTIC OF ARYPLO    66
     1 1050 SAMPLES NO.,0.0,53)                                         ARYPLO    67
C TO LABEL OX                                                           ARYPLO    68
      CALL SYMBOL (4.4,0.35,0.15,17HNUMBER OF SAMPLES,0.0,17)           ARYPLO    69
C                                                                       ARYPLO    70
C TO LABEL OY                                                           ARYPLO    71
      CALL SYMBOL (0.27,2.3,0.15,20HNORMALISED AMPLITUDE,90.0,20)       ARYPLO    72
C                                                                       ARYPLO    73
      RETURN                                                            ARYPLO    74
      END                                                               ARYPLO    75
```

```
      PROGRAM DATPOW(TAPE5.OUTPUT.TAPE6=OUTPUT.TAPE62)                          DATPOW     2
C                                                                               DATPOW     3
C    THIS IS THE MAIN PROGRAM FOR THE ESTIMATION AND PLOTTING OF                DATPOW     4
C      THE FADING SPECTRUM ON LINEAR AXES.                                      DATPOW     5
C                                                                               DATPOW     6
C                                                                               DATPOW     7
      DIMENSION XREAL(1024).XIMAG(1024).STOR3(257).XDATA(10).SDATA(1024)        DATPOW     8
     1.HDATA(502)                                                               DATPOW     9
      CALL START(2)                                                             DATPOW    10
      CALL PEN(1)                                                               DATPOW    11
      NOP=0                                                                     DATPOW    12
      N=1024                                                                    DATPOW    13
      PI=3.141592                                                               DATPOW    14
      NENTRY=1                                                                  DATPOW    15
      INVERT=2                                                                  DATPOW    16
C CLEAR XREAL AND XIMAG                                                         DATPOW    17
      DO 10 K=1.1024                                                            DATPOW    18
      XREAL(K)=0.0                                                              DATPOW    19
      XIMAG(K)=0.0                                                              DATPOW    20
   10 SDATA(K)=0.0                                                              DATPOW    21
      DO 603 I=1.10                                                             DATPOW    22
      XDATA(I)=0.0                                                              DATPOW    23
  603 CONTINUE                                                                  DATPOW    24
C READ DATA INTO XREAL                                                          DATPOW    25
      DO 11 I=1.1011.10                                                         DATPOW    26
      J=I+9                                                                     DATPOW    27
      READ (5.100) XDATA                                                        DATPOW    28
  100 FORMAT (F5.3.2X)                                                          DATPOW    29
      L=0                                                                       DATPOW    30
      DO 12 K=I.J                                                               DATPOW    31
      L=L+1                                                                     DATPOW    32
      XREAL(K)=XDATA(L)                                                         DATPOW    33
   12 CONTINUE                                                                  DATPOW    34
   11 CONTINUE                                                                  DATPOW    35
      READ (5.101) (XDATA(I).I=1.4)                                             DATPOW    36
  101 FORMAT (F5.3.2X)                                                          DATPOW    37
      L=0                                                                       DATPOW    38
      DO 13 K=1021.1024                                                         DATPOW    39
      L=L+1                                                                     DATPOW    40
      XREAL(K)=XDATA(L)                                                         DATPOW    41
   13 CONTINUE                                                                  DATPOW    42
C                                                                               DATPOW    43
C     TO REMOVE THE MEAN VALUE AND THE LINEAR TRENDS FROM THE ORIGINAL          DATPOW    44
C     TIME SERIES.                                                              DATPOW    45
C                                                                               DATPOW    46
      CALL REGRE (XREAL.N)                                                      DATPOW    47
C                                                                               DATPOW    48
C     TO APPLY A HAMMING DATA WINDOW.                                           DATPOW    49
C                                                                               DATPOW    50
      CALL TAPER (XREAL.N.PI)                                                   DATPOW    51
C                                                                               DATPOW    52
C     TO APPLY THE FOURIER TRANSFORM.                                           DATPOW    53
C                                                                               DATPOW    54
      CALL FASTF(XREAL.XIMAG.N)                                                 DATPOW    55
      DO 21 K=1.1024                                                            DATPOW    56
      SDATA(K)=XREAL(K)**2+XIMAG(K)**2                                          DATPOW    57
   21 CONTINUE                                                                  DATPOW    58
      H=0.0                                                                     DATPOW    59
      DO 24 K=1.11                                                              DATPOW    60
      H=H+SDATA(K)                                                              DATPOW    61
   24 CONTINUE                                                                  DATPOW    62
      HDATA(1)=H/11.0                                                           DATPOW    63
      R=H                                                                       DATPOW    64
      DO 25 K=1.501                                                             DATPOW    65
      R=R-SDATA(K)+SDATA(K+11)                                                  DATPOW    66
      HDATA(K+1)=R/11.0                                                         DATPOW    67
   25 CONTINUE                                                                  DATPOW    68
C TO TAKE THE SQRT OF HDATA                                                     DATPOW    69
      DO 26 K=1.502                                                             DATPOW    70
      HDATA(K)=SQRT(HDATA(K))                                                   DATPOW    71
   26 CONTINUE                                                                  DATPOW    72
C TO NORMALISE HDATA                                                            DATPOW    73
      BIG=HDATA(1)                                                              DATPOW    74
      DO 27 K=2.502                                                             DATPOW    75
      IF (HDATA'K).GT.BIG) BIG=HDATA(K)                                         DATPOW    76
```

```
   27 CONTINUE                                                          DATPOW     77
      DO 28 K=1.502                                                     DATPOW     78
   28 HDATA(K)=HDATA(K)/BIG                                             CATPOW     79
C                                                                       JATPOW     80
C       TO PLOT THE NORMALIZED FADING SPECTRUM ON LINEAR AXES.          DATPOW     81
C                                                                       DATPOW     82
      CALL POWPLO (HDATA,NOP)                                           DATPOW     83
C TO END PLOT                                                           DATPOW     84
      CALL ENPLOT (10.5)                                                DATPOW     85
      STOP                                                              DATPOW     86
      END                                                               DATPOW     87


      SUBROUTINE REGRE (XREAL,N)                                        REGRE      2
C                                                                       REGRE      3
C       THIS IS THE SUBROUTINE FOR THE REMOVAL OF THE MEAN AND THE      REGRE      4
C       LINEAR TRENDS.                                                  REGRE      5
C                                                                       REGRE      6
C                                                                       REGRE      7
      DIMENSION XREAL(1024),XIMAG(1024),STOR3(257),XDATA(10),SDATA(1024) REGRE      8
     1,HDATA(502)                                                       REGRE      9
C SUM SEQUENTIAL NUMBER 0 TO 1023 AND AVERAGE                           REGRE      10
      L=0                                                               REGRE      11
      DO 14 K=1,1023                                                    REGRE      12
      L=L+K                                                             REGRE      13
   14 CONTINUE                                                          REGRE      14
      AS=FLOAT(L)/1024.0                                                REGRE      15
C SUM ALL DATA AND AVERAGE                                              REGRE      16
      SUM=0.0                                                           REGRE      17
      DO 15 K=1,N                                                       REGRE      18
      SUM=SUM+XREAL(K)                                                  REGRE      19
   15 CONTINUE                                                          REGRE      20
      ASUM=SUM/1024.0                                                   REGRE      21
C SUM OF SQUARES OF THE SEQUENTIAL NUMBER AND AVERAGE                   REGRE      22
      M=0                                                               REGRE      23
      DO 16 K=1,1023                                                    REGRE      24
      M=M+K**2                                                          REGRE      25
   16 CONTINUE                                                          REGRE      26
      ASQ=FLOAT(M)/1024.0                                               REGRE      27
C SUM OF PRODUCTS OF SEQUENTIAL NUMBER AND DATA AMPLITUDE AND AVERAGE   REGRE      28
      P=0.0                                                             REGRE      29
      DO 17 K=1,N                                                       REGRE      30
      A=FLOAT(K)-1.0                                                    REGRE      31
      P=P+A*XREAL(K)                                                    REGRE      32
   17 CONTINUE                                                          REGRE      33
      AP=P/1024.0                                                       REGRE      34
C TO FIND THE REGRESSION SLOPE                                          REGRE      35
      U=AP-ASUM*AS                                                      REGRE      36
      D=ASQ-AS**2                                                       REGRE      37
C THE REGRESSION CURVE                                                  REGRE      38
      SLOPE=U/D                                                         REGRE      39
      C=ASUM-SLOPE*AS                                                   REGRE      40
      DO 18 K=1,1024                                                    REGRE      41
      V=FLOAT(K)-1.0                                                    REGRE      42
      Y=SLOPE*V+C                                                       REGRE      43
      XREAL(K)=XREAL(K)-Y                                               REGRE      44
   18 CONTINUE                                                          REGRE      45
      RETURN                                                            REGRE      46
      END                                                               REGRE      47


      SUBROUTINE TAPER (XREAL,N,PI)                                     TAPER      2
C                                                                       TAPER      3
C       THIS IS THE SUBROUTINE FOR THE APPLICAION OF A HAMMING WINDOW.  TAPER      4
C                                                                       TAPER      5
C                                                                       TAPER      6
      DIMENSION XREAL(1024),XIMAG(1024),STOR3(257),XDATA(10),SDATA(1024) TAPER      7
     1,HDATA(502)                                                       TAPER      8
      DO 19 K=1,1024                                                    TAPER      9
      V=FLOAT(K)-1.0                                                    TAPER      10
      H=0.08+0.46(1.0-COS(2*PI*V/N))                                    TAPER      11
      XREAL(K)=XREAL(K)*H                                               TAPER      12
   19 CONTINUE                                                          TAPER      13
      RETURN                                                            TAPER      14
      END                                                               TAPER      15
```

```
      SUBROUTINE FASTF(XREAL,XIMAG,ISIZE)                                    FASTF     2
C                                                                            FASTF     3
C THIS IS THE FOURIER TRANSFORM SUBROUTINE.                                  FASTF     4
C                                                                            FASTF     5
C                                                                            FASTF     6
      REAL XREAL(1),XIMAG(1)                                                 FASTF     7
      INTEGER L(12)                                                          FASTF     8
      EQUIVALENCE(L1,L(1)),(L2,L(2)),(L3,L(3)),(L4,L(4)),(L5,L(5)),          FASTF     9
     1(L6,L(6)),(L7,L(7)),(L8,L(8)),(L9,L(9)),(L10,L(10)),(L11,L(11)),       FASTF    10
     2(L12,L(12))                                                            FASTF    11
      PIE2=8.*ATAN(1.)                                                       FASTF    12
      N=IABS(ISIZE)                                                          FASTF    13
      IF(N-4)14,11,11                                                        FASTF    14
   11 IFACC=1                                                                FASTF    15
      IFACA=N/4                                                              FASTF    16
      IF(ISIZE)62,12,12                                                      FASTF    17
   62 DO 17 K=1,N                                                            FASTF    18
   17 XIMAG(K)=-XIMAG(K)                                                     FASTF    19
   12 ITIME=0                                                                FASTF    20
   16 IFCAB=IFACA*4                                                          FASTF    21
      ITIME=ITIME+2                                                          FASTF    22
      DO 80 LITLA=1,IFACA                                                    FASTF    23
      DO 82 IO=LITLA,N,IFCAB                                                 FASTF    24
      I1=IO+IFACA                                                            FASTF    25
      I2=I1+IFACA                                                            FASTF    26
      I3=I2+IFACA                                                            FASTF    27
      XSO=XREAL(IO)+XREAL(I2)                                                FASTF    28
      XS1=XREAL(IO)-XREAL(I2)                                                FASTF    29
      YSO=XIMAG(IO)+XIMAG(I2)                                                FASTF    30
      YS1=XIMAG(IO)-XIMAG(I2)                                                FASTF    31
      XS2=XREAL(I1)+XREAL(I3)                                                FASTF    32
      XS3=XREAL(I1)-XREAL(I3)                                                FASTF    33
      YS2=XIMAG(I1)+XIMAG(I3)                                                FASTF    34
      YS3=XIMAG(I1)-XIMAG(I3)                                                FASTF    35
      XREAL(IO)=XSO+XS2                                                      FASTF    36
      XIMAG(IO)=YSO+YS2                                                      FASTF    37
      X1=XS1+YS3                                                             FASTF    38
      Y1=YS1-XS3                                                             FASTF    39
      X2=XSO-XS2                                                             FASTF    40
      Y2=YSO-YS2                                                             FASTF    41
      X3=XS1-YS3                                                             FASTF    42
      Y3=YS1+XS3                                                             FASTF    43
      IF(LITLA-1)14,66,64                                                    FASTF    44
   66 XREAL(I2)=X1                                                           FASTF    45
      XIMAG(I2)=Y1                                                           FASTF    46
      XREAL(I1)=X2                                                           FASTF    47
      XIMAG(I1)=Y2                                                           FASTF    48
      XREAL(I3)=X3                                                           FASTF    49
      XIMAG(I3)=Y3                                                           FASTF    50
      GO TO 82                                                               FASTF    51
   64 XREAL(I2)=X1*CW1+Y1*SW1                                                FASTF    52
      XIMAG(I2)=Y1*CW1-X1*SW1                                                FASTF    53
      XREAL(I1)=X2*CW2+Y2*SW2                                                FASTF    54
      XIMAG(I1)=Y2*CW2-X2*SW2                                                FASTF    55
      XREAL(I3)=X3*CW3+Y3*SW3                                                FASTF    56
      XIMAG(I3)=Y3*CW3-X3*SW3                                                FASTF    57
   82 CONTINUE                                                               FASTF    58
      IF(LITLA-IFACA)65,80,14                                                FASTF    59
   65 CW1=COS(PIE2*FLOAT(LITLA)/FLOAT(IFCAB))                                FASTF    60
      Z=1.-CW1*CW1                                                           FASTF    61
      SW1=SQRT(Z)                                                            FASTF    62
      CW2=CW1*CW1-Z                                                          FASTF    63
      SW2=2.*CW1*SW1                                                         FASTF    64
      CW3=CW1*CW2-SW1*SW2                                                    FASTF    65
      SW3=CW1*SW2+CW2*SW1                                                    FASTF    66
   80 CONTINUE                                                               FASTF    67
      IF(IFACA-1)21,21,67                                                    FASTF    68
   67 IFACC=IFACC*4                                                          FASTF    69
      IFACA=IFACA/4                                                          FASTF    70
      IF(IFACA)14,68,16                                                      FASTF    71
   68 DO 40 K=1,N,2                                                          FASTF    72
      TEMPR=XREAL(K)+XREAL(K+1)                                              FASTF    73
      XREAL(K+1)=XREAL(K)-XREAL(K+1)                                         FASTF    74
      XREAL(K)=TEMPR                                                         FASTF    75
```

```
      XIMAG(K+1)=XIMAG(K)-XIMAG(K+1)
   40 XIMAG(K)=TEMPR
      ITIME=ITIME+1
   21 IF(ISIZE)69,166,18
   69 DO 19 K=1,N
   19 XIMAG(K)=-XIMAG(K)
      GO TO 166
   18 Z=N
      DO 177 K=1,N
      XREAL(K)=XREAL(K)/Z
  177 XIMAG(K)=XIMAG(K)/Z
  166 II=1
      DO 101 K=1,ITIME
      II=II*2
  101 L(K)=II
      DO 102 K=ITIME,11
  102 L(K+1)=1
      II=1
      DO 103 J1=1,2
      DO 103 J2=J1,L2,L1
      DO 103 J3=J2,L3,L2
      DO 103 J4=J3,L4,L3
      DO 103 J5=J4,L5,L4
      DO 103 J6=J5,L6,L5
      DO 103 J7=J6,L7,L6
      DO 103 J8=J7,L8,L7
      DO 103 J9=J8,L9,L8
      DO 103 J10=J9,L10,L9
      DO 103 J11=J10,L11,L10
      DO 103 J12=J11,L12,L11
      IF(II-J12)108,103,103
  108 TEMPR=XREAL(II)
      XREAL(II)=XREAL(J12)
      XREAL(J12)=TEMPR
      TEMPR=XIMAG(II)
      XIMAG(II)=XIMAG(J12)
      XIMAG(J12)=TEMPR
  103 II=II+1
   14 RETURN
      END
```

```
FASTF      77
FASTF      78
FASTF      79
FASTF      80
FASTF      81
FASTF      82
FASTF      83
FASTF      84
FASTF      85
FASTF      86
FASTF      87
FASTF      88
FASTF      89
FASTF      90
FASTF      91
FASTF      92
FASTF      93
FASTF      94
FASTF      95
FASTF      96
FASTF      97
FASTF      98
FASTF      99
FASTF     100
FASTF     101
FASTF     102
FASTF     103
FASTF     104
FASTF     105
FASTF     106
FASTF     107
FASTF     108
FASTF     109
FASTF     110
FASTF     111
FASTF     112
FASTF     113
FASTF     114
FASTF     115
FASTF     116
```

```
      SUBROUTINE POWPLO (HDATA,NOP)                                          POWPLO     2
C                                                                            POWPLO     3
C       THIS IS THE SUBROUTINE FOR THE PLOTTING OF THE FADING SPECTRUM.      POWPLO     4
C                                                                            POWPLO     5
C                                                                            POWPLO     6
      DIMENSION HDATA(502)                                                   POWPLO     7
C TO ESTABLISH PAGE ORIGIN                                                   POWPLO     8
      NOPY=1+NOP-3*(NOP/3)                                                   POWPLO     9
      IF (NOP.EQ.0) GO TO 500                                                POWPLO    10
      IF (NOPY.EQ.1) GO TO 502                                               POWPLO    11
      GO TO 501                                                              POWPLO    12
  500 CALL PLOT (0.0,1.0,3)                                                  POWPLO    13
      CALL PLOT (0.0,1.0,-1)                                                 POWPLO    14
      GO TO 503                                                              POWPLO    15
  501 CALL PLOT (0.0,9.0,3)                                                  POWPLO    16
      CALL PLOT (0.0,9.0,-1)                                                 POWPLO    17
      GO TO 503                                                              POWPLO    18
  502 CALL PLOT (10.5,-18.0,3)                                               POWPLO    19
      CALL PLOT (10.5,-18.0,-1)                                              POWPLO    20
  503 NOP=NOP+1                                                              POWPLO    21
C                                                                            POWPLO    22
C TO DRAW A RECTANGLE 8 BY 10 INCHES.                                        POWPLO    23
      CALL PLOT (0.0,8.0,2)                                                  POWPLO    24
      CALL PLOT (10.0,8.0,2)                                                 POWPLO    25
      CALL PLOT (10.0,0.0,2)                                                 POWPLO    26
      CALL PLOT (0.0,0.0,2)                                                  POWPLO    27
C                                                                            POWPLO    28
C TO DRAW AXES WITH ORIGIN AT (1.25,1.0)                                     POWPLO    29
      CALL PLOT (1.25,6.0,3)                                                 POWPLO    30
      CALL PLOT (1.25,1.0,2)                                                 POWPLO    31
      CALL PLOT (9.25,1.0,2)                                                 POWPLO    32
C                                                                            POWPLO    33
C TO SCALE AND MARK THE OX AXIS.                                             POWPLO    34
C                                                                            POWPLO    35
C THE 8 INCHES OX AXIS REPRESENTS 2.0 CYCLES FREQUENCY WITH 1.0 INCH         POWPLO    36
C REPRESENTING 0.25 CYCLE/SECOND.                                            POWPLO    37
      XINT=2.0/8.0                                                           POWPLO    38
      E=0.0                                                                  POWPLO    39
      DO 30 K=1,9                                                            POWPLO    40
      IF (K.LE.1) GO TO 400                                                  POWPLO    41
      E=E+1.0                                                                POWPLO    42
  400 FINT=XINT*E                                                            POWPLO    43
      XMARK=K-1                                                              POWPLO    44
      CALL PLOT (1.25+XMARK,1.0,3)                                           POWPLO    45
      CALL PLOT (1.25+XMARK,0.9,2)                                           POWPLO    46
      CALL NUMBER (XMARK+1.05,0.7,0.12,FINT,0.0,2)                           POWPLO    47
   30 CONTINUE                                                               POWPLO    48
C                                                                            POWPLO    49
C TO SCALE AND MARK OY AXIS (NORMALISED SCALE)                               POWPLO    50
      DO 25 K=1,11                                                           POWPLO    51
      SP=K-1                                                                 POWPLO    52
      ORDN=0.10*SP                                                           POWPLO    53
      YMARK=1.0+0.5*SP                                                       POWPLO    54
      CALL PLOT (1.25,YMARK,3)                                               POWPLO    55
      CALL PLOT (1.15,YMARK,2)                                               POWPLO    56
      CALL NUMBER (0.86,YMARK-0.05,0.12,ORDN,0.0,1)                          POWPLO    57
   25 CONTINUE                                                               POWPLO    58
C                                                                            POWPLO    59
C TO PLOT THE SPECTRUM                                                       POWPLO    60
C SINCE THE 8 INCHES OX AXIS REPRESENTS 2.0 CYCLES,SO THIS GIVES 408.8       POWPLO    61
C DIVISIONS OR 409 LINES IN THE UNFILTERED SPECTRUM.                         POWPLO    62
      Y1=1.0+5.0*HDATA(1)                                                    POWPLO    63
      XINT=8.0/408.0                                                         POWPLO    64
      XXINT=5.0*XINT                                                         POWPLO    65
      CALL PLOT (1.25+XXINT,Y1,3)                                            POWPLO    66
      DO 29 K=6,408                                                          POWPLO    67
      RN=K                                                                   POWPLO    68
      NR=K-4                                                                 POWPLO    69
      XN=1.25+XINT*RN                                                        POWPLO    70
      YN=1.0+5.0*HDATA(NR)                                                   POWPLO    71
      CALL PLOT (XN,YN,2)                                                    POWPLO    72
   29 CONTINUE                                                               POWPLO    73
C                                                                            POWPLO    74
C DRAW TITLE AND LABEL AXES                                                  POWPLO    75
      CALL SYMBOL (3.0,6.5,0.15,31HTHE POWER SPECTRUM FOR DATA-NO.,0.0,3)    POWPLO    76
```

```
     1 1)                                                                    POWPLO     77
C                                                                            POWPLO     78
C TO LABEL OX                                                                POWPLO     79
      CALL SYMBOL (3.0.0.35.0.15.30HFREQUENCY IN CYCLES PER SECOND.0.0.3     POWPLO     80
     1 0)                                                                    POWPLO     81
C                                                                            POWPLO     82
C  TO LABEL   OY                                                            POWPLO     83
      CALL  SYMBOL  (0.65.2.3.0.15.20HNORMALISED AMPLITUDE.90.0.20)          POWPLO     84
      RETURN                                                                 POWPLO     85
      END                                                                    POWPLO     86
```

```
      PROGRAM LOGPLO (INPUT.OUTPUT.TAPE5=INPUY.TAPE62)                       LOGPLO     2
C                                                                            LOGPLO     3
C     THIS IS THE PROGRAM FOR THE PLOTTING OF 30 POWER SPECTRAL ESTIMATES    LOGPLO     4
C     ON LOGARITHMIC AXES AND THE FITTING OF THE BEST POLYNOMIAL.            LOGPLO     5
C                                                                            LOGPLO     6
C                                                                            LOGPLO     7
      COMMON X(120).Y(120).XA(120).YA(120).XB(100).YB(100).W(30).SI(6).       LOGPLO     8
     7 P(6)                                                                  LOGPLO     9
      CALL START(2)                                                          LOGPLO     10
         CALL SCALEZ(1.)                                                     LOGPLO     11
      CALL BORDOFF                                                           LOGPLO     12
      CALL NEWPAGE                                                           LOGPLO     13
      DO 1 K=1.12                                                            LOGPLO     14
      KA=(K-1)*10+1                                                          LOGPLO     15
      KB=K*10                                                                LOGPLO     16
    1 READ(5.1000)(Y(I).I=KA.KB)                                             LOGPLO     17
 1000 FORMAT(10(F5.3.3X))                                                    LOGPLO     18
      DO 2 I=1.20                                                            LOGPLO     19
    2 X(I)=FLOAT(I)*0.05                                                     LOGPLO     20
      DO 3 I=21.30                                                           LOGPLO     21
    3 X(I)=FLOAT(I-20)*0.1+1.                                                LOGPLO     22
      DO 12 I=1.30                                                           LOGPLO     23
      X(I+30)=X(I)                                                           LOGPLO     24
      X(I+60)=X(I)                                                           LOGPLO     25
   12 X(I+90)=X(I)                                                           LOGPLO     26
C     TO DRAW THE LOGARITHMIC AXES.                                          LOGPLO     27
      HOR=6.                                                                 LOGPLO     28
      VER=6.                                                                 LOGPLO     29
      CALL LOGAX(2.0.2.0.1.HOR.3.-2.1.2.1)                                   LOGPLO     30
      CALL LOGAX(2.0.2.0.2.VER.2.-2.2.1.1)                                   LOGPLO     31
      DO 4 I=1.120                                                           LOGPLO     32
    4 CALL LOCATE(X(I).Y(I).XA(I).YA(I).1)                                   LOGPLO     33
      DO 5 I=1.30                                                            LOGPLO     34
      YB(I)=(YA(I)+YA(I+30)+YA(I+60)+YA(I+90))/4.                            LOGPLO     35
    5 W(I)=1.                                                                LOGPLO     36
      IA=6                                                                   LOGPLO     37
C     TO FIND THE BEST FITTING POLYNOMIAL.                                   LOGPLO     38
      CALL E02ABF(30.XA.YB.W.IA.NA.SI.P..TRUE.)                              LOGPLO     39
      DO 6 I=1.100                                                           LOGPLO     40
      XB(I)=XA(I)+(XA(30)-XA(1))*FLOAT(I-1)/99.                              LOGPLO     41
    6 YB(I)=P(1)+P(2)*XB(I)+P(3)*XB(I)**2+P(4)*XB(I)**3+P(5)*XB(I)**4        LOGPLO     42
     7+P(6)*XB(I)**5                                                         LOGPLO     43
      SIZ=0.09                                                               LOGPLO     44
      DO 7 I=1.120                                                           LOGPLO     45
      L=INT(FLOAT(I)/30.3)                                                   LOGPLO     46
C     TO PLOT THE  30 SPECTRAL ESTIMATES FROM EACH OF THE 4 TRIALS.          LOGPLO     47
    7 CALL SYMBOL(XA(I).YA(I).SIZ.L.0.0.-1)                                  LOGPLO     48
      CALL PLOT(XB(1).YB(1).3)                                               LOGPLO     49
      DO 8 I=1.99                                                            LOGPLO     50
    8 CALL PLOT(XB(I+1).YB(I+1).2)                                           LOGPLO     51
      CALL LOGAX(2.0.VER*2.+2..1.HOR.3.-2.-1.1.1)                            LOGPLO     52
      CALL LOGAX(HOR*3.+2..2.0.2.VER.2.-2.-1.2.1)                            LOGPLO     53
      CALL SYMBOL(8.2.0.65.0.35.16HFREQUENCY IN HZ..0.0.16)                  LOGPLO     54
      CALL SYMBOL(0.7.5.2.0.35.16HNORMALIZED POWER.90.0.16)                  LOGPLO     55
      DO 9 I=1.4                                                             LOGPLO     56
      CALL SYMBOL(3.0.5.0-FLOAT(I-1)/2.0.0.2.I-1.0.0.-1)                     LOGPLO     57
    9 CALL SYMBOL(3.2.4.9-FLOAT(I-1)/2.0.0.2.                                LOGPLO     58
     239H  TRIAL NO.    . WIND SPEED=      M/SEC..0.0.39)                    LOGPLO     59
      CALL SYMBOL(4.8.2.9.0.2.65HAVERAGE WIND SPEED=      M/SEC. . TEMPE     LOGPLO     60
     7RATURE GRADIENT=     C/CM..0.0.65)                                     LOGPLO     61
      CALL ENPLOT                                                            LOGPLO     62
      STOP                                                                   LOGPLO     63
      END                                                                    LOGPLO     64
```

```
      SUBROUTINE E02ABF(M,X,F,W,K1,N,SI,P,L)                                E02ABF     2
C                                                                           E02ABF     3
C     THIS IS THE SUBROUTINE FOR THE ESTIMATION OF THE BEST FITTING         E02ABF     4
C     POLYNOMIAL OF THE RIGHT DEGREE.                                       E02ABF     5
C                                                                           E02ABF     6
C                                                                           E02ABF     7
C     MARK 1 RELEASE.  NAG COPYRIGHT 1971                                   E02ABF     8
C     MARK 3 REVISED.                                                       E02ABF     9
C     MARK 4 REVISED. ER AM3-42                                             E02ABF    10
      DIMENSION X(M),F(M),W(M),SI(K1),P(K1)                                 E02ABF    11
      LOGICAL L                                                             E02ABF    12
      DIMENSION CTP(51),CPSAVE(51),CP(51),CLP(52)                           E02ABF    13
      DIMENSION XLP(450),TP(450),AL(51),BE(51),S(51)                        E02ABF    14
      K2=K1+1                                                               E02ABF    15
      K=K1-1                                                                E02ABF    16
      N=K                                                                   E02ABF    17
      DO 10 I=1,K1                                                          E02ABF    18
   10 CP(I)=0.0                                                             E02ABF    19
      BE(1)=0.0                                                             E02ABF    20
      CLP(2)=0.0                                                            E02ABF    21
      CLP(1)=0.0                                                            E02ABF    22
      DELSQ=0.0                                                             E02ABF    23
      OM=0.0                                                                E02ABF    24
      TW=0.0                                                                E02ABF    25
      SIMIN=0.0                                                             E02ABF    26
      ISWX=0                                                                E02ABF    27
      CTP(1)=1.0                                                            E02ABF    28
      ICOMP=1                                                               E02ABF    29
      DO 5 I=1,M                                                            E02ABF    30
      DELSQ=DELSQ+W(I)*F(I)**2                                              E02ABF    31
      TP(I)=1.0                                                             E02ABF    32
      XLP(I)=0.0                                                            E02ABF    33
      OM=OM+W(I)*F(I)                                                       E02ABF    34
    5 TW=TW+W(I)                                                            E02ABF    35
      S(1)=OM/TW                                                            E02ABF    36
      CP(1)=S(1)                                                            E02ABF    37
      DELSQ=DELSQ-S(1)*OM                                                   E02ABF    38
      XTEMP = M                                                             E02ABF    39
      SI(1) = ABS(DELSQ/(XTEMP - 1.0))                                      E02ABF    40
      A=4.0/(X(M)-X(1))                                                     E02ABF    41
      B=-2.0-A*X(1)                                                         E02ABF    42
      DO 11 I=1,M                                                           E02ABF    43
   11 X(I)=A*X(I)+B                                                         E02ABF    44
      DO 7 I=1,K                                                            E02ABF    45
      OU=0.0                                                                E02ABF    46
      DO 12 J=1,M                                                           E02ABF    47
   12 OU=OU+W(J)*X(J)*TP(J)**2                                              E02ABF    48
      AL(I+1)=OU/TW                                                         E02ABF    49
      XLW=TW                                                                E02ABF    50
      TW=0.0                                                                E02ABF    51
      OM=0.0                                                                E02ABF    52
      DO 4 J=1,M                                                            E02ABF    53
      OU=BE(I)*XLP(J)                                                       E02ABF    54
      XLP(J)=TP(J)                                                          E02ABF    55
      TP(J)=(X(J)-AL(I+1))*TP(J)-OU                                         E02ABF    56
      TW=TW+W(J)*TP(J)**2                                                   E02ABF    57
    4 OM=OM+W(J)*F(J)*TP(J)                                                 E02ABF    58
      BE(I+1)=TW/XLW                                                        E02ABF    59
      S(I+1)=OM/TW                                                          E02ABF    60
      DELSQ=DELSQ-S(I+1)*OM                                                 E02ABF    61
      KTEMP = M - I - 1                                                     E02ABF    62
      XTEMP = KTEMP                                                         E02ABF    63
      SI(I+1) = ABS(DELSQ/XTEMP)                                            E02ABF    64
      IF(L) GO TO 20                                                        E02ABF    65
      IF(ISWX.EQ.1)GO TO 21                                                 E02ABF    66
      IF(SI(I+1).LT.SI(I))GO TO 20                                          E02ABF    67
      N=I-1                                                                 E02ABF    68
      ICOMP = 1                                                             E02ABF    69
      ISWX=1                                                                E02ABF    70
      SIMIN=SI(I)                                                           E02ABF    71
      DO 13 J=1,K1                                                          E02ABF    72
   13 CPSAVE(J)=CP(J)                                                       E02ABF    73
      GO TO 20                                                              E02ABF    74
   21 IF (SI(I+1).GE.(0.6*SIMIN)) GO TO 20                                  E02ABF    75
      ICOMP  = 0                                                            E02ABF    76
```

```
      ISWX = 0                                                          E02ABF     77
      N = K                                                             E02ABF     78
20    DO 3 J=1,I                                                        E02ABF     79
      DU=CLP(J+1)*BE(I)                                                 E02ABF     80
      CLP(J+1)=CTP(J)                                                   E02ABF     81
      CTP(J)=CLP(J)-AL(I+1)*CTP(J)-DU                                   E02ABF     82
3     CP(J)=CP(J)+S(I+1)*CTP(J)                                         E02ABF     83
      CP(I+1)=S(I+1)                                                    E02ABF     84
      CTP(I+1)=1.0                                                      E02ABF     85
      CLP(I+2)=0.0                                                      E02ABF     86
      IF(ICOMP.EQ.0.OR.ISWX.EQ.0)GO TO 7                                E02ABF     87
      IF(I.NE.K)GO TO 7                                                 E02ABF     88
      DO 8 J=1,K1                                                       E02ABF     89
8     CP(J)=CPSAVE(J)                                                   E02ABF     90
7     CONTINUE                                                          E02ABF     91
      CLP(1)=1                                                          E02ABF     92
      CPSAVE(1)=1                                                       E02ABF     93
      P(1)=CP(1)                                                        E02ABF     94
      DO 30 I=2,K1                                                      E02ABF     95
      CLP(I)=1                                                          E02ABF     96
      CPSAVE(I)=B*CPSAVE(I-1)                                           E02ABF     97
30    P(I)=P(I)+CP(I)*CPSAVE(I)                                         E02ABF     98
      DO 33 J=2,K1                                                      E02ABF     99
      CLP(1)=CLP(1)*A                                                   E02ABF    100
      P(J)=CP(J)*CLP(1)                                                 E02ABF    101
      KK=2                                                              E02ABF    102
      J1=J+1                                                            E02ABF    103
      IF(J1.GT.K1)GO TO 40                                              E02ABF    104
      DO 34 I=J1,K1                                                     E02ABF    105
      CLP(KK)=A*CLP(KK)+CLP(KK-1)                                       E02ABF    106
      P(J)=P(J)+CP(I)*CLP(KK)*CPSAVE(KK)                                E02ABF    107
34    KK=KK+1                                                           E02ABF    108
33    CONTINUE                                                          E02ABF    109
40    A=1.0/A                                                           E02ABF    110
      DO 35 I=1,M                                                       E02ABF    111
35    X(I)=(X(I)-B)*A                                                   E02ABF    112
      RETURN                                                            E02ABF    113
      END                                                               E02ABF    114
```

APPENDIX V

APL/360 ROUTINE FOR LINEAR REGRESSION AND CORRELATION

```
      SIMPLE REGRESSION
      T←X SR Y
      ENTERED:10/08/67

   X AND Y ARE VECTORS GIVING THE (SAME NUMBER OF) OBSERVATIONS
ON AN INDEPENDENT VARIABLE X AND A DEPENDENT VARIABLE Y. T IS
A MATRIX WITH 5 ROWS AND 3 COLUMNS CONTAINING THE RESULTS OF
FITTING THE STRAIGHT LINE Y=A+B×X BY THE METHOD OF LEAST SQUARES
IN THE FOLLOWING FORMAT:
   ROW1: MEAN OF X, ST DEV OF X, 0
   ROW2: MEAN OF Y, ST DEV OF Y, 0
   ROW3: A, 0, 0
   ROW4: B, ST ERROR OF B, T-VALUE
   ROW5: ST ERROR OF ESTIMATE, R=SIMPLE CORR COEFF, R*2
```

```
      ∇SR[[]]∇
    ∇ ~→⊃ ⌈⍴ ⍬;N;MX;SX;MY;SY;B1;B0;R;RSQ;TV;SE;A;B
[1]   SX←((A←+/(X-MX←(+/X)÷N)*2)÷(N←(⍴X))-1)*0.5
[2]   SY←((B←+/(Y-MY←(+/Y)÷N)*2)÷N-1)*0.5
[3]   B0←MY-MX×B1←(+/(X-MX)×(Y-MY))÷A
[4]   SE←((B×1-RSQ←(R←B1×SX÷SY)*2)÷N-2)*0.5
[5]   TV←B1÷SB1←(SY÷SX)÷((N-2)÷(1-RSQ))*0.5
[6]   T←(5 3)⍴MX,SX,0,MY,SY,0,B0, 0 0 ,B1,SB1,TV,SE,R,RSQ
    ∇
```

APPENDIX VI

TABLE FOR CORRELATION COEFFICIENTS

n	SIGNIFICANCE LEVELS				
	·1	·05	·02	·01	·001
1	·98769	·99692	·999507	·999877	·9999988
2	·90000	·95000	·98000	·990000	·99900
3	·8054	·8783	·93433	·95873	·99116
4	·7293	·8114	·8822	·91720	·97406
5	·6694	·7545	·8329	·8745	·95074
6	·6215	·7067	·7887	·8343	·92493
7	·5822	·6664	·7498	·7977	·8982
8	·5494	·6319	·7155	·7646	·8721
9	·5214	·6021	·6851	·7348	·8471
10	·4973	·5760	·6581	·7079	·8233
11	·4762	·5529	·6339	·6835	·8010
12	·4575	·5324	·6120	·6614	·7800
13	·4409	·5139	·5923	·6411	·7603
14	·4259	·4973	·5742	·6226	·7420
15	·4124	·4821	·5577	·6055	·7246

n	SIGNIFICANCE LEVELS				
	·1	·05	·02	·01	·001
16	·4000	·4683	·5425	·5897	·7084
17	·3887	·4555	·5285	·5751	·6932
18	·3783	·4438	·5155	·5614	·6787
19	·3687	·4329	·5034	·5487	·6652
20	·3598	·4227	·4921	·5368	·6524
25	·3233	·3809	·4451	·4869	·5974
30	·2960	·3494	·4093	·4487	·5541
35	·2746	·3246	·3810	·4182	·5189
40	·2573	·3044	·3578	·3932	·4896
45	·2428	·2875	·3384	·3721	·4648
50	·2306	·2732	·3218	·3541	·4433
60	·2108	·2500	·2948	·3248	·4078
70	·1954	·2319	·2737	·3017	·3799
80	·1829	·2172	·2565	·2830	·3568
90	·1726	·2050	·2422	·2673	·3375
100	·1638	·1946	·2301	·2540	·3211